Metal Complexes of Alkyne-Functionalised 2,2':6',2"-Terpyridine Ligands

Inauguraldissertation

zur

Erlangung der Würde eines Doktors der Philosophie

vorgelegt der

Philosophisch-Naturwissenschaftlichen Fakultät

der Universität Basel

von

Ellen Jane Shardlow

aus Lothersdale, Grossbritannien.

Basel, Februar 2007.

Genehmigt von der Philosophisch-Naturwissenschaftlichen Fakultät der auf Antrag von:

Prof. Dr. C. E. Housecroft

Prof. Dr. A. Pfaltz

Basel, den 13 Februar 2007

Prof. Dr. H.-P. Hauri,
Dekan.

Abstract

4'-substituted-2,2':6',2"-terpyridine ligands which all contain a terminal alkyne functionality are synthesised and discussed in Chapter 2. These ligands have been designed with potential coupling to platinum(II) or gold(I) through the alkyne in mind and have varying degrees of flexibility built in. Ligands are intended to favour either polymer or macrocycle formation according to their flexibility and the various ways of achieving this are also discussed in Chapter 2.

The coupling of these ligands with platinum(II) and gold(I) are discussed separately in Chapters 3 and 4, respectively. The combination of the ligand flexibility with the coordination geometry at the metal centre is carefully considered in order to form building blocks of a specific shape which can then be reacted further at the pendant terpyridine moiety. The ligands have been fully characterised, some crystallographically. Luminescence spectra of these building blocks are measured. ^{31}P NMR spectroscopy is a particularly useful tool for characterisation of these molecules, especially in the case of the platinum(II) complexes, since this provides a means of determining the configuration of the phosphine ligands at the platinum(II) centre. Again, X-ray crystal data provide some invaluable information as to the arrangement of the molecules in the solid state, including interactions between metal atoms in the case of Au(I).

The final step in the formation of polymers or macrocycles is discussed in Chapter 5 where the platinum(II) and gold(I) containing building blocks are assembled into supramolecular structures by coordination of the pendant terpyridine moiety with iron(II). The resulting structures are fully characterised, and electrospray ionisation mass spectrometry is important in determining the size of the macrocycles formed. Pulsed-field gradient spin-echo NMR experiments help to determine the size of the products formed and X-ray crystal data for one structure have been obtained and are discussed.

Acknowledgements

I would first of all like to thank my supervisors Prof. Catherine Housecroft and Prof. Ed Constable for all your help and support over the last few years. I have learnt a great deal from working with you and it has been wonderful to work for supervisors who have been just as excited about my results as I was.

I would also like to thank the Constable/Housecroft group members both past and present for your help and friendship. In particular, thanks go to Jon for your time spent on all those complicated NMR experiments, I'll buy you some (more) beer when I've finished this thesis. Thanks to Lukas, Conor, Dan and Kate for MALDI mass spectroscopy measurements, Emma for her advice on UV/VIS spectroscopy and Valerie J, now in Boston, for being my librarian and sending me all those unavailable journal articles from the other side of the world. Thanks also to Hein. Your vast experience stopped me from making stupid mistakes on more than one occasion. I haven't got room to mention all my other colleagues by name but because of you I have thoroughly enjoyed my time in Basel and working with you all has been a great experience which I won't forget.

A special mention goes to Markus and Silvia for your expertise in X-ray crystallography. Without you both I wouldn't have a thesis, and I am still amazed at your willingness and ability to measure the worst possible crystal at a moment's notice, particularly when I must have told you on several occasions that this crystal is the "important one" and that I really need it doing straight away.

Thanks to Beatrice Erismann for your help and advice on the various intricacies of living in Switzerland. I would never have worked out all the many rules and regulations and I'm sure I would be in serious trouble for some minor misdemeanour by now if it wasn't for you.

Thank you to all my friends and family back in the UK. I am very grateful for your moral support given regularly down the end of a telephone, your regular visits which have kept me sane, and your frequent trafficking of bacon, black pudding and other items of food which have enabled me to live a normal life in Basel.

Last but not least I would like to acknowledge the financial support of the Schweizerischer Nationalfonds zur Förderung der Wissenschaflichen Forschung, Universität Basel and the Schweizerische Chemische Gesellschaft. With this support I have been able to carry out my own research as well as travel to an international conference in order to present my results and I am very grateful for this opportunity.

Contents

Abbreviations

General

A-Sol	MeCN, saturated KNO_3 and H_2O in a 14:2:1 ratio.
bpy	2,2'-Bipyridine
Cy	Cyclohexyl
DMF	*N,N*-Dimethylformamide
DMSO	Dimethylsulfoxide
HO-tpy	4'-Hydroxy-2,2':6',2"-terpyridine
NEM	*N*-Ethylmorpholine
OTf^-	Triflate
phen	Phenanthroline
ppm	Parts per million
TGA	Thermogravimetric analysis
THF	Tetrahydrofuran
TLC	Thin layer chromatography
TMS	Tetramethyl silane
Tpy	2,2':6',2"-Terpyridine
X	Substituent attached to a tpy, e.g. OH, phenyl, etc.

Experimental Methods

Nuclear Magnetic Resonance Spectroscopy

^{1}H NMR	Proton nuclear magnetic resonance spectroscopy
^{13}C NMR	Carbon nuclear magnetic resonance spectroscopy
^{31}P NMR	Phosphorus nuclear magnetic resonance spectroscopy
^{195}Pt NMR	Platinum nuclear magnetic resonance spectroscopy
COSY	Correlated spectroscopy
DOSY	Diffusion ordered spectroscopy
HMBC	Heteronuclear multiple bond correlation

HMQC	Heteronuclear multiple quantum correlation
NOESY	Nuclear overhauser effect spectroscopy
PGSE	Pulsed-field gradient spin-echo
δ	Chemical shift, ppm
J	Coupling constant in Hz
s	Singlet
d	Doublet
t	Triplet
dd	Doublet of doublets
ddd	Doublet of doublets of doublets
dt	Doublet of triplets
td	Triplet of doublets
m	Multiplet
br	Broad

Mass Spectrometry (MS)

ES	Electrospray ionisation
M	Parent ion
m/z	Mass to charge ratio
MALDI	Matrix assisted laser desorption ionisation

Ultra-Violet Visible (UV/VIS) Spectroscopy

MLCT	Metal-to-ligand charge transfer
λ_{max}	Wavelength at which maximum absorption occurs in nm
ε	Extinction coefficient in $M^{-1}cm^{-1}$

Infrared (IR) Spectroscopy

w	Weak
m	Medium

s	Strong
br	Broad

General Experimental

^{1}H, ^{13}C, ^{31}P and ^{195}Pt NMR spectra were recorded on Bruker DRX400 and 500 spectrometers. Chemical shifts for ^{1}H and ^{13}C spectra were referenced with respect to residual solvent peaks and TMS = δ 0ppm. ^{31}P was referenced with respect to 85% aqueous H_3PO_4 (δ 0ppm) (sometimes also with an internal reference of $[PF_6]^-$) and ^{195}Pt with respect to Na_2PtCl_4 (δ 0ppm). Compound labelling schemes are shown in each chapter.

IR spectra were recorded on a Shimadzu FTIR-8400S spectrophotometer with samples as solids using a Golden Gate ATR accessory.

ESI mass spectra were recorded using a Finnigan MAT LCQ spectrometer, and MALDI mass spectra were recorded using a PerSeptive Biosystems Voyager instrument.

Electronic absorption spectra were recorded on a Varian-Cary 5000 spectrophotometer and fluorescence spectra were recorded using a Shimadzu RF-5301 PC spectrofluorophotometer.

TGA experiments were carried out on a Mettler Toledo TGA/SDTA851^{e} machine.

Liquid crystals were examined under a Leica DMLP polarising microscope.

Chapter 1 Introduction

1.1 Supramolecular Chemistry

The field of supramolecular chemistry has grown in importance over the last couple of decades. In 1987 Jean-Marie Lehn won the Nobel Prize for Chemistry with his work in this area of research. But what exactly is supramolecular chemistry? There are many definitions of the phrase. Lehn himself describes supramolecular chemistry as "chemistry beyond the molecule",[1] where the molecules concerned are components of complex chemical systems and are held together by non-covalent intermolecular forces.[2] This type of system is often found in natural biological systems, though at the research level the field of supramolecular chemistry is entirely unnatural in character.

Unfortunately things are not as straightforward as they might first seem. Normally, non-covalent intermolecular forces are weak (often less than 10 % of the intramolecular bond energies) and the "bonds" are long, often much longer than the intramolecular distances. This in itself is not a problem. However, in the last few years there has been a great increase in the amount of supramolecular systems constructed by using the principles of coordination chemistry. A problem arises in the fact that the metal-ligand bonds are not long and the energies involved are significantly greater than traditional non-covalent forces such as van der Waals forces, π-stacking, or hydrogen bonds. Thus, there is some contradiction surrounding the definition of supramolecular chemistry.[3]

The growing amount of research into this field of chemistry has come about due to the greater need for smaller and smaller devices for applications in nanotechnology, defined as "the understanding and control of matter at dimensions of roughly 1 to 100 nanometers, where unique phenomena enable novel applications"[4] according to the National Nanotechnology Initiative in the USA. The creation of devices at this scale requires great precision and

control, and traditional organic synthesis is severely limited in terms of what it can deliver in this respect.[5] Not only do chemists have to develop the molecular technology, but they also have to develop the means of allowing these devices to communicate with the outside world as well as the appropriate structures to contain and service the devices.[6] The use of metals in forming coordination complexes is one way of achieving this control and order.

1.2 Metallosupramolecular Chemistry

Metallosupramolecular chemistry involves "the use of transition metal centres to control the assembly of novel supramolecular architectures."[7] There is a wide variety of transition metals, and each of these has a preferred coordination geometry as well as a preference for certain types of donor ligand.[8] The choice of a specific metal for coordination in supramolecular assembly therefore allows the design of building blocks based around these coordination geometries.

The use of a chelating ligand, such as a terpyridine, gives control and stability to any resulting supramolecular structure. Complexes of 2,2':6',2"-terpyridine ligands can be formed with various different metals in different oxidation states, bringing in a certain degree of versatility to these systems. The three nitrogen donors on each tpy form strong interactions with the metal ion and if the ligand is 4'- substituted, there is no chirality arising from the MN_6 core, unlike in systems where monosubstituted bpy ligands are used. This means the resulting structure is predictable, one of the most important qualities of this type of synthesis. Figure 1.1 shows the 2,2':6',2"-terpyridine ligand with ring atom numbering.

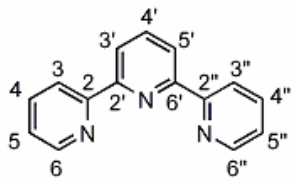

Figure 1.1: 2,2':6',2"-Terpyridine ligand showing ring atom numbering scheme.

If supramolecular compounds are to be useful as functional microporous materials they need to have several features. They should be cyclic with suitable cavities which can be accessed by smaller molecules. This means that there should be no catenation between different molecules and no counter ions which might take up valuable space inside the cavity. They should also be stable enough to resist removal of solvent or any other small molecules which fill the cavity on a temporary basis. Most of the compounds under investigation as potential molecular materials are supramolecular squares with $Re(CO)_3X$ as corner units where X = Cl or Br, two examples of these can be seen in figure 1.2.[11]

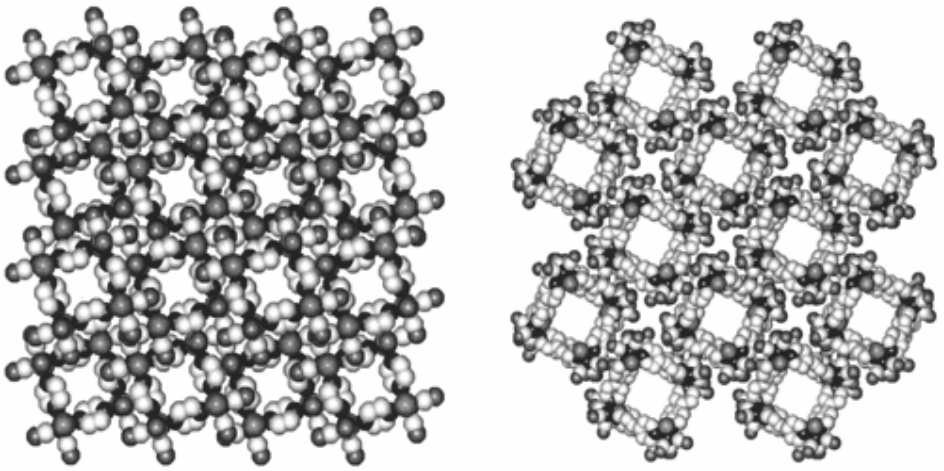

Figure 1.2: X-ray crystal structures of supramolecular compounds investigated as potential microporous materials clearly showing the square structure and the large empty cavities capable of hosting smaller molecules.[11]

The different metals available to the coordination chemist also bring unusual and interesting properties to a supramolecular structure. There is significant literature available on the use of metals in supramolecular assemblies for their luminescent and photophysical properties, such as ruthenium(II), iridium(III), osmium(II) and platinum(II)[9]. Yam has carried out significant research into the use of metal alkynyls as luminescent materials,[10] and there are also reports in the literature of supramolecular materials as molecular sieves, chemical sensors and catalysts.[11]

1.3 Molecular Self Assembly

Molecular self assembly involves the use of diverse interactions between molecules to construct nanoscale structures with a wide variety of functions. This is a phenomenon which is widely present in nature, for example, the formation of the DNA double helix, shown in figure 1.3 and the growth of the Tobacco Mosaic Virus.[6]

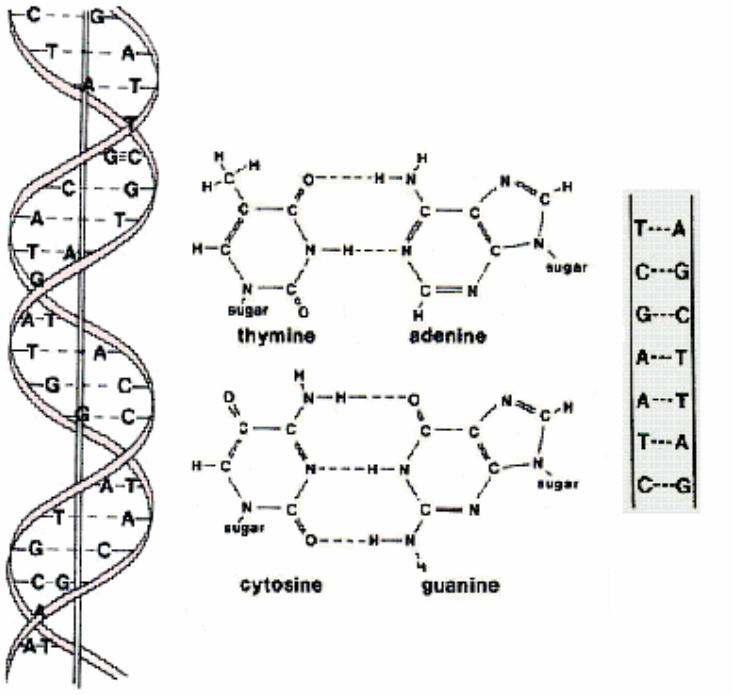

Figure 1.3: Probably the most important natural example of supramolecular self assembly in nature- the formation of the double helix of the DNA molecule. Base pairs are held together by hydrogen bonds.

Up until recently, the use of organic synthesis to produce large structures has been the only method available. However, although some relatively large molecules have been synthesised, such as vitamin B_{12}, it is clear that to synthesise any molecule on a nanometre scale would involve an incredible effort in terms of manpower, time and of course money. Lessons have to be learnt from nature, and nature has taught us that the most efficient way to produce large nanometre scale structures is to self assemble these from smaller subunits. It is highly important to understand the nature of the

interactions which are responsible for the self assembly[6] and this is where the field of coordination chemistry plays an important part.

1.4 2,2':6',2"-Terpyridine Ligands

The molecule 2,2':6',2"-terpyridine (tpy) has been known since 1932 when Morgan and Burstall heated pyridine and anhydrous iron(III) chloride in an autoclave.[12] Terpyridine was one of 20 products of this reaction, and since then the synthesis has been developed to give more specific results and better yields.

Terpyridine ligands have many applications apart from that in the field of supramolecular chemistry. The use of aryl substituents in the 4'- position gives a molecule which can be used in the colorimetric determination of iron(II) as well as having the potential for use in clinical chemistry. There are examples of the use of terpyridine ligands in the preparation of luminescent materials and these have potential as luminescent protein labels. [13]

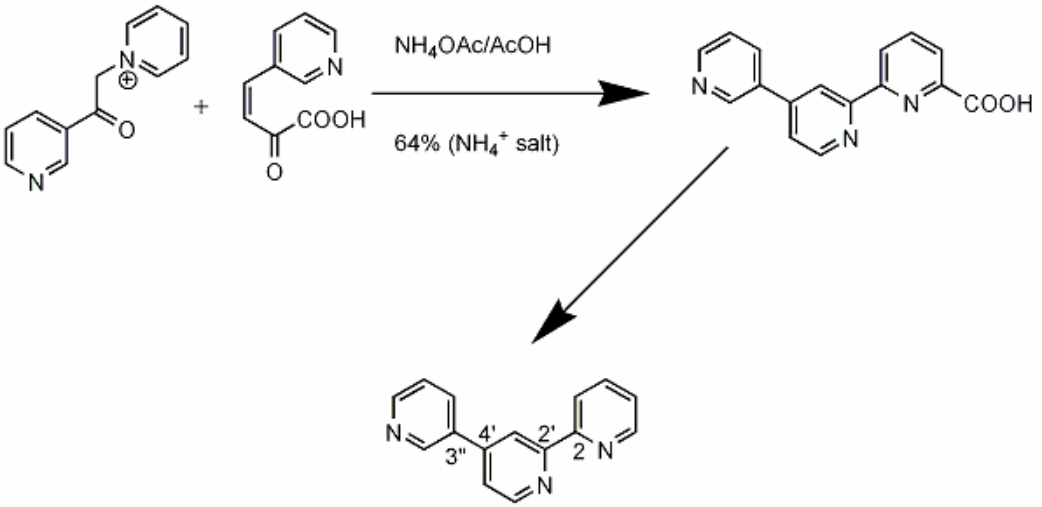

Figure 1.4: The original Kröhnke 2,2':4',3"-terpyridine synthesis.

These days there are many different synthetic routes to form substituted terpyridines. These are generally based on two different methods, ring closure and ring coupling. An example of the ring closure method is the Kröhnke synthesis,[14] shown in figure 1.4. This method is described by

Kröhnke in the literature for the synthesis of 2,2':4',3"-terpyridine. The other method is the direct coupling of the pyridine rings. This method is inefficient, producing on average less than 10 % yield of terpyridine.[13]

A useful method for directly forming a hydroxy-substituted terpyridine uses acetone and 2-acetylpyridine as reactants to generate 4'-hydroxy-2,2':6',2"-terpyridine (HO-tpy).[15] This can then be used as the starting point for further functionalisation of the terpyridine ligand. This method is possibly more useful for synthesis of building blocks for supramolecular self assembly since the product here has the nitrogen atoms positioned in a way which is suitable for coordination to an octahedral metal ion. In the original Kröhnke synthesis the donor atoms are positioned so that it is impossible for all three of them to coordinate simultaneously to the metal ion. Figure 1.5 shows ring closure to form 4'-substituted tpy directly.

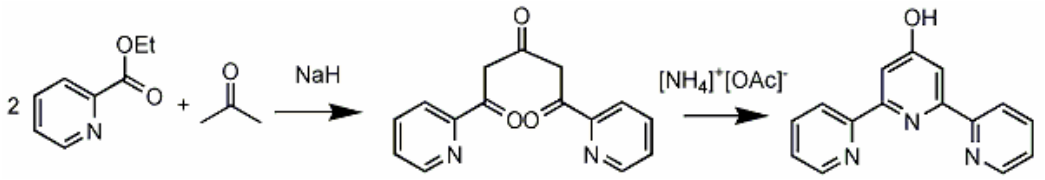

Figure 1.5: Formation of hydroxy-substituted terpyridine by the ring closure method.[15]

The hydroxyl group is a particularly useful functional group to include since it provides a means for attaching all sorts of other functionalities to the terpyridine ligand itself. The use of a base creates a nucleophile which can undergo substitution reactions and there are many examples in the literature of this.[16,17,18]

The use of substituted terpyridine ligands has now become widespread as a building block in supramolecular chemistry since these ligands readily coordinate to a wide variety of transition metal ions and can be substituted with many different functionalities. 4'-Substituted tpy when coordinated to an octahedral metal centre produces a rigid linear moiety which can produce molecular wires and rods. Figure 1.6 shows how substituents on 4'-

substituted tpy ligands are arranged linearly as part of an octahedral metal complex.

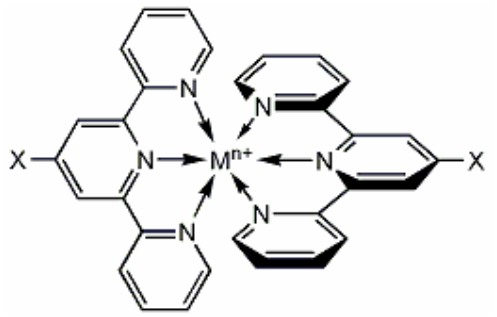

Figure 1.6: Octahedral metal complex of 4'-substituted 2,2':6',2"-terpyridine showing the overall linear arrangement of substituents, X.

There are many examples in the literature of 4'-substituted terpyridine ligands being used as precursors for large supramolecular architectures. The synthesis of terpyridine ligands bearing pendant naphthalene units was designed in order to provide a method for the self assembly of ligands and/or complexes in the solid state by use of π-stacking interactions of the naphthalene groups.[19] Terpyridine ligands have also been used in the core of metallodendrimers as a means to investigate the novel properties associated with a metal ion, such as iron(II) and cobalt(II), being embedded in the centre of a large macromolecular structure.[20] Terpyridines can also be found on the outside of dendrimers, providing a means of using the coordination of metal ions to assemble further generations of the dendrimer structure as shown in figure 1.7.[21]

The addition of an alkyne substituent onto a terpyridine in the 4'-position is useful for achieving further coordination or functionality. There are various methods in which this can be achieved, namely the direct attachment onto the terpyridine[22] or the use of a spacer of varying lengths to separate the alkyne from the terpyridine.[16,18,23] The alkyne functionality is useful as a means for the insertion of cobalt clusters[24,25,26] as well as reaction with square planar platinum complexes[27,28] to give a bis-tpy building block.

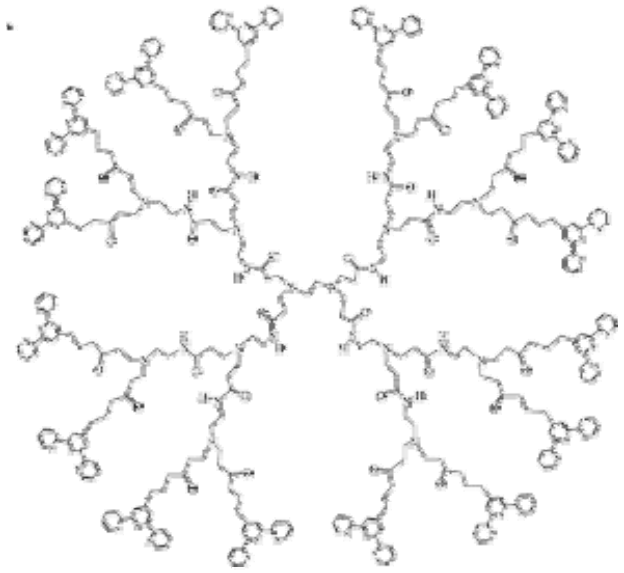

Figure 1.7: The use of the 4'-substituted 2,2':6',2"-terpyridine ligand as a functional group on the outside of a dendrimer.[21]

1.5 Iron(II) and Ruthenium(II) Terpyridine Complexes

There are several possible metals which can be complexed with terpyridine ligands. However we will concentrate on iron(II) and ruthenium(II) here. Both ruthenium(II) and iron(II) have the electron configuration d^6. In the case of ruthenium(II), complexes are always diamagnetic in a low spin electron configuration. Crystal field theory can be used to explain why this occurs since the electrons surrounding the metal centre are located in the d orbitals of the metal and there is electrostatic repulsion between these electrons and the electrons of the ligands. Both the metal electrons and the ligand electrons are dealt with as point charges for the purposes of crystal field theory. If we now consider the ligands arranged in an octahedral fashion around the metal, the electrons in the d_{z2} and d_{x2-y2} orbitals will point directly at the ligands and will therefore experience higher repulsion energy. The remaining d orbitals (d_{xy}, d_{xz} and d_{yz}) point between the ligands and experience less repulsion. This leads to a splitting of the d orbitals, called crystal field splitting. Depending on the metal centre and the ligand field, this splitting can be large or small resulting in higher or lower stabilisation effects. Each orbital can hold a maximum of two electrons and energy is required to

pair these electrons up in the orbitals. When there is a choice of orbitals for the electrons to occupy, the orbital occupation depends on whether a lower energy can be achieved by pairing the electron or promoting it to the higher level. Thus a lower crystal field splitting means that less energy is needed to promote the electron to the higher orbital than is needed to pair the electron and thus the complex is high spin. In the case of iron(II), complexes can be either low or high spin depending on the position of the ligands in the spectrochemical series, though the use of the terpyridine ligand means there is a strong crystal field splitting and therefore the complex is in a low spin configuration.[29,30] Figure 1.8 shows low spin and high spin configuration for a d^6 metal such as Fe(II).

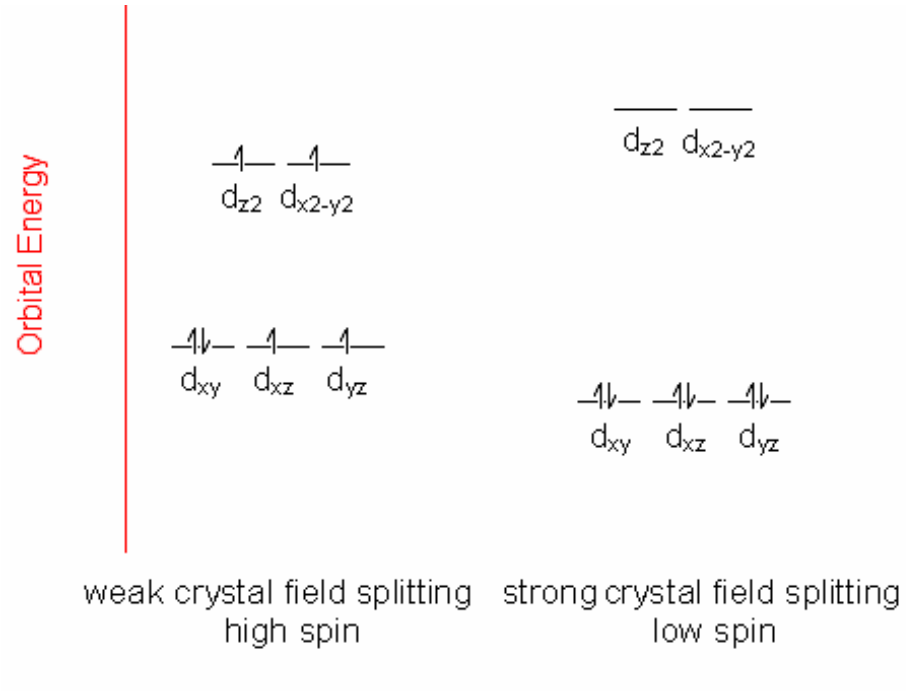

Figure 1.8: High and low spin electron configurations for a d^6 metal centre.

Both iron(II) and ruthenium(II) display octahedral coordination and readily form complexes with chelating nitrogen donor ligands such as tpy, bpy or phen. Two tpy ligands are coordinated to one metal ion compared to three bpy or phen ligands. The tpy ligand is symmetrical when monosubstituted in the 4'- position, whereas monosubstitution in bpy and phen leads to asymmetrical ligands. All three ligands can be seen in figure 1.9.

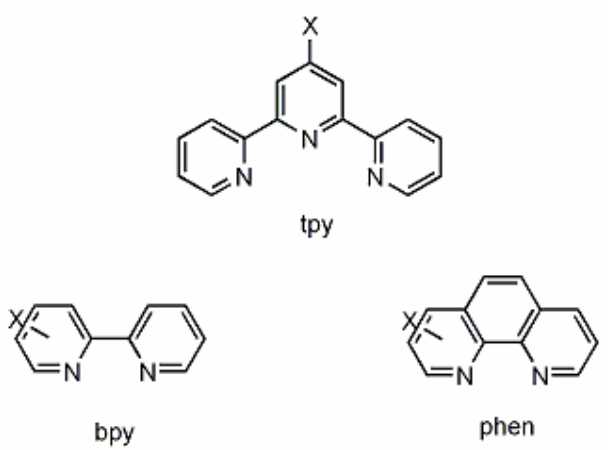

Figure 1.9: Symmetry of 4'-monosubstituted tpy compared to asymmetry of monosubstituted bpy and phen ligands.

When tpy is unsubstituted there are no isomers of an $M(tpy)_2$ unit and the product is symmetrical. However, the use of unsubstituted bpy or phen produces two enantiomers of an ML_3 unit. When the symmetrical 4'-substituted terpyridine ligand is coordinated to a metal ion, once again it allows for only one product with no isomers. This is a significant advantage over bpy or phen which, if monosubstituted, are asymmetrical. This asymmetry of monosubstituted bpy and phen means that on complexation with an octahedral metal ion, *fac* and *mer* isomerism occurs as shown in figure 1.10. Because of this, there is a significant advantage in using 4'-substituted tpy over substituted bpy and phen[31] for supramolecular self assembly as tpy complexes have highly predictable structures whereas bpy and phen complexes will produce a statistical mixture of different isomers which is not something which is sought after in this type of synthesis.

The main difference between iron(II) and ruthenium(II) is the way in which they can be used in the synthesis of self-assembled structures. The formation of iron-tpy complexes is done in one step at room temperature starting from two equivalents of the tpy ligand and an iron(II) salt. Usually the reaction is complete in a very short space of time. This gives a symmetrical complex in which both the terpyridine ligands are the same. The reaction

proceeds to give a deep purple coloured solution which is indicative of the formation of the bis-tpy complex.

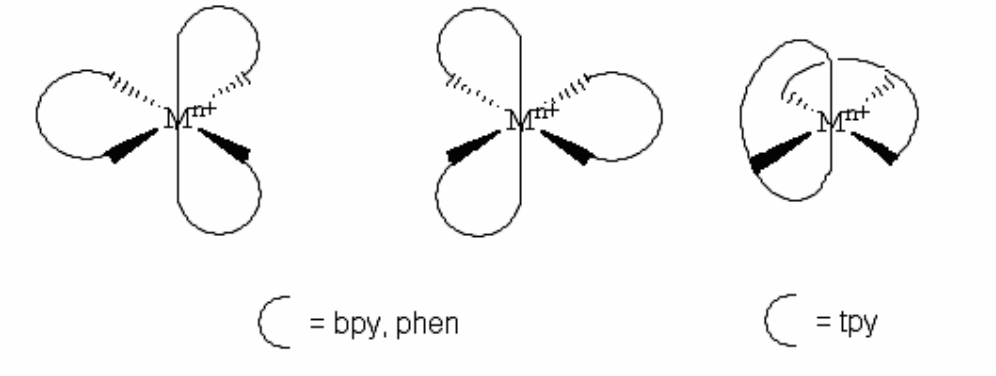

Figure 1.10: Enantiomers of octahedral bpy and phen complexes compared to the achiral tpy complex.

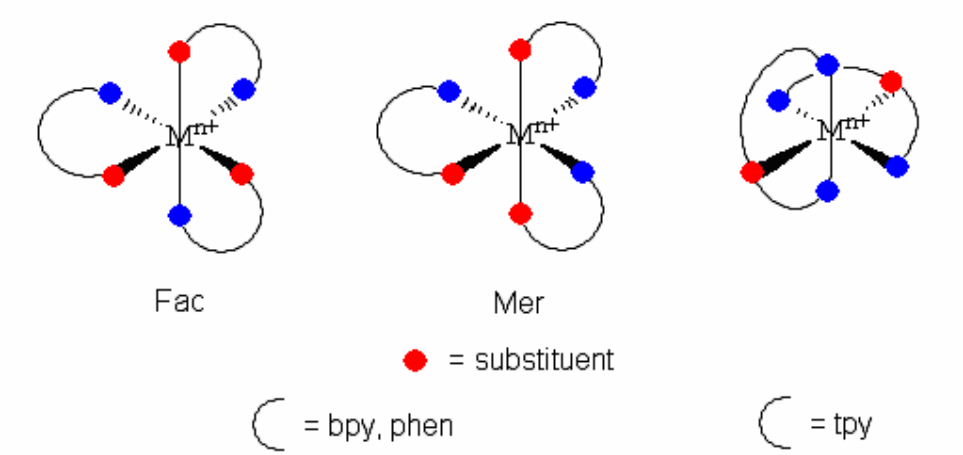

Figure 1.11: The possibility of *fac* and *mer* isomerism with monosubstituted bpy and phen complexes, but the formation of one species for 4'-monosubstituted tpy.

The reaction between iron(II) and terpyridine ligands has been used as a means to form molecular triangles in the group of Hogyu Han. The synthesis was reported as occurring simply by adding Fe(II) to an aqueous solution of the DNA-functionalised terpyridine ligands. This work, shown in figure 1.12, is a nice example of the use of two types of intermolecular forces in supramolecular self assembly, the hydrogen bonding between the base pairs in the complimentary DNA strands as well as coordination bonds between the transition metal and the nitrogen donors of the terpyridine ligand.[32]

In contrast, there are a few different methods for the formation of ruthenium-tpy complexes. An advantage of ruthenium over iron is that the reaction can be carried out in two steps, enabling an asymmetrical complex to be synthesised using two different substituted terpyridine ligands. In the first step $RuCl_3.xH_2O$ is reacted with one equivalent of terpyridine to form the insoluble ruthenium(III) complex $Ru(tpy)Cl_3$. This is then reduced to ruthenium(II) in the second step using a reducing agent such as N-ethyl morpholine while the second equivalent of the terpyridine ligand is added.[33] An alternative to this second step is to remove the chlorides from the mono complex using silver tetrafluoroborate[34] followed by addition of the second equivalent of the tpy ligand.

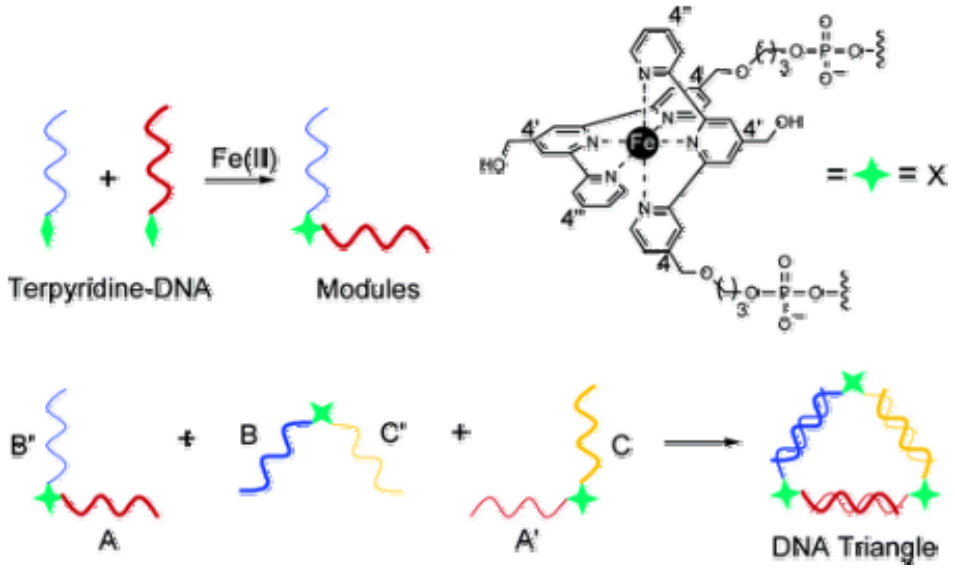

Figure 1.12: The formation of DNA triangles using iron(II) terpyridine complexes to form corner units.[32]

For a symmetrical complex, two equivalents of ligand can be used, with N-ethylmorpholine as above in a one-pot method. This also involves heating to reflux, usually for several hours, and so another method has been developed whereby the one-pot reaction mixture is heated in the microwave for very short times giving the desired symmetrical product in high yield.[35] Unfortunately the disadvantage of both of these methods is that a large amount of energy is put into the system. Having said that, the microwave method has significantly lower reaction times than the traditional thermal

method (several minutes compared to several hours) and therefore this method is an improvement on the thermal method. In both cases the large amount of energy needed can lead to decomposition of some less stable ligands during the reaction.

There are many examples in the literature of the use of terpyridine metal complexes in the construction of molecular cycles and polymers. The first reported examples of these were cycles based on bis-terpyridines with rigid spacers linking them together. The spacers were either linear or had a built in angle to them. The choice of angle predetermined the size of the macrocycle, and the use of alkynyl spacers played an important part in the synthesis of these rigid building blocks. Even with this seemingly rigid phenanthroline spacer it was reported that there was formation of both the tricyclic and tetracyclic compound, shown in figure 1.13. [36]

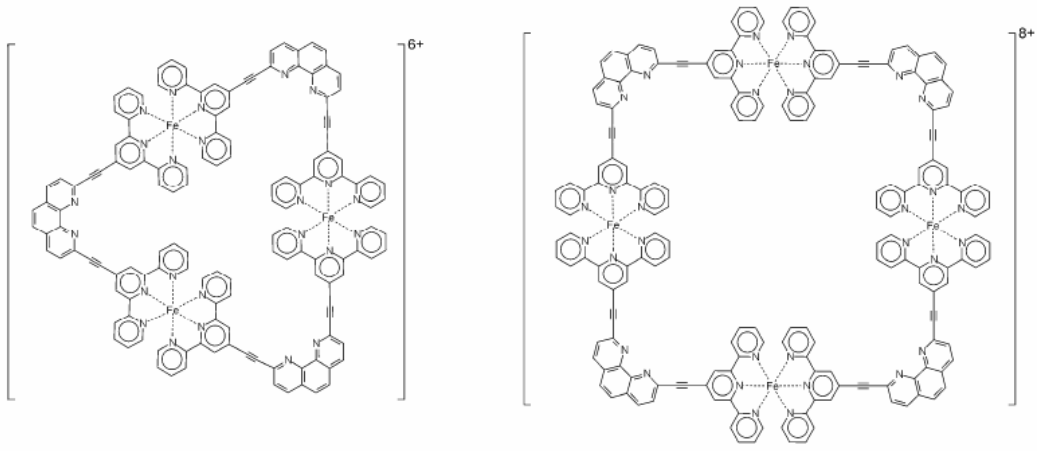

Figure 1.13: Formation of tricyclic and tetracyclic macrocycles using terpyridine complexes connected by a “rigid” spacer.[9]

Things become even more complicated when the spacer used is flexible. This type of system allows for the formation of various macrocycles and polymers, and indeed this is what has been observed in the majority of cases cited in the literature. In order to push the equilibrium to favour ring formation it is often necessary to perform these reactions at low concentration. In order to form a monocycle the spacer has to be sufficiently long enough so that the two terpyridine ligands can come together to form a

complex. Use of a spacer containing a naphthalene unit gives sufficient space to form a monocycle when the two tpy moieties are complexed with iron(II).[37] The formation of this complex is interesting because although the spacer is long enough for the complex to form, it is not long enough to allow free movement of the naphthalene ring. Therefore the conformation of the monocycle is locked, with the naphthalene occupying a cleft between the two terpyridine ligands. Since the naphthalene sits over one of the two tpy ligands, the tpy ligands are non-equivalent and the whole structure is therefore chiral. This arrangement can be seen in figure 1.14.

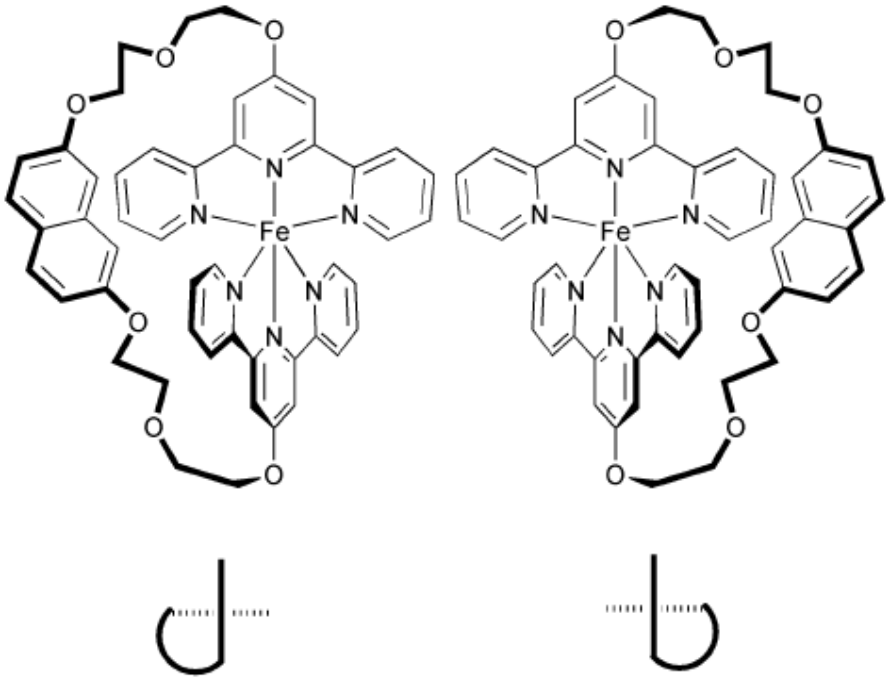

Figure 1.14: A conformationally locked chiral monocyclic iron(II) tpy complex with a naphthalene containing spacer, as well as a cartoon representation of its chirality.[37]

An example of terpyridine ligands connected with a flexible spacer shows how, on complexation of the terpyridine moieties with iron(II), two different macrocycles are formed, along with a small amount of polymeric material. In this case the length of the spacer is too short to allow a mono-cycle, and mass spectrometric evidence suggests the formation of a tri- and tetra-cycle.[38] Both these products are illustrated in figure 1.15.

As we have seen, choice of spacer is important in the design of supramolecular macrocycles and polymers. The use of alkyne spacers has been a popular choice in the literature, and these are also well known to form complexes with platinum and gold. This therefore begs the question “what properties could be added to a macrocycle by the use of alkynyl complexes as spacers in macrocycles such as the ones above?”

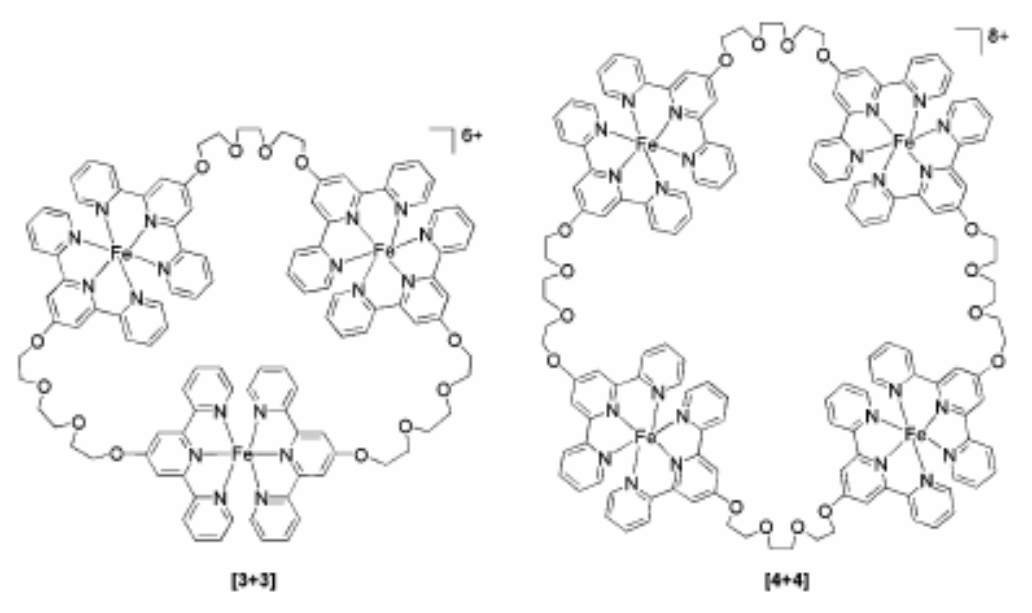

Figure 1.15: Formation of tri- and tetra-cycles with flexible spacers.[38]

1.6 Platinum(II) Alkynyl Complexes

Platinum is a transition metal commonly found in oxidation states +2 or +4. For the purposes of this thesis we will concentrate on the +2 state which has an electron configuration of d^8 at the platinum(II) centre. Platinum(II) complexes have a coordination number of 4. In theory, 4-coordinate d^8 platinum(II) complexes could have either a tetrahedral or square planar geometry, but in practice they are almost always square planar. This can be explained by crystal field theory.[29]

As described previously in the chapter, crystal field theory is a model where the ligand electrons create a field around the metal centre. This field is not spherical, due to the fact that electrons are found only in the d orbitals of

the metal which are arranged around the metal centre in an octahedral fashion. These orbitals are not equal in energy since two (d_{z2} and d_{x2-y2}) point directly at the ligands, therefore having a greater repulsion, while three (d_{xy}, d_{xz} and d_{yz}) point between the ligands and have a lower repulsion. The orbital diagram for a square planar complex is derived from the octahedral one by simple removal of the axial ligands, thus lowering the repulsive energies of those orbitals with a z component (z is taken to be the vertical axis) and meaning that the two orbitals with highest energy are those with no z component, the d_{x2-y2} and the d_{xy}. In contrast, the tetrahedral crystal field does not have the ligands pointing directly at the d orbitals of the metal. However, some point nearer than others and there is still an inequality in the orbitals. Figure 1.16 shows the crystal field splitting for the three geometries.

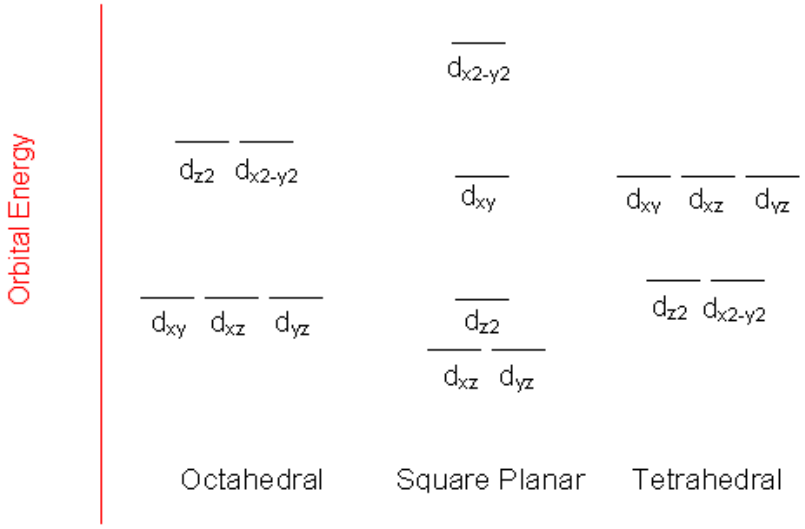

Figure 1.16: Crystal field splitting for octahedral, square planar and tetrahedral geometries.

Orbitals are filled with up to two electrons. This means that in the case of the d^8 metal centre, a square planar species would be diamagnetic, with all eight electrons paired up, and a tetrahedral species would be paramagnetic, with two unpaired electrons. When electrons are paired they require energy which can be offset by the energy gained by the stabilisation of the orbitals. Thus, a large crystal field splitting, and therefore a large stabilisation of the orbitals provides better compensation for the energy needed in pairing electrons than a smaller splitting. The crystal field splitting is affected by the

metal ion. Platinum(II) has a high crystal field splitting and when considering the stabilisation of the orbitals versus the energy saved by not pairing electrons as would be the case for a tetrahedral geometry, the square planar geometry is of lower energy and is therefore the geometry seen in virtually all d^8 platinum(II) complexes.

The synthesis of platinum(II) alkynyl complexes can be achieved by several methods. Firstly there is the use of organometallic reagents such as Grignard reagents, organolithium or organosodium reagents. An example of this is the way Chisholm uses propyne and BuLi to form the complex *trans*-$Pt(C{\equiv}CMe)_2(PMe_2Ph)_2$.[39] A second method involves transfer of the alkynyl group from less reactive species such as alkynyl tin, mercury and gold. Wrackemeyer[40] uses the alkylstannane method in his synthesis of *trans*-(alkynyl)chloro-bis(triethylphosphine)platinum(II) and Cross[41] uses the rather toxic alkynylmercury transfer method in his synthesis of *trans*-chlorobis(methyldiphenylphosphine)(phenylethynyl)platinum(II). A third, and probably the most common method uses copper iodide[42] as a catalyst with the most likely intermediate being a copper alkynyl complex. There is also the oxidative addition to platinum(0) and HX elimination from halogenoalkynyl complexes.[41] In all of these cases, the starting platinum complex has easily displaced ligands (such as halides) which are replaced by the nucleophilic alkynyl ligand on reaction. The above methods generate mostly the *trans* isomer if used with a monodentate ligand such as a phosphine, although the use of a chelating ligand, for example dppe, on the platinum(II) centre is a useful way to force the geometry to form the *cis* isomer, a popular corner unit for the formation of supramolecular squares. Figure 1.17 shows how the use of dppe forces the complex into a *cis* configuration compared to a non-chelating ligand where the complex is free to adopt a *trans* configuration. Use of the chelating phosphine dppe is exemplified in the work of Bruce.[43]

Platinum(II) alkynyl complexes have been shown to exhibit interesting luminescent properties which are unique to the presence of the alkynyl ligands.[10] The increasing demands over the past few years for new materials for use in the electronics industry has led to the investigation of this class of

compounds as potential molecular wires, sensors and other electronic materials. Studies have shown that the alkynyl ligand is a good σ- and π-donor although a poor π-acceptor.[44]

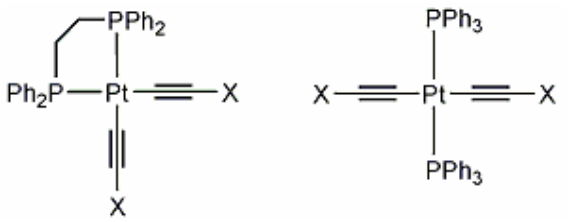

Figure 1.17: The use of chelating phosphine dppe forces the complex into a *cis* configuration (left) compared to the non-chelating phosphine (right) in which the complex is free to adopt the *trans* configuration.

Early work on the use of platinum polyynes as luminescent materials was done in the group of Hagihara.[45,46] However, the fact that these materials are polymers means that they are difficult to study and there are problems associated with molecular weight distribution, reproducibility and confirmation of the exact structure. This led Yam's group to study the design and synthesis of soluble metal alkynyls with luminescent properties which can potentially form building blocks for the supramolecular self assembly of luminescent organometallic oligomers, functional materials and molecular sensors.[10]

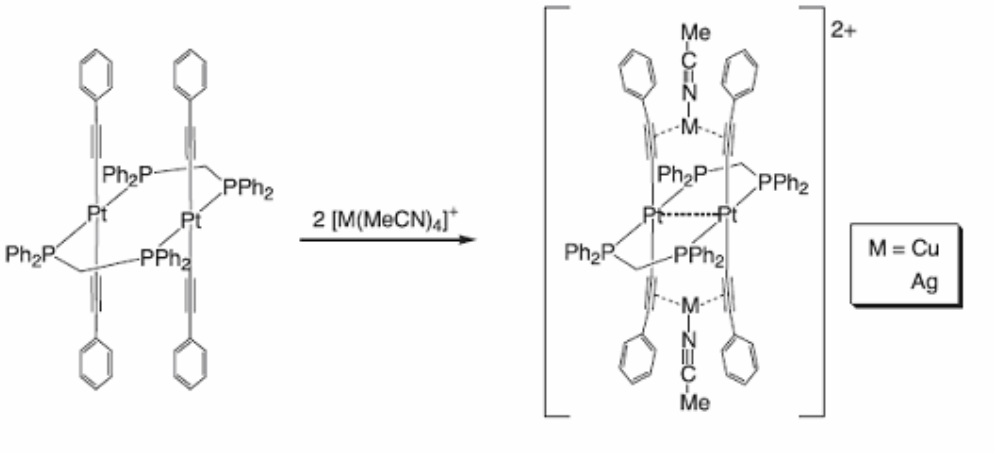

Figure 1.18: Coordination of different metals modifies the luminescence of this platinum complex which can act as a metal sensor.[47]

A recent example of the way platinum alkynyl complexes can be used as molecular sensors comes again from the work of Yam. Two square planar

platinum centres are linked via the use of a chelating phosphine ligand in a face to face arrangement. Studies have been done on the luminescence properties of this molecule and it has been shown that the further coordination of a second metal such as copper or silver to the alkynes modifies the luminescence and therefore the complex can act as a sensor for these metals.[47] Figure 1.18 shows the coordination of this second metal to the alkynes of the platinum complex.

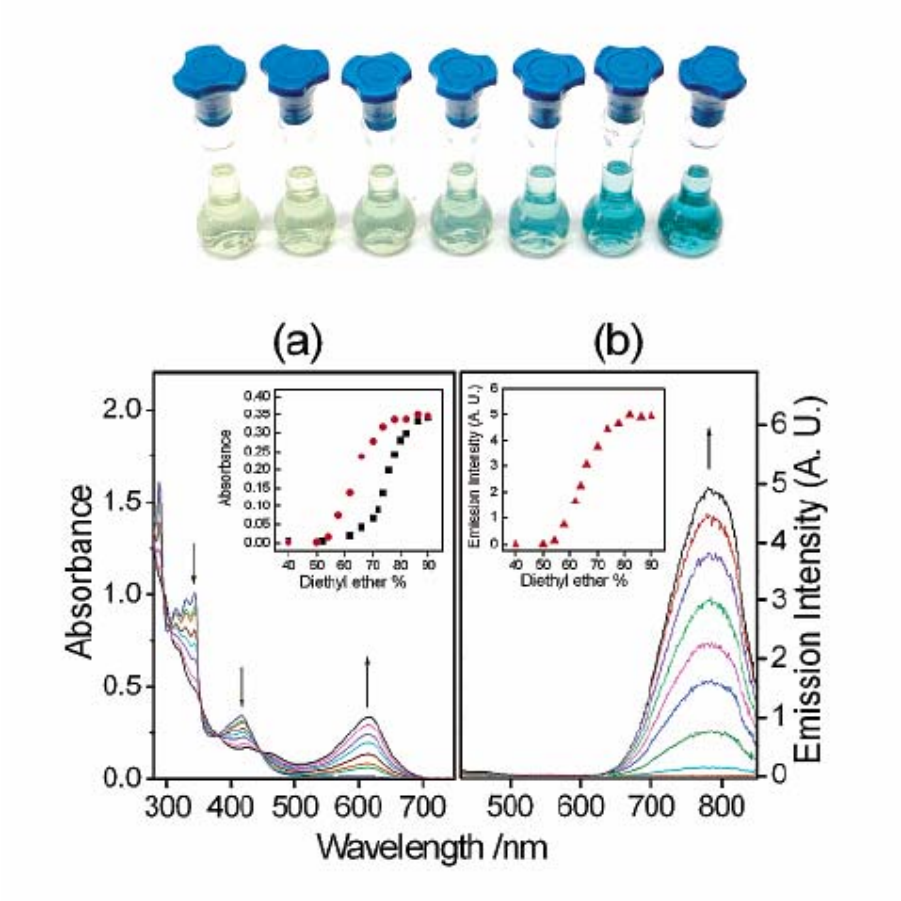

Figure 1.19: Colour changes of [Pt(tpy)C≡CC≡CH]OTf in solution with increasing diethyl ether content and its UV/VIS spectrum in MeCN (a), and emission spectrum in acetone (b).[48]

Alternatively, a simple linear platinum complex, [Pt(tpy)C≡CC≡CH]OTf has been shown to exist in two polymorphic forms, and solutions of either of these polymorphs have been shown to have varying luminescence properties depending on the composition of the solvent mixture. By increasing the amount of diethyl ether while keeping the concentration of the complex the same, the colour of the solution changes from yellow to green and finally to

blue and there are significant changes in the UV/VIS spectrum, shown in figure 1.19. This type of complex may eventually go on to act as a probe or reporter of environmental changes and may have other applications in materials science and sensor technology.[48,49]

The choice of the alkynyl ligand is also important in the design of supramolecular assemblies. It is a linear and rigid molecule which makes it a useful building block in the formation of large structures. It is well suited to forming the edge unit of squares and triangles and in combination with the right choice of metal centre it is a useful tool for the supramolecular chemist.

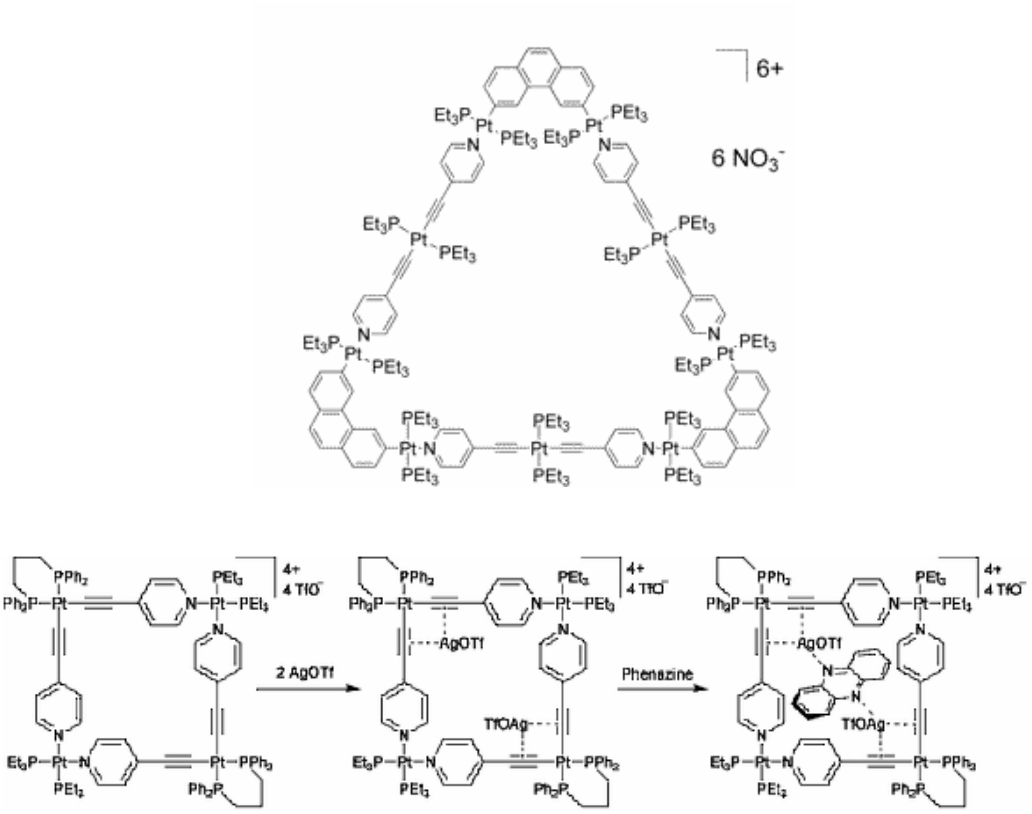

Figure 1.20: Stang's use of the platinum bis-alkyne unit to form the edges of triangles (above)[50] and the corners of molecular squares (below).[51]

Some examples of how the platinum(II) coordination geometry can be used in combination with the alkyne ligand include those in which Stang uses the square planar geometry of a bis-alkyne complex in a *trans* arrangement as a rigid linear building block in the self assembly of supramolecular triangles[50] as well as the use of a similar platinum complex, forced into the *cis*

configuration by use of a chelating phosphine ligand to form molecular squares which have the potential to form host-guest complexes.[51] Both of these are shown in figure 1.20

Bruce[43] makes use of a polyyne "edge" to give a greater cavity size for his molecular square, below in figure 1.21.

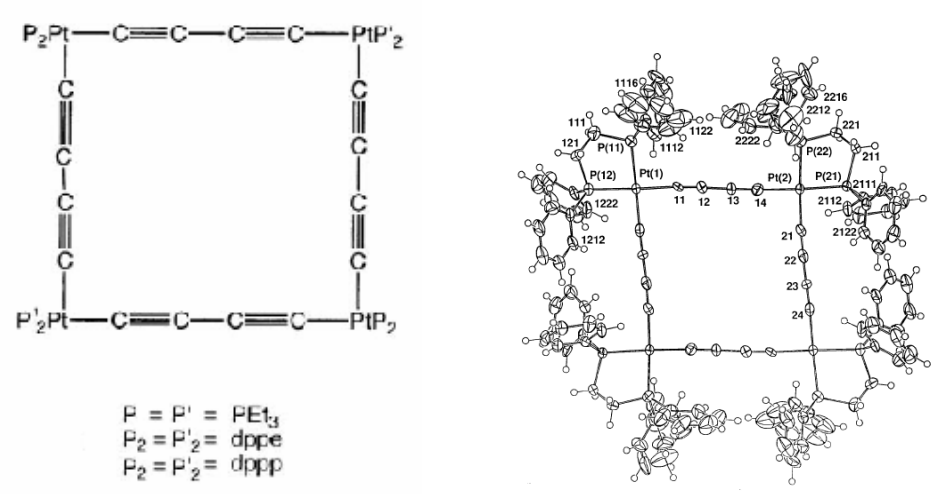

Figure 1.21: Bruce's molecular square. The use of the poly-alkyne chain for the edge units gives a larger cavity than using large aromatic systems.[43]

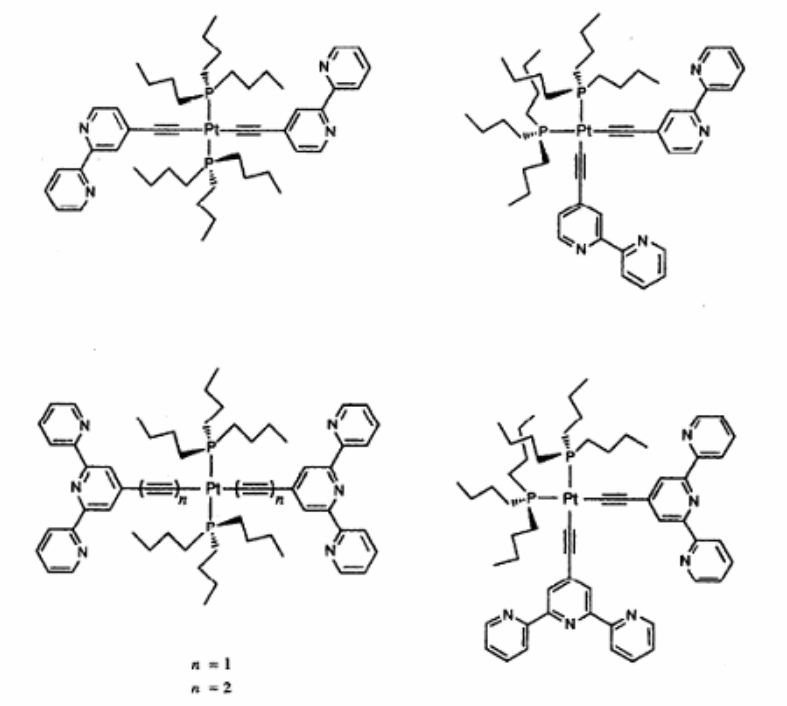

Figure 1.22: Ziessel's use of polypyridine ligands as precursors to molecular squares.[52,53]

In his work, Ziessel[52,53] starts to incorporate bipyridine and terpyridine ligands into his corner and edge units shown in figure 1.22 which have the potential to form complexes with other transition metals, closing up the square in the process.

Platinum is not the only metal which can be used in conjunction with alkynes to form large supramolecular architectures with interesting luminescence properties. Gold(I) alkynyl complexes are also commonly found in the literature and some of these are discussed in Section 1.7.

1.7 Gold(I) Alkynyl Complexes

In a similar way to platinum(II), gold forms alkynyl complexes. However, unlike platinum, gold is mainly found in the +1 and +3 oxidation states. Here we will concentrate on the +1 state, and this means that gold(I) alkynyl complexes are mostly linear[54] with a coordination number of two rather than 4-coordinate square planar like their platinum(II) analogues. This also means that in order to form a neutral complex as with platinum(II) analogues, one of the ligands must be neutral, for example a phosphine, since the alkynyl ligand is anionic (i.e. $RC{\equiv}C^-$).

There are two methods commonly used in the literature for the synthesis of phosphino-gold(I) alkynyl complexes which involve either the reaction of a gold alkynyl polymer with a suitable phosphine, or the reaction of a terminal alkyne with a phosphino-gold halide in the presence of a base, the most common one being the latter. By choosing a chelating phosphine, larger structures can be synthesised.

One important feature of gold complexes is the presence of Au…Au interactions. These are relatively weak but comparable in strength to hydrogen bonds and therefore an important factor in the supramolecular assembly of gold complexes in the solid state.[55] It is also thought that the

presence of these interactions gives rise to the luminescence often exhibited by these complexes.[56] Luminescence occurs when the interactions are short, around 3 Å. When the interactions are longer than this, no luminescence is observed. The choice of spacers used to link gold centres together can play an important part in the luminescent properties: gold centres can be held together or forced apart in order to switch luminescence on or off. Since the gold interactions also play an important part in the solubility of these complexes, by choosing linking groups which hinder interactions, solubility can be improved.[55]

In the group of Laguna, gold(I) complexes of the chelating phosphine bis(2-diphenylphosphinoethyl)phenylphosphine (triphos) have been synthesised, illustrated in figure 1.23, and their luminescent properties studied. This work has shown that in the case of gold(I) complexes, luminescence depends heavily on the ligand. In the cases of X = Cl, C_6F_5 and Fmes (2,4,6-tris(trifluoromethyl)phenyl) there is no luminescence, whereas in the case of X = Br and I there is luminescence. Thus the choice of a suitable ligand is important if synthesis of a luminescent gold complex is to be achieved.[57]

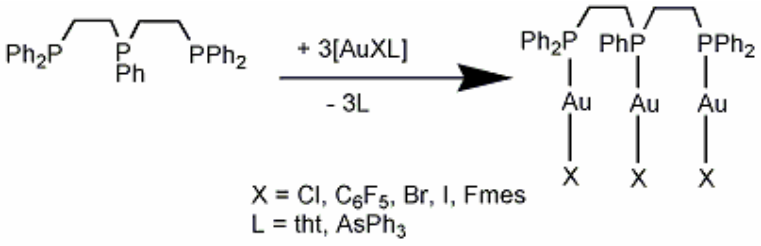

Figure 1.23: Synthesis of some luminescent gold(I) complexes.[57]

A nice example of the use of a chelating phosphine ligand in conjunction with an alkynyl ligand to form supramolecular structures containing gold centres is from the group of Puddephatt. Two gold centres are connected using a long organic spacer. The two gold centres are then connected at their other coordination site to close the ring using a chelating phosphine of varying lengths. Depending on the nature of the phosphine,

different supramolecular architectures can be formed resulting in either a single ring or a catenane as shown in figure 1.24.[58]

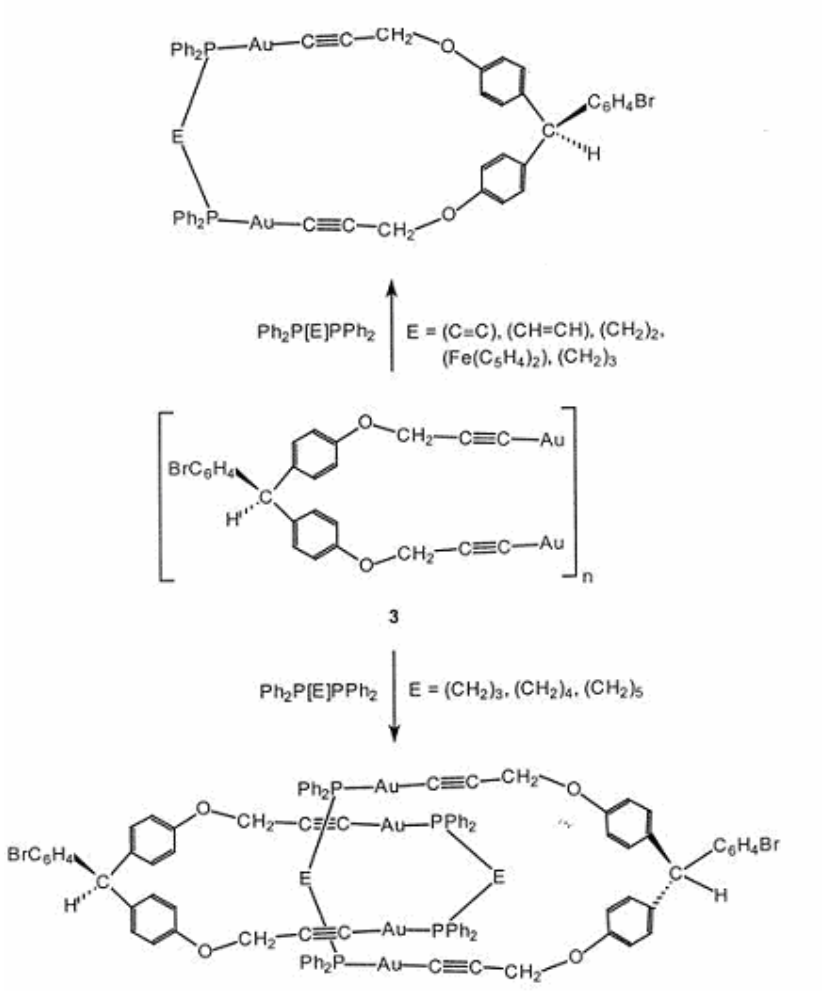

Figure 1.24: Formation of either a ring or a catenane containing gold centres in a linear arrangement (E = spacer).[58]

In later work done in the same group,[59] luminescence spectra were recorded for similar compounds where the chelating phosphines were the same as before and the alkyl spacer was varied. In the solid state two rings associate to form a pair and the Au…Au interactions can be clearly seen between the two rings in the pair, shown in figure 1.25. When the phosphine is shorter as in the case of dppm and dppe there is a short distance between the two gold centres of the same ring. This eliminates the need for pairing of rings since stabilisation due to Au…Au interactions is achieved in one ring. All

of the series of these compounds displayed luminescence, due to either Au…Au interactions in the same ring, or in a pair of rings, thus providing evidence that luminescence occurs as a result of these interactions.

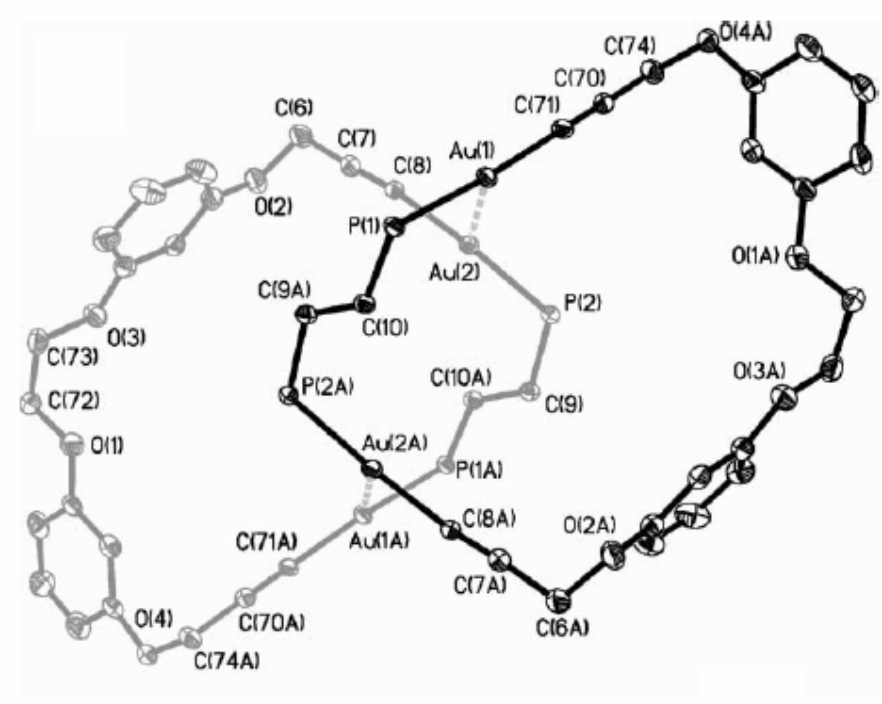

Figure 1.25: Crystal structure showing the presence of Au…Au interactions between the two rings.[59]

As with platinum(II) complexes, gold(I) complexes can potentially also have applications as molecular sensors. Yam's group has recently synthesised a series of gold(I) complexes functionalised with crown ethers. These molecules have been shown to exhibit a change in luminescence properties when binding of a metal cation occurs at the crown ether site. The complexes alone have been shown by X-ray crystallography (figure 1.26) to have the crown ether groups far apart. Therefore the gold centres are also far apart, far enough that there are no Au…Au interactions present. On binding of the metal cation, the crown ether groups come together to form a sandwich with the metal cation in the centre, thus bringing the two gold centres close enough together so that they can interact and therefore change the luminescence of the complex.[60]

Both gold(I) and platinum(II) alkynyl complexes have been shown to exhibit interesting luminescent properties, and these in combination with the structural properties of terpyridine complexes should, in theory, make for some potentially interesting supramolecular structures.

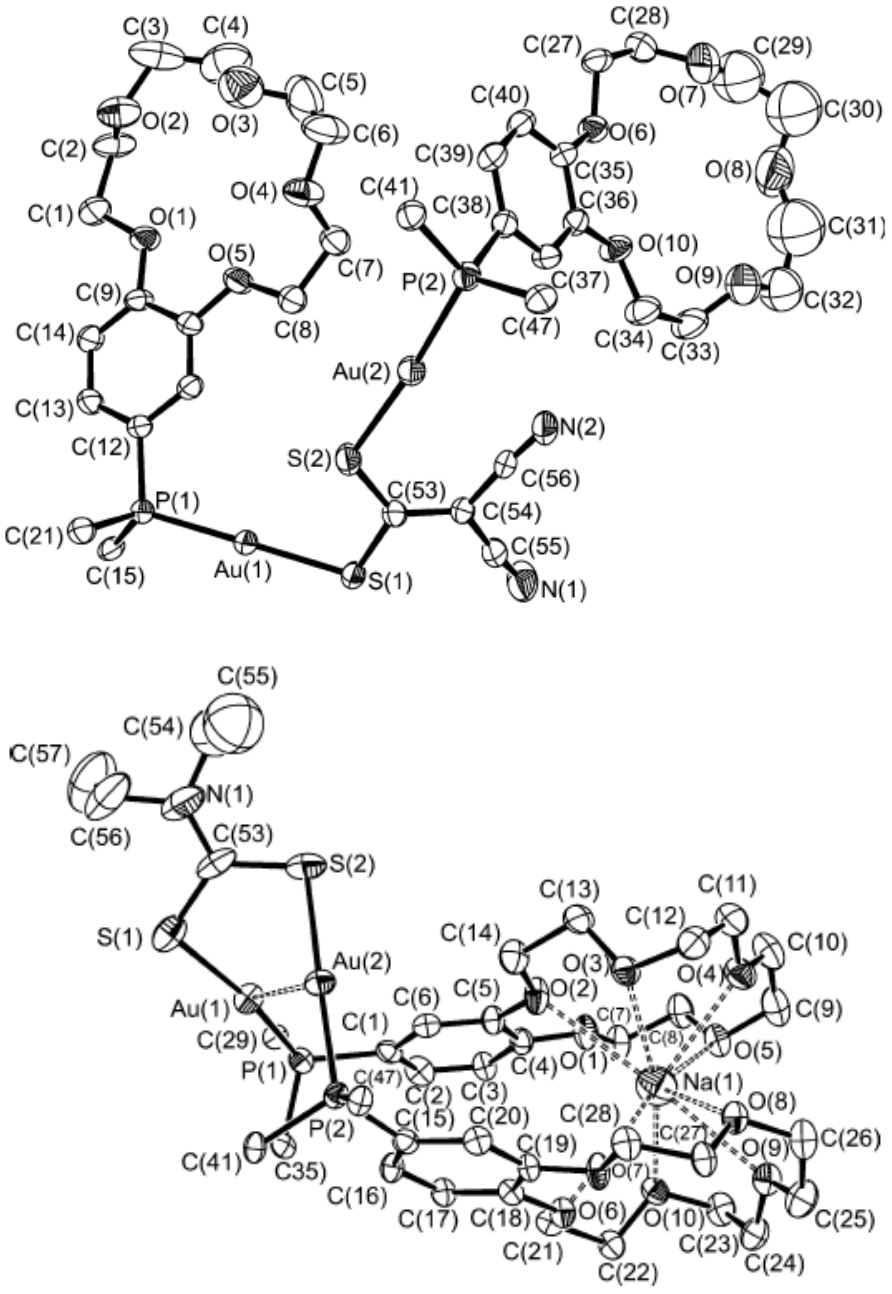

Figure 1.26: Two different examples of gold-containing molecular sensors; above [Au_2(μ-1,1-dicyanoethylene-2,2-dithiolate)Ph_2P-benzo-15-crown-5)$_2$] without a bound metal cation, and below, [{Au_2(μ-diethyldithiocarbamate)(Ph_2P- benzo-15-crown-5)$_2$}.Na](PF_6)$_2$ showing the bound sodium cation and the presence of Au…Au interactions.[60]

1.8 Aims

The aim of this thesis is the synthesis of 4'-substituted-2,2':6',2''-terpyridine ligands, all containing a terminal alkyne functionality. Coupling of these ligands at the alkyne site with platinum(II) and gold(I) is envisaged and the spectroscopic and structural properties of the resulting complexes will be investigated. The suitability of these complexes for the assembly of macrocycles or coordination polymers via further complexation at the terpyridine moiety will also be investigated.

1.9 References

[1] J.-M. Lehn, *Science*, 1993, **260**, 1762.

[2] J.-M. Lehn, *Proc. Natl. Acad. Sci. U.S.A.*, 2002, **99**, 4763.

[3] I. Dance, *New J. Chem*., 2003, **27**, 1.

[4] http://www.nano.gov/html/facts/whatIsNano.html

[5] C. A. Schalley, A. Lützen and M. Albrecht, *Chem. Eur. J.*, 2004, **10**, 1072.

[6] D. Philp and J. F. Stoddart, *Angew. Chem., Int. Ed*. *Engl.*, 1996, **35**, 1154.

[7] E. C. Constable, *Chem. Ind*., 1994, 56.

[8] E. C. Constable, *Pure Appl. Chem*., 1996, **68**, 253.

[9] H. Hofmeier and U. S. Schubert, *Chem. Soc. Rev*., 2004, **33**, 373.

[10] V. W.-W. Yam, *Acc. Chem. Res*., 2002, **35**, 555.

[11] P. H. Dinolfo and J. T. Hupp, *Chem. Mater*., 2001, **13**, 3113.

[12] G. T. Morgan and F. H. Burstall, *J. Chem. Soc. Abstr*., 1932, 20.

[13] A. M. W. Cargill-Thompson, *Coord. Chem. Rev*., 1997, **160**, 1.

[14] F. Kröhnke, *Synthesis*, 1976, 1.

[15] E.C. Constable and M. D. Ward, *J. Chem. Soc., Dalton Trans*. 1990, 1405.

[16] D. Armspach, E. C. Constable, C. E. Housecroft, M. Neuburger and M. Zehnder, *J. Organomet. Chem*., 1998, **550**, 193.

[17] D. Armspach, E. C. Constable, F. Diederich, C. E. Housecroft and J.- F. Nierengarten, *Chem. Eur. J*., 1998, **4**, 723.

[18] E. C. Constable, C. E. Housecroft, M. Neuburger, S. Schaffner and E. J. Shardlow, *CrystEngComm*, 2005, **7**, 599.

[19] H. S. Chow, E. C. Constable, C. E. Housecroft, M. Neuburger and S. Schaffner, *Dalton Trans*., 2006, 2881.

[20] E. C. Constable, C. E. Housecroft, M. Neuburger, S. Schaffner and L. J. Scherer, *Dalton Trans*., 2004, 2635.

[21] D. R. Blasini, S. Flores-Torres, D.-M. Smilgies and H. D. Abruña, *Langmuir*, 2006, **22**, 2082.

[22] V. Grosshenny and R. Ziessel, *J. Organomet. Chem*., 1993, **453**, C19.

[23] E. C. Constable, C. E. Housecroft, M. Neuburger, S. Schaffner and E. J. Shardlow, *Inorg. Chim. Acta*., 2007, in press.

[24] E. C. Constable, C. P. Hart and C. E. Housecroft, *Appl. Organomet. Chem.*, 2003, **17**, 383

[25] D. Armspach, E. C. Constable, C. E. Housecroft, M. Neuburger and M. Zehnder, *Supramol. Chem.*, 1996, **7**, 97.

[26] E. C. Constable, C. E. Housecroft and L. A. Johnston, *Inorg. Chem. Commun*., 1998, **1**, 68.

[27] E. C. Constable, C. E. Housecroft, M. Neuburger, S. Schaffner and E. J. Shardlow, *Dalton Trans*., 2005, **2**, 234.

[28] J. E. Beves, E. C. Constable, C. E. Housecroft, M. Neuburger, S. Schaffner and E. J. Shardlow, *Dalton Trans.*, 2007, in press.

[29] C. E. Housecroft and A. G. Sharpe, *Inorganic Chemistry 1st Ed*., 2001, Pearson, Harlow.

[30] E. C. Constable, G. Baum, E. Bill, R. Dyson, R. van Eldik, D. Fenske, S. Kaderli, D. Morris, A. Neubrand, M. Neuburger, D. R. Smith, K. Wieghardt, M. Zehnder and A. Zuberbühler, *Chem. Eur. J.,* 1999, **5**, 497.

[31] B. G. Lohmeijer and U. S. Schubert, *J. Polym. Sci. Part A. Polym. Chem.*, 2003, **41**, 1413.

[32] J. S. Choi, C. W. Kang, K. Jung, J. W. Yang, Y.-G. Kim and H. Han, *J. Am. Chem. Soc.*, 2004, **126**, 8606.

[33] E. C. Constable and M. W. C. Thompson, *New J. Chem*., 1992, **16**, 855.

[34] M. Beley, J. P. Collin, R. Louis, B. Metz and J. P. Sauvage, *J. Am. Chem. Soc.*, 1991, **113**, 8521.

[35] D. L. Greene and D. M. P. Mingos, *Transition Met. Chem*., 1991, **16**, 71.

[36] R. Ziessel, *Synthesis*, 1999, **11**, 1839.

[37] H. S. Chow, E. C. Constable, C. E. Housecroft and M. Neuburger, Dalton Trans. 2003, 4568.

[38] E. C. Constable, C. E. Housecroft and C. B. Smith, *Inorg. Chem. Commun*., 2003, **6**, 1011.

[39] R. A. Bell, M. H. Chisholm, D. A. Couch and L. A. Rankel, *Inorg. Chem*., 1977, **16**, 677.

[40] A. Sebald, C. Stader, B. Wrackmeyer and W. Bensch, *J. Organomet. Chem*., 1986, **311**, 233.

[41] R. J. Cross and M. F. Davidson, *J. Chem. Soc. Dalton Trans*., 1986, 1987.

[42] K. Sonogashira, T. Yatake, Y. Tohda, S. Takahashi and N. Hagihara, *J. Chem. Soc. Chem. Commun*., 1977, 291.

[43] M. I. Bruce, K. Costuas, J.-F. Halet, B. C. Hall, P. J. Low, B. K. Nicholson, B. W. Skelton and A. H. White, *J. Chem. Soc., Dalton Trans*., 2002, 383.

[44] U. Belluco, R. Bertani, R. A. Michelin and M. Mozzon, *J. Organomet. Chem*., 2000, **600**, 37.

[45] K. Sonogashira, S. Takahashi and N. Hagihara, *Macromolecules*, 1977, **10**, 879.

[46] S. Takahashi, M. Kariya, T. Yakate, K. Sonogashira and N. Hagihara, *Macromolecules*, 1978, **11**, 1063.

[47] V. W.-W. Yam and K. M.-C. Wong, *Top. Curr. Chem*., 2005, **257**, 1.

[48] V. W.-W. Yam, K. M.-C. Wong and N. Zhu, *J. Am. Chem. Soc.*, 2002, **124**, 6506.

[49] V. W.-W. Yam, *C. R. Chimie*, 2005, **8**, 1194.

[50] Y. K. Kryschenko, S. R. Seidel, A. M. Arif and P. J. Stang, *J. Am. Chem. Soc.*, 2003, **125**, 5193.

[51] J. A. Whiteford, P. J. Stang and S. J. Huang, *Inorg. Chem*., 1998, **37**, 5595.

[52] M. Hissler and R. Ziessel, *J. Chem. Soc., Dalton Trans*., 1995, 893.

[53] A. Harriman, M. Hissler, R. Ziessel, A. de Cian and J. Fisher, *J. Chem. Soc., Dalton Trans.*, 1995, 4067.

[54] M. I. Bruce, M. Jevric, B. W. Skelton, M. E. Smith, A. H. White and N. Zaitseva, *J. Organomet. Chem.*, 2006, **691**, 361.

[55] R. J. Puddephatt, *Coord. Chem. Rev*., 2001, **216-217**, 313.

[56]C. King, J. C. Wang, M. N. I. Kham and J. P.Fackler Jr., *Inorg. Chem*., 1989, **28**, 2145.

[57] M. Bardají, A. Laguna, J. Vicente and P. G. Jones, *Inorg. Chem*., 2001, **40**, 2675.

[58] C. P. McArdle, S. Van, M. C. Jennings and R. J. Puddephatt, *J. Am. Chem. Soc.*, 2002, **124**, 3959.

[59] W. J. Hunks, J. Lapierre, H. A. Jenkins and R. J. Puddephatt, *J. Chem. Soc., Dalton Trans.*, 2002, 2885.

[60] C.-K. Li, E. C.-C. Cheng, N. Zhu and V. W.-W. Yam, *Inorg. Chim. Acta*, 2005, **358**, 4191.

Chapter 2 2,2':6',2"-Terpyridine Ligands

2.1 2,2':6',2"-Terpyridine Ligands

4'-Substituted 2,2':6',2"-terpyridine ligands are well known in the literature[1] as building blocks for supramolecular self assembly. The use of an alkyne-functionalised tpy ligand is particularly useful in this type of self assembly since it can be reacted with other species, giving further opportunity for functionalisation, for example, addition of a carbaborane[2] or a cobalt cluster.[3] The alkyne functional group can also be reacted with a platinum(II) or gold(I) centre to form homoditopic ligands, leaving the tpy moiety free for coordination.

This chapter describes the synthesis and characterisation of several alkyne-functionalised tpy ligands. These are grouped into two types: the first being ligands having a flexible alkyl spacer between the tpy moiety and the alkyne, and being prepared from 4'-hydroxy-2,2':6',2"-terpyridine, and the second type being ligands with a rigid C_6H_4-spacer and synthesised from 4'-(n-bromophenyl)-2,2':6'2"-terpyridine. The rigid ligands have a predetermined angle built into them, achieved by the choice of placing the alkyne in either the meta or para positions. Figure 2.1 shows the different terpyridine ligands discussed in this chapter and the nomenclature used for describing them.

Syntheses were based on literature methods reported for 4'-(2-propyn-1-oxy)-2,2':6',2"-terpyridine[2] and 4'-(4-ethynylphenyl)-2,2':6',2"-terpyridine.[3]

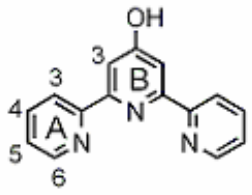

4'-Hydroxy-2,2':6',2"-terpyridine
HO-tpy

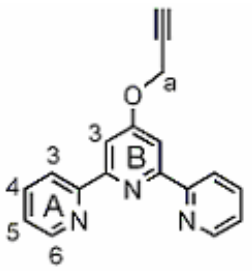

4'-(2-Propyn-1-oxy)-2,2':6',2"-terpyridine
1

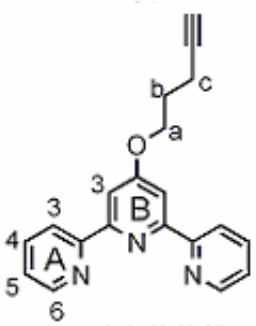

4'-(4-Pentyn-1-oxy)-2,2':6',2"-terpyridine
2

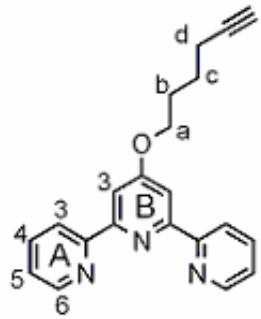

4'-(5-Hexyn-1-oxy)-2,2',6',2"-terpyridine
3

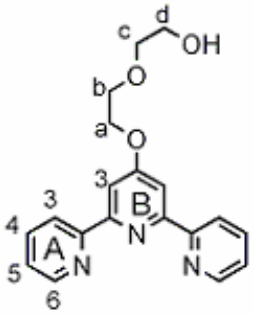

4'-[2-(2-Hydroxyethoxy)ethoxy]
-2,2':6',2"-terpyridine
4

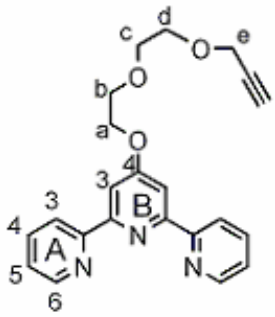

4'-(4,7,10-trioxa-10-dec-1-ynyl)-2,2':6',2"-terpyridine
5

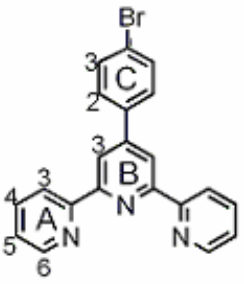

4'-(4-Bromophenyl)-2,2':6',2"-
terpyridine
6

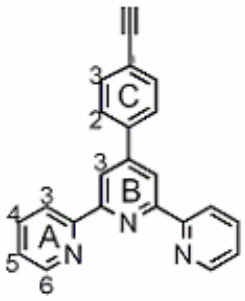

4'-(4-Ethynylphenyl)-2,2':6',2"-
terpyridine
7

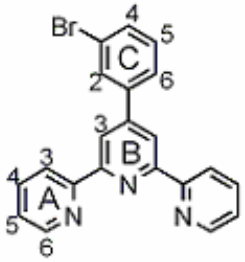

4'-(3-Bromophenyl)-2,2':6',2"-
terpyridine
8

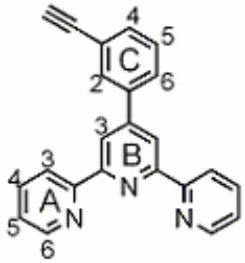

4'-(3-Ethynylphenyl)-2,2':6',2"-
terpyridine
9

4'-(3,5-Dibromophenyl)-2,2':6',2"-terpyridine
10

4'-(3,5-Diethynylphenyl)-2,2':6',2"-terpyridine
11

Figure 2.1: Numbering scheme for tpy ligands synthesised. Ligands **1**[2], **4**[4], **6**[5,6], **7**[3], **8**[7] and **10**[8] as well as **HO-tpy**[9] were prepared according to literature methods.

2.2 Synthesis of 4'-Hydroxy-2,2':6',2"-Terpyridine Derivatives

The ligand 4'-hydroxy-2,2':6',2"-terpyridine is a useful starting material for the synthesis of 4'-substituted terpyridine ligands. The synthesis of this starting material was reported in 1990 by Constable and Ward[9] and starts with the formation of a triketone by a double Claisen condensation reaction between two equivalents of ethyl 2-pyridine carboxylate and one of acetone.[10] The triketone is then reacted with ammonium acetate to close up the middle ring and form 2,6-bis(2'-pyridyl)-4-pyridone. The tautomer **HO-tpy** can be purified by recrystallisation from ethanol. The reaction scheme can be seen in figure 2.2.

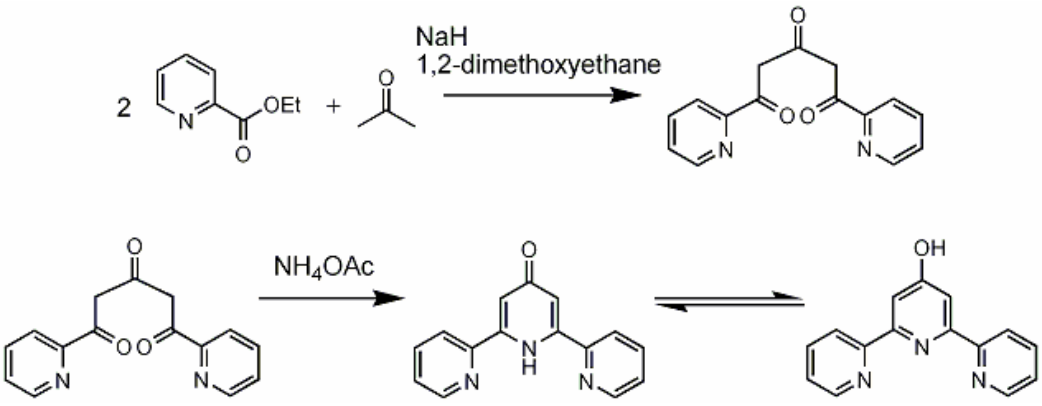

Figure 2.2: Formation of **HO-tpy** from two equivalents of ethyl 2-pyridine carboxylate and acetone.

Reactions of **HO-tpy** can produce different functionalised terpyridines as shown in figure 2.1. By using a base to deprotonate the hydroxy group, the resulting nucleophile can then be reacted with other species containing a good leaving group such as an alkyl halide. By choosing an alkyl halide with a terminal alkyne, this method can be used to generate a ligand which can go on to react with platinum(II) or gold(I) at a later stage.

This method (figure 2.3) is based on the reported synthesis of ligand **1**[2] where the use of propargyl bromide attaches a short alkyl spacer to the oxygen atom of the **HO-tpy** as well as providing the terminal alkyne functionality.

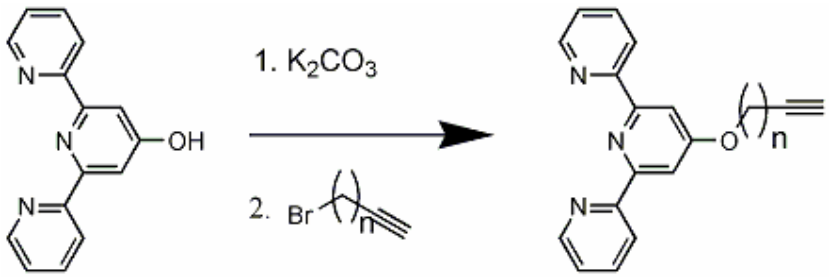

Figure 2.3: Synthesis of ligands **1**, **2** and **3** (n = 1, 3 and 4 respectively).

First of all, **HO-tpy** is suspended in acetonitrile and is deprotonated at room temperature using potassium carbonate as the base. After an hour, the halogenated compound is added and the reaction is stirred for 24 hours at 60 °C. During this time, a nucleophilic substitution reaction occurs in which the deprotonated **HO-tpy** attacks at the halogenated position of the alkyne compound. The bromide is a good leaving group and is eliminated as the C-O bond forms. The reaction mixture is then poured into water. This precipitates the product out of solution, as well as dissolving the excess base. Finally, the product is isolated by filtration as an off-white solid. Purification can be achieved by recrystallisation from hot ethanol. This method has proved successful for ligands **1**, **2** and **3** where n = 1, 3 and 4 respectively. Several attempts were made to synthesise the n = 2 ligand in the same way but to no avail.

This reaction worked well, giving a yield of the alkyne-substituted ligand of between 29 % and 66 %. The products were recrystallised from hot ethanol in the first instance. This usually produced large crystals which, in the case of **3** were suitable for X-ray crystallography. In the cases of **1** and **2**, X-ray quality crystals were obtained from a layered solution of CH_2Cl_2 and hexane. A search of the Cambridge database revealed that the X-ray crystal structure of ligand **1** had not previously been published, and so the structure was determined. In the case of **3**, both solvent systems produced suitable X-ray quality crystals. It was found that these were two different polymorphs, neither containing any solvent molecules.[11] Crystal structures of these ligands are discussed later in the chapter.

The known ligand **4**, was synthesised according to the literature method.[4] Once again, **HO-tpy** was used as the starting material for this synthesis and was deprotonated in the same way described above using potassium carbonate as the base in conjunction with potassium iodide. These reactants were stirred in DMF for half an hour at 70 ˚C before 2-(2-chloroethoxy)ethanol was added. As before, a nucleophilic substitution reaction occurs where the deprotonated **HO-tpy** acts as the nucleophile and the chloride is the leaving group. After removal of the solvent, the residue is suspended in CH_2Cl_2 and washed with NaOH followed by $NaHCO_3$ and finally water. After drying of the organic layer and removal of the solvent, the product is isolated as an oil which solidifies on standing.

Ligand **4** is then dissolved in acetonitrile. A stronger base than in the previous examples, in this case KOH, was used to remove the proton from the terminal OH group. After an hour, propargyl bromide was added and the reaction was stirred at 60 ˚C for 24 hours. Again the deprotonated hydroxyl group on the end of the spacer acts as a nucleophile in a substitution reaction with the propargyl bromide, the bromide acting as the leaving group. As before, the reaction mixture was poured into water, although this time since no precipitate formed, the product was extracted from solution with CH_2Cl_2. Finally the solvent was removed from the organic layer after drying over magnesium sulfate. Ligand **5** was isolated as a brown oil which later solidified

giving a good yield of around 50 %. Figure 2.4 shows the synthesis of ligand **4**, followed by reaction to form ligand **5** as the final product.

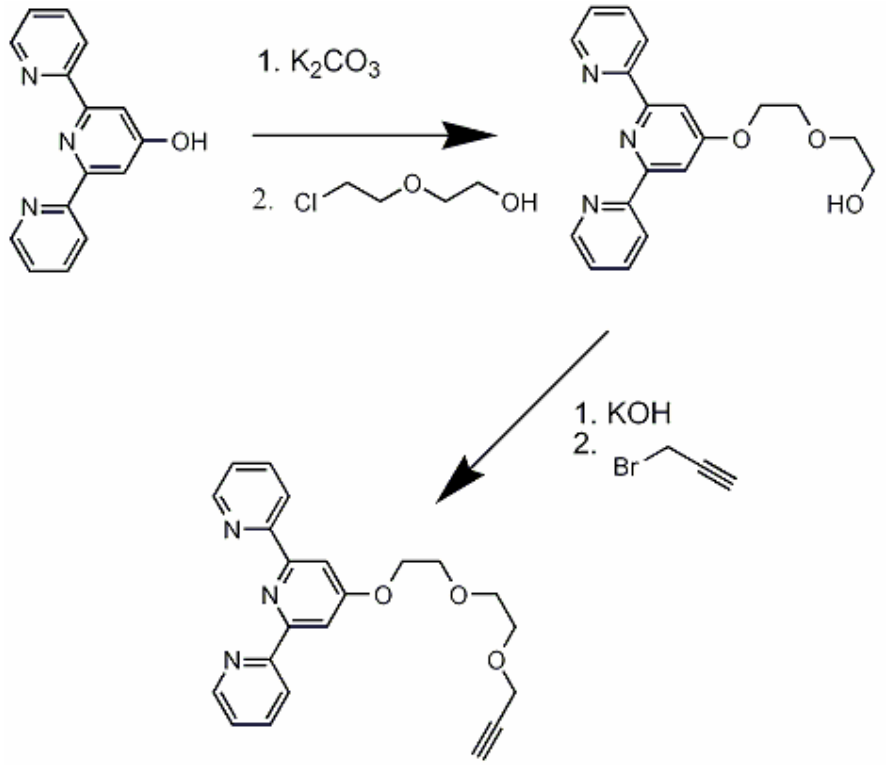

Figure 2.4: Synthesis of ligand **4** followed by reaction to form **5**.

X-ray quality crystals of this ligand were obtained from a $CDCl_3$ solution and the structure is discussed later in the chapter.

2.3 Characterisation

2.3.1 ^{1}H NMR Spectroscopy.

All the above ligands were characterised by ^{1}H NMR spectroscopy in a $CDCl_3$ solution. The protons in the aromatic region of the spectra all correspond to signals from known terpyridine ligands as is expected. The aliphatic region differs between ligands with the varying numbers of CH_2 groups. The signal which corresponds to the terminal alkyne function is clearly distinguishable due to the presence of coupling between the alkyne proton

and the CH_2 group nearest to it. Chemical shifts were assigned using COSY and NOESY experiments.

	A3	A4	A5	A6	B3	a	b	c	d	e	C≡C*H*
1	8.67	7.91	7.39	8.75	8.16	4.99					2.61
2	8.62	7.82	7.33	8.69	8.03	4.35	2.08	2.45			1.98
3	8.63	7.88	7.35	8.70	8.04	4.28	2.00	1.77	2.30		1.99
4	8.57	7.82	7.31	8.66	8.07	4.41	3.91	3.66	3.76		
5	8.59	7.84	7.32	8.68	8.03	4.40	3.89	3.73	3.78	4.21	2.44

Table 2.1: Table of ^{1}H NMR data for ligands **1**-**5**. Chemical shifts are shown in δ/ppm. The signal for the OH proton in **4** was not observed. See fig. 2.1 for atom labelling.

Table 2.1 shows the different chemical shifts for the protons in each of the 5 ligands synthesised. Shifts of **1** and **4** compare well with those cited in the literature.[2,4] All the signals for the terpyridine protons are comparable with each other, only showing slight differences from one ligand to another. In each of the ligands, proton a is always shifted the most down field due to its close proximity to the electronegative oxygen atom directly bound to the terpyridine unit.

In the aliphatic region of the spectra the assignment of peaks is not so straightforward. The order in which the peaks can be seen varies according to the length of the alkyl spacer. The proton coupled to the alkyne proton (c in ligand **2**, d in ligand **3**) is always the next highest field after a, and after that come b, c and the alkyne proton, with the chemical shifts being similar in the different ligands.

Figure 2.5 shows the ^{1}H NMR spectrum of **3**. This is typical of this series of ligands. The terpyridine peaks can be seen in the aromatic region and it is possible to see the downfield shift of a, due to its proximity to the terpyridine oxygen atom.

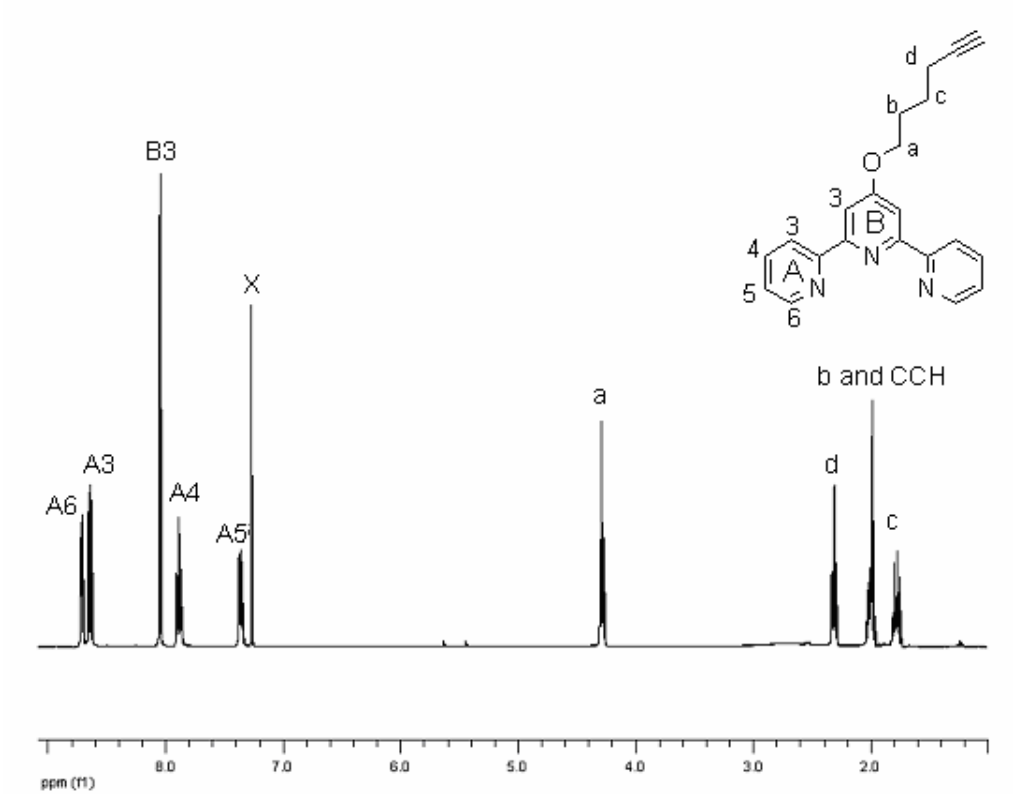

Figure 2.5: Representative 500 MHz ^{1}H NMR spectrum of ligand **3** in $CDCl_3$ (marked X).

The expansion of the aliphatic region of the spectrum is shown in figure 2.6. It is quite clear from looking at the coupling constants which signal is d, since this signal appears as a triplet of doublets. The largest coupling constant (J = 7.2 Hz) is similar in size to that seen in b and c, and arises due to coupling with the adjacent CH_2 group. The other smaller coupling constant (J = 2.4 Hz) corresponds to coupling between d and the alkyne proton. The coupling constant is small because coupling occurs between protons which are not attached to neighbouring carbons. This type of coupling pattern can be seen for all the flexible ligands in this series and is a useful diagnostic tool for the presence of the alkyne functionality. Signals for protons b and c can also be seen in figure 2.6. These signals are both quintuplets arising from coupling to 4 protons in approximately equal environments. In the case of b, the signal for the alkyne proton is superimposed on top, and the two signals therefore appear together.

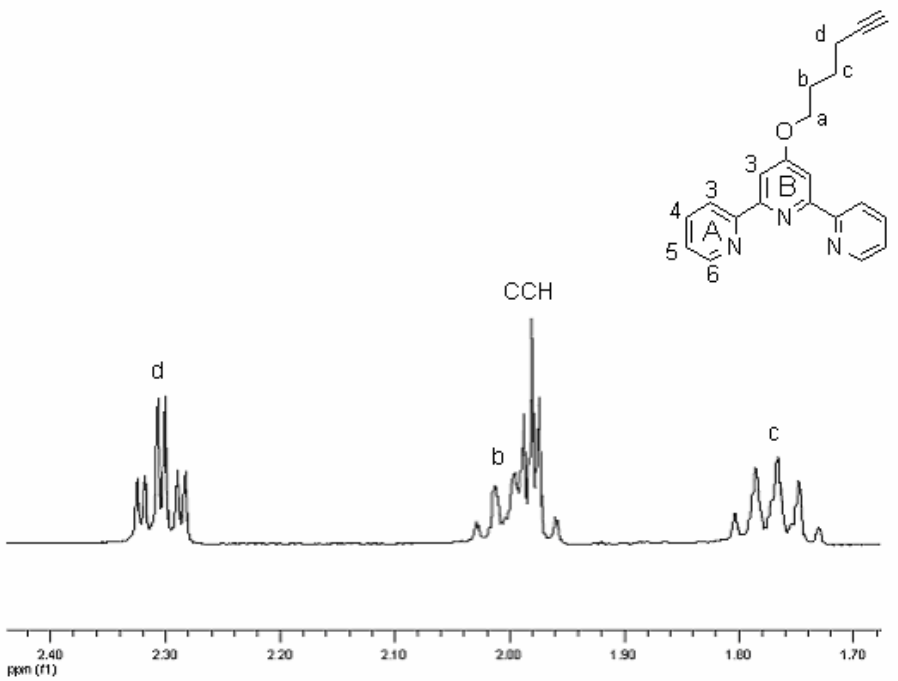

Figure 2.6: Expansion of the aliphatic region of the 500 MHz ^{1}H NMR spectrum of **3** in $CDCl_3$ showing clearly the small coupling between d and the alkyne proton.

The NMR spectrum of ligand **5** is shown in figure 2.7. Due to the nature of the spacer it was more difficult to assign the signals. Proton a could be easily assigned due to the fact that it appeared as a triplet as well as being the most downfield shifted. Proton e was also easy to assign based on the coupling to the alkyne proton as described for ligands **1**, **2**, and **3**.

Information from COSY NMR experiments made it possible to assign proton b since cross peaks could be seen to proton a. Likewise, c and d showed small cross peaks between them. These assignments are shown in figure 2.8.

It was not possible to assign c and d from the COSY alone so NOESY experiments were crucial in determining which peak was c and which was d. A very weak cross peak could be observed between b and c due to their proximity to each other and it was therefore possible to assign c and d based on this. An expansion of the region of the NOESY spectrum in question is shown in figure 2.9.

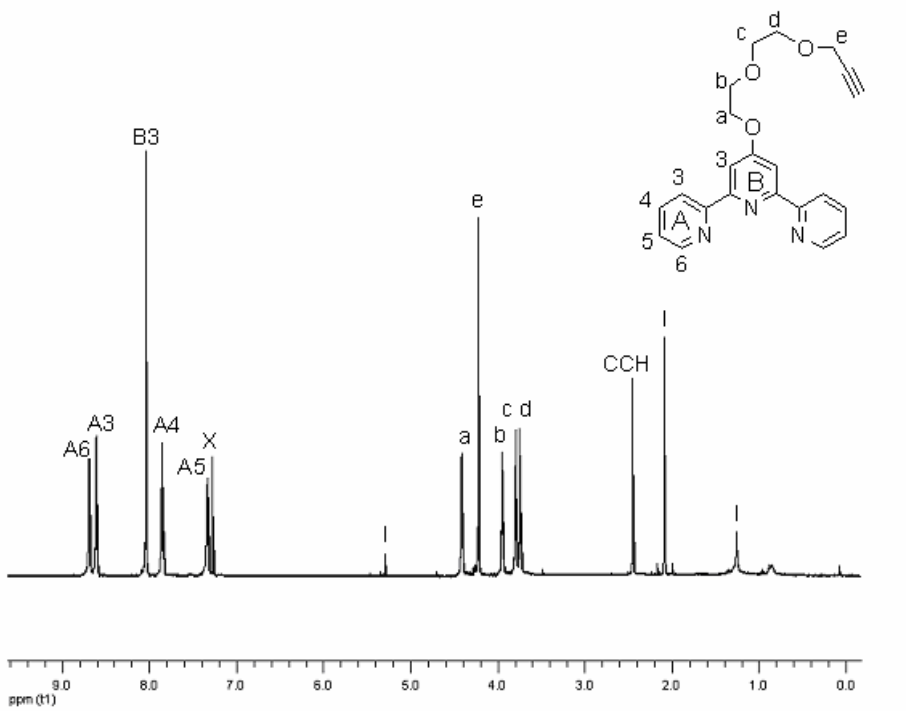

Figure 2.7: 500 MHz ^{1}H NMR spectrum of ligand **5** in $CDCl_3$. Protons c and d have very similar chemical shifts. X = residual $CHCl_3$, I = impurities.

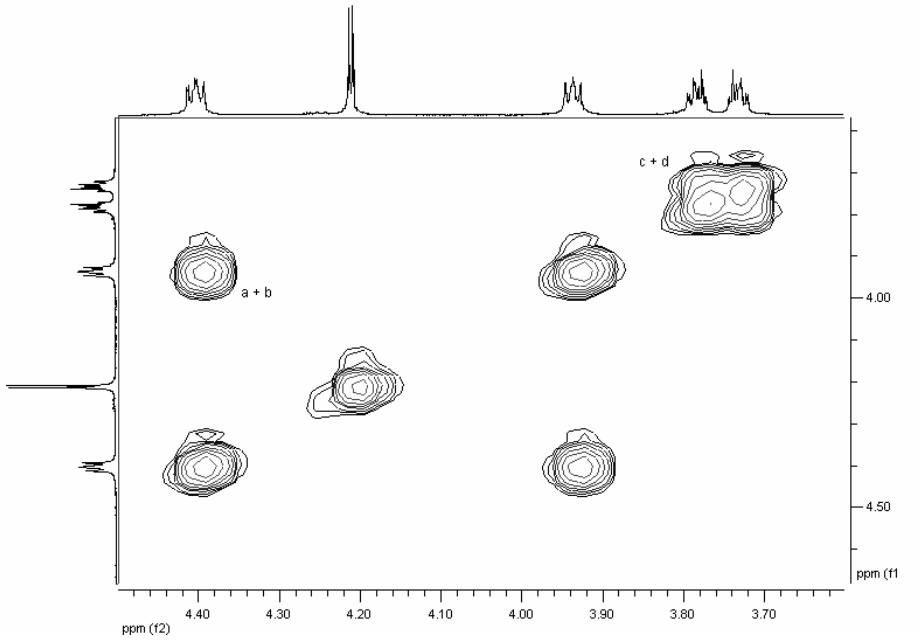

Figure 2.8: Expansion of the aliphatic region of the 500 MHz COSY spectrum of **5** in $CDCl_3$. Cross peaks between a and b can be clearly seen, cross peaks between c and d appear together.

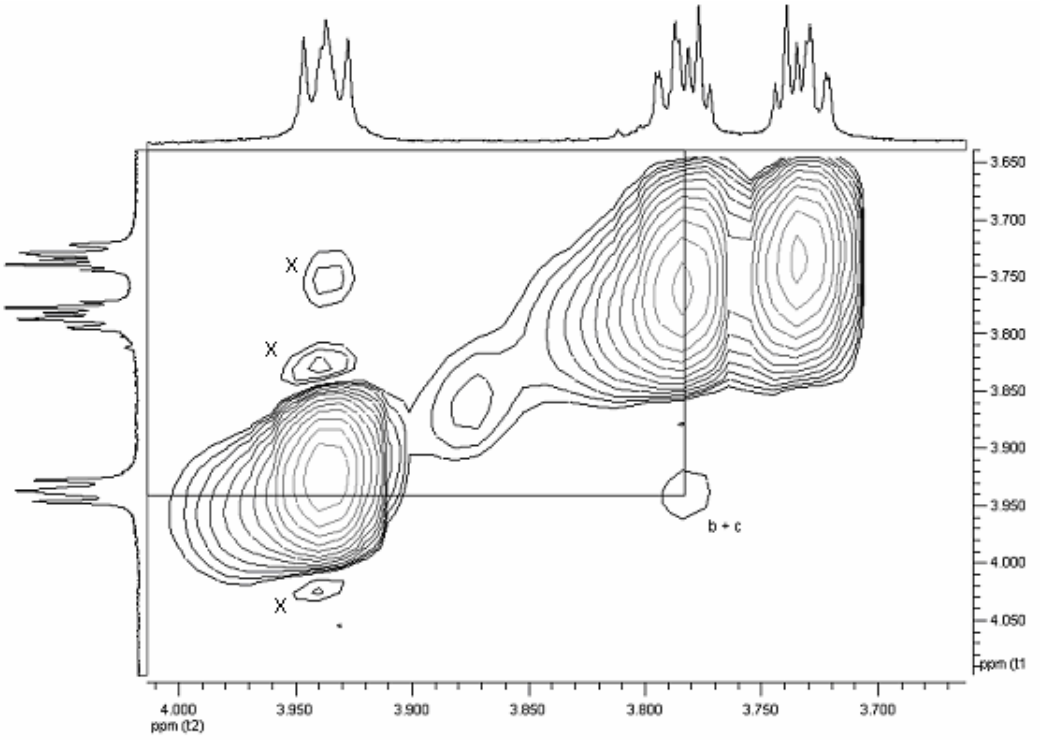

Figure 2.9: Expansion of the 500 MHz NOESY spectrum of ligand **5** in $CDCl_3$. The cross peak is very weak but shows the link between b and c. Signals marked X are due to breakthrough or noise.

2.3.2 ^{13}C NMR spectroscopy

Ligands were also characterised using ^{13}C NMR spectroscopy. All experiments were run with proton decoupling. This means that all signals appear as singlets since coupling to neighbouring protons is removed. Carbons were assigned using HMQC (Heteronuclear Multiple Quantum Coherence) and HMBC (Heteronuclear Multiple Bond Coherence) experiments and a table of data is shown in table 2.2. HMQC shows coupling between a proton and a directly bound carbon or other heteroatom, whereas HMBC shows longer range coupling between ^{1}H and ^{13}C, over a range of between 2 and 4 bonds.

	A2	A3	A4	A5	A6	B2	B3	B4
1	157.3/ 155.9	121.4	136.8	123.9	149.1	157.3/ 155.9	107.6	165.9

2	157.4/ 156.4	121.8	137.4	124.3	149.3	157.4/ 156.4	107.9	167.6
3	157.0/ 156.0	121.4	136.9	123.9	149.0	157.0/ 156.0	107.4	167.4
4	156.9/ 155.9	121.3	136.8	123.8	148.9	156.9/ 155.9	107.7	167.0
5	157.5/ 156.4	121.7	137.2	124.2	149.4	157.5/ 156.4	107.8	167.3

	a	b	c	d	e	*C*≡CH	C≡*C*H
1	55.9					77.6	76.3
2	66.8	28.4	15.5			83.6	69.5
3	67.6	28.0	68.8	18.1		84.0	68.8
4	67.9	69.9	72.8	61.7			
5	69.6	69.9	68.1	71.1	58.8	80.0	75.1

Table 2.2: Table of ^{13}C NMR spectroscopic data for ligands **1**-**5**. Chemical shifts are shown in δ/ppm.

There was difficulty in assigning peaks A2 and B2 despite the use of HMQC and HMBC techniques. Both these methods are 2D experiments and show cross peaks between ^{1}H and ^{13}C nuclei. Usually, once the ^{1}H spectrum has been assigned, HMQC can be used to assign the ^{13}C spectrum since cross peaks are seen between protons and the ^{13}C nuclei they are directly attached to.

Both A2 and B2 are quaternary carbons and have no protons directly attached to them, so the use of HMQC alone to assign the peaks was not possible. HMBC provides information on the carbons which are indirectly attached to protons, that is, neighbouring carbon atoms. Unfortunately this still could not provide enough information and peaks A2 and B2 still remain unambiguously unassigned. Figure 2.10 shows the ^{13}C spectrum of ligand **5**. Aliphatic and aromatic ^{13}C signals appear in a diagnostic region of the spectrum.

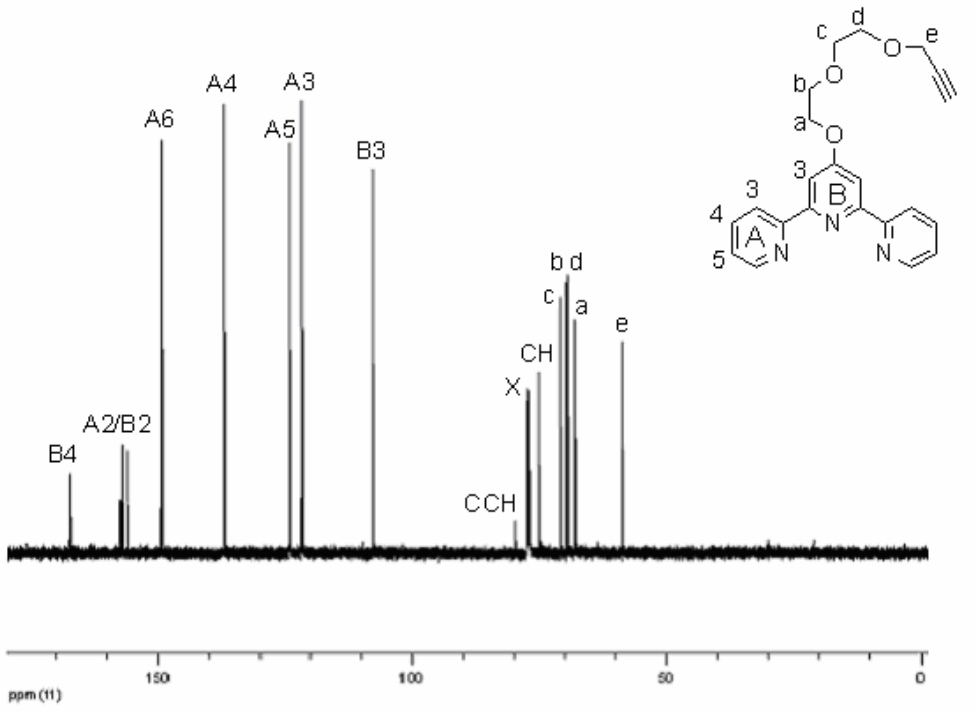

Figure 2.10: 125 MHz ^{13}C NMR spectrum of ligand **5** in $CDCl_3$ (X).

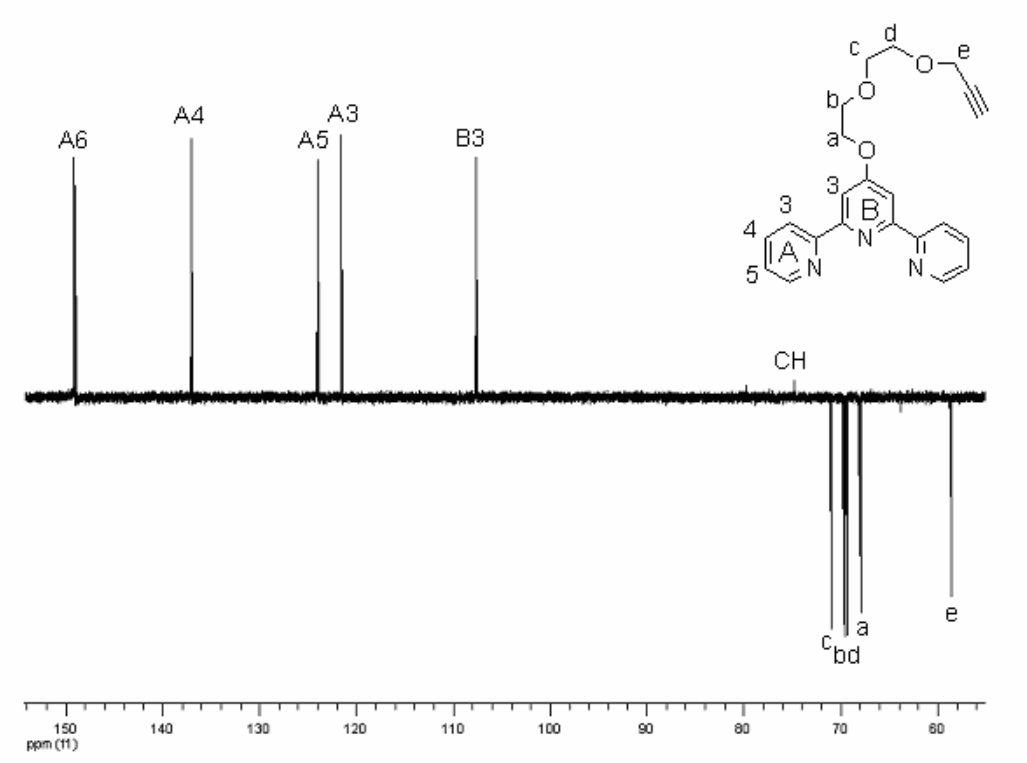

Figure 2.11: 125 MHz ^{13}C DEPT spectrum of **5** in $CDCl_3$.

Quaternary peaks can be identified by their relatively low intensity compared to other peaks, as well as DEPT (Distortionless Enhancement by Polarisation Transfer) experiments. In the DEPT spectrum, peaks assigned to CH_3 or CH groups appear pointing up, CH_2 peaks are inverted and quaternary carbon peaks do not appear at all. The DEPT spectrum of ligand **5** is shown in figure 2.11.

2.3.3 MALDI Mass Spectrometry

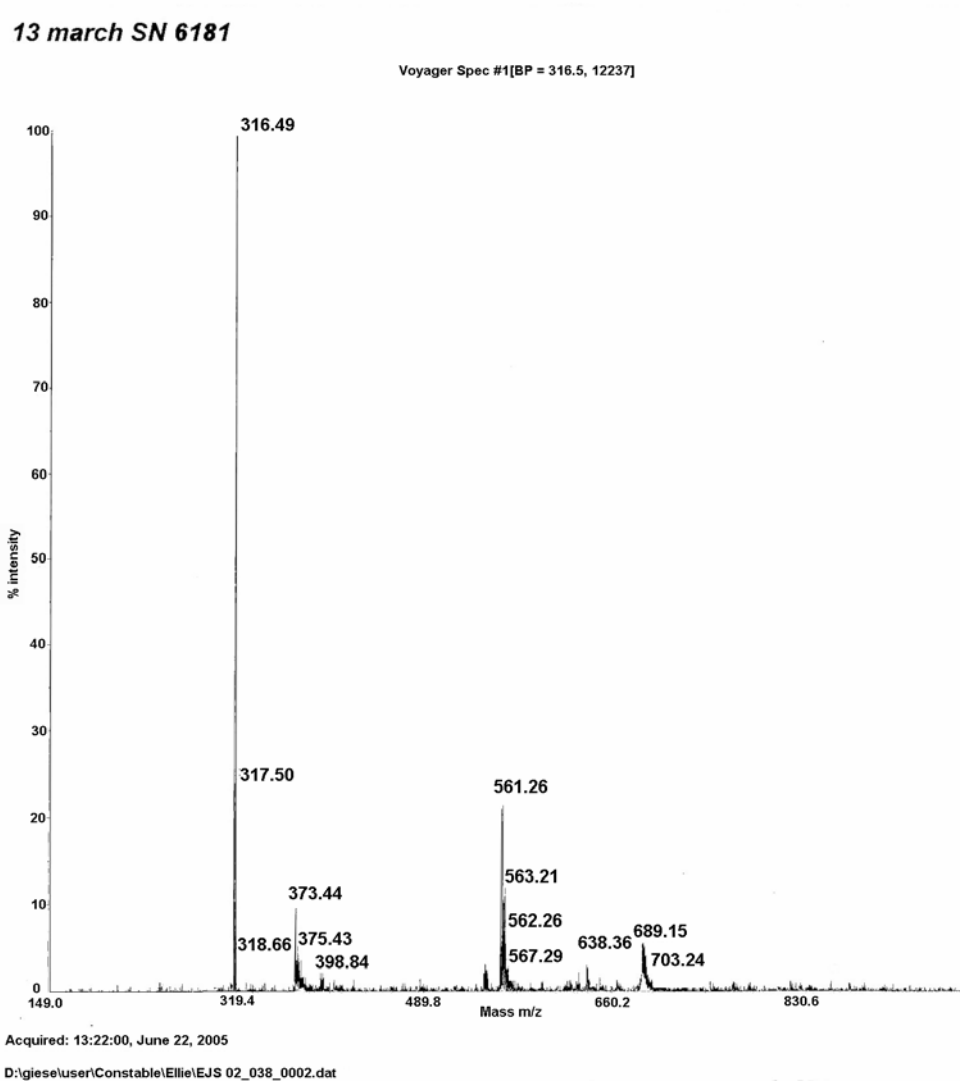

Figure 2.12: MALDI mass spectrum of ligand **2** showing M^+ = 316.49. The other peaks arise from 2(matrix), 3(matrix) and $[M + 2(matrix)]^+$ where the matrix is α-Cyano-4-hydroxycinnamic acid (Mw = 189.17).

MALDI mass spectroscopy, (or matrix assisted laser desorption/ionization) was a useful tool for confirmation of the molecular mass to charge ratio of the ligands. This is a technique in which a laser is used to ionise the molecules in question and the molecular weight of the fragments determines their velocities as they pass down the chamber to the detector. Molecular ions are generated by loss of an electron or addition of a proton, sodium or potassium ion.

In the MALDI mass spectrum of the ligands, peaks could often be seen for the molecular ion as well as sometimes the molecular ion plus sodium or potassium. Figure 2.12 shows the MALDI mass spectrum of ligand **2** which is typical. The base peak corresponds to the parent ion at m/z 316. The mass spectra of ligands **3** and **5** are similar and show the parent ion at m/z 330 and 377 respectively.

2.4 Synthesis of 4'-Phenyl-2,2':6',2"-Terpyridine Derivatives

A different method was used for the synthesis of the phenyl-substituted tpy ligands and this is shown in figure 2.13. Here the phenyl ring is directly connected to the terpyridine ligand with no bridging oxygen so **HO-tpy** was not used as the starting material for this synthesis. Instead, a solvent free method[5] was used to synthesise a bromo-substituted phenyl terpyridine using 3-bromo, 3,5-dibromo or 4-bromobenzaldehyde with 2-acetylpyridine. In this method the reactants are ground together with NaOH until a powder is formed from the liquid starting materials. After washing the powder with water the ring closure step is carried out by heating a mixture of the powder and ammonium acetate in acetic acid to reflux for 2 hours. The reaction mixture is finally poured into water to precipitate the product. The product is then recrystallised from hot ethanol.

Once these bromo-substituted ligands have been synthesised, the bromo functionality is converted to an alkyne. Ligands **6**, **8**, and **10** (figure 2.1)

were reacted with TMS-acetylene. Ligands **6** and **8** were converted to **7** and **9** (figure 2.1) respectively, although there were problems with the conversion of **10** into **11** and the synthesis of **11** using this method ultimately proved to be unsuccessful. Instead of obtaining a solid, off-white product as was the case for the mono-bromo compounds, a black solid (assumed to be polymeric) was obtained instead. This was completely insoluble in all solvents and remains uncharacterised.

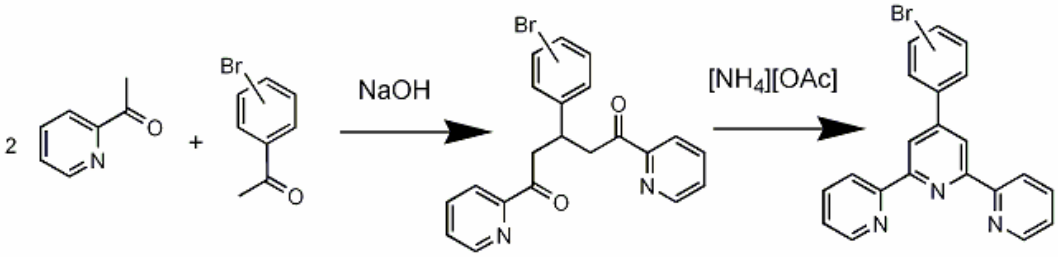

Figure 2.13: Synthesis of bromophenyl terpyridine ligands using a solvent free grinding method.[5]

The Sonogashira coupling[12,13] reactions were all catalysed by $[(Ph_3P)_2PdCl_2]$ in the presence of triphenylphosphine and copper(I) iodide. First of all the bromo compounds were stirred in triethylamine with the catalyst, phosphine and copper(I) iodide while the reaction mixture was heated to 60 ˚C and cooled back to 40 ˚C. The TMS-acetylene was added and the reaction mixture was stirred at 40 ˚C for 7 days in total. After removal of the solvent the crude product was purified by chromatography, and the product was isolated as an off-white solid.

The TMS protecting group was necessary in this synthesis to prevent the formation of polymers by the reaction at both ends of the acetylene. The protecting group was removed in the final step by dissolving the product in methanol and THF and stirring with K_2CO_3. After addition of water and CH_2Cl_2, the product was extracted into the CH_2Cl_2 layer, dried and (after removal of the solvent) isolated as an off-white solid. This method is reported in the literature for the formation of 4'-(4-ethynylphenyl)-2,2':6',2"-terpyridine[3] and the same method was employed for all these related ligands.

2.5 Characterisation

2.5.1 ^{1}H NMR Spectroscopy

The previously unknown ligand **9** was characterised by ^{1}H NMR spectroscopy. The chemical shifts of the known ligands **6**, **7** and **8** were also recorded experimentally and the data are shown for comparison in table 2.3. The NMR spectroscopic data recorded are in good agreement with those reported in the literature for ligands **6**[5,6] and **7**.[3] There were no reported NMR spectroscopic data in the literature for ligand **8**, so the data are reported here for the first time.

	A3	A4	A5	A6	B3	C2	C3	C4	C5	C6	C≡C*H*
6	8.70	7.93	7.41	8.76	8.74	7.75					
7	8.71	7.94	7.41	8.77	8.78	7.80					3.22
8	8.58	7.84	7.33	8.66	8.59	8.00		7.53/ 7.78	7.33	7.53/ 7.78	
9	8.67	8.04	7.54	8.77	8.68	8.08		7.75/ 7.94	7.55	7.75/ 7.94	4.34

Table 2.3: 500 MHz ^{1}H NMR chemical shifts (δ/ppm) for phenyl-tpy based ligands, in $CDCl_3$ for **6**-**8**, DMSO-d_6 for **9**.

Due to the poor solubility of these ligands, it was necessary to run the NMR spectrum for ligand **9** in DMSO rather than $CDCl_3$ in order to obtain well resolved spectra. Chemical shifts were assigned using COSY and NOESY techniques. Unfortunately there was still not enough information to assign protons C4 and C6.

Comparing the chemical shifts of **6** and **7** shows there is little difference in chemical shifts on going from the bromo to the alkyne compound. The larger difference in the chemical shifts of **8** and **9** is probably due to the effect of changing NMR solvent. It was not possible to purify ligand **9** due to its poor solubility and some small impurities can still be seen in the NMR spectrum shown in figure 2.14. It is also possible to see in this spectrum

how peaks C5 and A5 overlap. COSY NMR was very important in distinguishing between these two signals.

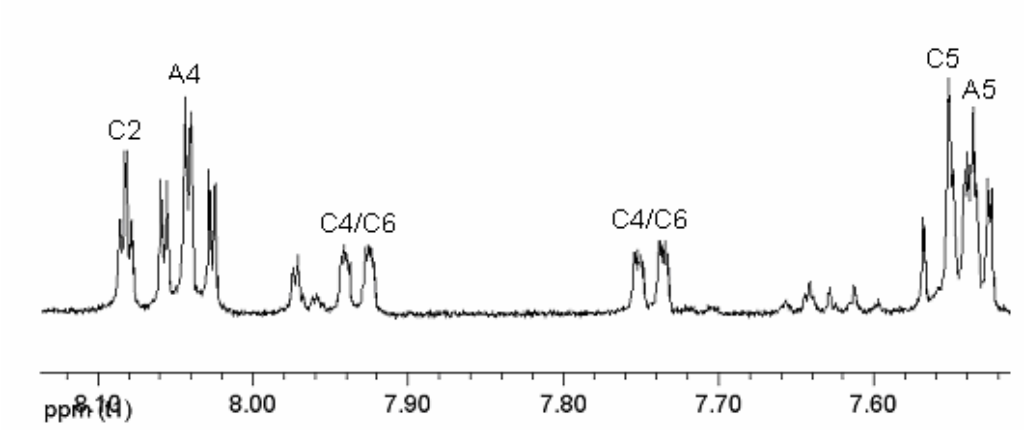

Figure 2.14: Expansion of the 500 MHz ^{1}H NMR spectrum of ligand **9** in DMSO-d_6 showing overlap of peaks C5 and A5.

2.5.2 ^{13}C NMR Spectroscopy

^{13}C NMR spectroscopy was once again a useful tool for characterisation of these phenyl substituted ligands. As was the case with the previous ligands, HMQC and HMBC techniques were essential in assigning each of the signals to a particular carbon atom. A table of data for the new ligand **9** and its precursor **8** is shown in table 2.4.

	A2	A3	A4	A5	A6	B2	B3	B4
8	155.8/ 155.9	121.3	136. 9	123.9	149.0	155.8/ 155.9	118.7	123.1
9	154.7/ 155.7	120.9	137.5	124.6	149.3	154.7/ 155.7	118.1	122.6

	C1	C2	C3	C4	C5	C6	*C*≡CH	C≡*C*H
8	140.5/ 148.7	130.4	140.5/ 148.7	126.0/ 131. 9	130.2	126.0/ 131. 9		

9	140.0/ 148.0	129. 5	140.0/ 148.0	126.1/ 132.2	131.5	126.1/ 132.2	82.9	81.6

Table 2.4: 500 MHz ^{13}C NMR data for ligands **8** and **9**, **8** in $CDCl_3$, **9** in DMSO-d_6.

The chemical shifts of both ligands **8** and **9** are very similar. The major difference between the NMR spectra is the change in the order of peaks C2 and C5. However, a different solvent was used for each ligand due to the poor solubility of **9** so this could explain the difference in the order of these two peaks which occur very close together. Figure 2.15 shows how the peaks were assigned using HMBC in ligand **8**. Cross peaks can clearly be seen between protons H(C4/C6) and carbon C(C5).

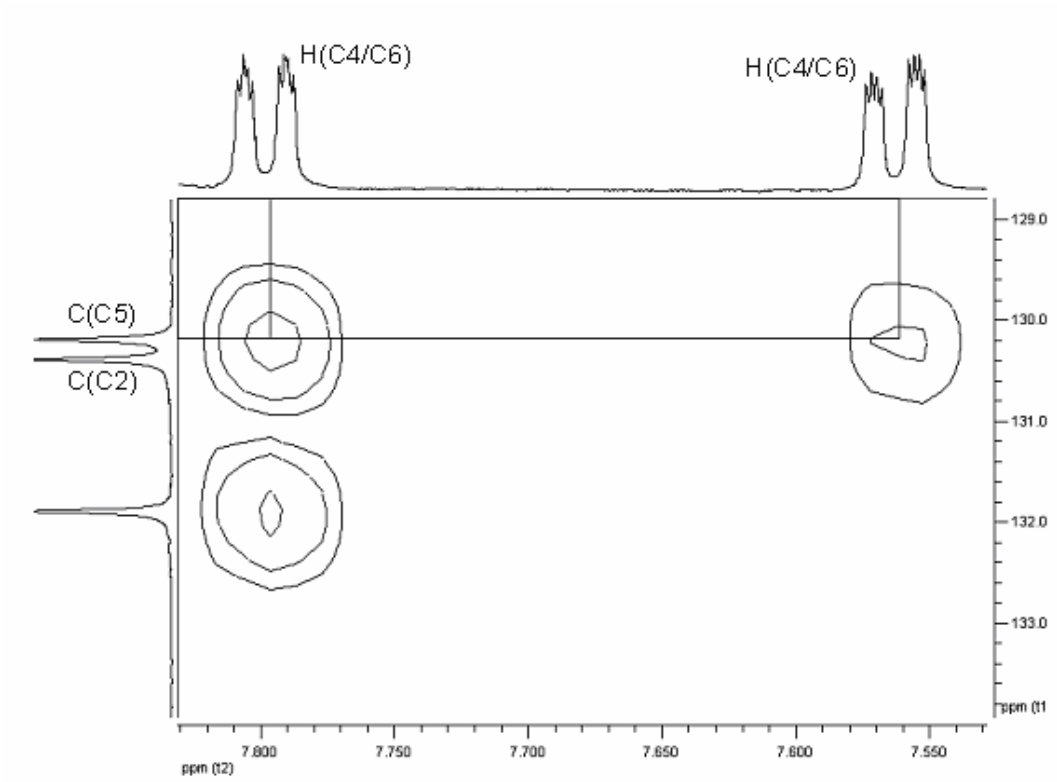

Figure 2.15: Expansion of part of the 500 MHz HMBC spectrum of ligand **8** in $CDCl_3$ showing cross peaks between H(C4/C6) and C(C5).

2.5.3 MALDI Mass Spectrometry

Ligand **9** was also characterised using MALDI mass spectrometry. A peak was seen at m/z 395 corresponding to $[M + K + Na]^+$.

2.6 Synthesis of Ligand **12**

A further alkyne-functionalised tpy ligand has also been synthesised. It was originally felt that this ligand would not be a suitable precursor for the self assembly of metallomacrocycles, however, it did have three alkyne moieties and was therefore deemed potentially useful in the formation of metal-alkyne complexes (discussed in chapter 4).

The synthesis of this ligand was not entirely straightforward (figure 2.16). The starting ligand was 4'-[1,1,1-tris(hydroxymethyl)methoxy]-2,2':6',2''-terpyridine,[14] and this has three pendant alcohol groups at which reaction to form the alkyne functionalised ligand can occur. A stronger base was needed than in the synthesis of ligand **1** from **HO-tpy** since the alcohol groups are now further removed from the tpy moiety. There were problems in obtaining the tris-alkyne ligand since there was always a significant amount of the mono- and bis- alkyne ligands produced and purification by chromatography on alumina using 0.5 % MeOH in $CHCl_3$ was possible, though difficult. The tris-alkyne product was finally obtained, though in a low yield (23 %), by the use of a large excess of propargyl bromide. Use of stoichiometric quantities produced the mono- or bis-alkyne ligands as the major products.

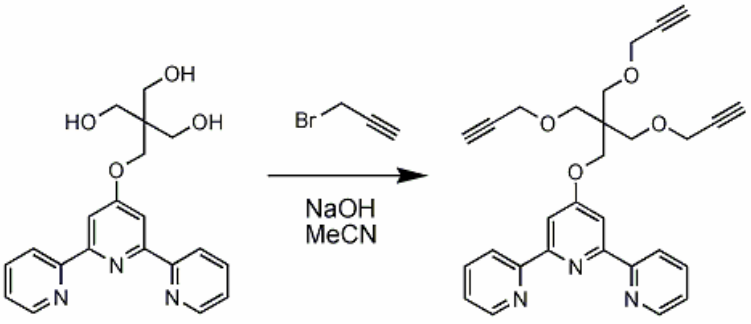

Figure 2.16: Synthesis of ligand **12**.

As ligand **12** was not originally intended to be used in the formation of metallomacrocycles, only minimal characterisation data has been obtained and this is reported in Chapter 6.

2.7 Crystal Structures

2.7.1 Ligand **1**

Single crystals suitable for X-ray crystallographic analysis were grown from a CH_2Cl_2 solution of **1** layered with hexane. An ORTEP representation of **1** is shown in figure 2.17 and figure 2.18 shows the packing of the molecules. Crystal data are given in the appendix and selected bond lengths and angles are given in table 2.5. Torsion angles of the tpy ligand are also shown in table 2.5.

Like most other uncoordinated 2,2':6',2"-terpyridine ligands, ligand **1** exists in a *trans*, *trans* conformation which minimises the interactions between lone pairs on each of the nitrogen atoms.[15] Ligand **1** deviates slightly from planarity, with torsion angles between the adjacent pyridine rings (defined in table 2.5) of 1.0(1) and 7.8(1) ° respectively. The bonds linking the rings of the tpy compare very well with similar systems such as the unsubstituted 2,2':6',2"-terpyridine, with C5-C6 having a length of 1.4879(16) and C10-C11 a length of 1.4901(16) Å. Bond angles in the tpy rings are also comparable with those in the same unsubstituted tpy.[16]

Hydrogen bonds of length 2.582 Å can be seen between N3 of one molecule and H18 of another, so that two ligand molecules are arranged in a pair. There is also hydrogen bonding between H16 of one ligand molecule and both O1 and C17 of another ligand molecule lying above. There is π-stacking (3.5 Å) between planes.

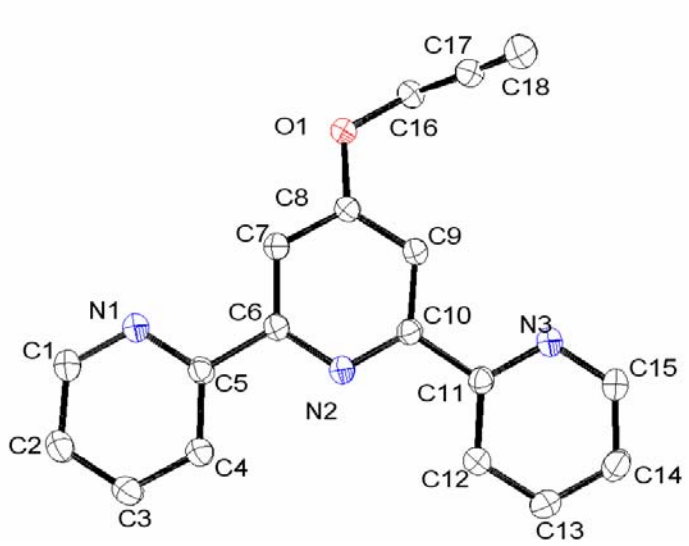

Figure 2.17: ORTEP representation of ligand **1**. Hydrogen atoms are omitted for clarity.

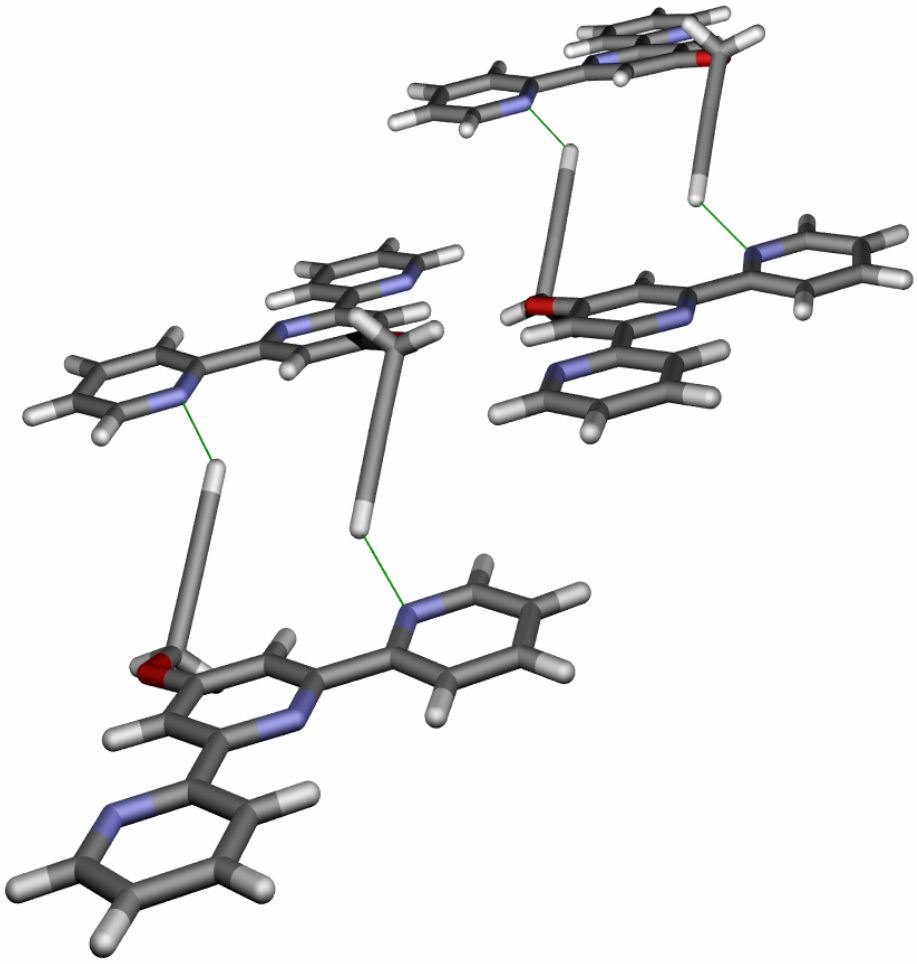

Figure 2.18: Molecules of ligand **1** arrange themselves into dimers held together by hydrogen bonds between H18 of one molecule and N3 of another.

Bond	Distance/Å	Bond	Distance/Å
N1-C5	1.3469(15)	C6-C7	1.3916(16)
C4-C5	1.3955(16)	C10-C9	1.3961(16)
C5-C6	1.4879(16)	C7-C8	1.3894(15)
N3-C11	1.3433(15)	C9-C8	1.3893(16)
C12-C11	1.3938(16)	C8-O1	1.3642 (13)
C11-C10	1.4901(16)	O1-C16	1.4406 (14)
N2-C6	1.3482(14)	C16-C17	1.4647 (18)
N2-C10	1.3413(14)	C17-C18	1.1838 (19)

Bonds	Angle/deg.	Bonds	Angle/deg.
C1-N1-C5	117.77(11)	C11-C10-N2	116.41(10)
N1-C5-C6	116.59(10)	C7-C8-O1	115.56(10)
C5-C6-N2	116.57(10)	C8-C9-O1	124.73(10)
C6-N2-C10	117.37(10)	C8-O1-C16	117.79(9)
C11-N3-C15	117.59(11)	O1-C16-C17	113.24(11)
N3-C11-C10	116.67(10)	C16-C17-C18	176.69(14)

N1-C5-C6-N12	1.0(1)	N2-C10-C11-N3	7.8(1)

Table 2.5: Selected bond lengths (Å), angles (˚) and torsion angles (˚) for ligand **1**.

2.7.2 Ligand **2**

Single crystals of ligand **2** which were suitable for X-ray crystallographic studies were grown from a solution of **2** in CH_2Cl_2 layered with hexane. An ORTEP representation is shown in figure 2.19 as well as the packing of the molecules in figure 2.20 and selected bond parameters are given in table 2.6. Crystal data are given in the appendix.

Once again the tpy ligand is in a *trans*, *trans* arrangement and there are torsion angles (defined in table 2.6) of 2.2(1) and 14.4(1) ˚ between the pyridine rings. This ligand also displays bond lengths which are comparable to the reported structure for the free 2,2':6',2"-terpyridine.[16]

Ligand **2** differs from **1** in the way its molecules are arranged in the solid state. There is a hydrogen bond of 2.3 Å between N1 of one molecule and H20 of another, but this time the molecules are not arranged in pairs, rather there is a zig-zag type of arrangement between molecules. Zig-zag chains of ligand molecules are stacked in planes (figure 2.21) and there is π-stacking of 3.4 Å between the least squares planes.

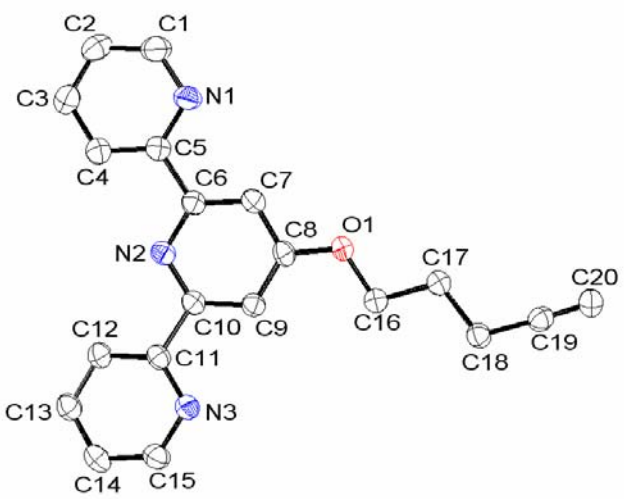

Figure 2.19: ORTEP representation of ligand **2**. Hydrogen atoms have been omitted for clarity.

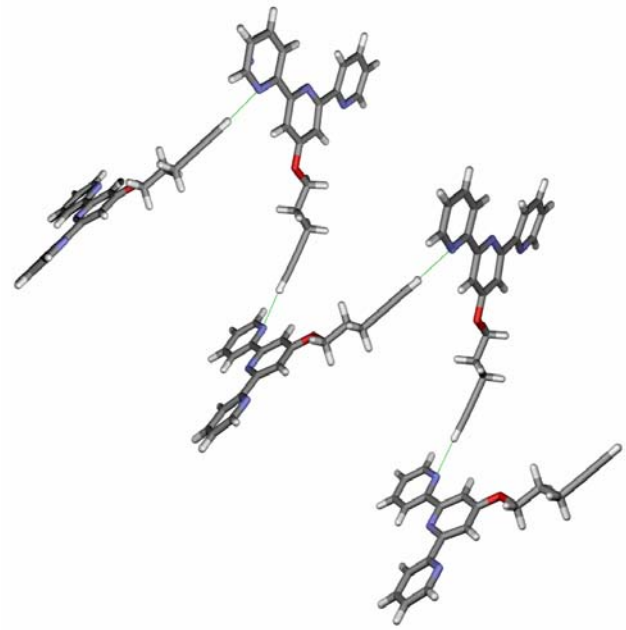

Figure 2.20: Arrangement of ligand **2** molecules in a zig-zag arrangement. This ligand does not arrange its molecules in dimers although hydrogen bonding does occur between H20 of one molecule and N1 of another.

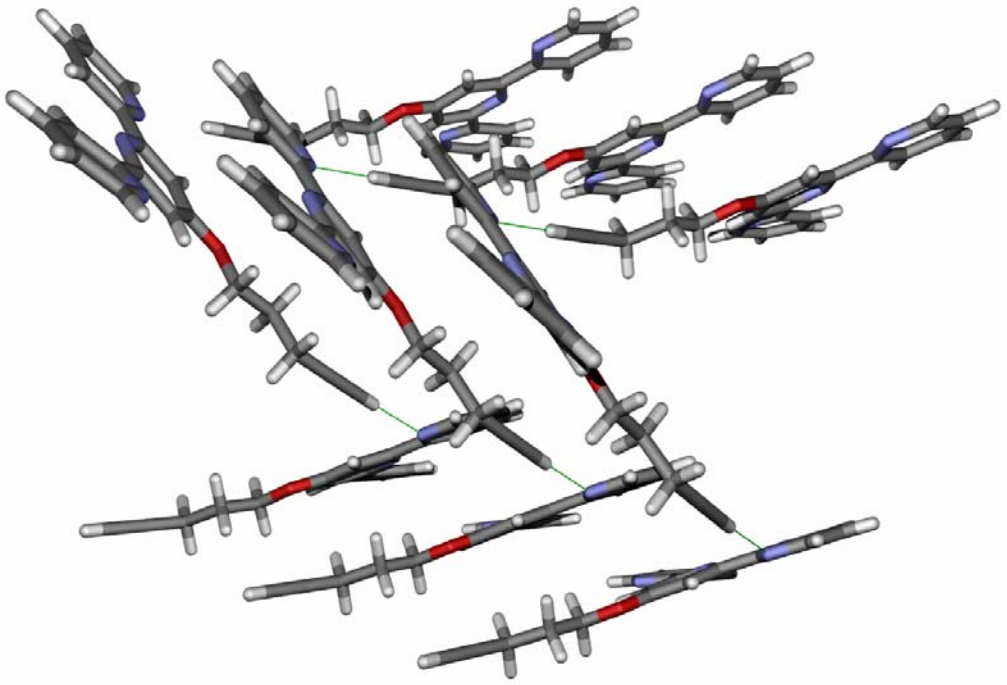

Figure 2.21: Zig-zag chains of ligand **2** molecules are arranged in planes which display π-stacking.

Bond	Distance/Å	Bond	Distance/Å
N1-C5	1.343(2)	C6-C7	1.381(2)
C4-C5	1.382(2)	C10-C9	1.388(2)
C5-C6	1.492(2)	C7-C8	1.398(2)
N3-C11	1.342(2)	C9-C8	1.385(2)
C12-C11	1.389(2)	C8-O1	1.3560(19)
C11-C10	1.494(2)	O1-C16	1.435(2)
N2-C6	1.351(2)	C16-C17	1.507(2)
N2-C10	1.338(2)	C17-C18	1.526(2)
C18-C19	1.468(2)		

Bonds	Angle/deg.	Bonds	Angle/deg.
C1-N1-C5	116.93(16)	C11-C10-N2	115.80(14)
N1-C5-C6	116.68(14)	C7-C8-O1	115.73(14)
C5-C6-N2	116.68(14)	C8-C9-O1	125.14(15)
C6-N2-C10	117.26(14)	C8-O1-C16	118.27(12)
C11-N3-C15	117.13(15)	O1-C16-C17	106.90(12)
N3-C11-C10	116.25(15)	C16-C17-C18	111.55(13)

C17-C18-C19	111.78(13)	C18-C19-C20	177.20(17)

N1-C5-C6-N2	2.2(1)	N2-C10-C11-N3	14.4(1)

Table 2.6: Selected bond lengths (Å), angles (˚) and torsion angles (˚) for ligand **2**.

2.7.3 Ligand **3**

The crystallisation of ligand **3** was achieved using two different solvent systems. X-ray quality crystals were obtained from a layered solution of CH_2Cl_2/hexane (**a**) as well as hot EtOH (**b**). Two solvent-free polymorphs were obtained. An ORTEP representation of ligand **3a** is shown in figure 2.22. At the molecular level, the structures of both polymorphs are very similar and as before, the rings of the tpy are in a *trans, trans* arrangement in both polymorphs. Bond parameters are shown in table 2.7. Crystal data for both polymorphs are given in the appendix. Bond lengths and angles in both **a** and **b** compare well with the published structure of the unsubstituted 2,2':6',2''-terpyridine.[16]

The major difference between the two forms is in the molecular packing. The crystals of **3a**, grown from a solution of **3** in CH_2Cl_2 layered with hexane were colourless plates. Ligand molecules form dimers due to hydrogen bonding between the alkyne H atom of one molecule and one of the tpy nitrogens of another molecule. These dimers arrange themselves into layers (shown in figure 2.23) and layers are all parallel to one another, with the b axis of the unit cell running parallel to these layers.

The crystals grown from hot EtOH, **3b**, were colourless prisms and once again molecules are arranged in dimers with the same type of hydrogen bonding between molecules as in **3a**. However, in this structure, the dimers are arranged orthogonal to one another, shown in figure 2.24.

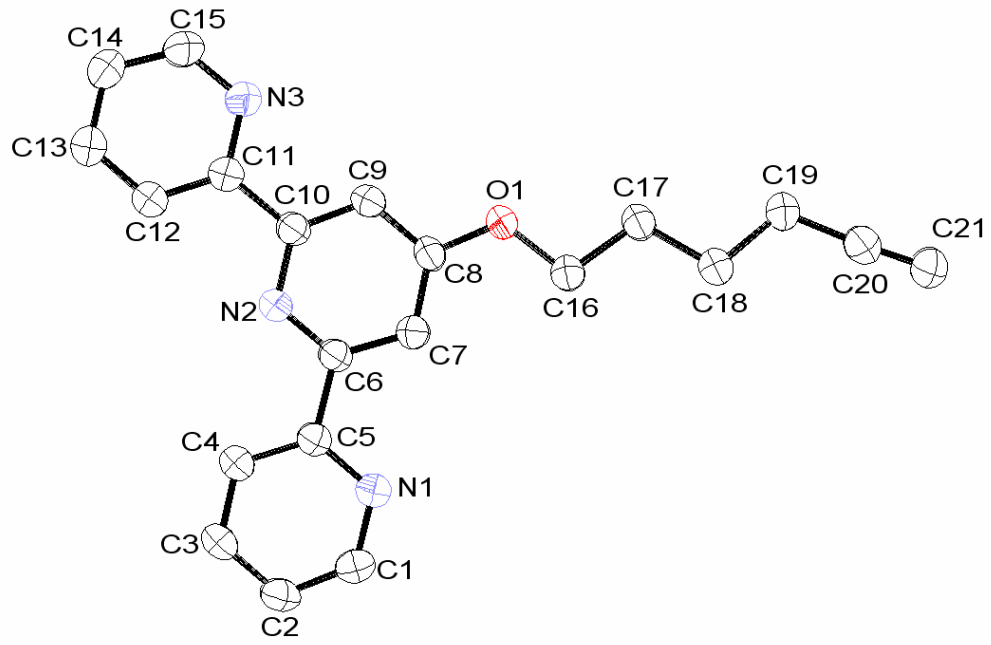

Figure 2.22: An ORTEP representation of ligand **3a**. Crystals here were grown from a solution of **3** in CH_2Cl_2 layered with hexane.

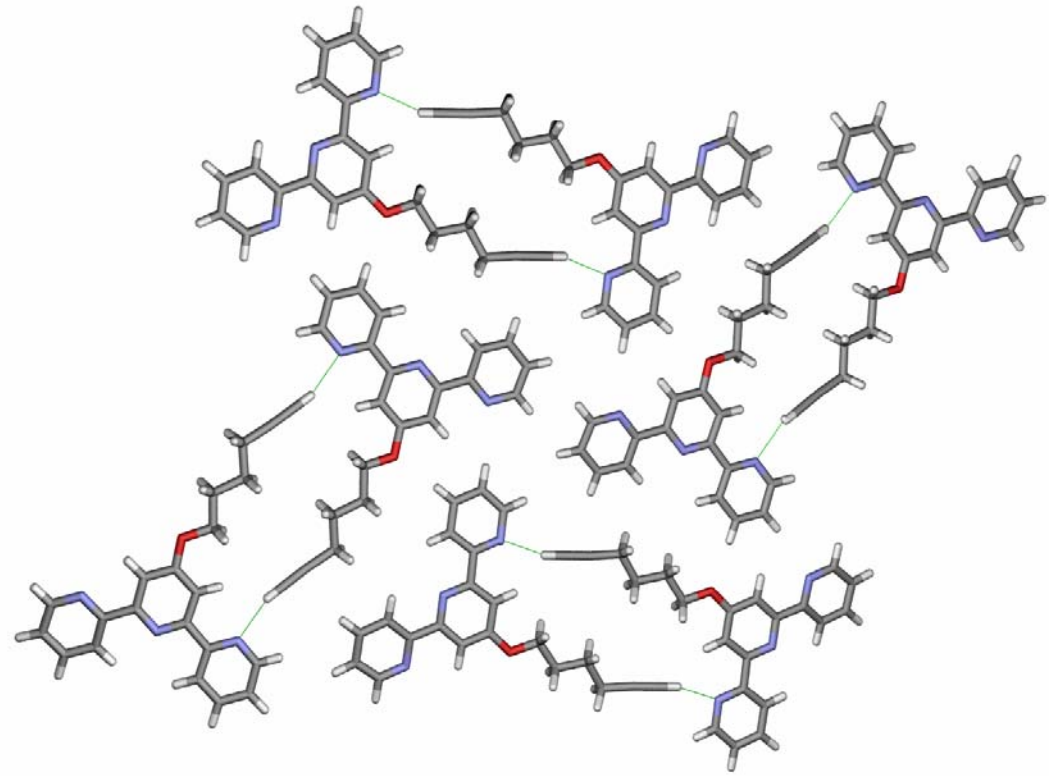

Figure 2.23: Packing of molecules of ligand **3a**. Crystals grown from a solution of **3** in CH_2Cl_2 layered with hexane. Ligand molecules shown here are hydrogen bonded in dimers with all sets of dimers forming the same layer.

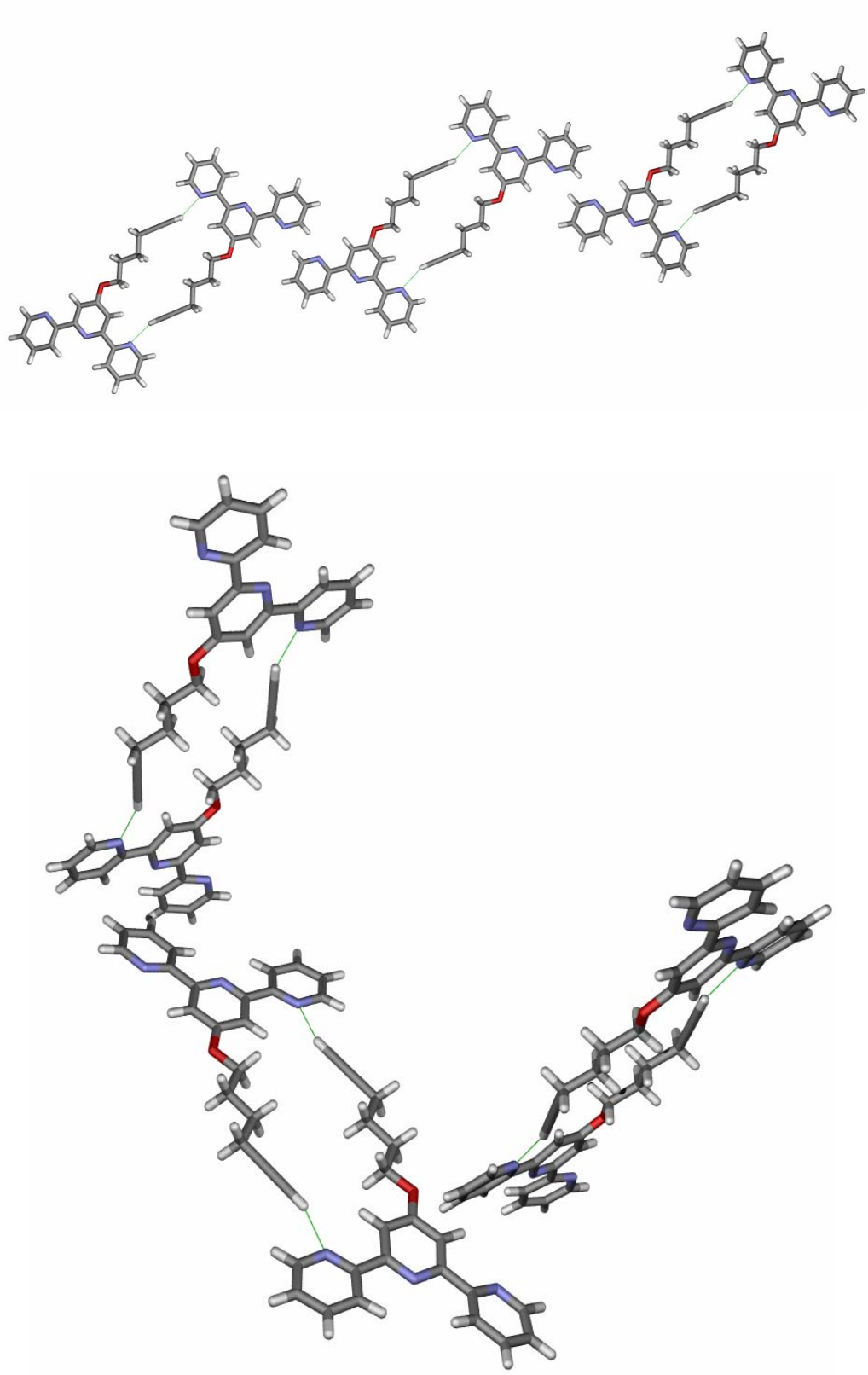

Figure 2.24: packing of molecules of ligand **3b**. Crystals grown from hot EtOH. Once again molecules are arranged as dimers (top) though here dimers are arranged perpendicular to one another (bottom).

Bond	Distance/Å	Distance/Å	Bond	Distance/Å	Distance/Å
	a	**b**		**a**	**b**
N1-C5	1.342(3)	1.338(2)	C6-C7	1.393(3)	1.389(2)
C4-C5	1.391(3)	1.385(2)	C10-C9	1.381(3)	1.379(2)
C5-C6	1.489(3)	1.488(2)	C7-C8	1.383(3)	1.388(2)
N3-C11	1.345(3)	1.343(2)	C9-C8	1.390(3)	1.384(2)
C12-C11	1.378(3)	1.386(2)	C8-O1	1.356(2)	1.3532(19)
C11-C10	1.488(3)	1.481(2)	O1-C16	1.432(3)	1.433(2)
N2-C6	1.339(3)	1.329(2)	C16-C17	1.510(3)	1.504(2)
N2-C10	1.349(3)	1.346(2)	C17-C18	1.520(3)	1.515(2)
C18-C19	1.526(3)	1.522(3)	C19-C20	1.467(3)	1.462(3)
C20-C21	1.180(3)	1.169(3)			

Bonds	Angle/deg.	Angle/deg.	Bonds	Angle/deg.	Angle/deg.
C1-N1-C5	117.5(2)	116.84(16)	C11-C10-N2	116.16(19)	115.20(14)
N1-C5-C6	116.80(19)	116.48(15)	C7-C8-O1	125.2(2)	124.35(16)
C5-C6-N2	115.76(18)	115.77(15)	C8-C9-O1	115.85(19)	116.11(14)
C6-N2-C10	116.99(18)	117.61(14)	C8-O1-C16	118.67(17)	118.54(13)
C11-N3-C15	116.9(2)	116.75(16)	O1-C16-C17	106.38(19)	106.62(14)
N3-C11-C10	116.3(2)	116.97(15)	C16-C17-C18	113.70(19)	112.43(15)
C17-C18-C19	109.91(19)	110.65(15)	C18-C19-C20	116.1(2)	113.74(17)
C19-C20-C21	176.1(3)	179.5(2)			

N1-C5-C6-N2	1.2(2)	9.1(2)	N2-C10-C11-N3	7.7(2)	12.7(2)

Table 2.7: Selected bond lengths (Å), angles (˚) and torsion angles (˚) for both the CH_2Cl_2 (**a**) and EtOH (**b**) polymorphs of ligand **3**.

The thermal behaviour of the EtOH polymorph **3b** was also investigated. On heating a sample of **3b** at a rate of 2 ˚C per minute a phase change was seen at a temperature of 98 ˚C. Further heating of the sample up to a temperature of 110 ˚C resulted in no further changes. Cooling the sample back down, also at a rate of 2 ˚C per minute did not show any phase changes. If the sample was then heated once again, this time from 60 ˚C rather than

room temperature, a different phase change to that observed during the first heating cycle was seen, at a temperature of 83 ˚C. If this sample is then allowed to return to room temperature naturally and allowed to rest for several hours, the same cycle of phase changes can be observed and this is reproducible for each heating and cooling cycle. It is possible that this observation is due to the formation of a third, metastable polymorph which is formed on slow cooling of the sample back to 60 ˚C.[17,11] The TGA curve of the heating and cooling cycles of **3b** can be seen in figure 2.25. Temperature and time are shown on the x axis and two peaks can be clearly seen, one resulting from a phase change at 98 ˚C on the first heating cycle and the second from a phase change at 83 ˚C on the second heating cycle.

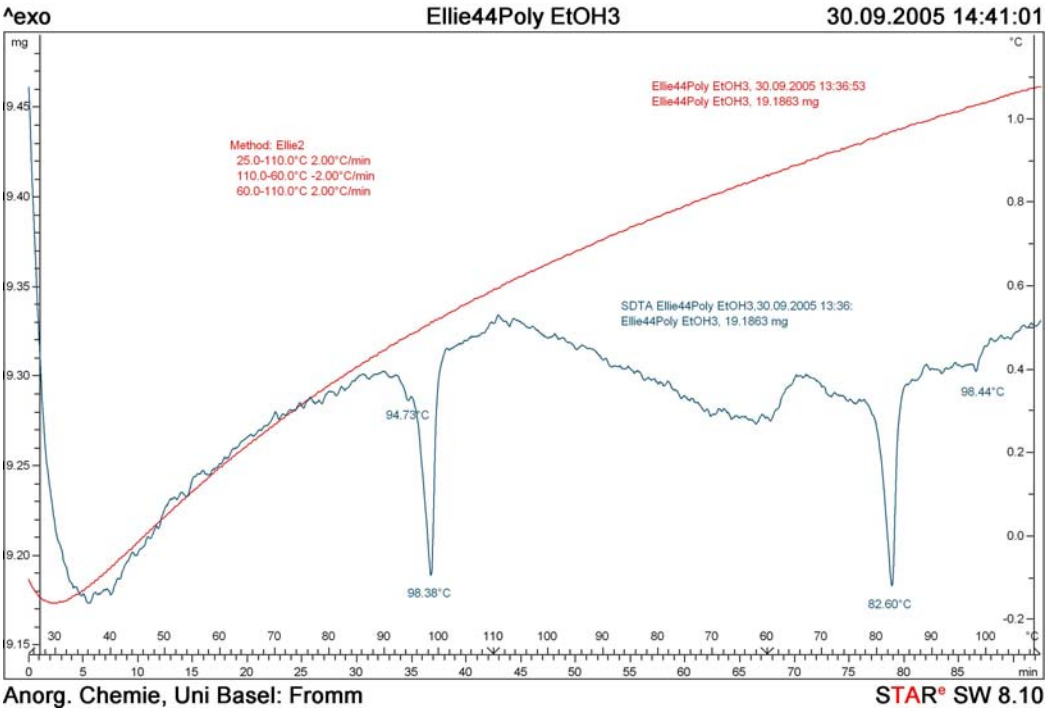

Figure 2.25: TGA trace of **3b** showing the two phase changes on heating and cooling.

Crystals of **3b** were observed under a polarising microscope. It was noted that on reaching a temperature just below 98 ˚C, the first phase change on the TGA trace, liquid crystalline behaviour was observed. Liquid crystals in which this behaviour is seen between a certain temperature range are called thermotropic and this type of liquid crystalline phase is a nematic one.[18]

Nematic phase liquid crystals are the most liquid-like of all the types. One or two molecular axes are oriented parallel to one another and this means that this type of phase has an orientational long range order. Molecules of a nematic phase are typically long and linear and have rotational freedom about the long molecular axis. Figure 2.26 shows the different phases and the degree of molecular order in each.

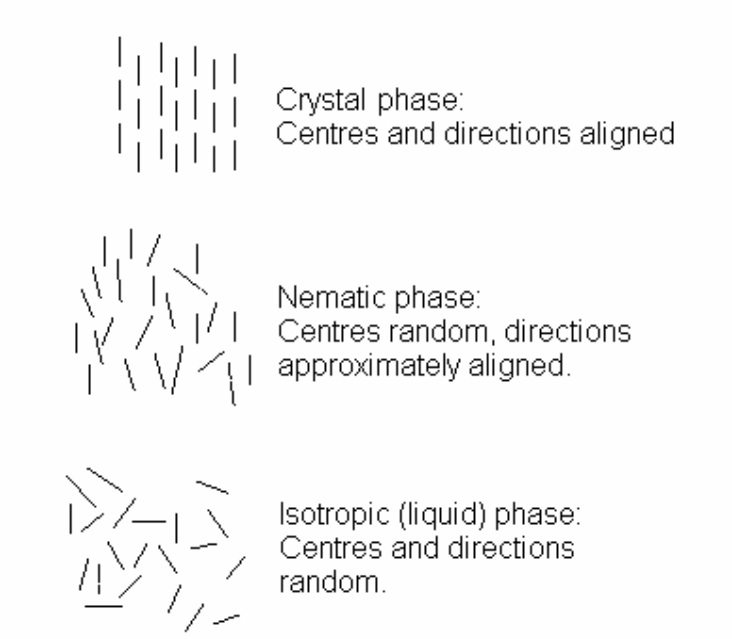

Figure 2.26: Molecular order on going from solid to liquid crystal to liquid phase.

Because of the parallel nature of nematic phase liquid crystals, these molecules possess an optical anisoptropy, or double refraction. The optical axis is parallel to the long molecular axis and if a polarising microscope is used to observe the liquid crystal behaviour, different textures can be observed depending on the orientation of the liquid crystal phase. Figure 2.27 shows a photograph of liquid crystals of **3b** taken down a polarising microscope. The typical nematic “thread like” pattern can be clearly seen, this pattern being the one which originally gave rise to the term “nematic”.

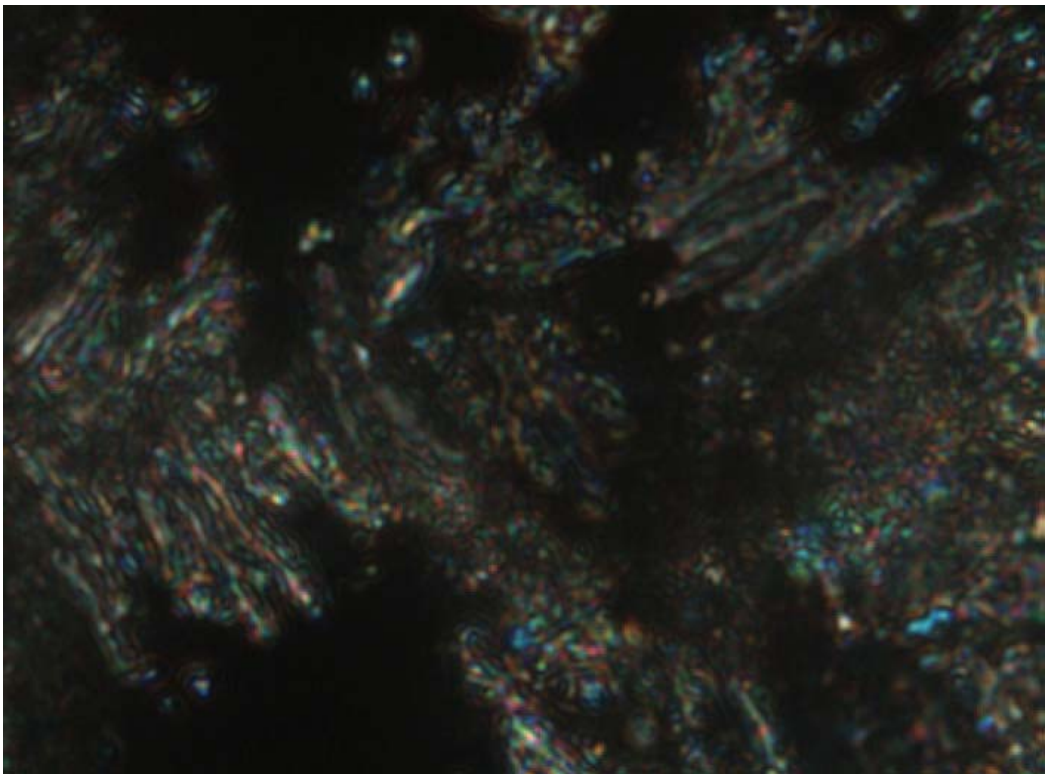

Figure 2.27: Photograph of liquid crystals of **3b** taken down a polarising microscope.

2.7.4 Ligand **5**

X-ray quality crystals of ligand **5** were grown from a $CDCl_3$ solution of **5**. An ORTEP representation is shown below in figure 2.28 and the packing of the molecules can be seen in figure 2.29 Once again, since this ligand is uncoordinated, the nitrogen atoms of the tpy rings are in a *trans*, *trans* arrangement. Again the bond lengths and angles compare well with those reported for the unsubstituted 2,2':6',2"-terpyridine.[16] Figure 2.29 shows the arrangement of pairs of molecules in dimers, due to hydrogen bonds of length 2.26 Å between H22 of one molecule and N3 of another. The presence of several oxygen atoms in this ligand means that there is also hydrogen bonding between H17 of one molecule and O3 (2.612 Å) of the other. Dimers are stacked on top of each other in a chair like conformation and stacks of chairs run perpendicular to one another. The tpy regions of the stacks are not in close enough proximity to one another to permit any π-stacking interactions. Selected bond parameters are shown in table 2.8.

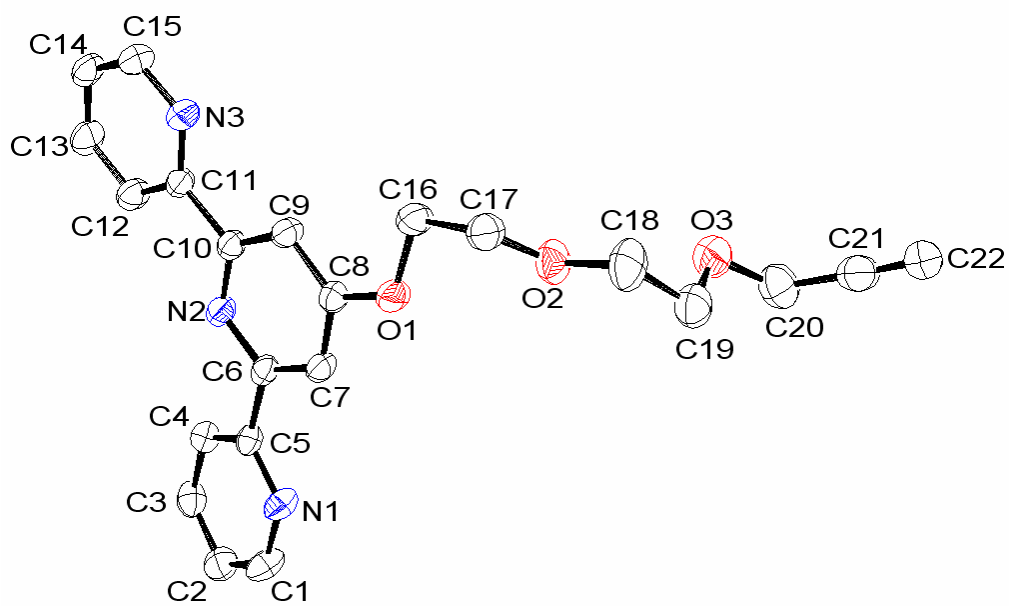

Figure 2.28: ORTEP representation of ligand **5**. Hydrogen atoms are omitted for clarity.

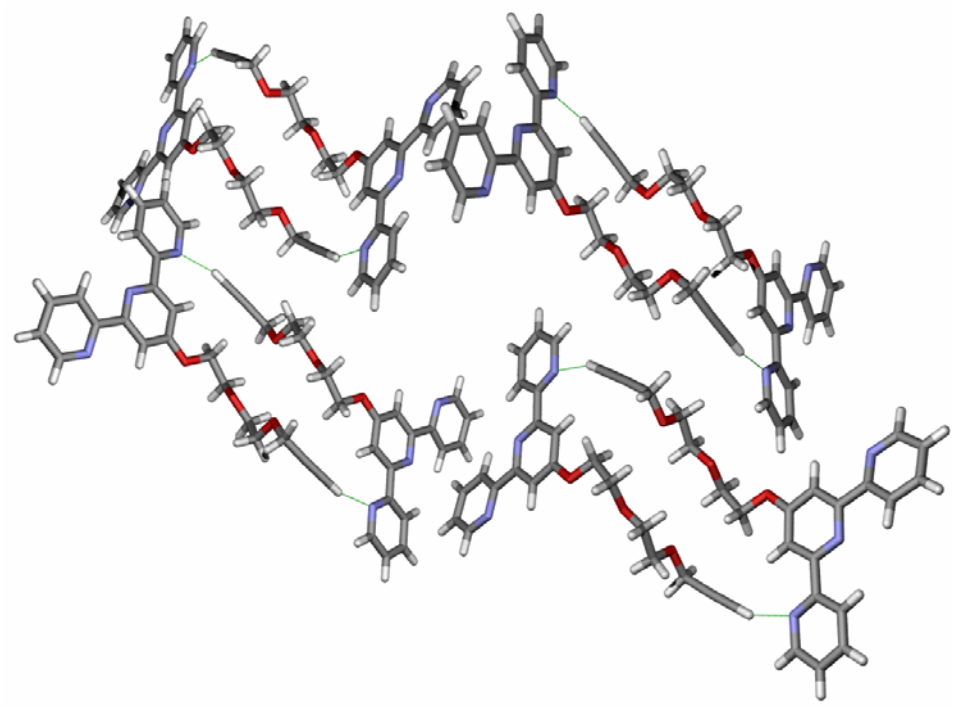

Figure 2.29: Arrangement of molecules of ligand **5** in dimers due to hydrogen bonding between H22 of one molecule and N3 of another. Dimers are arranged perpendicular to one another.

Bond	Distance/Å	Bond	Distance/Å
N1-C5	1.337(3)	C6-C7	1.371(3)

C4-C5	1.390(3)	C10-C9	1.388(3)
C5-C6	1.479(3)	C7-C8	1.386(3)
N3-C11	1.334(3)	C9-C8	1.391(3)
C12-C11	1.383(3)	C8-O1	1.351(3)
C11-C10	1.495(3)	O1-C16	1.422(3)
N2-C6	1.342(3)	C16-C17	1.489(3)
N2-C10	1.332(3)	C17-O2	1.419(3)
C18-C19	1.500(4)	O2-C18	1.410(3)
C19-O3	1.392(3)	O3-C20	1.415(4)
C20-C21	1.466(4)	C21-C22	1.170(4)

Bonds	Angle/deg.	Bonds	Angle/deg.
C1-N1-C5	116.9(2)	C11-C10-N2	115.30(19)
N1-C5-C6	117.3(2)	C7-C8-O1	116.19(18)
C5-C6-N2	115.51(19)	C8-C9-O1	124.5(2)
C6-N2-C10	117.73(19)	C8-O1-C16	117.93(16)
C11-N3-C15	117.4(2)	O1-C16-C17	108.00(18)
N3-C11-C10	117.1(2)	C16-C17-O2	108.8(2)
C17-O2-C18	110.6(2)	O2-C18-C19	109.6(3)
C18-C19-O3	111.0(2)	C19-O3-C20	112.2(2)
O3-C20-C21	112.1(3)	C20-C21-C22	177.5(3)

N1-C5-C6-N2	12.5(2)	N2-C10-C11-N3	6.5(2)

Table 2.8: Selected bond lengths (Å), angles (˚) and torsion angles (˚) of ligand **5**.

2.8 Conclusion

Several different tpy ligands have been synthesised and their NMR spectroscopic and mass spectrometric characteristics have been discussed in this chapter. X-ray crystal structures have been obtained for most of the ligands.

2.9 References

[1] H. Hofmeier and U. S. Schubert, *Chem. Soc. Rev.*, 2004, **33**, 373 and references therein.

[2] D. Armspach, E. C. Constable, C. E. Housecroft, M. Neuburger and M. Zehnder, *J. Organomet. Chem.*, 1998, **550**, 193.

[3] E. C. Constable, C. E. Housecroft, L. A. Johnston, D. Armspach, M. Neuburger and M. Zehnder, *Polyhedron*, 2001, **20**, 483.

[4] D. Armspach, E. C. Constable, F. Diederich, C. E. Housecroft and J.-F. Nierengarten, *Chem. Eur. J.*, 1998, **4**, 723.

[5] G. W. Cave and C. L. Raston, *J. Chem. Soc. Perkin Trans.*, 2001, 3258.

[6] W. Spahni and G. Calzaferri. *Helv. Chim. Acta*, 1984, **67**, 450.

[7] S. Bonnet, J.-P. Collin and J.-P. Sauvage, *Chem. Commun.*, 2005, 3195.

[8] C. Patoux, J.-P. Launay, M. Beley, S. Chodorowski-Kimmes, J.-P. Collin, S. James and J.-P. Sauvage, *J. Am. Chem. Soc.*, 1998, **120**, 3717.

[9] E. C. Constable and M. D. Ward, *J. Chem. Soc. Dalton Trans.*, 1990, 1405.

[10] B. G. Lohmeijer and U. S. Schubert, *J. Polym. Sci. Part A. Polym. Chem.*, 2003, **41**, 1413.

[11] E. C. Constable, C. E. Housecroft, M. Neuburger, S. Schaffner and E. J. Shardlow, *CrystEngComm.*, 2005, **7**, 599.

[12] K. Sonogashira, Y. Tohda and N. Hagihara, *Tetrahedron. Lett.*, 1975, 4467.

[13] K. Sonogashira, *J. Organomet. Chem.*, 2002, **653**, 46.

[14] E. C. Constable, C. E. Housecroft, M. Cattalini and D. Phillips, *New J. Chem.*, 1998, **22**, 193.

[15] A. M. W. Cargill Thompson, *Coord. Chem. Rev.*, 1997, **160**, 1.

[16] C. A. Bessel, R. F. See, M. R. Churchill and K. J. Takeuchi, *J. Chem. Soc. Dalton Trans.*, 1992, 3223.

[17] B. Perrenot and G. Widmann, *Thermochim. Acta*, 1994, **234**, 31.

[18] H. Stegemeyer, *Topics in Physical Chemistry, Vol. 3: Liquid Crystals*, Steinkopff Darmstadt, 1994.

Chapter 3 Platinahomoditopic Ligands

3.1 Platinum(II) Alkynyl Complexes

Platinum(II) alkynyl complexes are well studied in the literature because of their interesting luminescence properties. These compounds have more recently been investigated as potential molecular wires and sensors due to the increasing demands for new materials for the electronics industry.[1,2,3]

This chapter describes the synthesis of several platinahomoditopic ligands from various alkyne-functionalised terpyridine ligands, the synthesis of these ligands having been discussed in Chapter 2. By coupling two terpyridine ligands to a platinum centre via their alkyne functionality, a platinahomoditopic ligand can be created, that is to say a platinum-containing ligand with two identical sets of donor atoms. All of the platinum complexes described have a square planar geometry and a *trans* configuration. They differ in the nature of the spacer between the alkyne and the terpyridine, some are more flexible than others, and some are completely rigid. Auxiliary ligands are various phosphines, PEt_3, P^nBu_3 and PPh_3. P^iPr_3 and PCy_3 were also tried but with no success. These are varying sizes and have different Tolman cone angles.

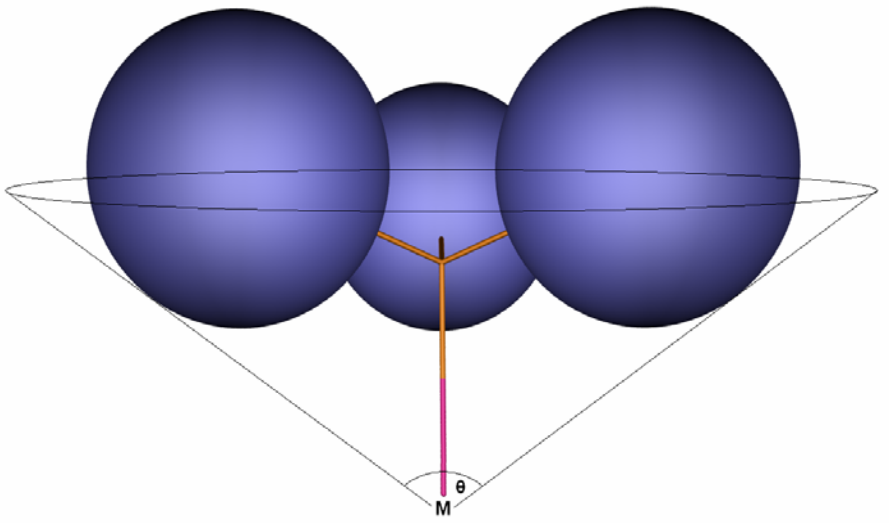

Figure 3.1: Representation of the Tolman cone angle, θ. The blue spheres represent the space taken up by an R group.

The cone angle is a measure of the steric bulk of the phosphine and is found by estimating the angle of a cone formed by taking the metal atom to be the apex of the cone.[4] Figure 3.1 shows how the Tolman cone angle is derived and table 3.1 shows cone angles for the phosphine groups discussed in this chapter.

Phosphine	Tolman Cone Angle
PEt_3	132
P^nBu_3	132
PPh_3	145
P^iPr_3	160
PCy_3	170

Table 3.1: Tolman cone angles (˚) for selected phosphine ligands.

3.2 Synthesis of Platinahomoditopic Ligands

As described in Chapter 1, there are a number of methods for synthesising platinum(II) alkynyl complexes. Most of the literature examples use a copper(I) iodide catalyst with a base such as triethylamine, and this is the method used for the synthesis of the platinahomodiopic ligands discussed in this chapter. Figure 3.2 shows the nomenclature and numbering scheme for the homoditopic ligands discussed in this chapter.

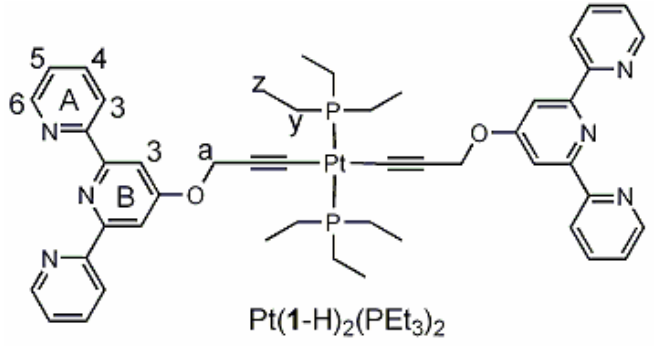

$Pt(\mathbf{1}\text{-}H)_2(PEt_3)_2$

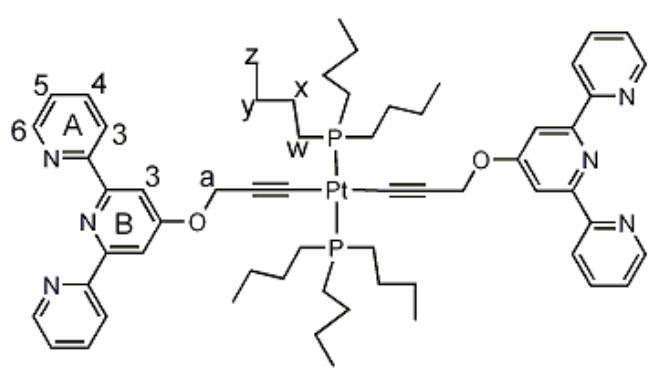

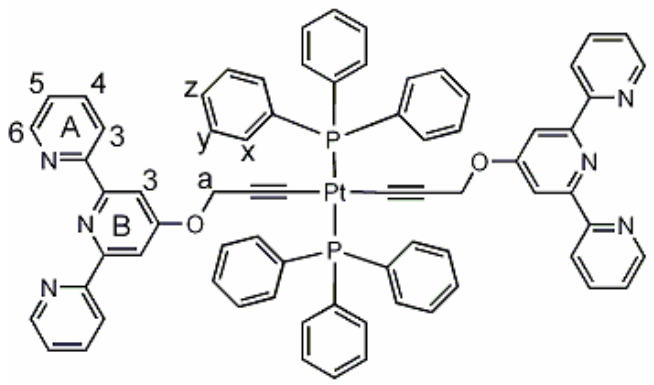

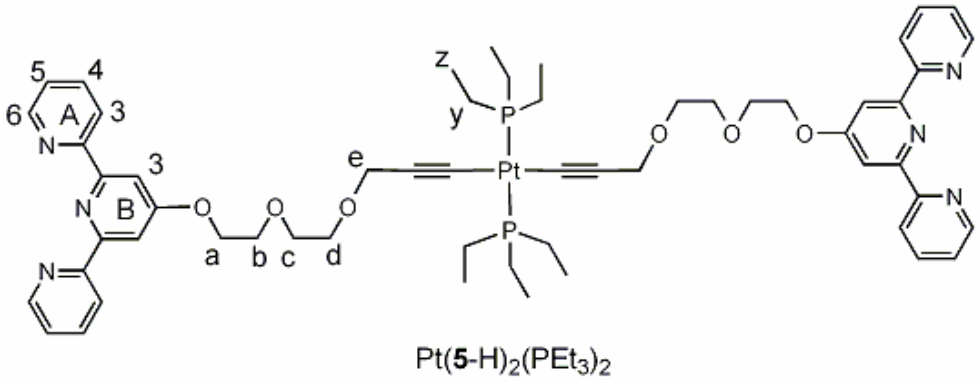

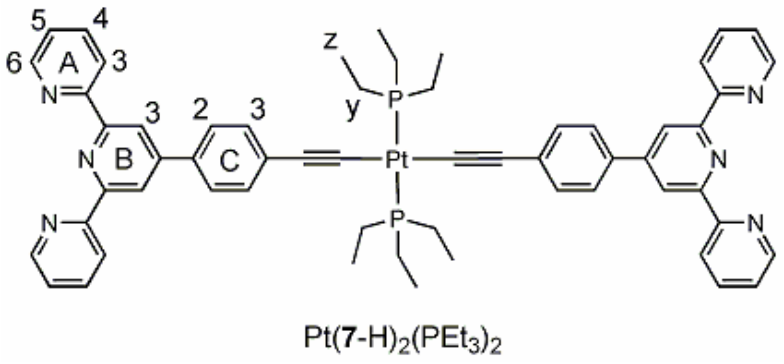

Figure 3.2: Numbering scheme for platinahomoditopic ligands.

Alkyne functionalised tpy ligands have two potential moieties for reaction with platinum(II). Either the reaction can take place at the alkyne as desired, or alternatively complexation of the tpy can occur with platinum(II), leaving the alkyne free. All of the reactions described later in this chapter produced the desired reaction at the alkyne with no evidence of coupling to the tpy. It is thought that this coupling reaction proceeds via the formation of a copper(I) alkynyl complex as an intermediate. The exact mechanism is not known, but figure 3.3 shows the proposed reaction scheme for the process.[5]

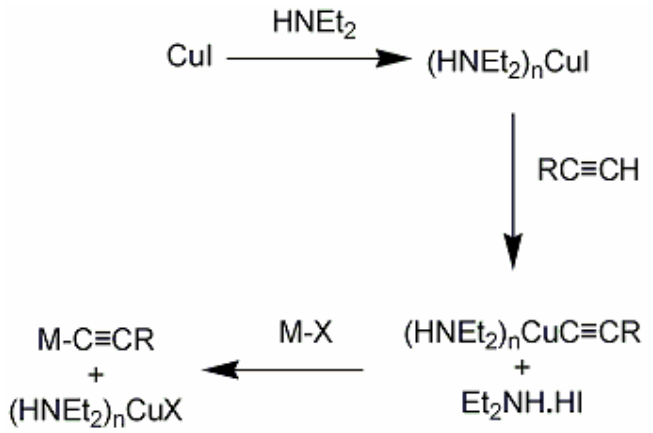

Figure 3.3: Proposed reaction scheme[5] for the CuI catalysed formation of M-alkyne bonds. For syntheses discussed in this chapter, M = Pt(II), X = I and $HNEt_2$ was replaced by NEt_3.

The synthesis of the platinahomoditopic ligands described in this chapter can be straightforward. An excess of the alkyne functionalised tpy ligand along with a $PtI_2(PR_3)_2$ complex and a catalytic amount of copper(I) iodide is stirred at room temperature for 5 days in a 50:50 mixture of CH_2Cl_2 and NEt_3 (figure 3.4). It is important for all the reactants to be soluble in the solvent chosen which is why it was necessary to add CH_2Cl_2 to the NEt_3. If the reactants are not soluble enough, then the reaction does not proceed to completion and sometimes not at all. The use of CH_2Cl_2 can occasionally cause problems. X-ray crystal structures obtained from the reaction of $PtI_2(PCy_3)_2$ with ligand **3** have shown that the CH_2Cl_2 is able to take part in a reaction with the starting platinum complex and results in the formation of a platinum bis-chloride bis-phosphine complex. Since chloride ligands are significantly less labile than iodide, this can prevent subsequent substitution of

the alkyne tpy ligand and if this is the case, the formation of the platinahomoditopic ligand is not observed. Other solvent systems have been investigated, such as a mixture of THF, DMF and NEt_3, though these were more problematic in terms of the purification of the final product. Products resulting from reactions where this solvent system was used were usually oily due to the presence of remaining solvent which is difficult to remove and therefore the CH_2Cl_2/NEt_3 mixture was the solvent system of choice for most of these reactions.

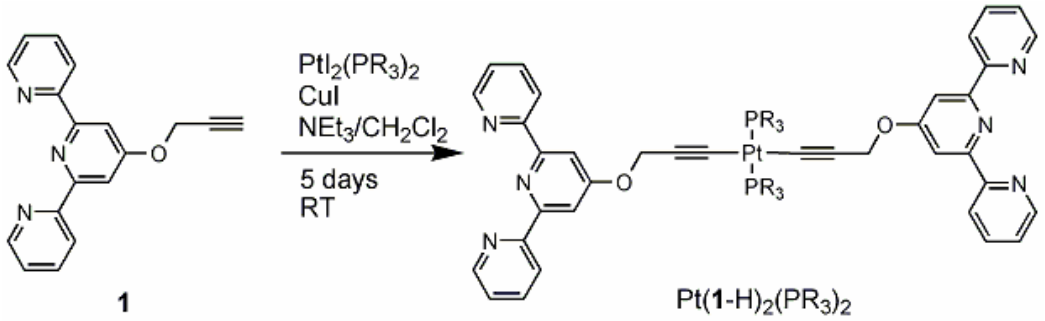

Figure 3.4: The synthesis of platinahomoditopic ligands[6]

As well as the correct choice of solvent system, around 4 or 5 equivalents of the tpy ligand is usually necessary in order to ensure the reaction goes to completion. Using a stoichiometric amount of tpy sometimes results in the formation of a mixture of products, both the mono- and bis-complexes as well as some remaining unreacted bis-iodide complex. Proton NMR spectroscopy is a useful tool for monitoring the reaction, especially in the reaction of ligand **5** with $PtI_2(PEt_3)_2$.[7] There is a significant change in the chemical shift of the e protons on going from free ligand to the mono and finally the bis complex and if there is still a significant quantity of the mono complex the reaction can be left to react for a few more days. ^{31}P NMR is also a useful tool for characterisation of the complexes since the presence of platinum satellites confirms coordination at the platinum centre. The coupling constants between the two satellite peaks can be used to determine the geometry at the metal centre since coupling of around 2300 Hz shows a *trans* geometry and coupling of around 3000 Hz shows a *cis* geometry. The NMR spectra of all the platinum complexes synthesised are discussed in more detail in Section 3.3.

Ligand **3** (figure 3.5) was used in attempts to synthesise Pt(**3**-H)$_2$(PCy$_3$)$_2$. This time, the phosphines are very sterically hindered due to the presence of the cyclohexyl groups and it was thought that by using ligand **3** where the spacer is longer than in **1** or **2** there would still be enough distance between the platinum(II) centre and the bulky tpy groups for the reaction to occur. Unfortunately this was not the case and crystals obtained from the products of the reaction confirmed the formation of PtCl$_2$(PCy$_3$)$_2$.[8] This could possibly be due to the fact that the reaction between the alkyne and the platinum(II) either does not occur at all or occurs very slowly, leaving more time for the substitution of the iodide by chloride which comes from the CH_2Cl_2 solvent used in the reaction. Once the chloride substitution has taken place there is even less chance for reaction between alkyne and platinum(II) to occur since, as discussed already, the chloride is much less labile than the iodide ligand.

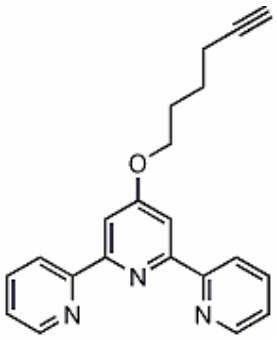

Figure 3.5: Ligand **3** was used in attempts to synthesise Pt(**3**-H)$_2$(PCy$_3$)$_2$.

Attempts to synthesise Pt(**2**-H)$_2$(PEt$_3$)$_2$ from ligand **2** (figure 3.6) and PtI$_2$(PEt$_3$)$_2$ were also unsuccessful. ^{31}P NMR spectra showed the presence of 3 P-Pt environments, one which was identified as being the starting material PtI$_2$(PEt$_3$)$_2$. The major environment in the ^{31}P spectrum came at δ 11.3 ppm. This is similar to the literature values[9,10] for Pt(CCR)$_2$(PEt$_3$)$_2$ (R = H and CH_3) The presence of a signal at δ 12 ppm in the ^{1}H NMR spectrum was reminiscent of the signal arising from the NH group of the tautomer of **HO-tpy** seen in the NMR spectrum of **HO-tpy** suggesting there had also been

cleavage at the ether bond of the ligand. Attempts to separate the fractions were unsuccessful.

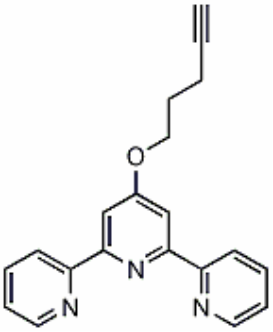

Figure 3.6: Ligand **2** was used in attempts to synthesise Pt(**2**-H)$_2$(PEt$_3$)$_2$.

When ligand **7** (figure 3.7) was first used in attempts to synthesise a rigid platinum complex from the reaction with PtI$_2$(PPh$_3$)$_2$ the solvent used was NEt$_3$ only. This ligand was much less soluble than **1** and after a while an orange precipitate formed in the reaction vessel. This was collected by filtration and found to be virtually insoluble in water as well as all common organic solvents. It was not possible to record an NMR spectrum due to its insolubility although the IR spectrum did show peaks similar to those of the free ligand suggesting the resulting compound was in some way related.

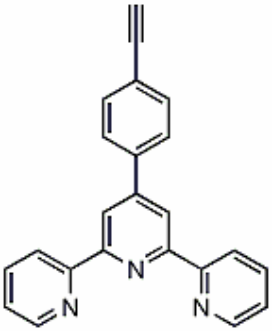

Figure 3.7: Ligand **7** was used in attempts to synthesise Pt(**7**-H)$_2$(PPh$_3$)$_2$.

A saturated solution of the orange product in CH$_2$Cl$_2$ layered with hexane produced crystals suitable for X-ray diffraction studies and the structure was confirmed as a copper(I) complex[11] containing two copper atoms coordinated to the nitrogen atoms of the tpy. The crystal structure of

this product is discussed later in the chapter in Section 3.4. It was interesting to note that there was no platinum in the product and that the triphenylphosphine ligands which had previously been coordinated to the platinum(II) had now migrated to the copper(I). The alkyne moiety remained uncoordinated. Figure 3.8 shows the X-ray crystal structure of the resulting copper(I) complex. Hydrogen atoms have been omitted for clarity.

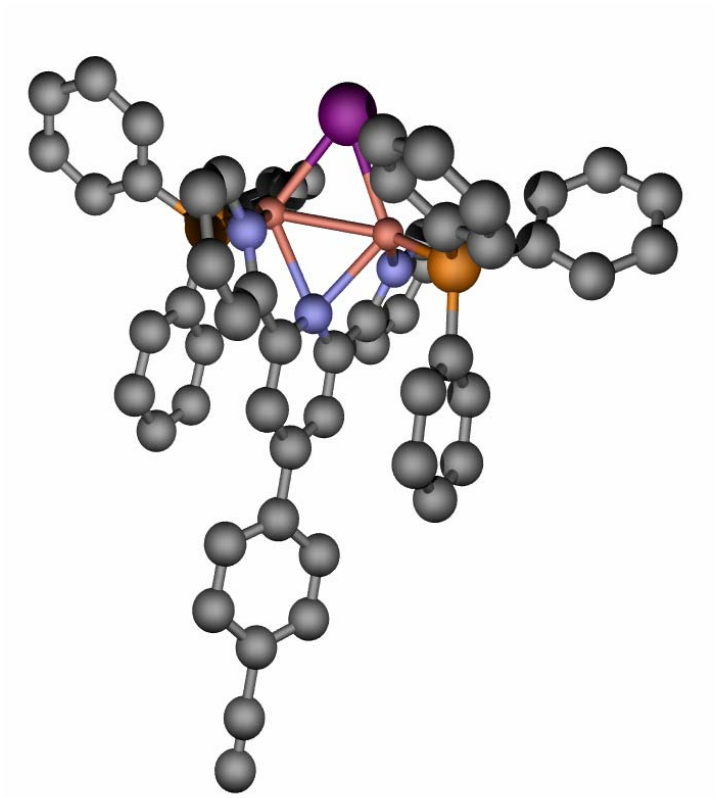

Figure 3.8: Structure of the cation $[Cu_2(PPh_3)_2(\mu\text{-}I)(\mu\text{-}\mathbf{7})]^+$ from X-ray determination of the iodide salt. Hydrogen atoms have been omitted for clarity.

This result was then investigated further using a stoichiometric amount of copper(I) iodide rather than a catalytic amount and the formation of the same orange precipitate was again observed. This unexpected result suggests that formation of copper(I) complexes is in competition with the formation of platinum(II) complexes and that platinum(II) complex formation only occurs when the tpy ligand is highly soluble. A similar platinum(II) complex, $Pt(\mathbf{7}\text{-}H)_2(PEt_3)_2$, was finally achieved by the use of a THF/DMF/NEt_3 solvent system, however attempts to purify the product by crystallisation from

a saturated solution of the product in CH_2Cl_2 layered with hexane produced the same insoluble orange solid seen in the original reaction and no crystals of the platinum(II) complex. Likewise, the use of $PtI_2(P^nBu_3)_2$ in the reaction with ligand **7** produced similar results though the product was even less soluble than its ethyl counterpart and attempts at purification again produced an insoluble orange solid.

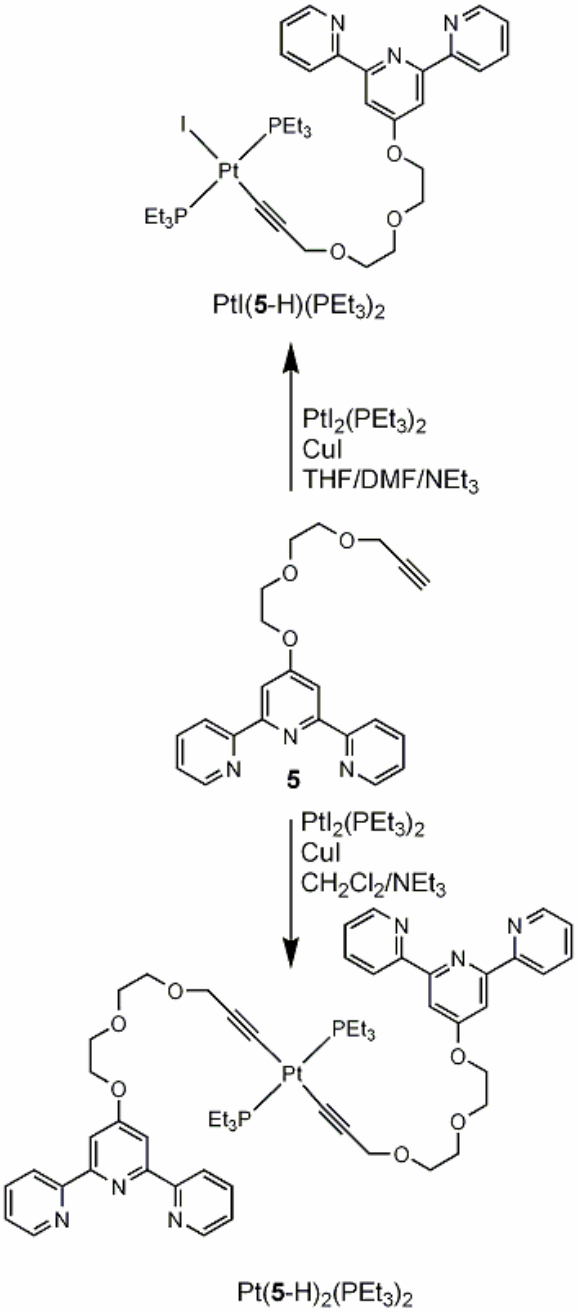

Figure 3.9: Mono and bis Pt(II) complexes formed from the reaction of ligand **5** with $PtI_2(PEt_3)_2$ in different solvent combinations. Using a large excess of ligand **5** facilitates the formation of the bis complex.

Purification of the platinahomoditopic ligands can normally be achieved by column chromatography. The solid phase is alumina and a mixture of CH_2Cl_2 and acetone is used as the eluent. Usually a quantity of 1 % acetone is used which is sufficient to elute the excess ligand first. This can be recovered and can be used again. Increasing the quantity of acetone in the eluent to about 5 % then elutes the product. If there is any mono complex (PtI(**L**-H)$(PR_3)_2$, where **L** is an alkyne substituted tpy ligand) in the mixture, this is eluted after the free ligand but before the bis complex. All tpy containing fractions can be detected by spotting a small amount on an alumina covered TLC plate dipped in an aqueous solution of $FeCl_2.4H_2O$. If the spot appears purple, this confirms the presence of a tpy containing fraction. The product is eluted as the second or third fraction, depending on if there is any of the mono complex present. Once the solvent is removed from the separated fractions, the product is isolated as a white solid or oil in yields ranging from 38 % for Pt(**5**-H)$_2(PEt_3)_2$ to 71 % for Pt(**1**-H)$_2(PEt_3)_2$. In early trial reactions the mono complex PtI(**5**-H)(PEt_3) was isolated from the reaction mixture when the solvent mixture used in the reaction was THF/DMF/NEt_3. Figure 3.9 shows the mono and bis complexes formed during the reaction of ligand **5** with $PtI_2(PEt_3)_2$.

Since the goal of this work is ultimately to synthesise heterometallic macrocycles containing both platinum(II) and iron(II), attempts were also made to take an iron(II) tpy complex bearing pendant alkyne moieties and couple this to a platinum(II) centre using the afore-mentioned methodology. This was attempted using the complex [Fe(**5**$)_2$][PF_6]$_2$, the synthesis and characterisation of this iron(II) complex is discussed in Chapter 5. On workup of the reaction mixture and analysis of the products it was clear to see from the absence of the ^{31}P NMR signal corresponding to the $PtI_2(PEt_3)_2$ starting material as well as loss of the diagnostic triplet signal of the alkyne proton in the ^{1}H NMR that reaction of the platinum(II) centre had taken place. There were several different environments in the ^{31}P NMR spectrum and, from the different J_{PtP} values, it could be seen that these included products with both *cis* and *trans* geometries. Attempts to separate the products by chromatographic methods were made and the ^{1}H NMR spectra of the

fractions obtained were recorded. It was suggested from analysis of the spectra obtained that reaction had taken place at the platinum(II) centre, however, only at the expense of cleavage of the polyethyleneoxy chain. The products observed in the ^{1}H NMR spectra of the fractions were cleavage products and it was concluded therefore that this was not a viable method for the formation of heterometallic macrocycles.[7]

3.3 Characterisation

3.3.1 ^{1}H NMR Spectroscopy

The homoditopic ligands Pt(**1**-H)$_2$(PEt$_3$)$_2$, Pt(**1**-H)$_2$(P^{n}Bu$_3$)$_2$, Pt(**5**-H)$_2$(PEt$_3$)$_2$ and Pt(**7**-H)$_2$(PEt$_3$)$_2$ were characterised by ^{1}H NMR spectroscopy in a $CDCl_3$ solution. Pt(**1**-H)$_2$(PPh$_3$)$_2$ was recorded in C_6D_6 solution due to its poorer solubility in chloroform. The protons in the aromatic region of the spectra all correspond to signals from the tpy ligands discussed in Chapter 2. As with the free tpy ligands, the aliphatic region differs between ligands with the varying numbers of CH_2 groups. The signal, which in the free ligand corresponds to the terminal alkyne functionality, is missing since the alkyne is now bound to the platinum(II) centre. This is a very useful indication of Pt-C bond formation and any free ligand impurities can easily be seen in the ^{1}H NMR spectra. Another useful indication of successful Pt-C bond formation is the signal corresponding to proton e. In the free ligand this appears as a doublet due to coupling to the alkyne proton. In the platinum complex the same signal now appears as a triplet as well as being shifted downfield slightly. Figure 3.10 shows an expansion of the aliphatic region of the proton NMR of Pt(**5**-H)$_2$(PEt$_3$)$_2$. The signal for proton e can be clearly seen as well as a small doublet to higher field which arises from a small amount of free ligand still in the sample. Chemical shifts were assigned using COSY and NOESY experiments although with these techniques alone it was not possible to distinguish between protons c and d. Table 3.2 shows the ^{1}H chemical shifts for the platinahomoditopic ligands synthesised in this chapter, all recorded in

$CDCl_3$ apart from Pt(**1**-H)$_2$(PPh_3)$_2$ and Pt(**7**-H)$_2$(P^nBu_3)$_2$ which were recorded in C_6D_6.

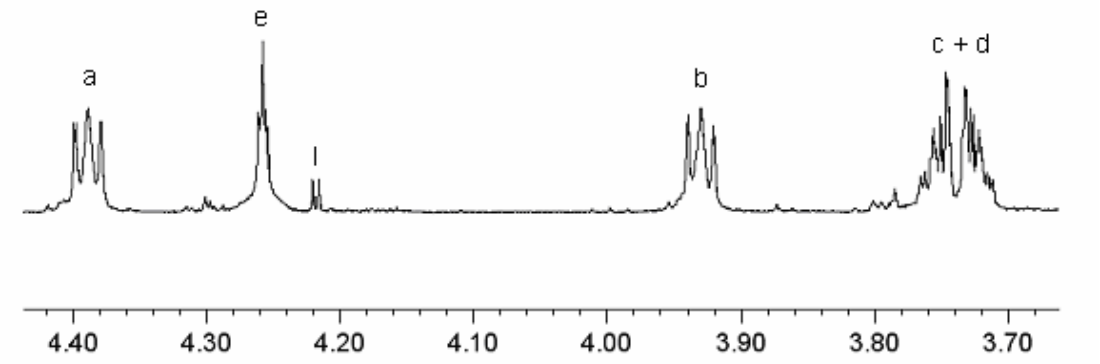

Figure 3.10: Expansion of the 500 MHz ^{1}H NMR of Pt(**5**-H)$_2$(PEt_3)$_2$ in $CDCl_3$ showing the aliphatic region. The peak for the e protons can be clearly seen to be a triplet rather than a doublet as in the free ligand. An impurity arising from the uncoordinated ligand **5** is marked l.

	A3	A4	A5	A6	B3
Pt(**1**-H)$_2$(PEt_3)$_2$	8.58	7.82	7.30	8.65	8.06
Pt(**1**-H)$_2$(P^nBu_3)$_2$	8.58	7.82	7.30	8.65	8.05
Pt(**1**-H)$_2$(PPh_3)$_2$	8.74	7.30	6.70	8.38	8.33
PtI(**5**-H)(PEt_3)$_2$	8.66	7.89	7.37	8.72	8.08
Pt(**5**-H)$_2$(PEt_3)$_2$	8.52	7.84	7.33	8.67	8.03
Pt(**7**-H)$_2$(PEt_3)$_2$	8.73	7.88	7.38	8.67	8.73
Pt(**7**-H)$_2$(P^nBu_3)$_2$	8.77	7.34	6.79	8.61	9.18

	a	b	c	d	e	w	x	y	z
Pt(**1**-H)$_2$(PEt_3)$_2$	4.96							1.83	0.88
Pt(**1**-H)$_2$(P^nBu_3)$_2$	4.94					1.85	1.33	1.25	0.77
Pt(**1**-H)$_2$(PPh_3)$_2$	4.18						6.95		
PtI(**5**-H)(PEt_3)$_2$	4.44	3.98	3.77	3.73	4.29			2.18	1.15
Pt(**5**-H)$_2$(PEt_3)$_2$	4.39	3.93	3.74		4.26			2.03	1.10

	C2	C3

w	x	y	z

Pt(**7**-H)$_2$(PEt$_3$)$_2$	7.41/ 7.81	7.41/ 7.81			2.23	1.28
Pt(**7**-H)$_2$(P^{n}Bu$_3$)$_2$	7.65/ 7.57	7.65/ 7.57	2.19	1.73	1.48	0.96

Table 3.2: ^{1}H Chemical shifts (δ/ppm) of platinahomoditopic ligands synthesised in this chapter. Spectra were recorded at 500 MHz in $CDCl_3$ with the exception of Pt(**1**-H)$_2$(PPh$_3$)$_2$ and Pt(**7**-H)$_2$(P^{n}Bu$_3$)$_2$ which were recorded in C_6D_6.

3.3.2 ^{13}C NMR Spectroscopy

Platinum(II) complexes were also characterised using ^{13}C NMR spectroscopy. Peaks were assigned (see experimental, chapter 6) using HMQC and HMBC techniques. Figure 3.11 shows the HMBC spectrum of Pt(**5**-H)$_2$(PEt$_3$)$_2$ which enables the distinction between protons c and d which was not possible using COSY and NOESY alone. A cross peak can clearly be seen in the HMBC spectrum between proton b and carbon c, and in turn, between carbon c and proton d.

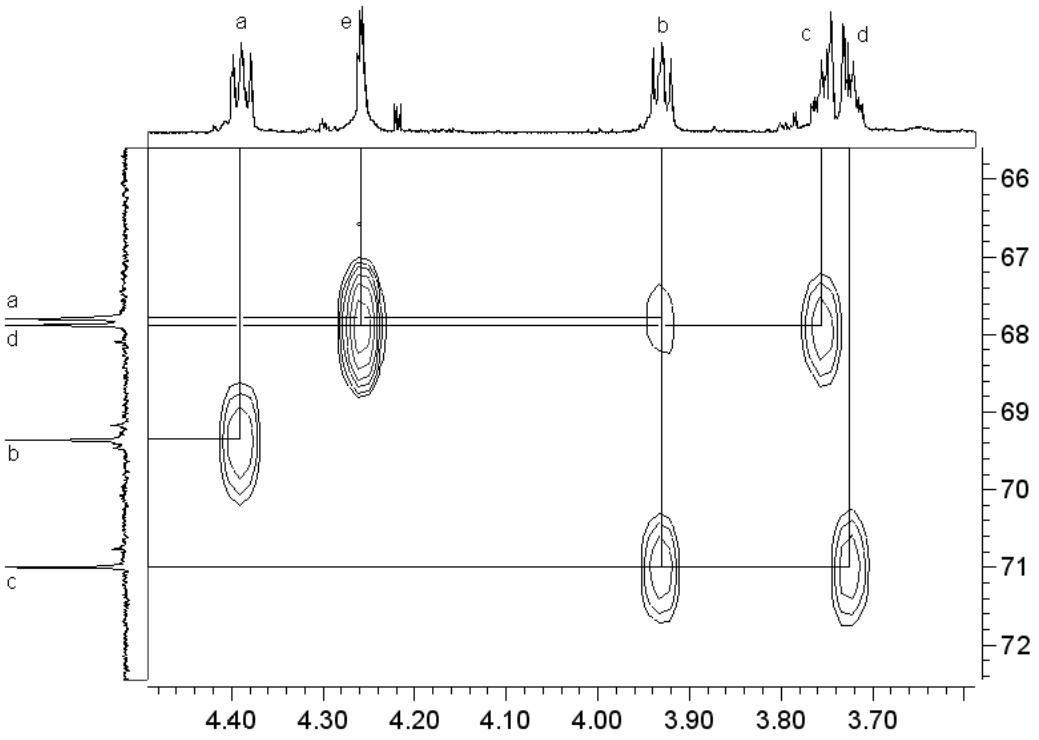

Figure 3.11: Expansion of the aliphatic region of the 500 MHz HMBC spectrum of Pt(**5**-H)$_2$(PEt$_3$)$_2$ in $CDCl_3$.

For the free ligands, as well as the platinum(II) complexes, ^{13}C NMR spectra were proton-decoupled. This means that in the free ligand, most signals appeared as singlets apart from those associated with the phosphine groups. However, in the platinum(II) complexes, one of the alkyne signals appears as a triplet in the ^{13}C spectrum with coupling of around 14 Hz. This is characteristic of the formation of the complex since the coupling arises from coupling of the carbon to the two identical phosphorus atoms and is good evidence that the complex has formed.

Table 3.3 shows the ^{13}C chemical shifts of the platinahomoditopic ligands discussed in this chapter. Spectra were recorded at 500 MHz in $CDCl_3$ solution apart from Pt(**1**-H)$_2$(PPh$_3$)$_2$ which was recorded in C_6D_6. The ^{13}C NMR spectra of Pt(**7**-H)$_2$(PEt$_3$)$_2$ and Pt(**7**-H)$_2$(P^{n}Bu$_3$)$_2$ are not listed in this table since the decomposition in solution to an insoluble orange solid meant that it was not possible to record a clean ^{13}C NMR spectrum in a reasonable time frame.

	A2	A3	A4	A5	A6	B2	B3	B4
Pt(**1**-H)$_2$(PEt$_3$)$_2$	156.6/ 156.2	121.1	136.6	123.5	148.8	156.6/ 156.2	108.1	166.6
Pt(**1**-H)$_2$(P^{n}Bu$_3$)$_2$	157.0/ 156.6	121.7	137.2	124.1	149.3	157.0/ 156.6	108.7	167.1
Pt(**1**-H)$_2$(PPh$_3$)$_2$	152.2/ 157.0	121.2	136.4	123.4	149.3	152.2/ 157.0	109.0	167.4
PtI(**5**-H)(PEt$_3$)$_2$	156.0/ 157.1	121.4	136.8	123.9	149.0	156.0/ 157.1	107.4	167.0
Pt(**5**-H)$_2$(PEt$_3$)$_2$	157.1/ 156.1	121.3	136.8	123.8	149.0	157.1/ 156.1	107.4	167.0

	a	b	c	d	e
Pt(**1**-H)$_2$(PEt$_3$)$_2$	58.7				
Pt(**1**-H)$_2$(P^{n}Bu$_3$)$_2$	58.7				
Pt(**1**-H)$_2$(PPh$_3$)$_2$	58.8				
PtI(**5**-H)(PEt$_3$)$_2$	67.9	69.4	71.0	68.3	61.2
Pt(**5**-H)$_2$(PEt$_3$)$_2$	67.8	69.4	71.0	67.9	60.9

	w	x	y	z	*C*≡CPt	C≡*C*Pt
Pt(**1**-H)$_2$(PEt$_3$)$_2$			15.8	8.0	101.2	104.8
Pt(**1**-H)$_2$(P^{n}Bu$_3$)$_2$	23.4	26.5/ 24.1	26.5/ 24.1	13.7	100.4	104.9
Pt(**1**-H)$_2$(PPh$_3$)$_2$	131.6	135.5	130.3		108.2/ 105.2	108.2/ 105.2
PtI(**5**-H)(PEt$_3$)$_2$			16.5	8.3	94.9	83.3
Pt(**5**-H)$_2$(PEt$_3$)$_2$			16.1	8.2	103.2	101.4

Table 3.3: ^{13}C Chemical shifts of platinahomoditopic ligands synthesised in this chapter. Spectra were recorded at 125 MHz apart from Pt(**1**-H)$_2$(P^{n}Bu$_3$)$_2$ and Pt(**1**-H)$_2$(PPh$_3$)$_2$ which were recorded at 100 MHz. Spectra were run in $CDCl_3$ with the exception of Pt(**1**-H)$_2$(PPh$_3$)$_2$ which was run in C_6D_6.

DEPT spectra were also recorded. This enabled the distinction between different carbon environments since CH_3 and CH environments appear pointing up, CH_2 environments point down and quaternary carbons do not appear at all. The major difference therefore between the free ligand and the platinum complexes in terms of the DEPT spectra is the disappearance of the alkyne CH carbon in the free ligand since this carbon atom is now bound to platinum. Figure 3.12 shows the DEPT spectrum of Pt(**1**-H)$_2$(PEt$_3$)$_2$ recorded at 125 MHz in $CDCl_3$ solution. There are now no peaks in the aliphatic region belonging to the alkyne carbons. Carbons a and y which are both CH_2 environments, are now inverted.

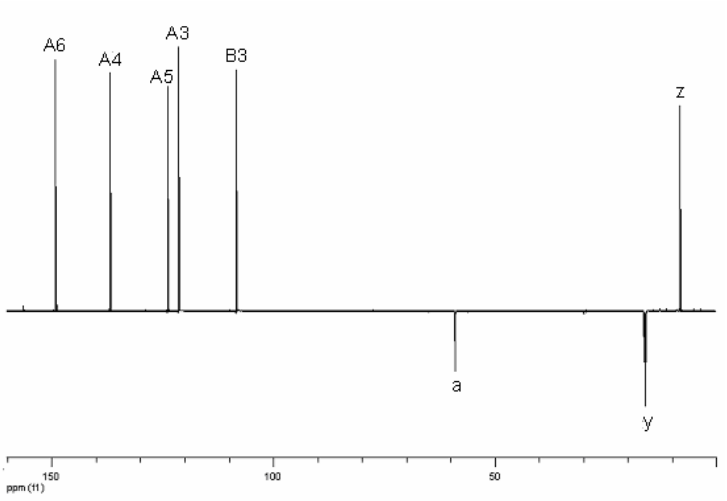

Figure 3.12: DEPT spectrum of Pt(**1**-H)$_2$(PEt$_3$)$_2$ recorded at 125 MHz in $CDCl_3$ solution.

3.3.3 ^{31}P NMR Spectroscopy

Phosphorus (^{31}P) NMR spectroscopy is also a useful tool for characterisation of the complexes. There is clearly a difference between those phosphorus atoms which are uncoordinated and those which are coordinated to platinum(II). ^{195}Pt is an NMR active nucleus with an abundance of 33.8 % which therefore means that satellite signals are observed in the ^{31}P NMR spectra. These arise from coupling of ^{31}P to this 33.8 % of NMR active platinum. The coupling constant between these satellite peaks is a good indication of the coordination geometry at the platinum(II) centre. A coupling constant of around 2300 Hz is characteristic of a *trans* geometry whereas a coupling of around 3000 Hz is characteristic or a *cis* geometry. Figure 3.13 shows the phosphorus NMR spectrum of Pt(**1**-H)$_2$(PEt$_3$)$_2$ with clear satellite peaks arising from coupling between ^{31}P and the small amount of NMR active ^{195}Pt. Coupling here is 2340 Hz which confirms the geometry of the complex is *trans*.

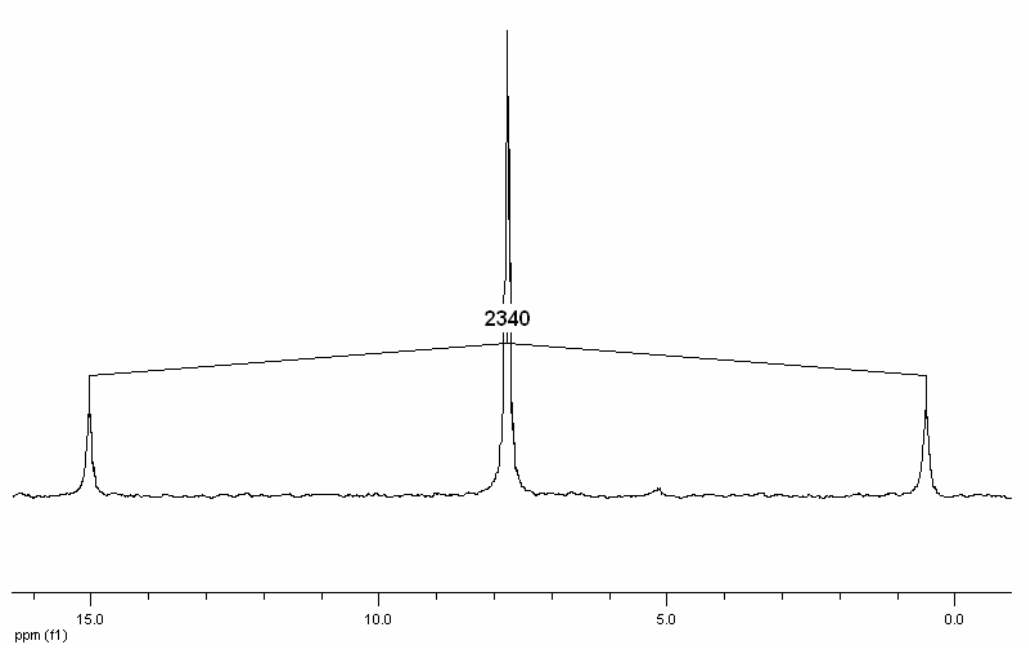

Figure 3.13: 500 MHz ^{31}P NMR of Pt(**1**-H)$_2$(PEt$_3$)$_2$ in $CDCl_3$ showing two satellite peaks with a coupling constant of around 2300 Hz characteristic of trans geometry. Signals are referenced to 85 % H_3PO_4 (aq.) at δ 0 ppm.

Table 3.4 shows the ^{31}P NMR signals referenced to H_3PO_4 (aq., 85 %) of the various platinum(II) complexes synthesised in this chapter.

Compound	δ/ppm
Pt(**1**-H)$_2$(PEt$_3$)$_2$	10.8
Pt(**1**-H)$_2$(P^{n}Bu$_3$)$_2$	-0.4
Pt(**1**-H)$_2$(PPh$_3$)$_2$	20.2
PtI(**5**-H)(PEt$_3$)$_2$	8.8
Pt(**5**-H)$_2$(PEt$_3$)$_2$	7.9
Pt(**7**-H)$_2$(PEt$_3$)$_2$	11.6
Pt(**7**-H)$_2$(P^{n}Bu$_3$)$_2$	0.9

Table 3.4: ^{31}P NMR chemical shifts (δ/ppm) of platinum complexes. All samples were recorded in $CDCl_3$ apart from Pt(**1**-H)$_2$(PPh$_3$)$_2$ and Pt(**7**-H)$_2$(P^{n}Bu$_3$)$_2$ which were run in C_6D_6. All spectra were recorded at 202 MHz apart from Pt(**1**-H)$_2$(P^{n}Bu$_3$)$_2$ and Pt(**7**-H)$_2$(P^{n}Bu$_3$)$_2$ which were recorded at 162 MHz. Signals were referenced to H_3PO_4 (aq., 85 %).

3.3.4 MALDI Mass Spectrometry

The platinahomoditopic ligands synthesised in this chapter were also characterised by MALDI mass spectrometry. A brief overview of the MALDI technique is given in Section 2.3.3. The platinum(II) complexes synthesised here are all neutral species and therefore to appear in the MALDI spectrum they must acquire a charge. This is usually done by loss of an electron or alternatively addition of a proton, sodium or potassium ion. MALDI spectra were recorded for all the complexes and on most occasions the molecular ion, $[M]^+$, was seen. The base peak is often a fragment of the molecule in question. Figure 3.14 shows the MALDI spectrum of Pt(**1**-H)$_2$(PEt$_3$)$_2$ which is typical of this series of complexes. This example clearly shows the molecular ion at m/z 1003 and in this case the base peak corresponds to $[M\text{-(tpy-O)}]^+$. The matrix used to record this particular spectrum was 2,5-dihydroxybenzoic acid.

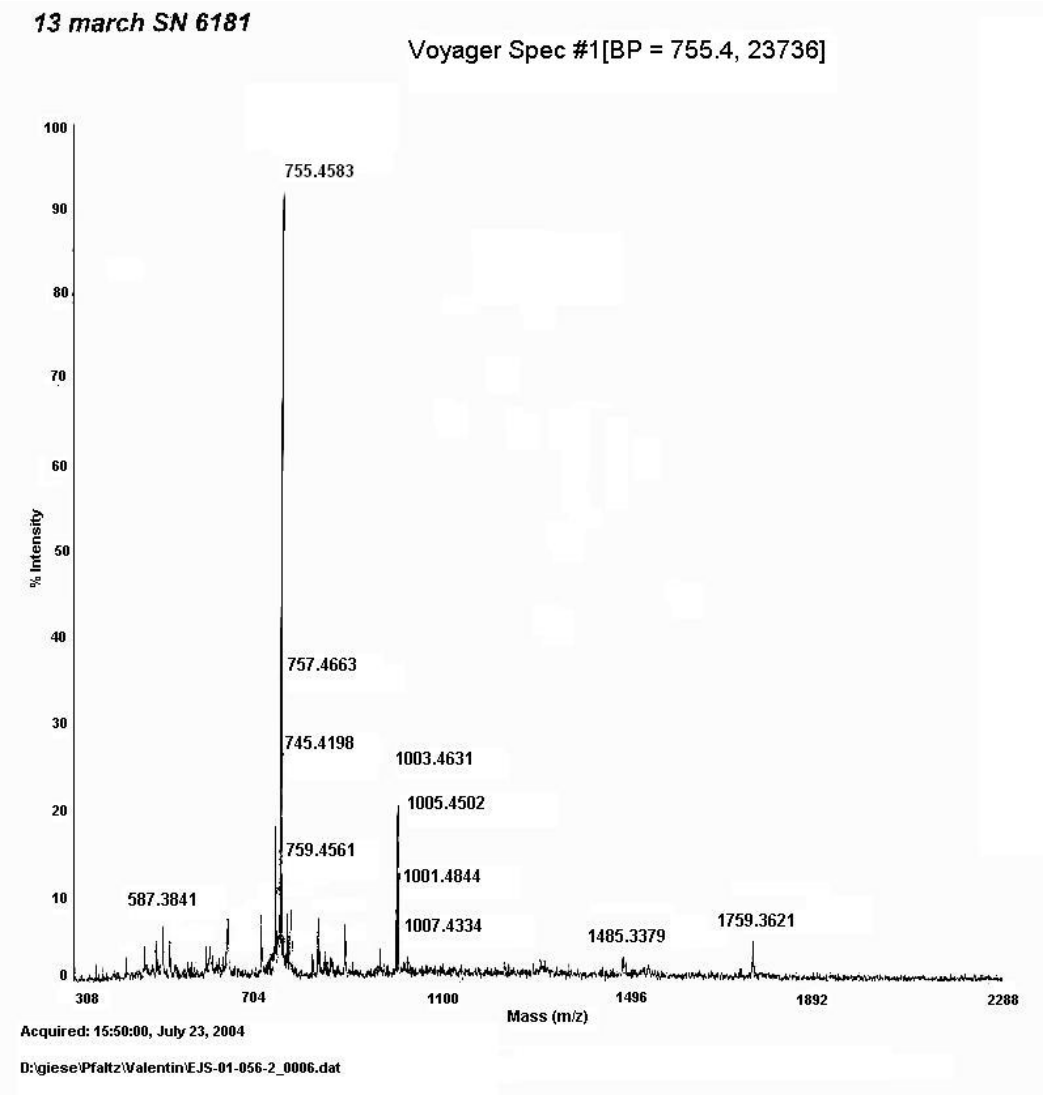

Figure 3.14: MALDI mass spectrum of Pt(**1**-H)$_2$(PEt$_3$)$_2$ recorded with a matrix of 2,5-dihydroxybenzoic acid.

3.3.5 UV/VIS and Luminescence Spectroscopy

UV/VIS and fluorescence spectra of the complexes were recorded in CH_2Cl_2 solution. In the UV/VIS spectra there are usually three bands around 200-350 nm although sometimes one or more of these is not seen or appears only as a shoulder. The lowest energy band arises from the transition between the alkyne π and π* orbitals. The other bands arise from the charge transfer between the alkyne π orbitals and the metal (n+1p) orbitals.[12]

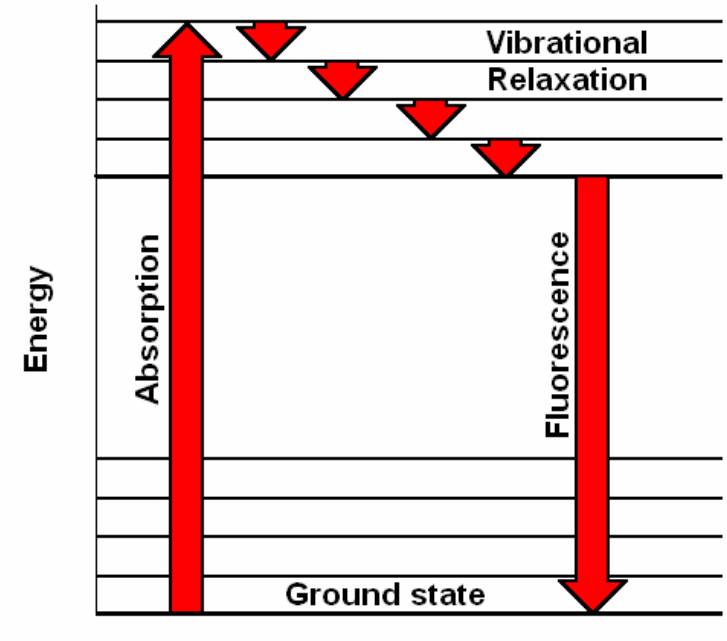

Figure 3.15: The fluorescence process- absorption and vibrational relaxation leads to short lived emission of a photon of lower energy (higher wavelength).

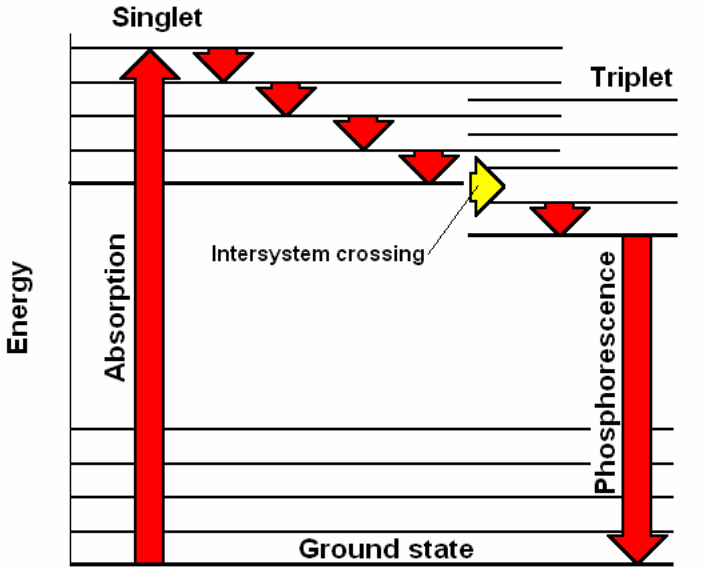

Figure 3.16: The phosphorescence process- absorption and vibrational relaxation followed by intersystem crossing to the triplet state leads to long lived emission of a photon of lower energy (higher wavelength).

When a molecule is irradiated with light of a certain wavelength it absorbs energy and becomes excited. The molecule gradually loses small amounts of energy by colliding with neighbouring molecules which is termed vibrational relaxation. However, to lose the large amount of energy needed to return completely to the ground state, it emits a photon.[13] This process is

called fluorescence and is illustrated in figure 3.15. The wavelength of this emission is what is measured in fluorescence spectroscopy and the irradiation wavelength is chosen based on the UV/VIS absorption spectrum since this gives the wavelength at which maximum absorptions occur. Similar is the process of phosphorescence. In this case emission is much longer lived since a forbidden change in spin state occurs before the photon is emitted. This can be seen in figure 3.16.

In the luminescence spectra of the complexes, a band can usually be seen around 400-450 nm. This is thought to be a fluorescence process due to the $S_1 \rightarrow S_0$ transition.[14] Tables 3.5 and 3.6 show UV/VIS and luminescence data for platinum complexes synthesised in this chapter.

	C	A (ε)	A (ε)	A (ε)
Pt(**1**-H)$_2$(PEt$_3$)$_2$	1.88x10^{-5}	246 (68900)	278 (69550)	
Pt(**1**-H)$_2$(P^{n}Bu$_3$)$_2$	3.75x10^{-5}	254 (19100)	279 (20700)	
Pt(**1**-H)$_2$(PPh$_3$)$_2$	1.30x10^{-5}	246 (70500)	278 (66700)	302 (36600)
PtI(**5**-H)(PEt$_3$)$_2$	4.80x10^{-5}	239 (48000)	276 (40400)	
Pt(**5**-H)$_2$(PEt$_3$)$_2$	3.89x10^{-5}	242 (27450)	277 (27200)	308 (10300))
Pt(**7**-H)$_2$(PEt$_3$)$_2$	9.12x10^{-5}	291 (16700)		
Pt(**7**-H)$_2$(P^{n}Bu$_3$)$_2$	1.11x10^{-5}	233 (73250)	285 (67900)	348 (61500)

Table 3.5: UV/VIS data for platinum(II) complexes recorded in CH_2Cl_2 solution apart from Pt(**1**-H)$_2$(PPh$_3$)$_2$ which was recorded in $CHCl_3$. C (mol dm^{-3}), A (nm), ε (dm^3 mol^{-1} cm^{-1}).

	C	Irradiation/nm	Emission/nm
Pt(**1**-H)$_2$(PEt$_3$)$_2$	1.88x10^{-5}	292	450
Pt(**1**-H)$_2$(P^{n}Bu$_3$)$_2$	3.75x10^{-5}	322	452
Pt(**1**-H)$_2$(PPh$_3$)$_2$	1.30x10^{-5}	325	455
PtI(**5**-H)(PEt$_3$)$_2$	3.89x10^{-5}	300	440
Pt(**5**-H)$_2$(PEt$_3$)$_2$	9.12x10^{-6}	300	396
Pt(**7**-H)$_2$(PEt$_3$)$_2$	1.11x10^{-5}	348	416

Table 3.6: Luminescence data for platinum(II) complexes in CH_2Cl_2 solution apart from Pt(**1**-H)$_2$(PPh$_3$)$_2$ which was recorded in $CHCl_3$. C (mol dm^{-3}), irradiation and emission (nm).

In the case of Pt(**7**-H)$_2$(PEt$_3$)$_2$, the UV/VIS spectrum of this complex differs from those of the complexes with alkyl spacers. The tail of a band can be seen around 200 nm in the spectrum of Pt(**7**-H)$_2$(PEt$_3$)$_2$, but the maximum of this absorption overlaps with the solvent cut-off and therefore was not determined. Shoulders can be seen around 300 nm and 400 nm but the only resolved peak was that at 291 nm. The UV/VIS spectrum of Pt(**7**-H)$_2$(PEt$_3$)$_2$ is shown in figure 2.17.

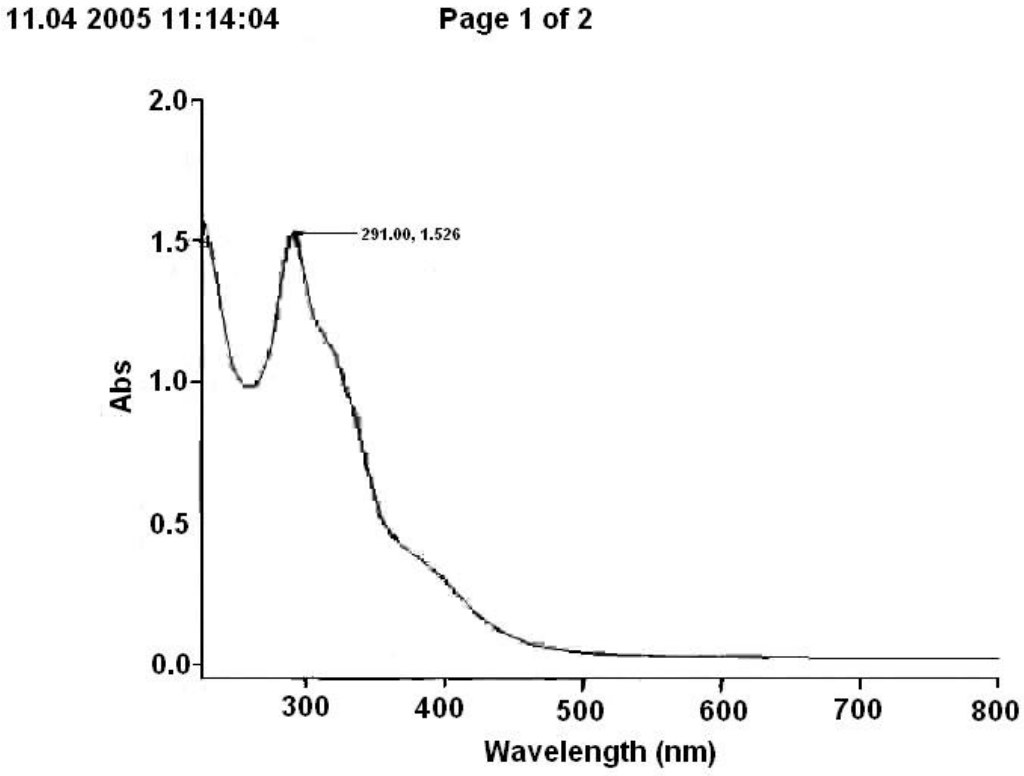

Figure 2.17: UV/VIS spectrum of Pt(**7**-H)$_2$(PEt$_3$)$_2$.

3.4 Crystal Structures

3.4.1 Pt(**1**-H)$_2$(P^{n}Bu$_3$)$_2$[6]

Crystals of Pt(**1**-H)$_2$(P^{n}Bu$_3$)$_2$ suitable for X-ray diffraction were grown from a solution of the product in CH_2Cl_2 layered with hexane. There are no solvent molecules present in the crystal lattice. An ORTEP representation is

shown in figure 3.18 as well as a packing diagram in figure 3.19; crystal data are given in the appendix and selected bond parameters are shown in table 3.7.

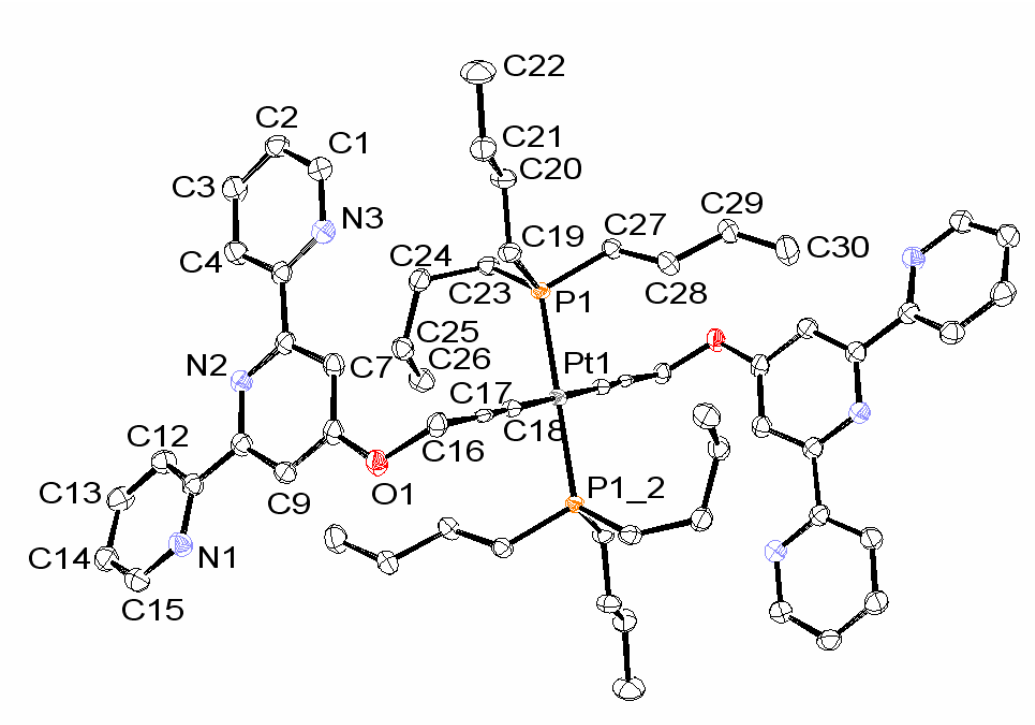

Figure 3.18: ORTEP representation of Pt(**1**-H)$_2$(P^{n}Bu$_3$)$_2$. Crystals were grown from a CH_2Cl_2 solution layered with hexane.

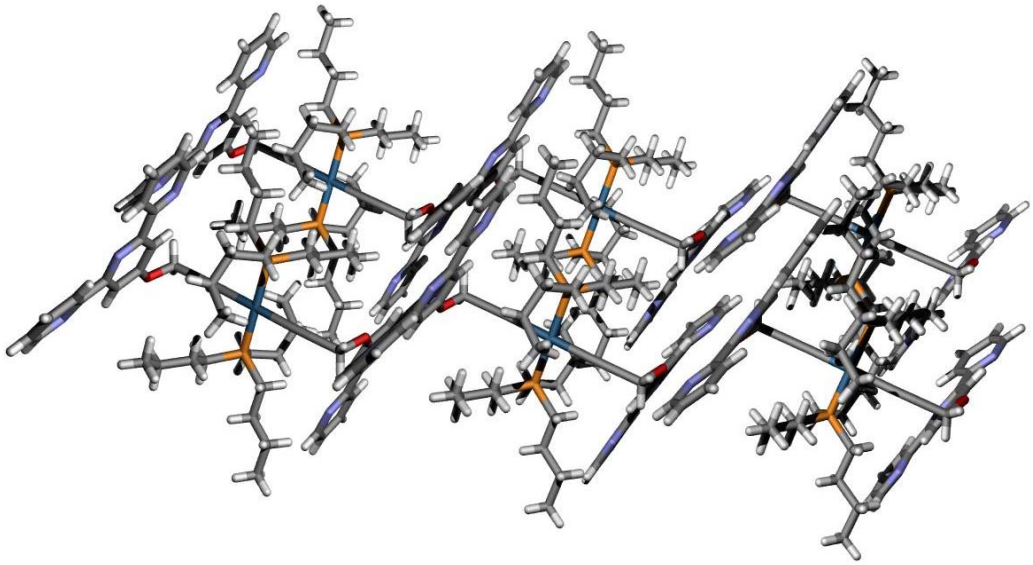

Figure 3.19: Packing diagram of Pt(**1**-H)$_2$(P^{n}Bu$_3$)$_2$. Molecules are stacked in rows and there are no solvent molecules present.

The X-ray crystal structure shows the platinum atom lying on an inversion centre. The molecule shows square planar geometry as is expected for a d^8 Pt(II) complex. The *trans* configuration is consistent with the coupling constants seen in the ^{31}P NMR spectrum.

There is no π-stacking between the tpy rings in the solid state and rows of molecules are held together by several hydrogen bonds. The first hydrogen bond forms between N1 on one molecule and H16 of the molecule in the next row. The second hydrogen bond forms between H9 on the first molecule and O1 of the second. This continues with bonds between O1 and H9 as well as C16 and N1, in a symmetrical arrangement. The tpy rings are not quite planar and have torsion angles of 15.6(2) Å and 3.5(2) Å respectively (defined in table 3.7).

Bond	Distance/Å	Bond	Distance/Å
Pt1-P1	2.2960(4)	Pt1-C18	2.0233(19)
C17-C-18	1.099(3)	C16-C17	1.542(2)
O1-C16	1.455(2)	C8-O1	1.357(2)

Bonds	Angle/deg.	Bonds	Angle/deg.
P1-Pt1-P1_2	179.995	C18-Pt1-C18_2	179.994
P1-Pt1-C18	92.67(5)	P1-Pt1-C18_2	87.33(5)
C17-C18-Pt1	177.55(16)	C16-C17-C18	175.70(18)
O1-C16-C17	111.92(14)	C8-O1-C16	117.35(14)

N1-C11-C10-N2	15.6(2)	N2-C6-C5-N3	3.5(2)

Table 3.7: Selected bond lengths (Å), angles (˚) and torsion angles (˚) for Pt(**1**-H)$_2$(P^{n}Bu$_3$)$_2$.

This compound has a similar structure to a square planar platinum(II) complex made in the group of Ziessel.[15] In the literature complex there is no spacer between the tpy and the alkyne, the alkyne is directly attached to the tpy, whereas in the compound above the presence of an O-CH_2 spacer between the tpy and the alkyne makes the complex above slightly more

flexible. Bond lengths are similar between the two compounds and so are the bond angles.

3.4.2 Pt(**1**-H)$_2$(PPh$_3$)$_2$.2C$_6$H$_6$[6]

Crystals of Pt(**1**-H)$_2$(PPh$_3$)$_2$.2C$_6$H$_6$ were grown from a solution in benzene. An ORTEP representation of the structure is shown in figure 3.20. As with the R = Bu complex, the platinum(II) lies on an inversion centre. The complex is square planar and has a *trans* geometry which agrees with the coupling constant seen in the ^{31}P NMR spectrum. There are slight torsion angles between the tpy rings of 5.1(5) Å and 3.0(4) Å respectively (defined in table 3.8). Selected bond lengths and angles are shown in table 3.8 and crystal data is given in the appendix.

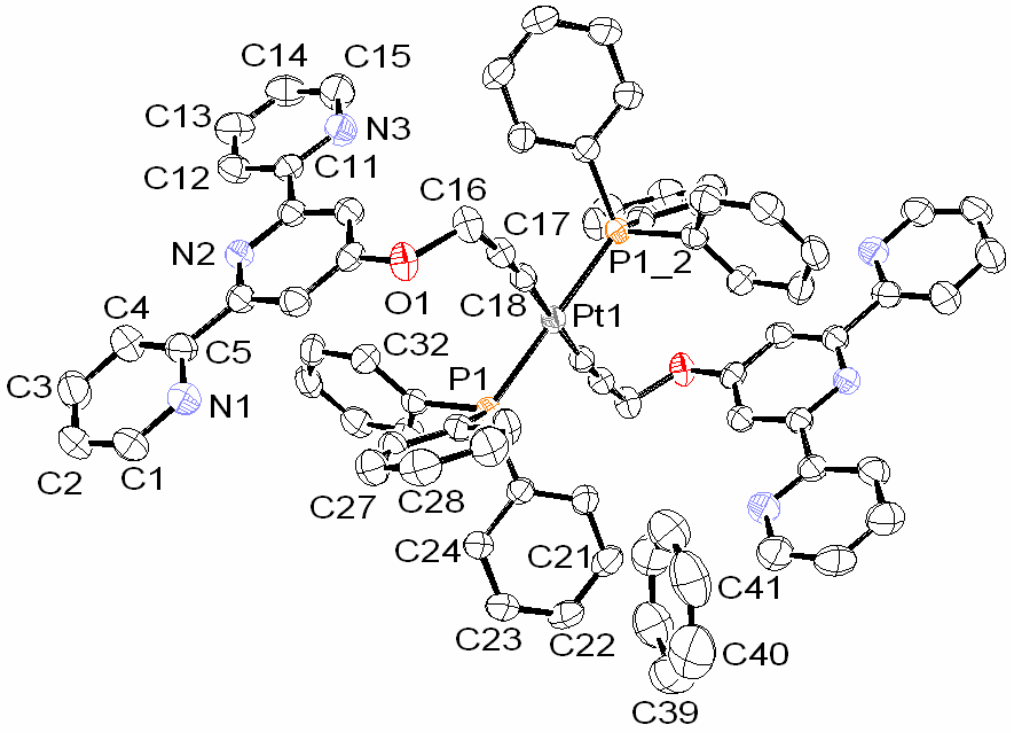

Figure 3.20:ORTEP representation of Pt(**1**-H)$_2$(PPh$_3$)$_2$.2C$_6$H$_6$ with one solvent molecule shown. Crystals grown from a solution of the compound in C$_6$H$_6$.

Molecules of Pt(**1**-H)$_2$(PPh$_3$)$_2$ are stacked in columns. In this structure there are benzene solvent molecules present and these can be seen in the

packing diagram (figure 3.21). Solvent molecules are stacked in columns which separate the columns of Pt(**1**-H)$_2$(PPh$_3$)$_2$. There are no π-stacking interactions in the unit cell due to the fact that the pyridine rings are offset from each other.

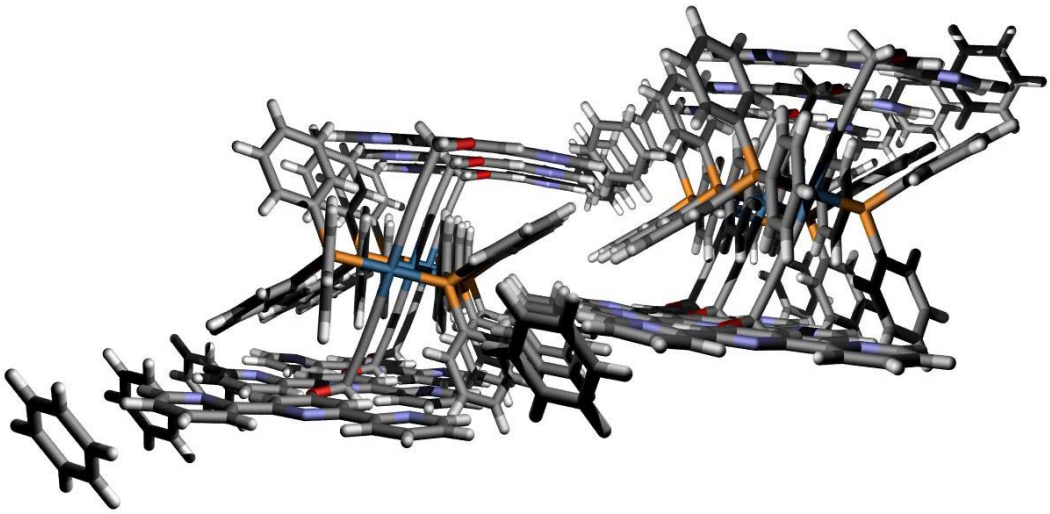

Figure 3.21: Packing of Pt(**1**-H)$_2$(PPh$_3$)$_2$. Molecules are arranged in rows separated by columns of benzene solvent molecules.

Bond	Distance/Å	Bond	Distance/Å
Pt1-P1	2.3175(10)	Pt1-C18	1.993(5)
C17-C-18	1.210(7)	C16-C17	1.452(7)
O1-C16	1.449(6)	C8-O1	1.364(6)

Bonds	Angle/deg.	Bonds	Angle/deg.
P1-Pt1-P1_2	180.00	C18-Pt1-C18_2	180.00
P1-Pt1-C18	89.07(13)	P1-Pt1-C18_2	90.93(13)
C17-C18-Pt1	176.5(4)	C16-C17-C18	175.8(5)
O1-C16-C17	112.7(4)	C8-O1-C16	117.6(3)

N1-C5-C6-N2	5.1(5)	N2-C10-C11-N3	3.0(4)

Table 3.8: Selected bond lengths (Å), angles (˚) and torsion angles (˚) for Pt(**1**-H)$_2$(PPh$_3$)$_2$.

3.4.3 $[Cu_2(PPh_3)_2(\mu\text{-}I)(\mu\text{-}\mathbf{7})]I$[11]

Crystals of $[Cu_2(PPh_3)_2(\mu\text{-}I)(\mu\text{-}\mathbf{7})]I$ were grown from a saturated solution of the compound in CH_2Cl_2 layered with hexane. An ORTEP representation is shown in figure 3.22 and the packing of the molecules is shown in figure 3.23. There is a significant torsion of the tpy of 25.2(5) ° (defined in table 3.9) due to the coordination to two copper atoms. Selected bond parameters are shown in table 3.9 and crystal data is given in the appendix.

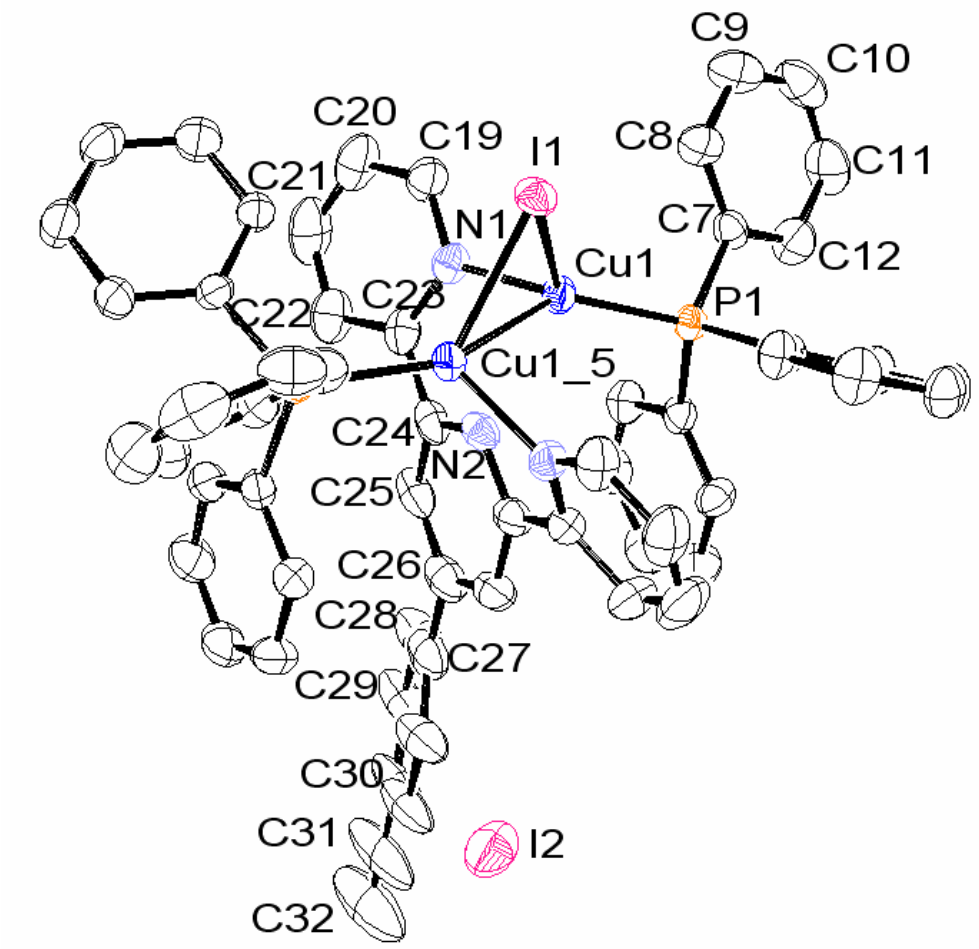

Figure 3.22: ORTEP representation of $[Cu_2(PPh_3)_2(\mu\text{-}I)(\mu\text{-}\mathbf{7})]I$ grown from a saturated solution of the compound in CH_2Cl_2 layered with hexane.

The complex $[Cu_2(PPh_3)_2(\mu\text{-}I)(\mu\text{-}\mathbf{7})]I$ is symmetrical about a C_2 axis running through the length of the molecule from I1 to C32. It is also chiral since the tpy unit has a helical twist about it and crystallises in the chiral

space group $C222_1$. This means that the molecule has resolved itself on crystallisation, rather than crystallising as a racemate.

The copper atoms have approximately tetrahedral coordination with a Cu-Cu bond of length 2.6508(8) Å. The iodide counterion, I2, is located at a distance of 3.377 Å from C28 of one molecule as well as 2.923 Å from C32 of another molecule.

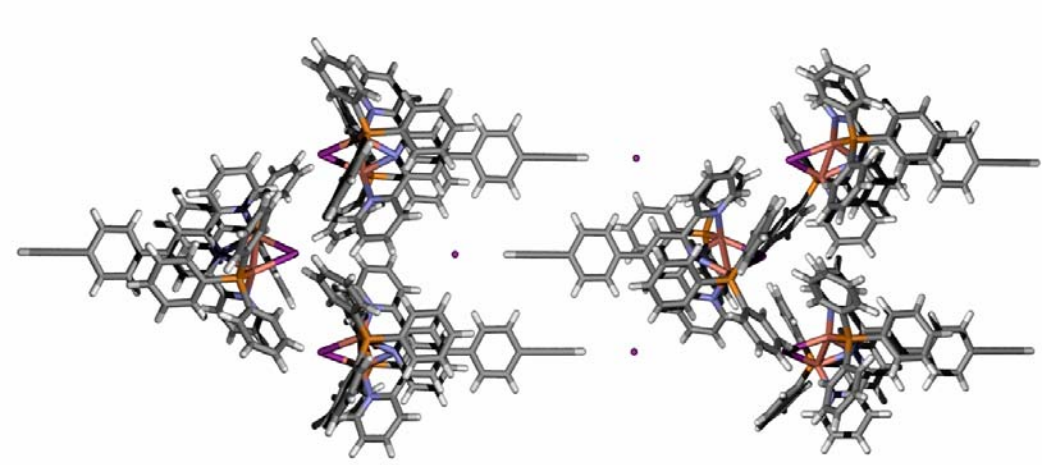

Figure 3.23: Packing of $[Cu_2(PPh_3)_2(\mu\text{-}I)(\ \mu\text{-}\mathbf{7})]I$.

Bond	Distance/Å	Bond	Distance/Å
Cu1-Cu1_5	2.6508(8)	Cu1-N1	2.019(3)
Cu1-P1	2.1975(9)	Cu1-I1	2.6216(5)
C26-C27	1.521(8)	C30-C31	1.526(10)
C31-C32	1.143(8)		

Bonds	Angle/deg.	Bonds	Angle/deg.
Cu1-I1-Cu1_5	60.74(2)	I1-Cu1-Cu1_5	59.631(10)
I1-Cu1-P1	124.08(3)	I1-Cu1-N1	104.39(9)
I1-Cu1-N2	114.59(5)	Cu1_5-Cu1-N1	91.13(9)

N1-C23-C24-N2	25.2(5)

Table 3.9: Selected bond lengths (Å), angles (˚) and torsion angles (˚) for $[Cu_2(PPh_3)_2(\mu\text{-}I)(\mu\text{-}\mathbf{7})]I$.

3.5 Conclusion

In this chapter the synthesis of several platinahomoditopic ligands has been discussed. These molecules have been fully characterised using standard spectroscopic techniques and their electronic and luminescence properties have been recorded. X-ray crystal structures have been obtained for some complexes and these have been discussed.

3.6 References

[1] V. W.-W. Yam, *Acc. Chem. Res.*, 2002, **35**, 555.

[2] U. Belluco, R. Bertani, R. A. Michelin and M. Mozzi, *J. Organomet. Chem.*, 2000, **600**, 37.

[3] K. M.-C. Wong, C.-K. Hui, K.-L. Yu and V. W.-W. Yam, *Coord. Chem. Rev.*, 2002, **229**, 123.

[4] C. A. Tolman, *Chem. Rev.*, 1977, **77**, 313.

[5] K. Sonogashira, T. Yatake, Y. Tohda, S. Takahashi and N. Hagihara, *J. Chem. Soc. Chem. Comm.*, 1977, 291.

[6] J. E. Beves, E. C. Constable, C. E. Housecroft, M. Neuburger, S. Schaffner and E. J. Shardlow, *Dalton Trans.*, 2007, in press.

[7] E. C. Constable, C. E. Housecroft, M. Neuburger, S. Schaffner and E. J. Shardlow, *Inorg. Chim. Acta*, 2007, in press.

[8] A. Del Pra and G. Zanotti, *Inorg. Chim. Acta*, 1980, **39**, 137.

[9] A. Sebald, C. Stader, B. Wrackmeyer and W. Bensch, *J. Organomet. Chem.*, 1986, **311**, 233.

[10] A. Sebald, B. Wrackmeyer and W. Beck, *Z. Naturforsch.,* 1983, **B38**, 45.

[11] E. C. Constable, C. E. Housecroft, M. Neuburger, S. Schaffner and E. J. Shardlow, *Inorg. Chem. Comm.*, 2005, **8**, 743.

[12] U. Belluco, R. Bertani, R. A. Michelin and M. Mozzon, *J. Organomet. Chem.*, 2000, **600**, 37.

[13] P. W. Atkins, *The Elements of Physical Chemistry 2nd Ed.*, Oxford University Press, 1999.

[14] T. J. McKay, J. A. Bolger, J. Staromlynska and J. R. Davy, *J. Chem. Phys.*, 1998, **108**, 5537.

[15] A. Harriman, M. Hissler, R. Ziessel , A. De Cian and J. Fisher, *J. Chem. Soc. Dalton Trans.*, 1995, 4067.

Chapter 4 Gold(I) Alkynyl Complexes

4.1 Gold(I) Alkynyl Complexes

Having investigated platinum(II) alkynyl complexes as potential precursors to supramolecular macrocycles, an obvious extension of the methodology was to use gold(I) as an alternative to platinum(II). Gold(I) alkynyl complexes are well known in the literature for their luminescence properties which is thought arise due to their Au…Au interactions.[1,2] These interactions are also very useful in supramolecular chemistry since they play an important part in the self assembly of gold(I) complexes in the solid state.[3,4,5,6] It has also been shown that luminescence is dependent on the ligand used[7] and so the investigation of gold(I) complexes of alkyne functionalised tpy ligands as luminescent materials is particularly important.

Gold(I) complexes have been studied as luminescent sensors[8] where the luminescence properties of the complex vary on further coordination of a metal at a remote site. This is something which could in theory apply to the gold(I) systems discussed in this chapter since the presence of pendant tpy moieties means there is a site available for coordination which could then alter the luminescence properties of the whole complex.

Due to time limitations only a brief investigation of some gold(I) complexes was possible and preliminary results are presented in this chapter. It was not possible to investigate all the ligands discussed in Chapter 2 in reactions with gold(I) and it may be that the resulting luminescence of these potential complexes would be different depending on the ligand used. The numbering scheme for complexes discussed in this chapter is shown in figure 4.1.

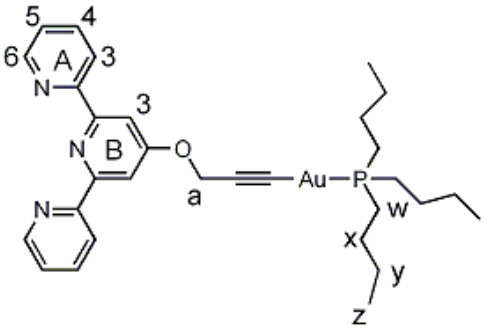

Au(**1**-H)(P^nBu_3)

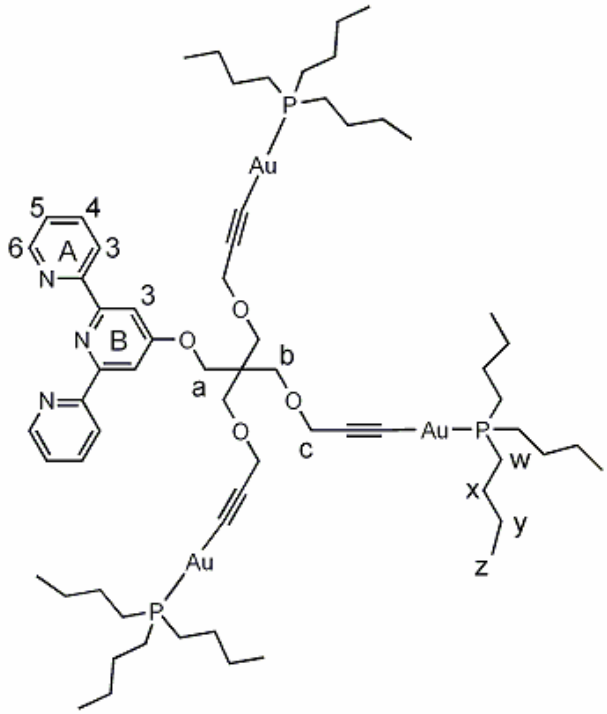

(AuP^nBu_3)$_3$(**12**-3H)

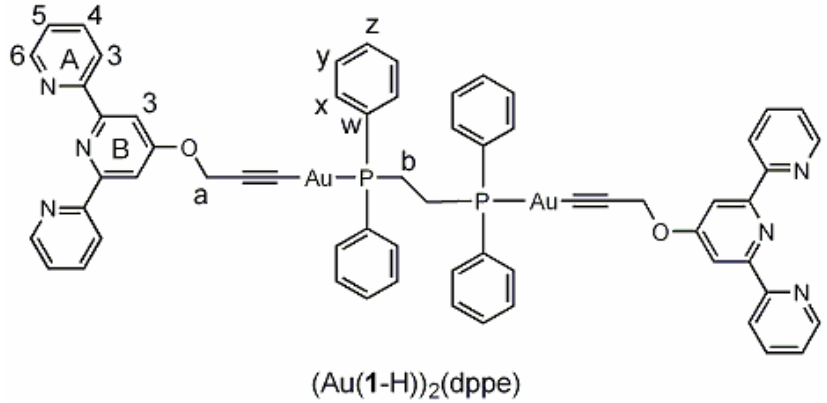

(Au(**1**-H))$_2$(dppe)

Figure 4.1: Numbering scheme for gold(I) complexes discussed in this chapter.

4.2 Synthesis of Gold(I) Alkynyl Complexes

The synthesis of these gold(I) complexes proceeded using the same method as that used for platinum(II). A base, in this case NEt_3, is used to deprotonate the alkyne, CuI is used as a catalyst and a gold(I) chloride complex is used as the starting material. As is the case for a large number of literature gold acetylide complexes, [2,6,9,10,11] a phosphine is used as the auxiliary ligand. The main difference between gold(I) and platinum(II) is that while platinum(II) complexes are of square planar geometry, gold(I) complexes are usually linear.[12]

In order to create a homoditopic ligand from a gold(I) complex it is therefore necessary to use a chelating phosphine in order to connect two gold(I) atoms together, thus providing the possibility for two tpy moieties, and this has the further possibility that the chelating phosphine used will bring the gold(I) atoms closer together, thus increasing the likelihood that Au…Au interactions will be present.[13] Figure 4.2 shows the synthesis of gold(I) containing homoditopic ligands by this method. Various different length spacers can be used for the chelating phosphine. These can be simple alkyl chains or, alternately, something more complicated such as bis(diphenylphosphino)ferrocene.

Most of the gold(I) complexes discussed in this chapter are synthesised using ligand **1** although one other ligand (**12**) was also used as a trial for multicentred gold(I) alkyne complexes (see figure 4.3). It was felt that since ligand **12** had three alkyne moieties, it was a suitable model ligand for the formation of multimetal systems. The successful formation of the compounds Au(**1**-H)(P^nBu_3) and (AuP^nBu_3)$_3$(**12**-3H) demonstrates that this method for the coupling of gold(I) with alkynes is viable. The same method can in theory be used with the other tpy ligands discussed in Chapter 2 although time restraints did not permit investigation of these in this thesis.

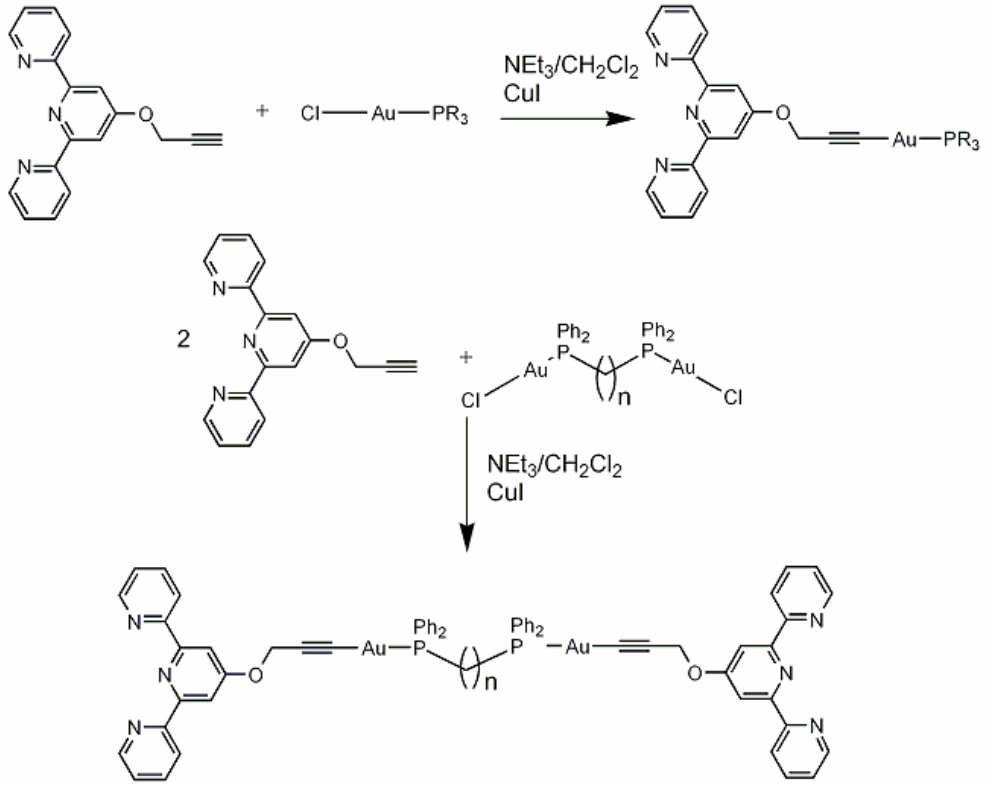

Figure 4.2: Synthesis of gold(I) alkyne complexes containing both mono- and bis-phosphine ligands.

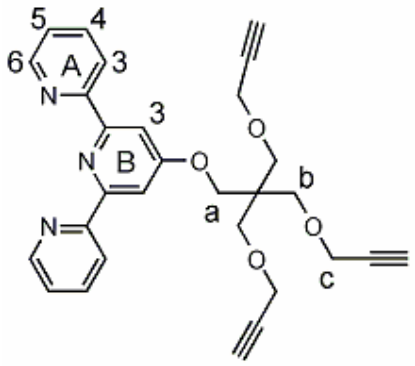

Figure 4.3: Ligand **12** was thought to be a suitable test molecule for the formation of multicentred gold(I) alkynyl complexes.

A trial of the proposed methodology was carried out using the simple gold(I) complex, $ClAu(P^nBu_3)$,[14] which has a monodentate phosphine. It was thought that this would prove the general concept and if successful, could then be extended to more complicated complexes. The synthesis of this first gold(I) complex was straightforward. Ligand **1** was reacted with $ClAu(P^nBu_3)$ using CuI as a catalyst in a 50:50 mixture of NEt_3 and CH_2Cl_2. The reaction

proceeded as with the platinum(II) analogues and a precipitate formed. The product was purified by column chromatography using 1 % acetone in CH_2Cl_2 as the eluent. The single fraction was shown to contain a tpy binding unit by spotting a small amount of eluent onto an alumina covered TLC plate followed by dipping this in an aqueous solution of $FeCl_2.4H_2O$. The presence of a purple colour was indicative of a tpy moiety. This fraction was collected and the solvent removed to give Au(**1**-H)(P^nBu_3) in a yield of 45 %.

The same method was used in the reaction of ligand **12** with ClAu(P^nBu_3). This also proceeded to give a precipitate which was collected by filtration. This was purified by column chromatography on alumina using 1 % acetone in CH_2Cl_2 as the eluent. The only fraction was shown to contain a tpy moiety as above and this fraction was collected and the solvent removed, although the yield was significantly lower than in the previous reaction (8 %). The compound $(AuP^nBu_3)_3$(**12**-3H) was characterised. Single crystals were grown from acetonitrile solution.

Characterisation of Au(**1**-H)(P^nBu_3) and $(AuP^nBu_3)_3$(**12**-3H) by various methods, including ^1H, ^{13}C and ^{31}P NMR spectroscopy, mass spectrometry, IR spectroscopy and X-ray crystallography showed that there had indeed been formation of the gold-carbon bond and that complexation had been successful. Importantly, there was a change in the chemical shift in the ^{31}P NMR spectrum as well as loss of the signal corresponding to the alkyne proton in the ^1H NMR spectrum. Mass spectrometry showed peaks arising from the molecular ion in both complexes. The characterisation of both these complexes is discussed in more detail later in the chapter.

Having established that this alkyne coupling was a viable method, investigation of various gold(I) complexes of chelating phosphines was the next step. These chelating phosphines included dppm, dppe, dppf and dpph (figure 4.4). Results from these studies were mixed and the only success was using dppe, where an X-ray crystal structure of the desired product was obtained.

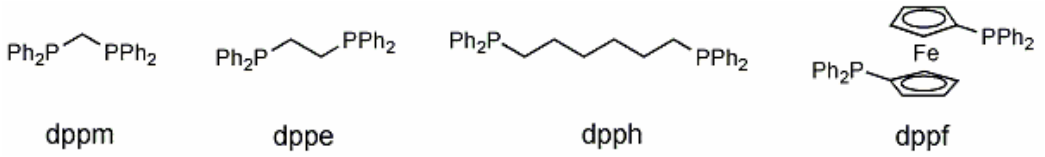

Figure 4.4: Bis-phosphines used in forming ditopic ligands by reaction with gold(I).

Ligand **1** was reacted with $(AuCl)_2$(dppm) using the above method. This produced a mixture of products and attempts at separating this using column chromatography were unsuccessful. Leaving a sample in $CDCl_3$ solution resulted in decomposition of the product. At this point it was decided to continue with the next step, the reaction of the product with Fe(II), since it was felt that attempts at recrystallisation would result in decomposition. The result of the addition of $FeCl_2.4H_2O$ to the mixture produced from the reaction of **1** with $(AuCl)_2$(dppm) was still a mixture, chromatography was once again unsuccessful, however attempts at crystallisation did produce a colourless crystal in a purple solution. This was confirmed by X-ray crystallography to be a $[(dppm)_2Au_3Cl_2][PF_6]$ cluster (shown schematically in figure 4.5). The structure is discussed in Section 4.4.3.

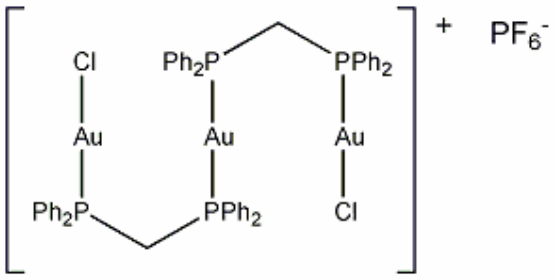

Figure 4.5: Gold(I) dppm complex formed during the attempted reaction of **1** with dppm.

The reaction of ligand **1** with $(ClAu)_2$(dppf)[15] (figure 4.6) was also problematic. The solid obtained from the reaction gradually became purple in colour. This indicated coordination of the tpy unit to the Fe(II), but the only source of Fe(II) in the reaction mixture was the ferrocene unit and it seems rather unlikely that tpy can remove Fe(II) from the ferrocenyl moiety. There were problems with solubility, and purification by chromatography was unsuccessful. Due to the low solubility, crystallisation was not an option and it was again decided to continue and react the mixture with Fe(II). A mixture

was obtained which was not possible to separate by chromatography and crystallisation was attempted. One colourless crystal was suitable for X-ray diffraction and this proved to be the original starting material, $(ClAu)_2(dppf)$.[16,17,18]

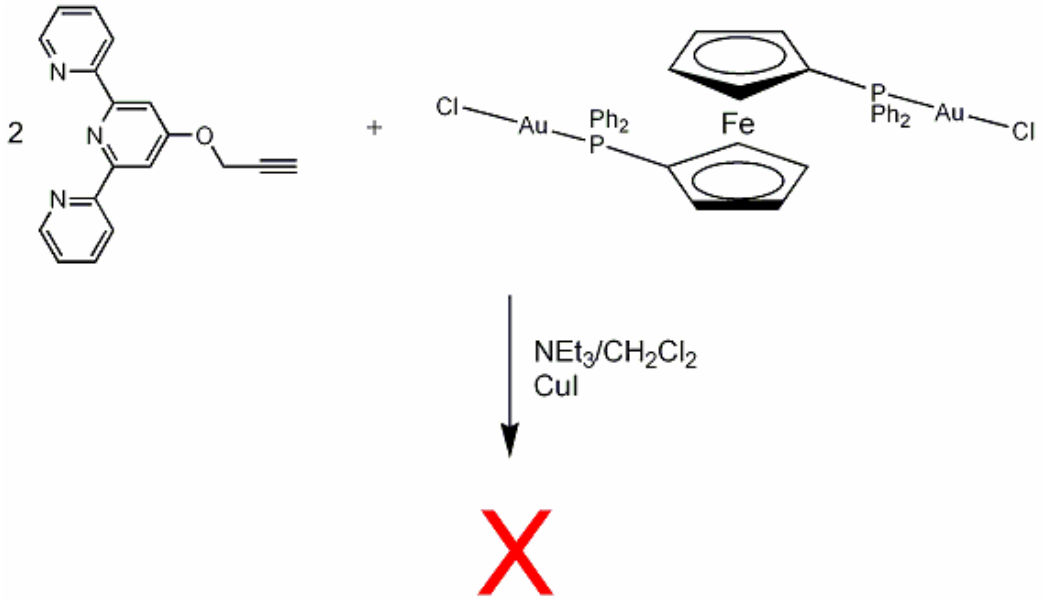

Figure 4.6: The reaction of ligand **1** with $(ClAu)_2(dppf)$ was unsuccessful.

The reaction of ligand **1** with $(ClAu)_2(dpph)$ was also unsuccessful. On first attempt, no reaction occurred at all. On repeating the experiment a reaction did occur giving an insoluble black precipitate which was removed from the reaction mixture. After removal of the solvent from the filtrate, NMR spectroscopy showed that there were no signals in the aliphatic region which could correspond to the alkyl spacer of the dpph part of the molecule. The aromatic region of the spectrum showed several overlapping peaks, many of which were broadened, and it was therefore concluded that the reaction had not produced the desired product.

The reaction of $(ClAu)_2(dppe)$[19,20,21] with ligand **1** in the presence of CuI proceeded successfully to produce a precipitate. This precipitate was collected by filtration and purified by column chromatography on alumina using 1 % acetone in CH_2Cl_2 as the eluent. There was only one fraction which was confirmed as having a tpy moiety present by spotting a small

amount of eluent onto an alumina covered TLC plate and then dipping this into an aqueous $FeCl_2.4H_2O$ solution, the presence of a purple colour confirming the presence of the $Fe(II)(tpy)_2$ chromophore. The solvent was removed from this fraction and X-ray quality crystals were grown easily. The structure of the product is discussed later in the chapter.

4.3 Characterisation

4.3.1 ^{1}H NMR Spectroscopy

Gold(I) complexes were characterised using ^{1}H NMR spectroscopy. Complexes were all soluble in $CDCl_3$. It was possible to assign signals based on the ^{1}H NMR spectrum for ligand **1** as well as the relative integrals of the signals. Chemical shifts are shown in table 4.1.

	A3	A4	A5	A6	B3
Au(**1**-H)(P^{n}Bu$_3$)	8.54	7.79	7.26	8.65	8.04
(Au(**1**-H))$_2$(dppe)	8.55	7.78	7.25	8.63	8.06
(AuP^{n}Bu$_3$)$_3$(**12**-3H)	8.55	7.78	7.25	8.66	7.98

	a	b	c
Au(**1**-H)(P^{n}Bu$_3$)	5.01		
(Au(**1**-H))$_2$(dppe)	5.00	1.94	
(AuP^{n}Bu$_3$)$_3$(**12**-3H)	4.30	3.71	4.22

	w	x	y	z
Au(**1**-H)(P^{n}Bu$_3$)	1.67	1.48	1.38	0.87
(Au(**1**-H))$_2$(dppe)		7.56	7.34	
(AuP^{n}Bu$_3$)$_3$(**12**-3H)	1.66	1.50	1.38	0.88

Table 4.1: Table of 400 MHz ^{1}H NMR spectroscopic data for gold(I) complexes in $CDCl_3$. Chemical shifts are shown in δ/ppm. Atom labelling is shown in figure 4.1.

From looking at table 4.1 it can be seen that there is very little difference in chemical shifts of the tpy protons in the three gold(I) complexes. As with the platinum(II) complexes, the loss of the diagnostic signal for the alkyne proton is evidence for the formation of the gold(I) complex. This can be seen in the ^{1}H NMR of (AuP^{n}Bu$_3$)$_3$(**12**-3H) where a small amount of the unreacted tpy ligand can be seen as an impurity in the spectrum, shown in figure 4.7. It is also possible to see that the chemical shifts of the protons do not change much when the alkyne is coordinated to the gold(I) centre. The signal which shifts the most is that of proton c, nearest to the gold(I) centre.

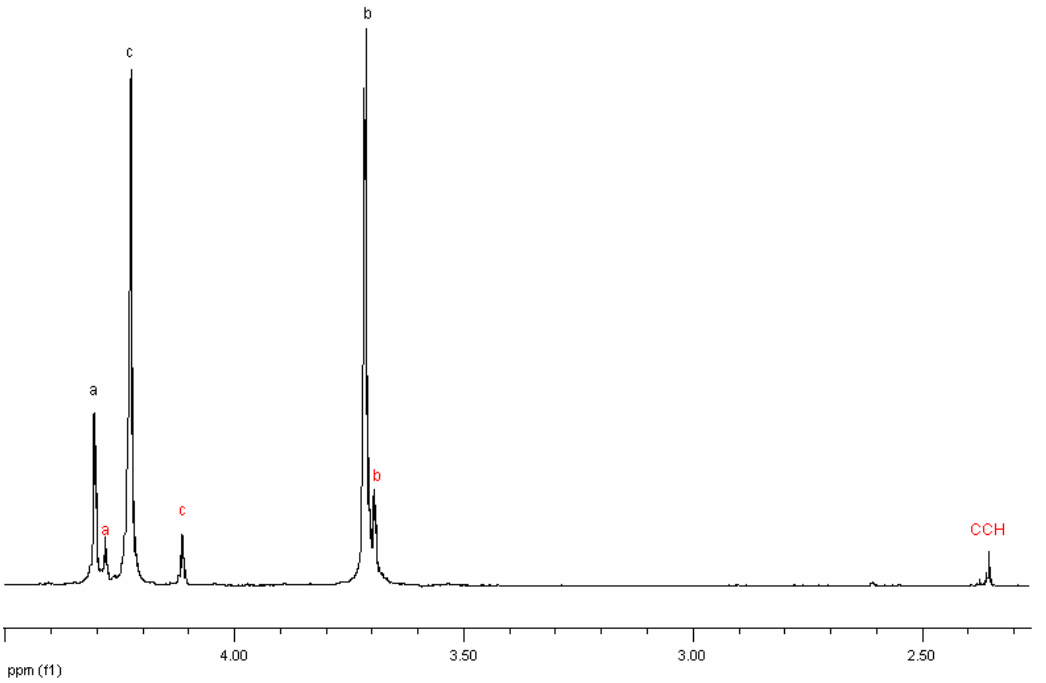

Figure 4.7: Expansion of the 400 MHz ^{1}H NMR spectrum of (AuP^{n}Bu$_3$)$_3$(**12**-3H) in $CDCl_3$ (peaks marked in black). Ligand **12** impurities are marked in red.

4.3.2 ^{13}C NMR Spectroscopy

Gold(I) complexes were also characterised using ^{13}C NMR spectroscopy. It was possible to assign the signals based on comparison with the ^{13}C NMR spectra of ligand **1** and ligand **12** in the cases of Au(**1**-H)(P^{n}Bu$_3$) and (AuP^{n}Bu$_3$)$_3$(**12**-3H). Table 4.2 shows the ^{13}C NMR chemical shifts for the three gold(I) complexes discussed in this chapter.

	A2	A3	A4	A5	A6	B2	B3	B4
Au(**1**-H)(P^nBu_3)	157.4/ 156.7	121.7	137.0	124.0	149.4	157.4/ 156.7	108.2	166.9
$(Au(\mathbf{1}\text{-H}))_2$(dppe)	157.0/ 156.2	121.3	136.7	123.9	149.0	157.0/ 156.2	107.8	166.6
$(AuP^nBu_3)_3$(**12**-3H)	156.6/ 156.4	121.1	136.5	123.3	148.9	156.6/ 156.4	107.8	167.4

	a	b	c
Au(**1**-H)(P^nBu_3)	57.7		
$(Au(\mathbf{1}\text{-H}))_2$(dppe)	57.1	23.7	
$(AuP^nBu_3)_3$(**12**-3H)	68.0	69.3	60.0

w	x	y	z
25.87	24.63	27.58	14.02
128.5	133.3, 132.2, 129.5		
25.4	24.2	27.1	13.6

	C≡CAu	C≡*C*Au	*C*$(CH_2)_4$
Au(**1**-H)(P^nBu_3)	97.2	107.9	
$(Au(\mathbf{1}\text{-H}))_2$(dppe)	97.0	107.5	
$(AuP^nBu_3)_3$(**12**-3H)	Not seen	100.1	44.9

Table 4.2: 100 MHz ^{13}C NMR chemical shifts for gold(I) complexes. NMR spectra were recorded in $CDCl_3$.

4.3.3 ^{31}P NMR Spectroscopy

Gold, unlike platinum, does not have an NMR active nuclei. This has a consequence for the ^{31}P NMR since there are now no satellite peaks present in the ^{31}P spectrum and all peaks appear as singlets. ^{31}P chemical shifts of phosphorus atoms in the gold(I) complexes are given in table 4.3.

Compound	δ/ppm
Au(**1**-H)(P^nBu_3)	25.7
$(Au(\mathbf{1}\text{-H}))_2$(dppe)	36.5
$(AuP^nBu_3)_3$(**12**-3H)	25.8

Table 4.3: 162 MHz ^{31}P NMR spectroscopic data for gold(I) complexes. Chemical shifts are shown in δ/ppm. Signals were referenced to H_3PO_4 (aq., 85 %) δ 0 ppm.

4.3.4 MALDI Mass Spectrometry

Gold(I) complexes were characterised by MALDI mass spectrometry. A brief explanation of the MALDI technique is given in Section 2.3.3. Like their platinum(II) analogues, the gold(I) complexes discussed here are neutral species and need to acquire a charge to appear in the MALDI spectrum.

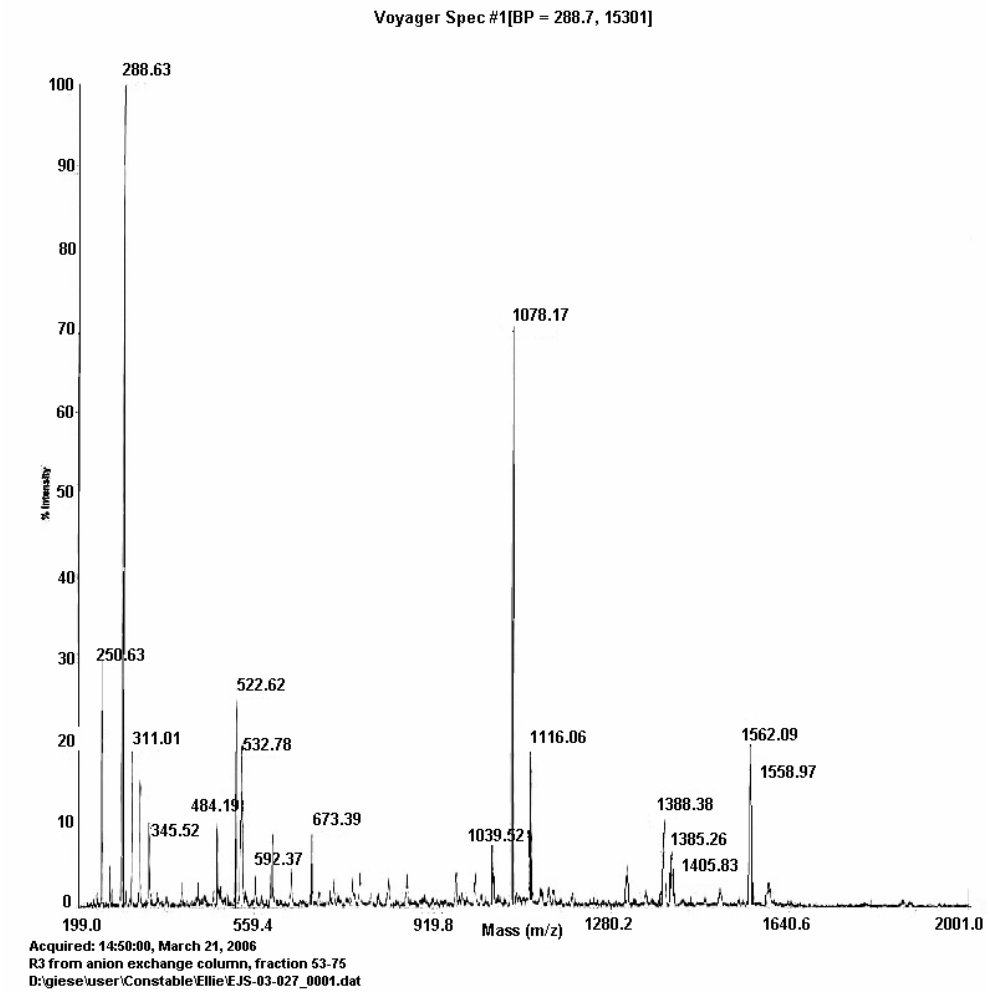

Figure 4.8: MALDI mass spectrum of (Au(**1**-H))$_2$(dppe) run with a matrix of α-Cyano-4-hydroxycinnamic acid of mass 189. Peaks can be seen for $[M - \mathbf{1}]^+$ (1078), $[M - \mathbf{1} + K]^+$ (1116), $[M + Na]^+$ (1388) and $[M + K]^+$ (1405).

The MALDI spectrum of (Au(**1**-H))$_2$(dppe) is shown in figure 4.8 Peaks can be seen for $[M - (\mathbf{1}\text{-H}) + H]^+$ (1078), $[M - (\mathbf{1}\text{-H}) + K]^+$ (1116), $[M + Na]^+$ (1388) and $[M + K]^+$ (1405). The peak at m/z 1562 is of a larger mass than the

product and possibly arises from some kind of aggregate of the product or impurity.

This spectrum as well as those of the other two gold(I) complexes was run with a matrix of α-cyano-4-hydroxycinnamic acid, of Mw 189. The matrix can sometimes appear in the spectrum as an addition to the mass of a molecular ion (for example peaks are often seen for $[M + matrix]^+$) and so it is important to know the mass of the matrix in order to assign the peaks seen in the mass spectrum. The MALDI spectrum of Au(**1**-H)(P^nBu_3) showed peaks for the molecular ion $[M]^+$ (686) as well as $[M + Na]^+$ (707), and the spectrum of $(AuP^nBu_3)_3$(**12**-3H) showed $[M]^+$ (1679), $[M – (P^nBu_3)]^+$ (1477), $[M – 2(P^nBu_3)]^+$ (1274), $[M – 3(P^nBu_3)]^+$ (1078) and $[\mathbf{12}]^+$ (483).

4.3.5 UV/VIS Spectroscopy

The gold(I) complexes synthesised in this chapter were characterised by UV/VIS spectroscopy (table 4.4). A brief outline of this technique is given in Section 3.3.5. In contrast to their platinum(II) analogues, the gold(I) complexes discussed here were non-luminescent. It is thought that Au…Au interactions give rise to luminescence in gold(I) complexes and the observation that the tpy-containing complexes synthesised here were non-luminescent is probably due to the fact that in none of these complexes were there two gold(I) centres in a single molecule in close proximity (~3 Å). Interactions were seen in the solid state between two separate molecules of $(AuP^nBu_3)_3$(**12**-3H) (see Section 4.4.2), but since these interactions are not present in solution this molecule was also non-luminescent.

	C	A (ε)	A (ε)	A (ε)
Au(**1**-H)(P^nBu_3)		247	277	
$(AuP^nBu_3)_3$(**12**-3H)	$2.39x10^{-5}$	249 (106200)	278 (72700)	
$(Au(\mathbf{1}\text{-H}))_2$(dppe)	$4.62x10^{-5}$	233 (55500)	253 (sh) (37900)	277 (30400)

Table 4.4: UV/VIS absorption data for gold(I) complexes recorded in CH_2Cl_2 solution. C (mol dm^{-3}), A (nm), ε ($dm^3\ mol^{-1}\ cm^{-1}$).

4.4 Crystal Structures

4.4.1 Au(**1**-H)(P^nBu_3)

X-ray quality crystals of Au(**1**-H)(P^nBu_3) were grown by slow evaporation of the filtrate from the reaction mixture, the solvent being a 50:50 mixture of NEt_3 and CH_2Cl_2. There were two types of crystal present after a week, the gold complex shown here and ligand **1**. Crystals were separated by eye, the crystals of ligand **1** being large blocks and the crystals of Au(**1**-H)(P^nBu_3) being long needles. An ORTEP representation of Au(**1**-H)(P^nBu_3) is shown in figure 4.9 and a diagram of the packing of the molecules can be seen in figure 4.10. Selected bond parameters are shown in table 4.5 and crystal data are given in the appendix.

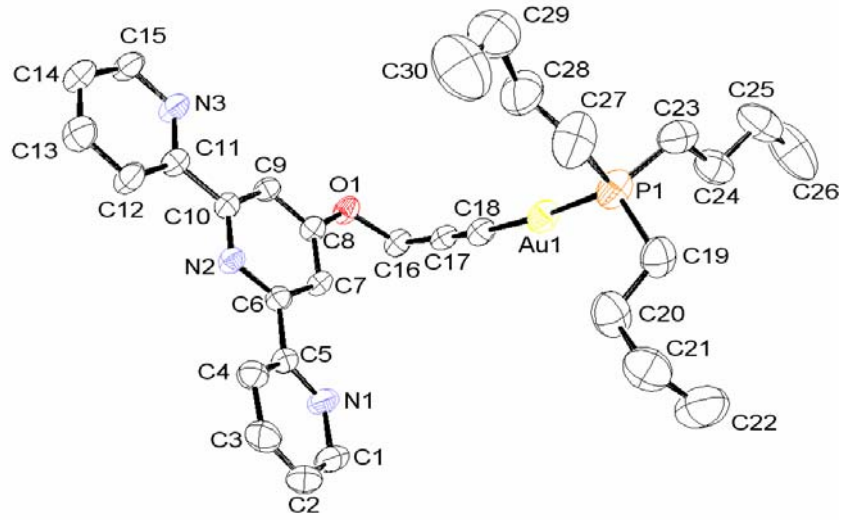

Figure 4.9: ORTEP representation of Au(**1**-H)(P^nBu_3). Crystals were grown by slow evaporation from solution where the solvent was a 50:50 mix of NEt_3 and CH_2Cl_2.

The structure of the molecule is fairly simple. As expected, the alkyne carbon atoms as well as the gold(I) centre are colinear. The Au-C-C vector is not completely straight as would be expected, but rather there is a slight bend and bond angles along this line are typically around 175 ˚ rather than 180 ˚ (defined in table 4.5). There are small torsion angles between the pyridine rings of the tpy of 11.9 and 3.6 ˚ (defined in table 4.5).

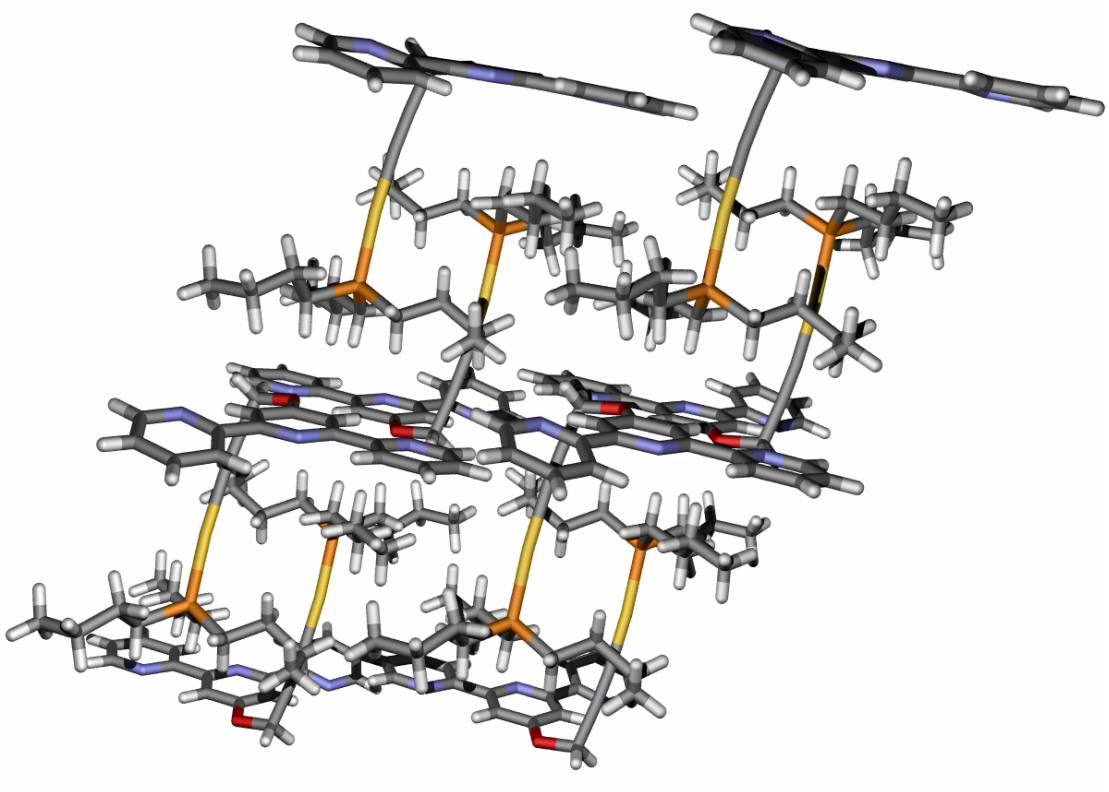

Figure 4.10: Diagram of the packing of Au(**1**-H)(P^{n}Bu$_3$).

Molecules of this simple gold(I) complex are packed such that the tpy moieties form a layer with the phosphine groups pointing alternately up and down to form a layer between the tpy layers. This arrangement effectively separates the tpy layers from one another and prevents any π-stacking. Gold atoms are at a distance of 5.2 Å from one another which is too large to permit any Au…Au interactions.

Bond	Distance/Å	Bond	Distance/Å
Au1-P1	2.2787(12)	C16-C17	1.467(5)
C18-Au1	2.018(4)	O1-C16	1.443(4)
C17-C18	1.186(5)	C8-O1	1.367(4)
C8-C7	1.383(4)	P1-C19	1.821(4)
C6-C7	1.391(5)	P1-C23	1.800(5)
N2-C6	1.345(4)	P1-C27	1.844(5)
C5-C6	1.491(4)		

Bonds	Angle/deg.	Bonds	Angle/deg.
C18-Au1-P1	175.09(11)	N2-C6-C7	123.8(3)
C17-C18-Au1	175.3(3)	N2-C10-C9	123.1(3)
C16-C17-C18	176.7(4)	Au1-P1-C27	111.86(17)
O1-C16-C17	111.5(3)	Au1-P1-C23	112.03(14)
C8-O1-C16	117.4(3)	Au1-P1-C19	117.01(16)
C7-C8-C9	119.1(3)		

N1-C5-C6-N2	11.9(4)	N2-C10-C11-N3	3.6(3)

Table 4.5: Selected bond lengths (Å), bond angles (˚) and torsion angles (˚) for Au(**1**-H)(P^nBu_3).

4.4.2 $(AuP^nBu_3)_3$(**12** – 3H)

Crystals of $(AuP^nBu_3)_3$(**12** – 3H) were grown from CD_3CN solution. An ORTEP representation is shown in figure 4.11 and a packing diagram is shown in figure 4.12. Selected bond parameters are shown in table 4.6 and crystal data are given in the appendix. Gold(I) atoms are close enough together in this structure to permit Au…Au interactions. These have a distance of 3.1 Å and link adjacent molecules together to form chains.

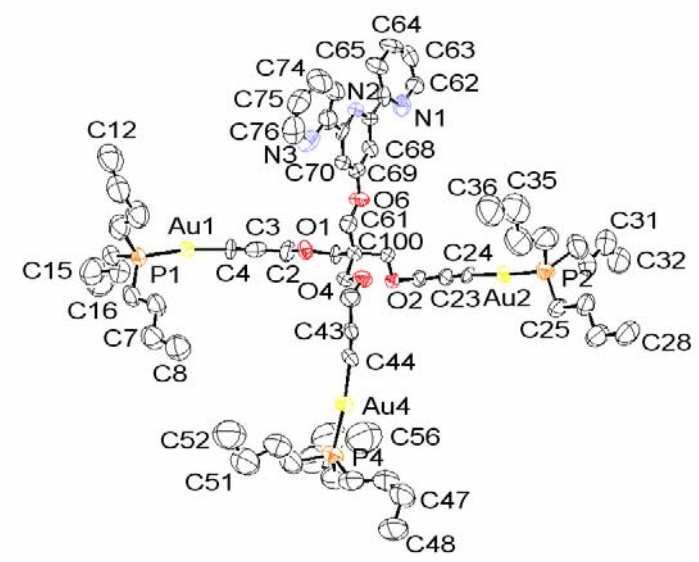

Figure 4.11: ORTEP representation of $(AuP^nBu_3)_3$(**12** – 3H).

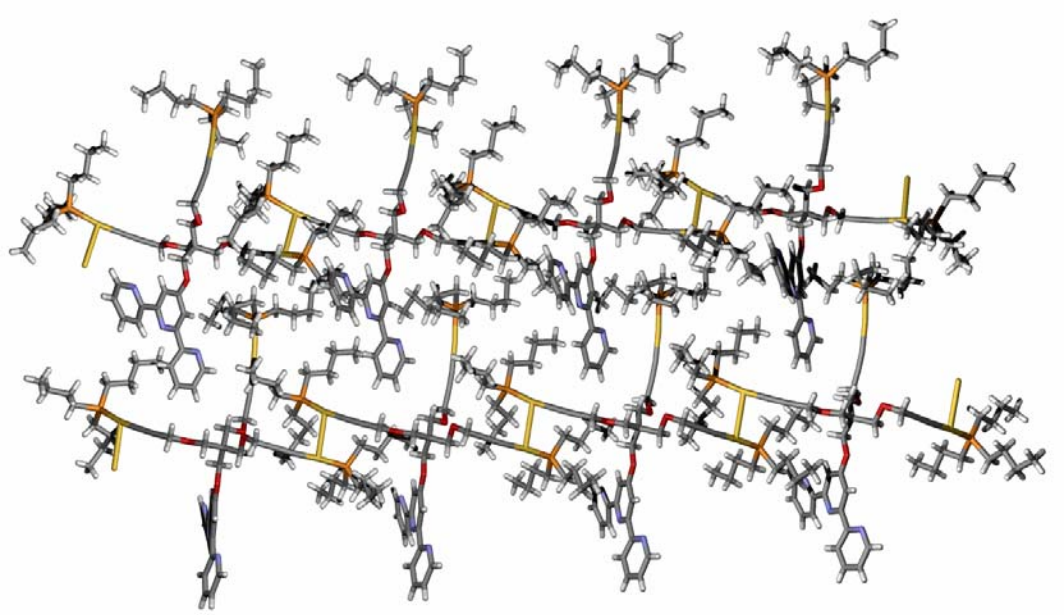

Figure 4.12: Packing diagram of $(AuP^nBu_3)_3$(**12** – 3H). Au…Au interactions can be seen between molecules so that molecules are arranged in chains.

As with the simple gold(I) complex Au(**1**-H)(P^nBu_3), this complex displays an alkyne-gold(I) bond. This is expected to be linear but once again deviates slightly from linearity. The pyridine rings of the tpy are not co-planar (torsion angles are 9.0 and 14.9 °). Torsion angles are defined in table 4.6.

Bond	Distance/Å	Bond	Distance/Å
Au1-P1	2.278(5)	C24-C23	1.18(2)
Au1-C4	1.993(14)	C23-C22	1.49(2)
C4-C3	1.17(2)	C22-O2	1.408(18)
C3-C2	1.46(3)	O2-C21	1.399(18)
C2-O1	1.45(2)	C100-C1	1.53(2)
O1-C1	1.425(18)	C100-C41	1.52(2)
Au4-P4	2.262(5)	C100-C61	1.51(2)
Au4-C44	2.027(18)	C100-C21	1.53(2)
C44-C43	1.16(2)	C61-O6	1.43(2)
C43-C42	1.47(2)	O6-C69	1.377(19)
C42-O4	1.42(2)	C69-C68	1.39(2)
O4-C41	1.391(19)	C69-C70	1.35(2)

Au2-P2	2.259(5)	Au2-C24	2.006(13)

Bonds	Angle/deg.	Bonds	Angle/deg.
Au2-Au1-P1	100.43(13)	C5-P1-C13	101.8(9)
Au2-Au1-C4	87.3(5)	C9-P1-C13	95.9(11)
P1-Au1-C4	171.7(5)	Au2-P2-C25	115.9(5)
Au1-Au2-P2	100.68(13)	Au2-P2-C29	116.7(9)
Au1-Au2-C24	82.9(4)	C25-P2-C29	114.5(11)
P2-Au2-C24	176.4(4)	Au2-P2-C33	116.2(10)
P4-Au4-C44	174.3(6)	C25-P2-C33	109.6(12)
Au1-P1-C5	111.4(6)	C29-P2-C33	78.1(14)
Au1-P1-C9	116.2(8)	Au4-P4-C45	113.8(9)
C5-P1-C9	112.0(12)	Au4-P4-C49	110.2(9)
Au1-P1-C13	117.8(7)	C45-P4-C49	101.0(12)
Au4-P4-C53	125.3(9)	C45-P4-C53	104.1(13)
C49-P4-C53	99.0(14)	C100-C1-O1	108.4(14)
C3-C2-O1	112.1(15)	C2-C3-C4	176.3(18)
Au1-C4-C3	178.5(16)	C23-C22-O2	114.2(14)
C5-C6-C7	114.1(14)	Au2-C24-C23	175.0(15)
C100-C21-O2	109.5(12)	C100-C41-O4	110.0(12)
C22-C23-C24	178.5(16)	C42-C43-C44	176.4(19)
C43-C42-O4	114.3(16)	C21-C100-C41	111.7(13)
Au4-C44-C43	172.2(17)	C21-C100-C61	109.0(13)
C21-C100-C1	108.6(14)	C41-C100-C61	107.6(14)
C1-C100-C41	109.7(13)	C22-O2-C21	111.5(11)
C1-C100-C61	110.4(14)	C61-O6-C69	118.1(13)
C2-O1-C1	111.3(13)	C71-N2-C67	118.6(14)
C42-O4-C41	113.9(13)	C100-C61-O6	110.2(13)
C66-N1-C62	117.9(20)	C76-N3-C72	112.3(20)

N1-C66-C67-N2	9.0(2)	N2-C72-C73-N3	14.9(2)

Table 4.6: Selected bond lengths (Å), angles (˚) and torsion angles (˚) of $(AuP^{n}Bu_3)_3$(**12** – 3H).

4.4.3 $[Au_3Cl_2(dppm)_2][PF_6]$

X-ray quality crystals of $[Au_3Cl_2(dppm)_2][PF_6]$ were grown from a solution of the complex in CH_2Cl_2 layered with hexane. The structure of another salt, $[Au_3Cl_2(dppm)_2]Cl$, has previously been determined.[22] However, there are significant differences between the structures of the $[Au_3Cl_2(dppm)_2]^+$ cations in the two salts. The structure described here is asymmetric, whereas the literature structure has C_2 symmetry, with both the gold(I) centres attached to chloride ligands being equivalent. There is some disorder in two of the phenyl rings and an ORTEP representation is shown in figure 4.13. A packing diagram is shown in figure 4.14 and selected bond parameters are shown in table 4.7. Crystal data are given in the appendix.

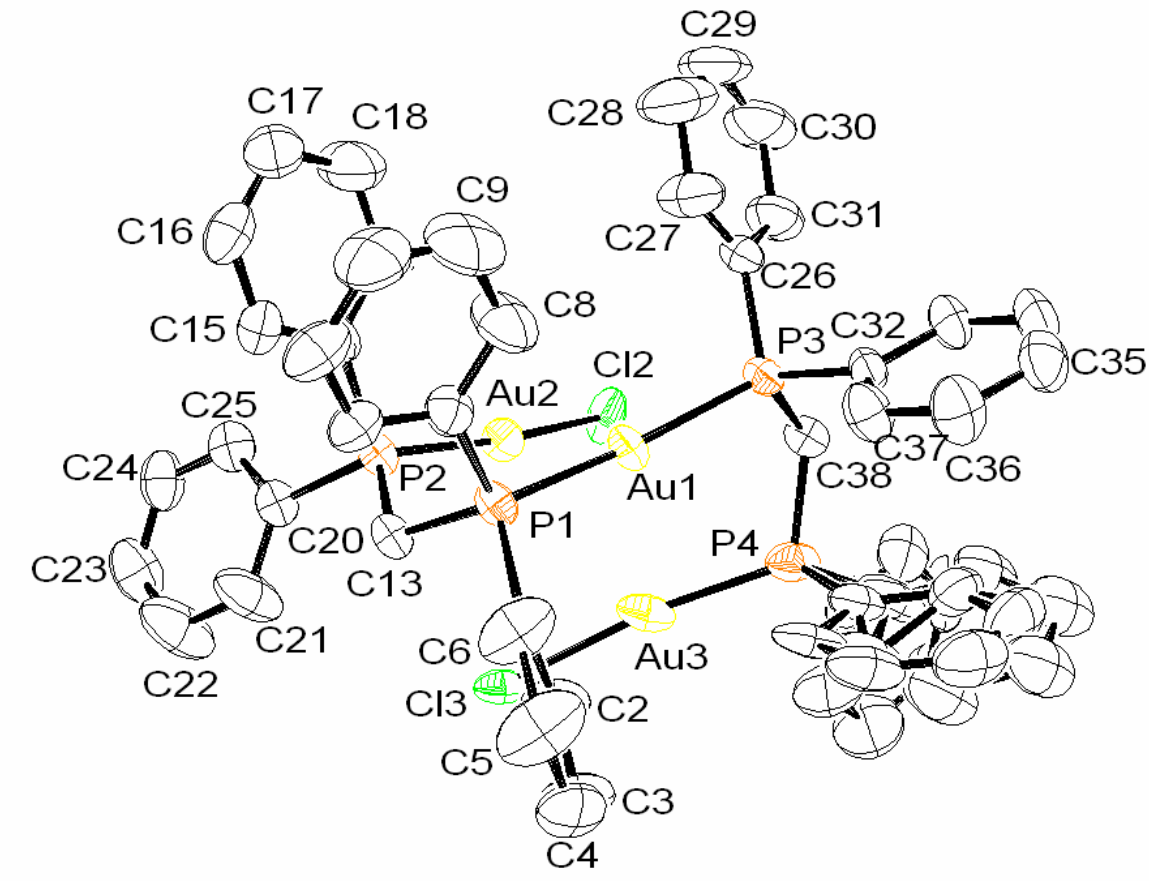

Figure 4.13: ORTEP representation of the $[Au_3Cl_2(dppm)_2]^+$ cation in $[Au_3Cl_2(dppm)_2][PF_6]$. The phenyl rings attached to P4 are disordered.

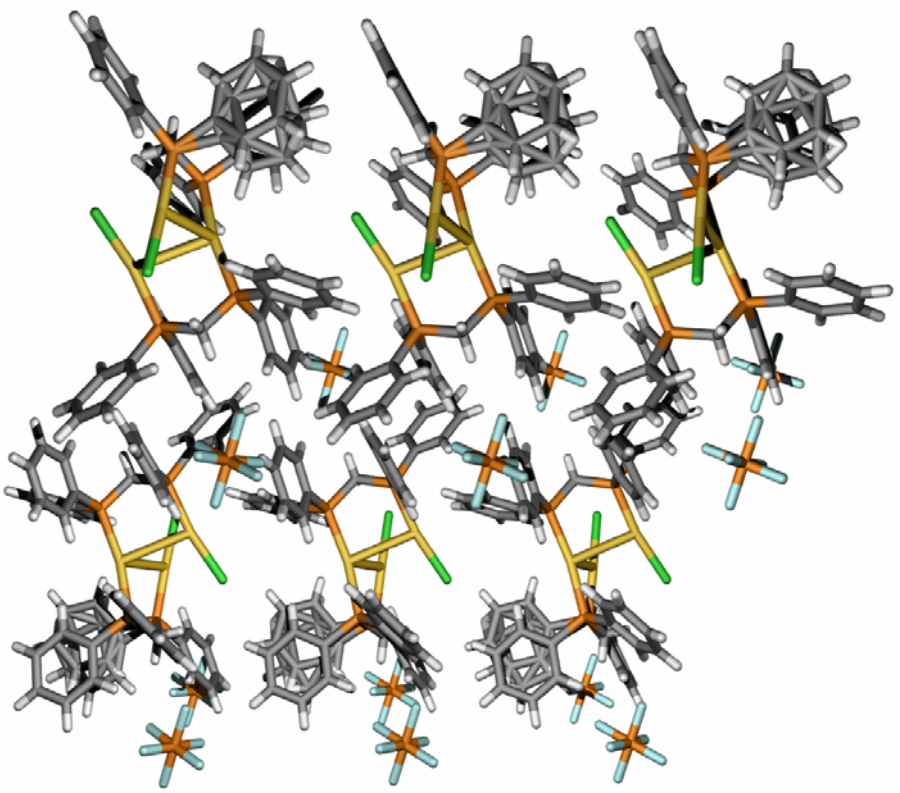

Figure 4.14: Packing diagram of $[Au_3Cl_2(dppm)_2][PF_6]$. The hexafluorophosphate counterions can be seen amongst the phenyl groups. Two phenyl groups per molecule are disordered.

The structure of this gold(I) complex shows short distances between each adjacent pair of Au atoms. These distances are short enough to allow for Au…Au interactions and are 3.2 Å between Au1-Au3 and Au1-Au2, and 3.3 Å between Au2-Au3. These differ from the literature structure[22] where the reported Au-Au distances are 3.1 and 3.7 Å respectively.

Bond	Distance/Å	Bond	Distance/Å
Cl2-Au2	2.3496(17)	P4-Au3	2.242(2)
Au2-P2	2.2442(17)	Au3-Cl3	2.3559(18)
P2-C13	1.814(7)	P2-C14	1.805(7)
C13-P1	1.832(7)	P2-C20	1.823(7)
P1-Au1	2.3048(17)	P3-C26	1.814(7)
Au1-P3	2.3083(16)	P3-C32	1.817(7)
P3-C38	1.832(7)	P1-C7	1.812(7)
C38-P4	1.822(7)	P1-C1	1.815(7)

Bonds	Angle/deg.	Bonds	Angle/deg.
Cl2-Au2-P2	169.64(7)	Au1-P3-C38	113.9(2)
Au2-P2-C13	115.4(2)	Au1-P3-C26	111.9(3)
Au2-P2-C14	111.4(2)	Au1-P3-C32	113.3(2)
Au2-P2-C20	113.1(2)	P3-C38-P4	111.3(4)
P2-C13-P1	114.0(3)	C38-P4-Au3	115.6(3)
P1-Au1-P3	167.01(6)	P4-Au3-Cl3	171.67(7)

Table 4.7: Selected bond lengths (Å) and bond angles (˚) for $[Au_3Cl_2(dppm)_2][PF_6]$.

4.4.4 $(Au(\mathbf{1}\text{-}H))_2(dppe).4CHCl_3$

X-ray quality crystals of $(Au(\mathbf{1}\text{-}H))_2(dppe).4CHCl_3$ were grown from a solution in $CHCl_3$ and there are solvent molecules present in the structure. An ORTEP representation is shown in figure 4.15 as well as a packing diagram in figure 4.16. Selected bond parameters are given in table 4.8 and crystal data are given in the appendix.

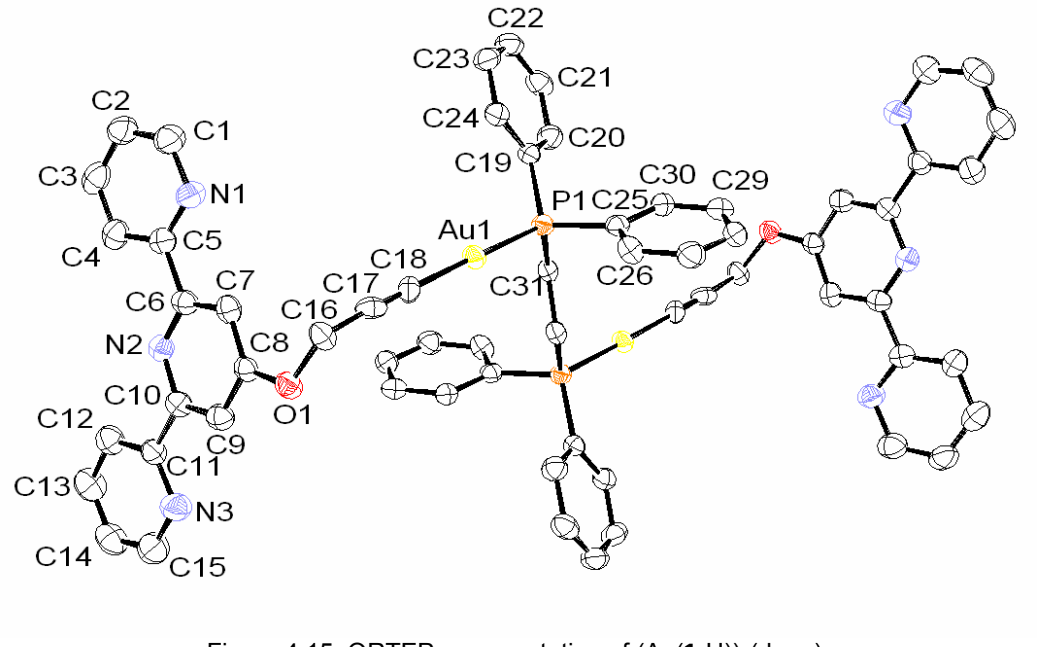

Figure 4.15: ORTEP representation of $(Au(\mathbf{1}\text{-}H))_2(dppe)$.

The gold(I) complex (Au(**1**-H))$_2$(dppe) displays an inversion centre situated between C31 and C31_2. There is a slight deviation from linearity along the Au1-C18-C17 axis with bond angles being 176-179 ˚. The P atoms have a near tetrahedral geometry with bond angles in the range 113-114 ˚. The pyridine rings of the tpy are not co-planar and there are torsion angles of 5.8 and 6.4 ˚ (defined in table 4.8).

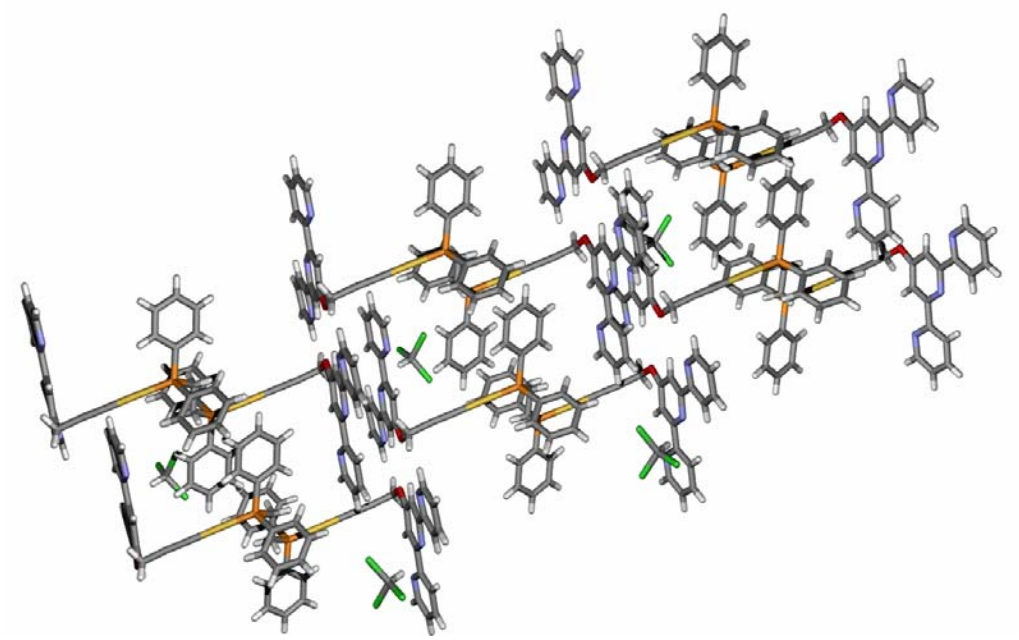

Figure 4.16: Packing diagram of (Au(**1**-H))$_2$(dppe).4CHCl$_3$. Solvent molecules can be seen in the structure.

The packing of the complex (Au(**1**-H))$_2$(dppe) is reminiscent of that of Au(**1**-H)(P^{n}Bu$_3$) in that the tpy moieties are arranged in layers separated by the phosphine groups of the molecule. There are hydrogen bonds (C16H16…N3 = 2.5 Å) between H16 of one molecule and N3 of another, as well as between O1 and H9 (O1…H9C9 = 2.6 Å). CHCl$_3$ solvent molecules are present in the crystal lattice; some are disordered and these are not shown on the packing diagram.

Bond	Distance/Å	Bond	Distance/Å
Au1-P1	2.2748(13)	C7-C8	1.391(8)
P1-C31	1.837(5)	C8-C9	1.383(8)
C31-C31_2	1.523(10)	C9-C10	1.387(8)

Au1-C18	2.062(6)	C10-N2	1.350(7)
C17-C18	1.117(8)	C5-C6	1.502(8)
C16-C17	1.481(8)	C10-C11	1.491(8)
O1-C16	1.449(7)	P1-C19	1.814(5)
C8-O1	1.361(7)	P1-C25	1.815(6)

Bonds	Angle/deg.	Bonds	Angle/deg.
P1-C31-C31_2	110.6(5)	C8-O1-C16	119.0(4)
Au1-P1-C31	113.25(17)	Au1-P1-C25	113.75(18)
C18-Au1-P1	178.79(17)	Au1-P1-C19	114.36(18)
C17-C18-Au1	177.6(5)	C7-C8-O1	124.7(5)
C16-C17-C18	176.2(6)	C6-C7-C8	117.5(5)
O1-C16-C17	112.3(5)	N2-C6-C7	123.2(5)

N1-C5-C6-N2	5.8(5)	N2-C10-C11-N3	6.4(5)

Table 4.8: Selected bond lengths (Å), bond angles (˚) and torsion angles (˚) for (Au(**1**-H))$_2$(dppe).

4.4.5 $(AuCl)_2$(dppf)

X-ray quality crystals of $(AuCl)_2$(dppf) were grown from a MeCN solution. The structure differs from those published in the literature,[16,17,18] although two of these known structures are solvates. The literature complex which is not a solvate[16] crystallised in the monoclinic space group whereas the structure obtained here crystallised in the triclinic space group. The phenyl rings are rotated slightly differently in the two structures and therefore the structure obtained here is a polymorph. The differences between the two structures can be seen in figure 4.17. An ORTEP representation is shown in figure 4.18 and a packing diagram is shown in figure 4.19. Selected bond parameters are shown in table 4.9 and crystal data are given in the appendix.

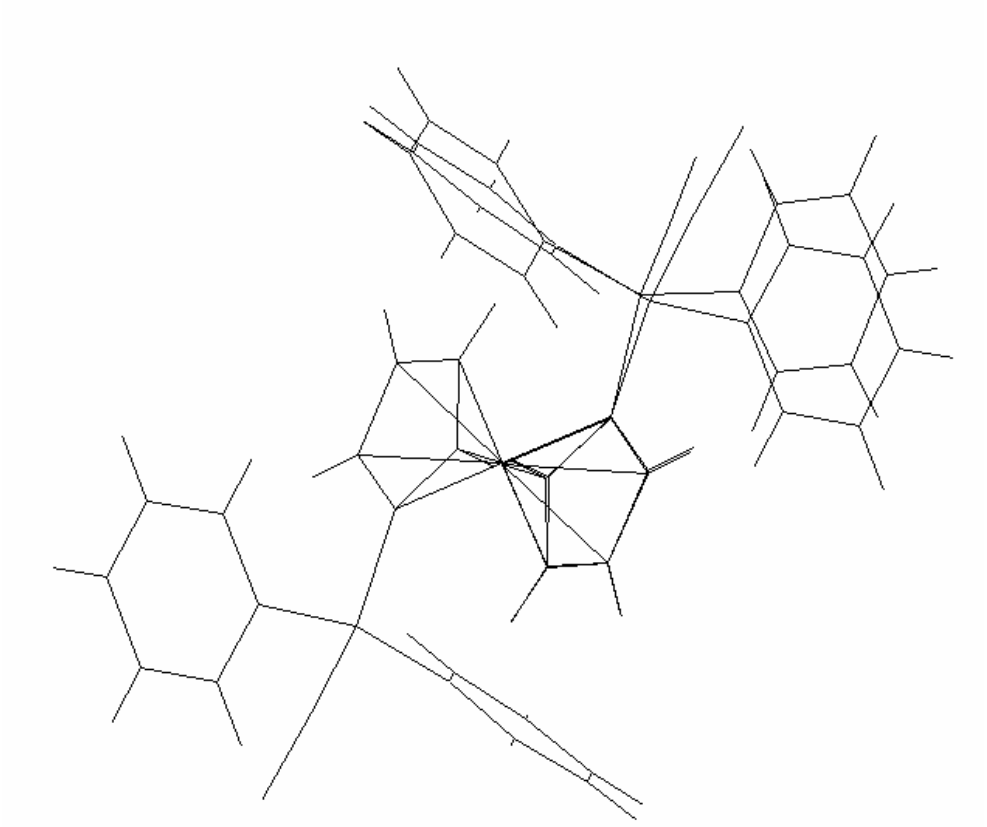

Figure 4.17: Diagram showing the structure of $(AuCl)_2(dppf)$ obtained overlaid on the literature structure.[16] The difference between the phosphine groups in the two structures can clearly be seen, demonstrating that these two structures are polymorphs.

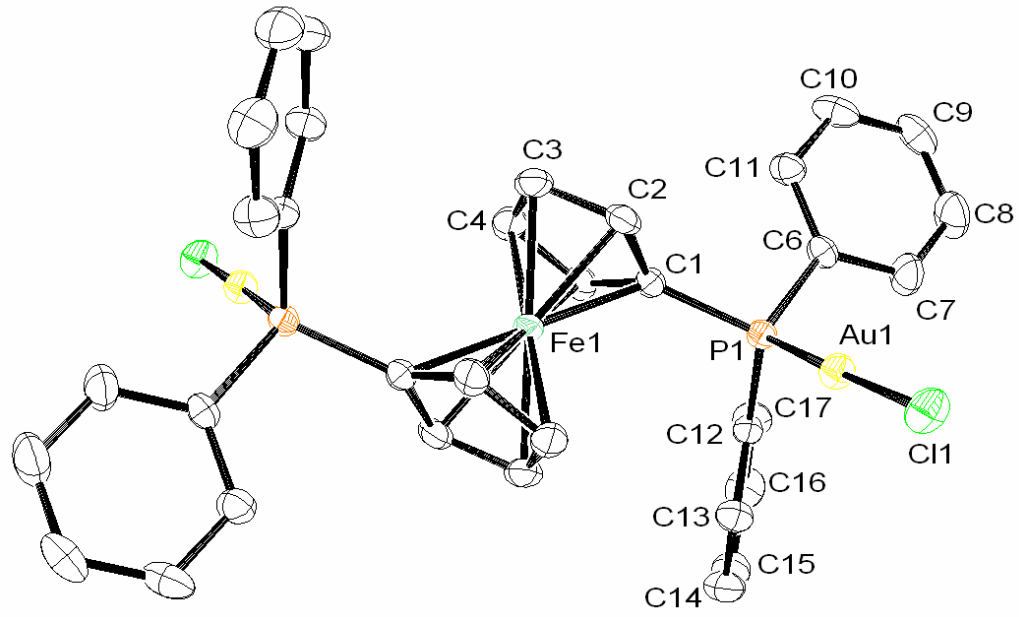

Figure 4.18: ORTEP representation of $(AuCl)_2(dppf)$.

The molecule possesses an inversion centre situated at the Fe(II) centre. The Cl1-Au1-P1 unit deviates little from linearity with a bond angle of 179 °.

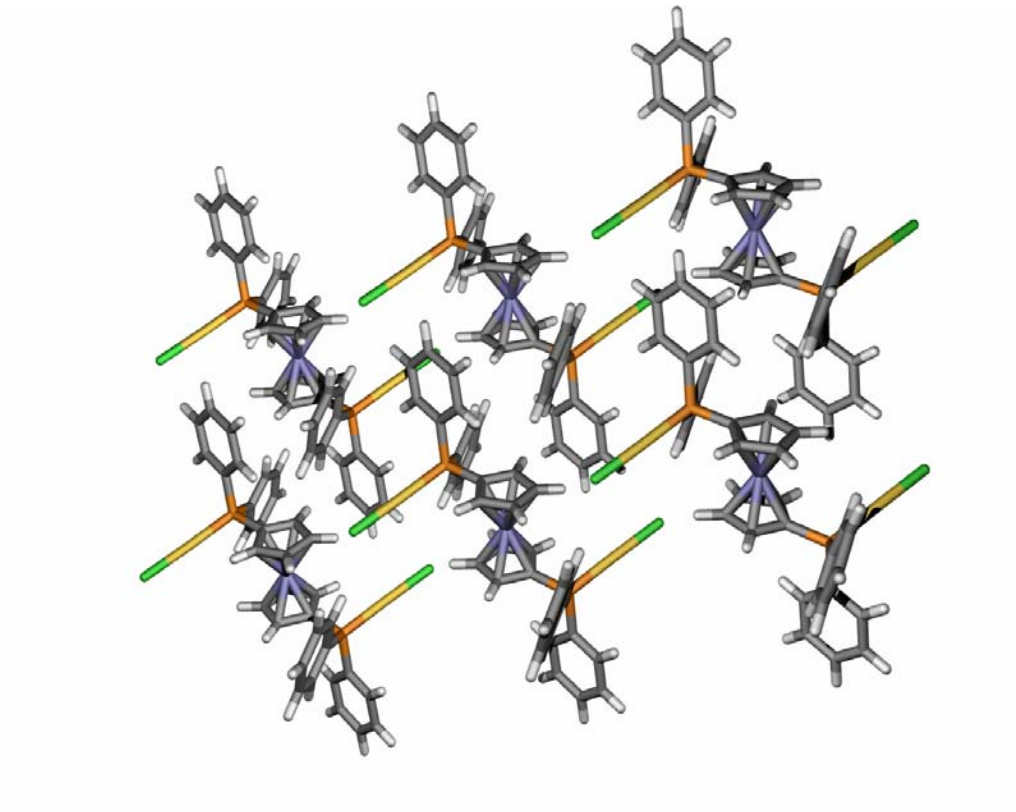

Figure 4.19: Packing diagram of $(AuCl)_2$(dppf). The complex crystallised without solvent molecules.

The packing of the molecules can be seen in figure 4.19. The gold(I) chloride moieties point in alternating directions which enables the molecules to interlock, the chloride ligands pointing at the ferrocene of a neighbouring molecule.

Bond	Distance/Å	Bond	Distance/Å
Cl1-Au1	2.2838(8)	C1-C2	1.436(4)
Au1-P1	2.2283(7)	C2-C3	1.422(5)
P1-C1	1.793(3)	C3-C4	1.411(5)
P1-C6	1.821(3)	C4-C5	1.429(4)
P1-C12	1.811(3)	C5-C1	1.428(4)
C1-Fe1	2.033(3)		

Bonds	Angle/deg.	Bonds	Angle/deg.
Cl1-Au1-P1	178.51(2)	Au1-P1-C12	112.80(10)
Au1-P1-C1	113.78(10)	P1-C1-Fe1	131.79(15)
Au1-P1-C6	112.85(10)		

Table 4.9: Selected bond lengths (Å) and angles (˚) for $(AuCl)_2$(dppf).

4.5 Conclusion

The coupling of gold(I) to alkyne functionalised tpy ligands has been achieved in three cases although problems were encountered when using certain bidentate phosphines. The molecules were characterised using NMR spectroscopy, mass spectrometry and UV/VIS spectroscopy and X-ray crystal structures were obtained from all reactions although these were not always the desired product.

4.6 References

[1] C. King, J. C. Wang, M. N. I. Kham and J. P. Fackler, *Inorg. Chem.*, 1989, **28**, 2145.

[2] W. J. Hunks, J. Lapierre, H. A. Jenkins and R. J. Puddephatt, *J. Chem. Soc., Dalton Trans.*, 2002, 2885.

[3] R. J. Puddephatt, *Coord. Chem. Rev*., 2001, **216-217**, 313.

[4] C. P. McArdle, S. Van, M. C.Jennings and R. J. Puddephatt, *J. Am. Chem. Soc.*, 2002, **124**, 3959.

[5] N. C. Habermehl, M. C. Jennings, C. P. McArdle, F. Mohr and R. J. Puddephatt, *Organometallics*, 2005, **24**, 5004.

[6] M. Ferrer, L. Rodríguez, O. Rossell, F. Pina, J. C. Lima, M. F. Bardia and X. Solans, *J. Organomet. Chem.*, 2003, **678**, 82.

[7] M. Bardají, A. Laguna, J. Vicente and P. G. Jones, *Inorg. Chem*., 2001, **40**, 2675.

[8] C.-K. Li, E. C.-C. Cheng, N. Zhu and V. W.-W. Yam, *Inorg. Chim. Acta*, 2005, **358**, 4191.

[9] C. P. McArdle, J. J. Vittal and R. J. Puddephatt, *Angew. Chem. Int. Ed.*, 2000, **39**, 3819.

[10] C. P. McArdle, M. C. Jennings, J. J. Vittal and R. J. Puddephatt, *Chem. Eur. J.*, 2001, **7**, 3572.

[11] G. Jia, R. J. Puddephatt, J. D. Scott and J. J. Vittal, *Organometallics*, 1993, **12**, 3565.

[12] M. I. Bruce, M. Jevric, B. W. Skelton, M. E. Smith, A. H. White and N. Zaitseva, J. Organomet. Chem., 2006, **691**, 361.

[13] S.-K. Yip, W. H. Lam, N. Zhu and V. W.-W. Yam, *Inorg. Chim. Acta*, 2006, **359**, 3639.

[14] B. M. Sutton, E. McGusty, D. T. Waltz and M. J. DiMartino, *J. Med. Chem.* 1972, **11**, 1095.

[15] S. M. Draper and C. E. Housecroft, *J. Organomet. Chem.*, 1992, **435**, 9.

[16] D. T. Hill, G. R. Girard, F. L. McCabe, R. K. Johnson, P. D. Stupik, J. H. Zhang, W. M. Reiff and D. S. Eggleston, *Inorg. Chem.*, 1989, **28**, 3529.

[17] F. Canales, M. C. Gimeno, P. G. Jones, A. Laguna and C. Sarroca, *Inorg.Chem*., 1997, **36**, 5206.

[18] O. Crespo, M. C. Gimeno, P. G. Jones and A. Laguna, *Acta Crystallogr.,Sect. C*, 2000, **56**, 1433.

[19] S. J. Berners-Price, M. A. Mazid and P. J. Sadler, *J. Chem. Soc. Dalton Trans.*, 1984, 969.

[20] F. Cariati, L. Naldini, G. Simonetta and L. Malatesta, *Inorg. Chim. Acta*, 1967, **1**, 315.

[21] C. A. McAuliffe, R. V. Parish and P. D. Randall, *J. Chem. Soc. Dalton Trans.*, 1979, **11**, 1730.

[22] I. J. B. Lin, J. M. Hwang, D.-F. Feng, M. C. Cheng and Y. Wang, *Inorg. Chem.*, 1994, **33**, 3467.

Chapter 5 Iron(II) Complexes of 2,2':6',2"-Terpyridine Ligands and the Assembly of Heterometallic Macrocycles

5.1 Iron(II) 2,2':6',2"-Terpyridine Complexes

Iron(II) tpy complexes display octahedral coordination[1,2,3] and, due to the high crystal field splitting of the tpy ligand, are always in a low spin configuration.[4] The tpy ligand is symmetrical when mono-substituted, and therefore complexes of the type $[M(tpyX)_2]^{2+}$ (X = 4'-substituent) are achiral and neither do they possess any other type of isomerism (such as the *fac mer* isomerism seen with complexes of bpy and phen).[3] Thus, their structures are highly predictable, a characteristic desirable in supramolecular self-assembly.

5.2 Synthesis of Iron(II) Complexes

For the purposes of this chapter, the term "tpy" refers to ligands of the type discussed in Chapter 2, as well as the platinahomoditopic ligands discussed in Chapter 3 and the gold containing ligands discussed in Chapter 4. The synthesis of iron(II) bis(tpy) complexes is straightforward and occurs in one step at room temperature.[4] Two equivalents of the ligand are reacted with one equivalent of an iron(II) salt, usually iron(II) chloride, in methanol. A purple colour appears instantly and this is an indication of the formation of the $[Fe(tpy)_2]^{2+}$ chromophore. Addition of an aqueous solution of ammonium hexafluorophosphate, and removal of some of the methanol, precipitates the hexafluorophosphate salt as a purple solid. Figure 5.1 shows the general synthesis of $[Fe(tpy)_2]^{2+}$ containing complexes.

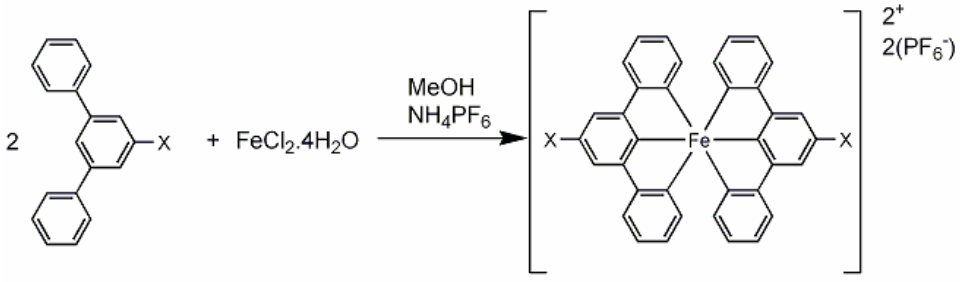

Figure 5.1: Synthesis of $[Fe(tpy)_2]^{2+}$ complexes.

Two model Fe(II) bis(tpy) complexes were synthesised in this way, [Fe(**4**)$_2$][PF$_6$]$_2$ and [Fe(**5**)$_2$][PF$_6$]$_2$ (figure 5.2). This was a good way of testing the methodology as well as providing characterisation data which would be useful for comparative purposes at a later stage. Both complexes were synthesised with no need for purification, and X-ray quality crystals of [Fe(**5**)$_2$][PF$_6$]$_2$ were grown from a solution of the complex in MeCN layered on top of toluene. The crystal structure of this complex is discussed later in the chapter.

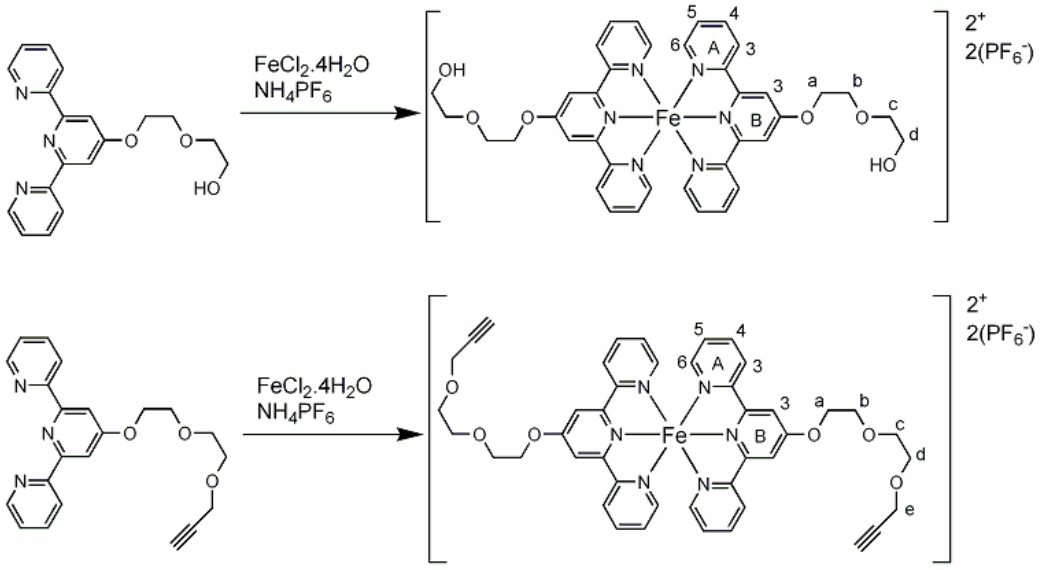

Figure 5.2: Synthesis of [Fe(**4**)$_2$][PF$_6$]$_2$ and [Fe(**5**)$_2$][PF$_6$]$_2$ complete with numbering scheme.

The same method was attempted in forming the iron(II) complex of Au(**1**-H)(P^{n}Bu$_3$). Since the phosphine P^{n}Bu$_3$ was not a chelating phosphine there was no opportunity for the formation of macrocycles or polymers, and a model iron(II) bis(tpy) complex was formed containing pendant gold(I) moieties (figure 5.3). However, due to the formation of a brown decomposition product after a period of time in solution, it was not possible to obtain well resolved NMR spectroscopic data on this complex.

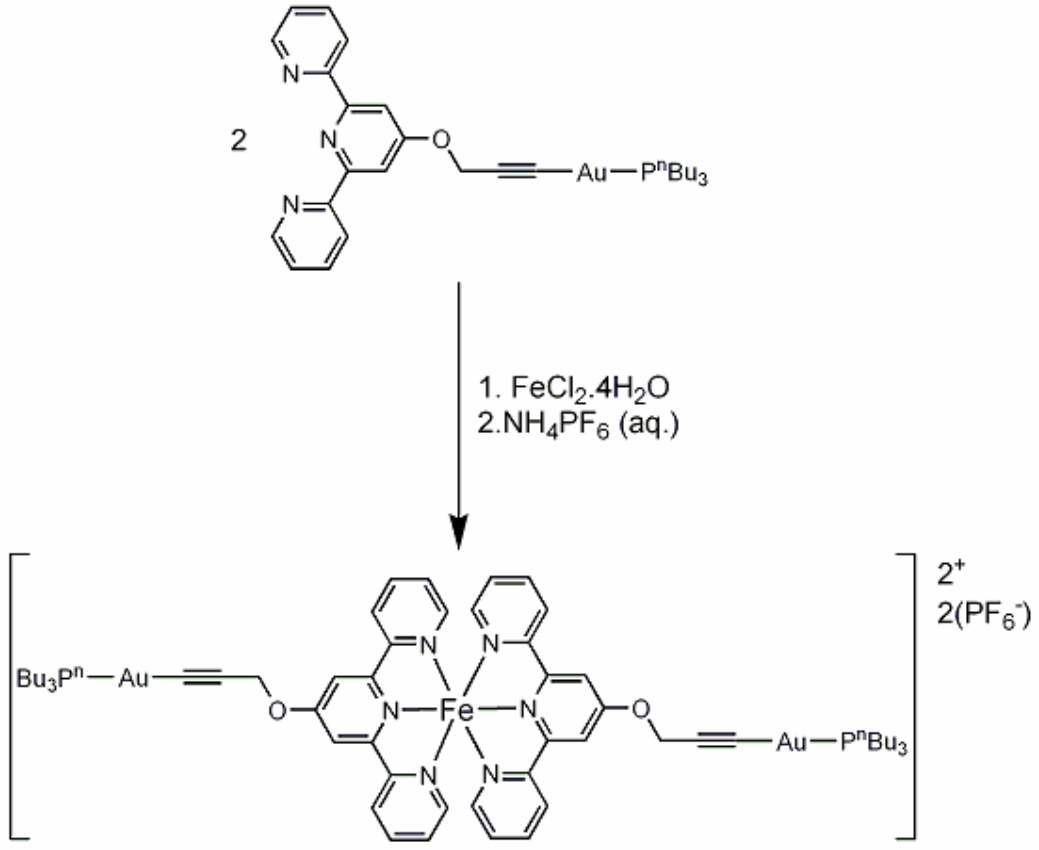

Figure 5.3: The iron(II) bis(tpy) complex formed from the reaction of Au(**1**-H)(P^{n}Bu$_3$) with $FeCl_2.4H_2O$.

The general reaction of Pt(**L**-H)$_2$(PR$_3$)$_2$ (where Pt(**L**-H)$_2$(PR$_3$)$_2$ is of the type discussed in Chapter 3) with $FeCl_2.4H_2O$ should proceed to give either a polymer or a macrocycle since there are now two tpy moieties available for coordination per single molecule. The result should, in theory, be influenced by two factors: the flexibility of the spacer between the tpy and the alkyne, as well as the steric bulk of the auxiliary phosphine groups on the platinum(II) centre. In the first instance, the reaction of ligand Pt(**1**-H)$_2$(PEt$_3$)$_2$ (i.e. one with a short spacer) with Fe(II) gave a mixture of three products. Recrystallisation of this mixture from a toluene/MeCN solution gave X-ray quality crystals and the structure was confirmed as that of [2+2] macrocycle [Fe$_2${Pt(**1**-H)$_2$(PEt$_3$)$_2$}$_2$][PF$_6$]$_4$.[5] Figure 5.4 shows the formation of the [2+2] macrocycle from the reaction of Pt(**1**-H)$_2$(PEt$_3$)$_2$ with $FeCl_2.4H_2O$.

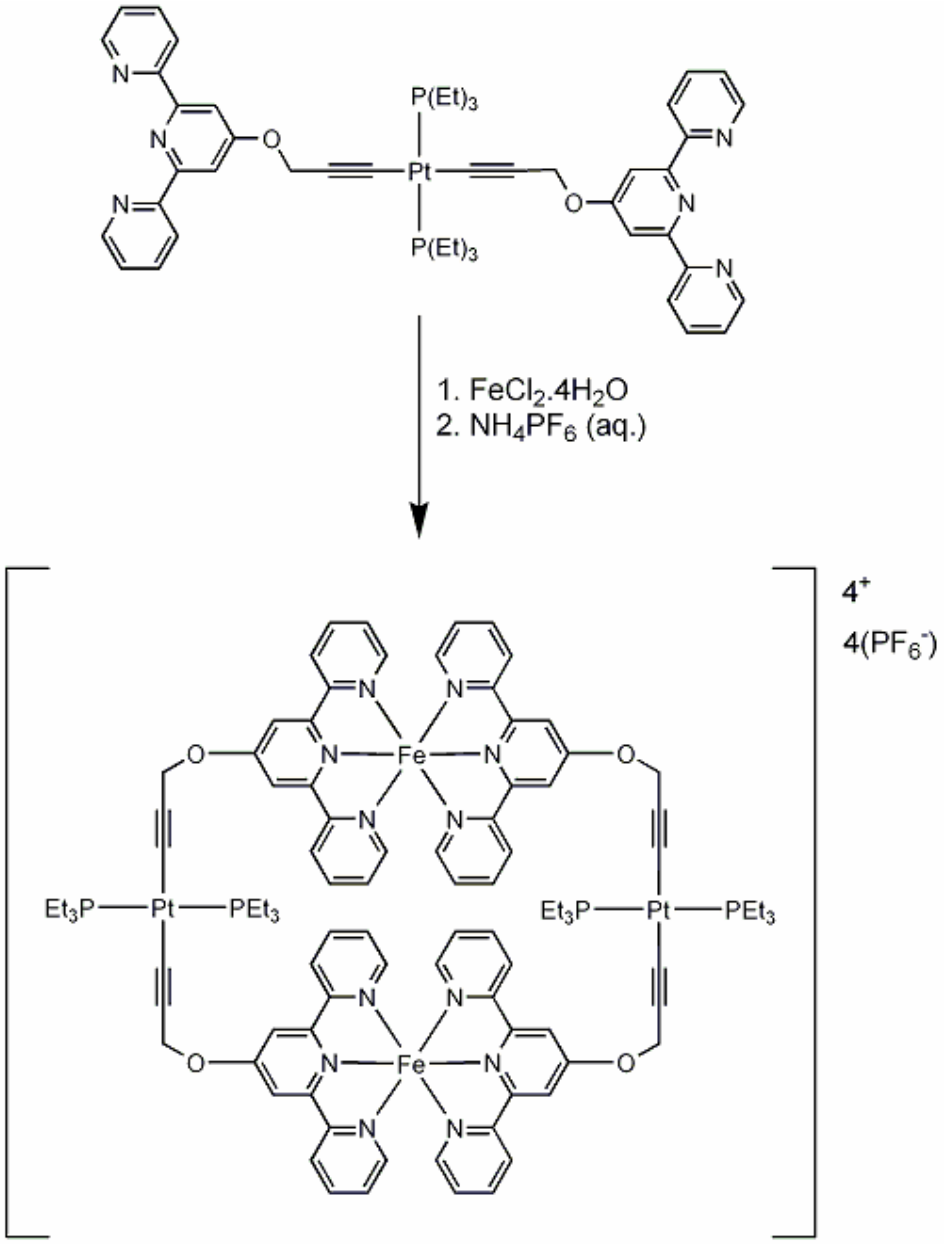

Figure 5.4: The formation of a [2+2] macrocycle from the reaction of Pt(**1**-H)$_2$(PEt$_3$)$_2$ with $FeCl_2.4H_2O$.

The same reaction conditions were used in the reaction of Pt(**1**-H)$_2$(P^{n}Bu$_3$)$_2$ and Pt(**1**-H)$_2$(PPh$_3$)$_2$ with $FeCl_2.4H_2O$. In each case, a mixture was produced once again, and attempts to separate the products by chromatography were unsuccessful and so attempts at crystallisation were made. After several months, it was apparent that crystals had not grown and the ^{31}P NMR spectra of [Fe$_n${Pt(**1**-H)$_2$(PEt$_3$)$_2$}$_n$][PF$_6$]$_{2n}$, [Fe$_n${Pt(**1**-H)$_2$(P^{n}Bu$_3$)$_2$}$_n$][PF$_6$]$_{2n}$ and [Fe$_n${Pt(**1**-H)$_2$(PPh$_3$)$_2$}$_n$][PF$_6$]$_{2n}$ solutions were

recorded. It was noted that over the period of months the ratios of the signals in the ^{31}P NMR spectra had changed. Since it was not possible to separate the components of the mixture, it was decided to try using the technique of PGSE (pulsed-field gradient spin-echo) NMR spectroscopy to gain information about the components of the mixtures. This technique as well as the results obtained is discussed further in Section 5.2.2.

Results of the PGSE NMR spectroscopy of all three mixtures showed that one of the components of each mixture had a calculated radius of between 9.7 and 10 Å; the other components had larger radii. The calculated radius of 9.7 Å was in good agreement with the radius measured form the X-ray crystal structure of $[Fe_2\{Pt(\mathbf{1}\text{-}H)_2(PEt_3)_2\}_2][PF_6]_4$ (see section 5.4.2), therefore the sets of peaks of this radius were assigned to the [2+2] macrocycle in each case. It was then possible to assign ^{1}H NMR peaks to macrocycles of different radii by making a DOSY plot (see later), and in turn it was possible to correlate ^{1}H NMR signals with signals observed in the ^{31}P NMR spectrum. From looking at how the peaks changed on standing in solution for several hours, it was proposed that the initial reaction mixture consisted of the kinetic products, metallomacrocycles of sizes larger than [2+2], and that over time, the distribution of products changed to favour the thermodynamic [2+2] product. This observation explains the growth of crystals of the [2+2] macrocycle, as well as why crystals of larger size cycles were never obtained.

Having established that platinum(II) containing macrocycles of different sizes interconvert in solution, reaction of the model complex, Au(**1**-H)(P^nBu_3) with iron(II) was carried out. Attempts at separating the product chromatographically still gave a mixture, and this decomposed in solution over a short period to form a brown precipitate visible in the NMR tube. This precluded the recording of well resolved NMR spectra.

A similar study of the reaction of the gold(I) containing ditopic ligand $(Au(\mathbf{1}\text{-}H))_2(dppe)$ with Fe(II) was also carried out. Again an inseparable mixture was produced. The NMR spectra of the mixture were recorded and

attempts at crystallisation were made. Crystals suitable for X-ray diffraction studies were not obtained and the NMR spectra of the mixture were recorded again. Significantly, the ^{31}P spectrum had changed, with a new signal growing in. The ^{31}P spectrum of this complex is discussed in more detail later in the chapter. Due to time constraints, the PGSE NMR spectrum of this product was not recorded. However, by analogy with the Pt(II) containing systems it is assumed that a similar interconversion between macrocycles takes place.

Reaction of the mixtures produced from attempts to form (Au(**1**-H))$_2$(dppm) and (Au(**1**-H))$_2$(dppf) with Fe(II) also gave inseparable mixtures. ^1H NMR spectra were broad and attempts at growing crystals suitable for X-ray diffraction produced only colourless crystals, one being $[Au_3Cl_2(dppm)_2][PF_6]$ (see Section 4.4.3 for structure) and the other being $(AuCl)_2$(dppf) (see Section 4.4.5 for structure). It therefore seems that there are more problems with gold(I) containing ditopic ligands than with their platinum(II) analogues and further investigation of these systems is warranted.

5.3 Characterisation

5.3.1 ^1H NMR Spectroscopy

Iron(II) bis(tpy) complexes were characterised by ^1H NMR spectroscopy. A corresponding numbering scheme to those used in Chapters 2, 3 and 4 is used for assignments of peaks. NMR spectra of iron complexes synthesised in this chapter were run in CD_3CN solutions.

The main difference between the ^1H NMR spectra of the uncoordinated tpy ligands discussed in earlier chapters and those of the coordinated tpy regions discussed here is the change in the order of the peaks. In the spectra of uncoordinated tpy ligands, the protons almost always come in the order A6, A3, B3, A4 and A5, with A6 being of highest chemical shift.[6] On coordination, this order changes and B3 now has the highest chemical shift, followed by A3,

A4, A6, and A5. This movement of the tpy signals, in particular the B3 signal, is diagnostic of coordination. Figure 5.5 compares the ^{1}H NMR spectra of uncoordinated ligand **5** with the iron(II) complex $[Fe(\mathbf{5})_2][PF_6]_2$.[7] The difference between the aromatic regions of the two spectra can be clearly seen. As expected, there is not a huge difference between the two aliphatic regions. The signals for the a protons (see figure 5.2 for numbering scheme) are most significantly shifted since these are the protons nearest the tpy region. Although different solvents were used for the platinahomoditopic ligand ($CDCl_3$) and the iron(II) complex (CD_3CN), solvent effects are negligible and the differences in the spectra arise wholly from coordination of the tpy moiety to iron(II).

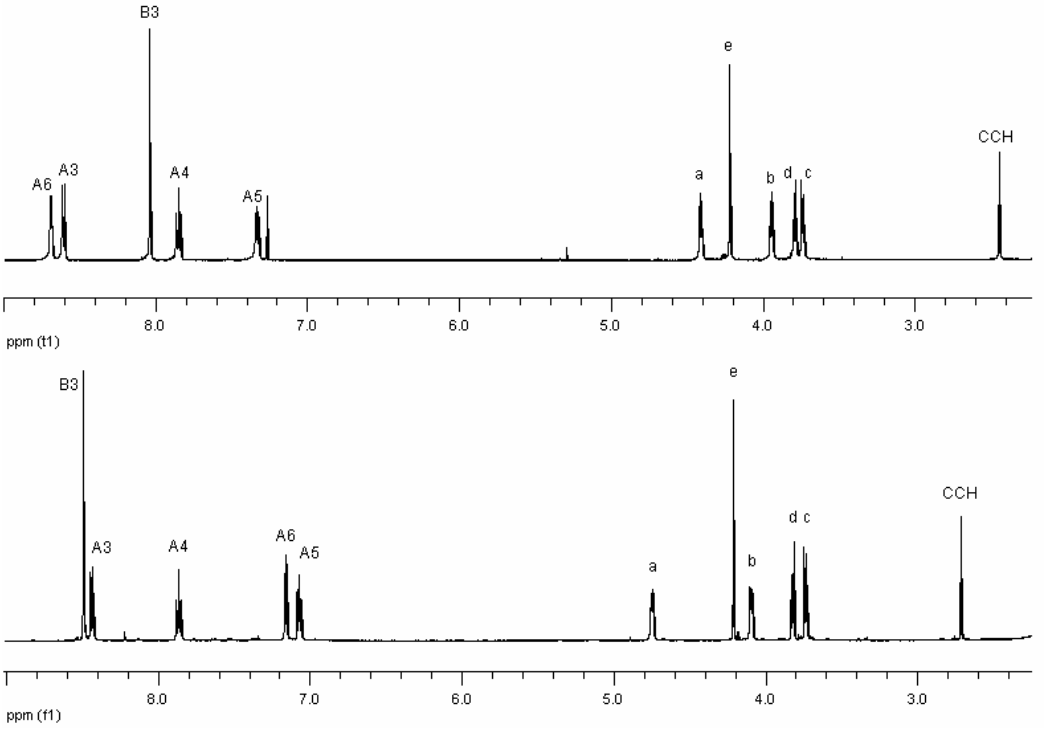

Figure 5.5: Comparison of the 500 MHz ^{1}H NMR spectra of ligand **5** (above) run in $CDCl_3$ solution and $[Fe(\mathbf{5})_2][PF_6]_2$ (below) run in CD_3CN solution.

If the tpy is a homoditopic ligand, the iron(II) complex formed is a heterometallic macrocycle. Formation of this type of complex is accompanied by a shift of the B3 proton to even higher ppm values. This has been seen in the reaction of $Pt(\mathbf{1}\text{-}H)_2(PEt_3)_2$ with Fe(II) to form $[Fe_2\{Pt(\mathbf{1}\text{-}H)_2(PEt_3)_2\}_2][PF_6]_4$[5]

where the B3 proton shifts from δ 8.06 ppm to δ 8.56 ppm as well as in the reaction of Pt(**5**-H)$_2$(PEt$_3$)$_2$ with Fe(II) to form [Fe{Pt(**5**-H)$_2$(PEt$_3$)$_2$}][PF$_6$]$_2$.[7]

Chemical shifts of protons in [Fe{Pt(**5**-H)$_2$(PEt$_3$)$_2$}][PF$_6$]$_2$ were assigned using COSY and NOESY techniques. [Fe{Pt(**5**-H)$_2$(PEt$_3$)$_2$}][PF$_6$]$_2$ could only be characterised as part of a mixture since its formation was accompanied by significant cleavage of the ether bonds along the spacer and the resulting mixture was not separated with any success. Therefore, COSY and NOESY played a significantly more important part in the assignment of peaks for this compound than for any other. The B3 signal proved a good starting point because of its larger change in chemical shift than the other components of the mixture, and cross peaks between this and other aromatic protons enabled the assignment of all signals. The other components of the mixture were assumed to be cleavage products similar to [Fe(**4**)$_2$][PF$_6$]$_2$, based on ^{1}H chemical shifts as well as the presence of a signal in the ^{31}P spectrum corresponding to the literature reported[8] chemical shift for Pt(C≡CR)$_2$(PEt$_3$)$_2$ where R = H or CH$_3$. The chemical shifts for all other protons in the mixture showed significant overlap.

As discussed earlier in the chapter, the NMR spectra of the products obtained from reaction of platinahomoditopic ligands with Fe(II) was more complicated than with the model complexes. Leaving a sample standing in solution for several days or even weeks resulted in changes in both the ^{1}H and ^{31}P NMR spectra. Heating of the samples meant that changes happened at a faster rate and monitoring of the ^{1}H and ^{31}P together meant that the spectra could be correlated. Peaks were assigned in the ^{1}H NMR spectrum due to PGSE NMR spectroscopy (discussed in Section 5.3.2) and once these were correlated with the ^{31}P signals, interconversion of the macrocycles was monitored using ^{31}P NMR. The results of this interconversion study are discussed in Section 5.3.4.

Table 5.1 shows chemical shifts of protons in representative iron complexes discussed in this chapter. As discussed, peaks were assigned from mixtures using PGSE NMR spectroscopy. It was not possible to assign

protons in the ^{1}H NMR spectrum of $[Fe_n\{Pt(\mathbf{1}\text{-}H)_2(PPh_3)_2\}_n][PF_6]_{2n}$ since all signals were overlapping and it was impossible to distinguish between them.

	A3	A4	A5	A6	B3
$[Fe(\mathbf{4})_2][PF_6]_2$	8.44	7.86	7.07	7.16	8.49
$[Fe(\mathbf{5})_2][PF_6]_2$	8.43	7.86	7.06	7.16	8.48
$[Fe_2\{Pt(\mathbf{1}\text{-}H)_2(PEt_3)_2\}_2][PF_6]_4$	8.27	7.79	6.96	6.93	8.56
$[Fe_2\{Pt(\mathbf{1}\text{-}H)_2(P^nBu_3)_2\}_2][PF_6]_4$	8.27	7.84	6.97	6.91	8.49
$[Fe\{Pt(\mathbf{5}\text{-}H)_2(PEt_3)_2\}][PF_6]_2$	8.39	8.01	7.15	7.07	8.63

	a	b	c	d	e	OH	CCH
$[Fe(\mathbf{4})_2][PF_6]_2$	4.76	4.10	3.73			2.84	
$[Fe(\mathbf{5})_2][PF_6]_2$	4.74	4.09	3.73	3.82	4.21		2.71
$[Fe_2\{Pt(\mathbf{1}\text{-}H)_2(PEt_3)_2\}_2][PF_6]_4$	5.35						
$[Fe_2\{Pt(\mathbf{1}\text{-}H)_2(P^nBu_3)_2\}_2][PF_6]_4$	5.33						
$[Fe\{Pt(\mathbf{5}\text{-}H)_2(PEt_3)_2\}][PF_6]_2$	4.92	4.04	3.65	3.54	4.12		

	w	x	y	z
$[Fe_2\{Pt(\mathbf{1}\text{-}H)_2(PEt_3)_2\}_2][PF_6]_4$			2.03	0.96
$[Fe_2\{Pt(\mathbf{1}\text{-}H)_2(P^nBu_3)_2\}_2][PF_6]_4$	Not observed.	1.47	1.25	0.60
$[Fe\{Pt(\mathbf{5}\text{-}H)_2(PEt_3)_2\}][PF_6]_2$			1.66	0.72

Table 5.1: 500 MHz ^{1}H chemical shifts for representative iron(II) complexes recorded in CD_3CN. The peak for the w protons in $[Fe_2\{Pt(\mathbf{1}\text{-}H)_2(P^nBu_3)_2\}_2][PF_6]_4$ is not observed since it overlaps with the solvent peak.

5.3.2 PGSE NMR Spectroscopy

When the reaction of tpy ligands $Pt(\mathbf{1}\text{-}H)_2(PR_3)_2$ (R = Et, Bu and Ph) with Fe(II) was carried out, it was observed that the ^{1}H and also the ^{31}P NMR spectra were not clean. The samples were left standing at room temperature for several weeks and on re-recording the ^{1}H and ^{31}P NMR spectra it was

noted that the ratio of the signals had changed since the first time the spectra were recorded. This observation prompted further investigation of these three mixtures.

The use of pulsed-field gradient spin-echo (PGSE) diffusion NMR spectroscopy was a useful tool in trying to determine the size of macrocycles produced from these reactions.[9] This is a technique which is used to determine the diffusion coefficients[10] of molecules in solution and this information can then be used to calculate an approximate radius for the molecules in question using the Stokes-Einstein equation (equation 5.1).[11] This technique has in the past been applied to various different systems including metallomacrocycles[12,13] and was applied to the macrocycles $[Fe_n\{Pt(\mathbf{1}\text{-}H)_2(PR_3)_2\}_n][PF_6]_{2n}$ where R = Et, Bu and Ph.

$$D = \frac{k_b T}{6\pi\eta r_H}$$

Equation 5.1: Stokes-Einstein equation for calculating the hydrodynamic radius (r_H) from the diffusion coefficient (D). T is absolute temperature, k_b is the Boltzmann constant and η is the viscosity of the solvent.

The aim of this study (carried out in conjunction with Jon Beves) was to confirm which NMR signals belong to which individual species, as well as to assign relative sizes to each of the components of each mixture. The signals in the ^{1}H NMR spectrum for the B3 protons of two components were suitably well resolved so that these could be used to determine the diffusion coefficients of each component. Hydrodynamic radii were calculated for each signal and a DOSY plot was obtained which correlates each signal with its calculated radius. Figure 5.6 shows the DOSY plot of the aromatic region of the ^{1}H NMR for $[Fe_n\{Pt(\mathbf{1}\text{-}H)_2(PEt_3)_2\}_n][PF_6]_{2n}$.

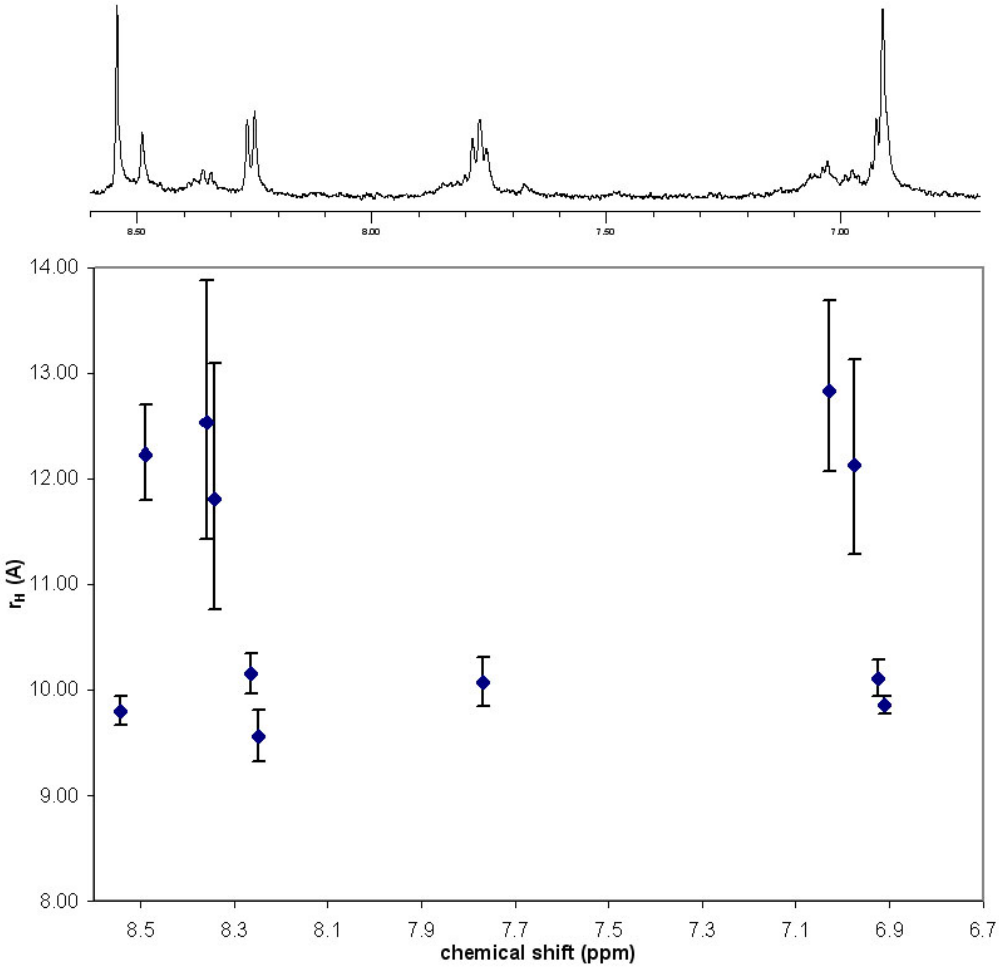

Figure 5.6: DOSY plot of the aromatic region of the ^{1}H NMR spectrum of macrocycles $[Fe_n\{Pt(\mathbf{1}\text{-}H)_2(PEt_3)_2\}_n][PF_6]_{2n}$. There is good agreement with there being one macrocycle of radius approximately 10 Å as well as several other larger species of radius ~12-13 Å. The spectrum was run in CD_3CN at 500 MHz.

The ^{31}P NMR spectrum showed that the crude reaction mixture obtained on adding iron(II) to the platinahomoditopic ligand $Pt(\mathbf{1}\text{-}H)_2(PEt_3)_2$ contained three species although the ^{1}H NMR signal corresponding to the B3 proton for one of these species was not well enough resolved to obtain a diffusion coefficient. The important point to note from the DOSY plot in figure 5.6 is that the ^{1}H NMR signals fall into two bands. The major component is assigned to the [2+2] macrocycle. The value for r_H of 9.7 Å gives a molecular diameter of 19.4 Å and this is in good agreement with that estimated from the X-ray crystal structure of 18-19 Å (see Section 5.4.2). Although the error bars are large, it can be seen clearly that the minor component has a significantly larger radius than the [2+2] macrocycle. Molecular modelling showed that

there is significant strain in a [1+1] macrocycle, indicating that only products of size [2+2] and larger are able to form. This observation is in accordance with the results seen in the DOSY plot. The second solution species has a radius obtained from the DOSY plot of approximately 12-12.5 Å which suggests the formation of a [3+3] macrocycle, $[Fe_3\{Pt(\mathbf{1}\text{-}H)_2(PEt_3)_2\}_3][PF_6]_6$. It would seem that on reaction of $Pt(\mathbf{1}\text{-}H)_2(PEt_3)_2$ with $FeCl_2.4H_2O$ at either room temperature or at reflux in MeOH, a mixture of three kinetic products is obtained, most probably $[Fe_2\{Pt(\mathbf{1}\text{-}H)_2(PEt_3)_2\}_2][PF_6]_4$, $[Fe_3\{Pt(\mathbf{1}\text{-}H)_2(PEt_3)_2\}_3][PF_6]_6$ and $[Fe_4\{Pt(\mathbf{1}\text{-}H)_2(PEt_3)_2\}_4][PF_6]_8$. On allowing the solution to stand for a period of several weeks the two larger species convert to $[Fe_2\{Pt(\mathbf{1}\text{-}H)_2(PEt_3)_2\}_2][PF_6]_4$, the thermodynamic product. Similar results have been observed where R = ^{n}Bu and Ph, but well resolved DOSY spectra were difficult to obtain.

5.3.3 ^{13}C NMR Spectroscopy

Iron(II) complexes were characterised by ^{13}C NMR spectroscopy and spectra were obtained in CD_3CN solution. Table 5.2 shows the ^{13}C NMR chemical shifts for representative iron(II) tpy complexes synthesised in this chapter. Due to the small quantities obtained it was not possible to record well resolved spectra for the $[Fe_2\{Pt(\mathbf{1}\text{-}H)_2(P^nBu_3)_2\}_2][PF_6]_4$ and $[Fe_2\{Pt(\mathbf{1}\text{-}H)_2(PPh_3)_2\}_2][PF_6]_4$ complexes. It was also not possible to observe the signals corresponding to the alkyne carbons in $[Fe_2\{Pt(\mathbf{1}\text{-}H)_2(PEt_3)_2\}_2][PF_6]_4$.

	A2	A3	A4	A5	A6
$[Fe(\mathbf{4})_2][PF_6]_2$	161.7/ 158.9	124.5	139.3	128.1	154.3
$[Fe(\mathbf{5})_2][PF_6]_2$	161.7/ 158.9	124.4	139.3	128.0	154.3
$[Fe_2\{Pt(\mathbf{1}\text{-}H)_2(PEt_3)_2\}_2][PF_6]_4$	161.1/ 159.0	124.3	139.4	127.9	153.9

	B2	B3	B4
$[Fe(\mathbf{4})_2][PF_6]_2$	161.7/ 158.9	112.3	168.8
$[Fe(\mathbf{5})_2][PF_6]_2$	161.7/ 158.9	112.4	168.7

$[Fe_2\{Pt(\mathbf{1}\text{-}H)_2(PEt_3)_2\}_2][PF_6]_4$	161.1/ 159.0	113.2	168.3

	a	b	c	d	e
$[Fe(\mathbf{4})_2][PF_6]_2$	71.0	69.8	73.7/ 62.0	73.7/ 62.0	
$[Fe(\mathbf{5})_2][PF_6]_2$	70.9	69.8	69.9	71.3	58.7
$[Fe_2\{Pt(\mathbf{1}\text{-}H)_2(PEt_3)_2\}_2][PF_6]_4$	61.7				

	w	x	y	z	*C*≡CR	C≡*C*R
$[Fe(\mathbf{4})_2][PF_6]_2$						
$[Fe(\mathbf{5})_2][PF_6]_2$					80.8	75.7
$[Fe_2\{Pt(\mathbf{1}\text{-}H)_2(PEt_3)_2\}_2][PF_6]_4$			17.1	8.7	Not observed.	

Table 5.2: 125 MHz ^{13}C chemical shifts for representative iron(II) complexes synthesised. All spectra were recorded in CD_3CN.

^{13}C NMR chemical shifts were assigned using HMQC and HMBC techniques. As expected there is very little difference in the chemical shifts of carbon atoms between complexes $[Fe(\mathbf{4})_2][PF_6]_2$ and $[Fe(\mathbf{5})_2][PF_6]_2$.

5.3.4 ^{31}P NMR Spectroscopy

Iron(II) bis(tpy) complexes were characterised by ^{31}P NMR spectroscopy. Since all complexes were isolated as the hexafluorophosphate salts, the septet arising from this could be used as an internal reference (δ -144.6 ppm). As for the platinahomoditopic ligands, the macrocycles formed from these starting materials contain phosphorus atoms bound directly to the platinum(II) centre. This means that the coupling constant of the satellite peaks arising from coupling of the ^{31}P nuclei to NMR active ^{195}Pt (I = ½ , 33.8 %) is a useful way of confirming that the geometry around the Pt(II) centre remains *trans* and has not changed to *cis* on coordination of the tpy with Fe(II). As with the platinahomoditopic ligands, a coupling constant of around 2300 Hz is indicative of *trans* geometry, one around 3000 Hz indicates *cis*.

With the Au(I) ditopic ligands there are no satellites and so the ^{31}P NMR signals for these complexes appear as singlets. Table 5.3 shows ^{31}P chemical shifts for Fe(II) complexes synthesised in this chapter.

Compound	δ/ppm
$[Fe_2\{Pt(\mathbf{1}\text{-}H)_2(PEt_3)_2\}_2][PF_6]_4$	12.0
$[Fe_2\{Pt(\mathbf{1}\text{-}H)_2(P^nBu_3)_2\}_2][PF_6]_4$	3.0
$[Fe\{Pt(\mathbf{5}\text{-}H)_2(PEt_3)_2\}][PF_6]_2$	8.8
$[Fe\{Au(\mathbf{1}\text{-}H)(P^nBu_3)\}_2][PF_6]_2$	36.3

Table 5.3: 202 MHz ^{31}P chemical shifts (δ/ppm) for Fe(II) complexes. All shifts are referenced with respect to the internal reference of PF_6^- at δ -144.6 ppm. All spectra were recorded in CD_3CN solution.

The observation that the ratio of the different peaks in the ^{31}P NMR was changing over time prompted attempts to interconvert the macrocycles by heating the samples. Monitoring the conversion by ^{31}P NMR spectroscopy showed that this was indeed the case. A new solution of $[Fe_n\{Pt(\mathbf{1}\text{-}H)_2(P^nBu_3)_2\}_n][PF_6]_{2n}$ in CD_3CN was heated at around 55 ˚C for a total of 247 hours. The ^{31}P NMR spectrum was recorded periodically and the relative integrals of the different signals were noted.

Figure 5.7 shows a graph of the relative integrals of the ^{31}P NMR signals of the species versus time. Integrals were measured with respect to PF_6^- (which was set to 100). The graph clearly shows how the species assigned to the [2+2] species using PGSE NMR spectroscopy increases with time at the expense of the other, larger, species. There are some anomalies in the graph, the most important one being the increase in the quantity of larger species at the start of the measurements before the eventual decrease. These anomalies can most likely be explained by the fact that the integration of NMR spectra is not an exact science. Although care was taken to measure the integrals from approximately the same point of each spectrum there are always going to be slight differences in the width of the integral and therefore the calculation. Integrals were corrected using the automatic integration correction function which is built into the software used to view and compare

NMR spectra and this in itself means there is a certain margin of error in each point on the graph.

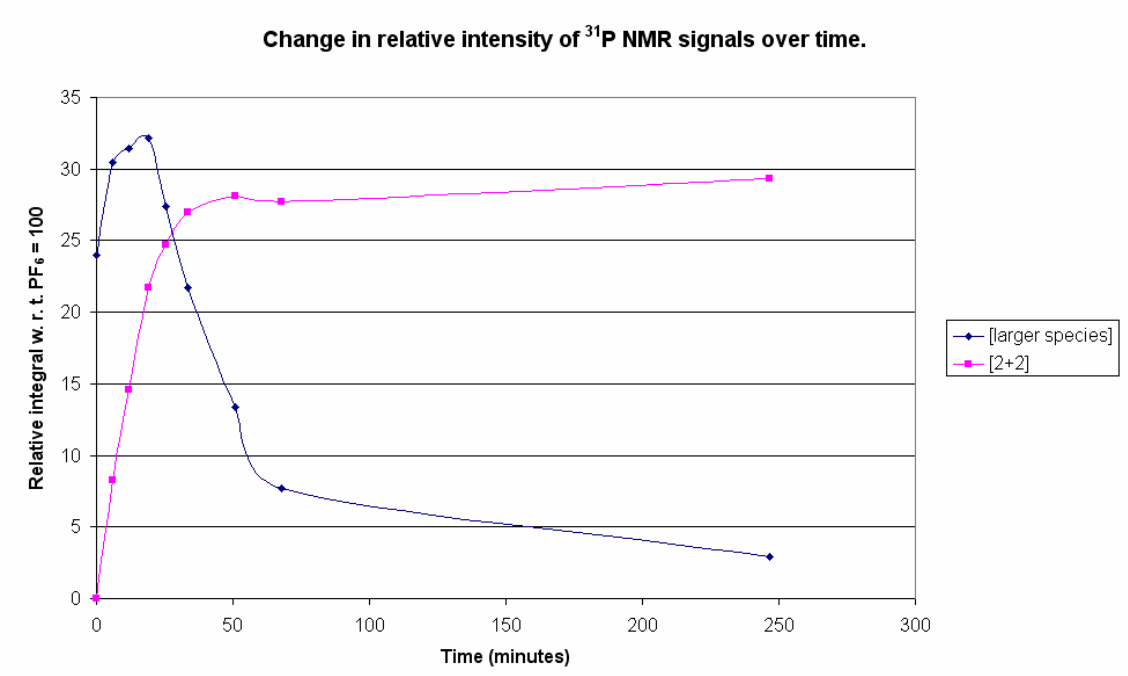

Figure 5.7: Graph of the relative intensity of ^{31}P NMR signals with respect to an internal reference of PF_6^- over time.

If we take the PF_6^- out of the equation and plot a graph of the ratio of the integrals of the [2+2] macrocycle to the larger species against time the results are much clearer. It is easy to see from the graph in figure 5.8 how the relative quantity of the [2+2] species increases at the expense of the larger species. Due to problems with loss of solvent from the sample over the first 24 hour period, the line of best fit on the graph in figure 5.8 does not pass through zero. For much of this 24 hour period the sample had no solvent in and therefore the larger components of the mixture were unable to convert into the [2+2] macrocycle. After 24 hours the solvent was replaced and further monitoring of the conversion showed that there was a linear relationship between the ratio of the macrocycles and the time the sample was in solution at elevated temperature.

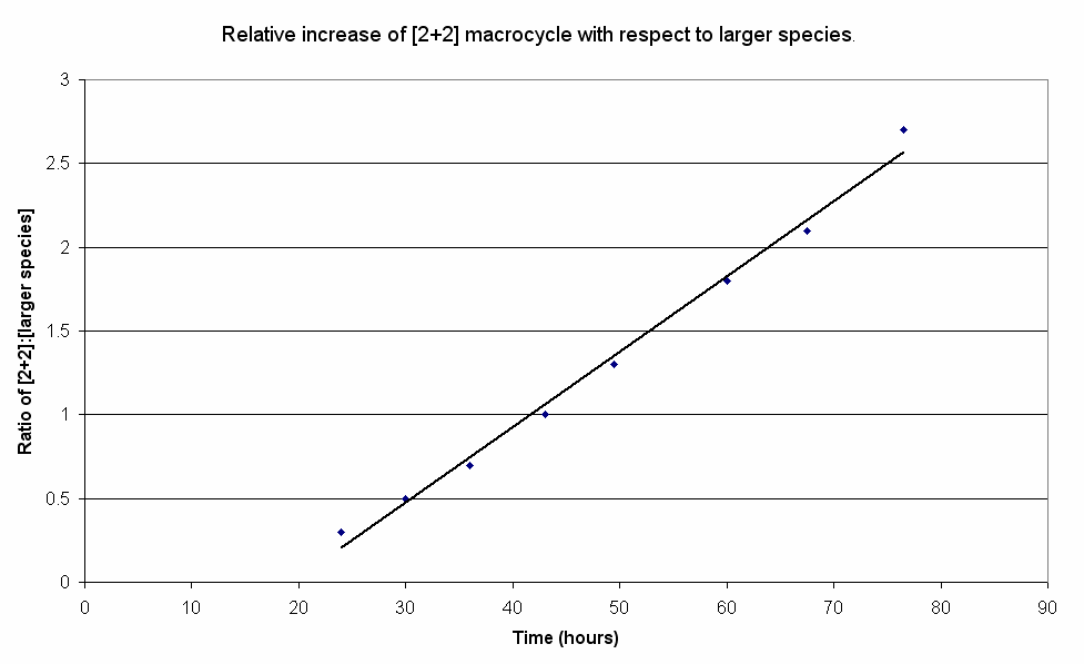

Figure 5.8: Graph showing the increase of the [2+2] species relative to larger species. Points were plotted as a ratio of [2+2]:[larger species], integrals were not calculated with respect to an internal reference of PF_6^-.

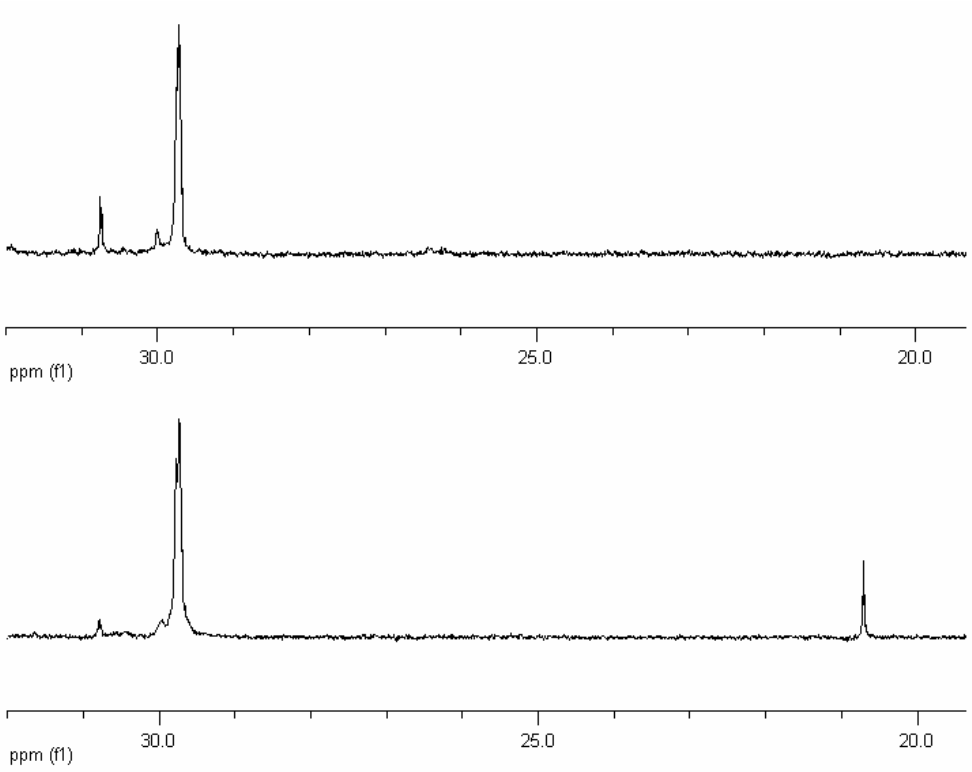

Figure 5.9: 162 MHz ^{31}P NMR spectra of $[Fe_n\{(Au(\mathbf{1}\text{-}H))_2(dppe)\}_n][PF_6]_{2n}$ recorded in CD_3CN before (above) and after (below) standing in MeCN solution at room temperature for several days.

Reaction of (Au(**1**-H))$_2$(dppe) with Fe(II) also produced a mixture, several peaks being seen in the ^{31}P NMR spectrum. Standing a sample of this mixture in solution for several days resulted in a change in the NMR signals, similar to those observed with the platinum(II) analogues. Figure 5.9 shows the two ^{31}P NMR spectra of the mixture obtained from the reaction of (Au(**1**-H))$_2$(dppe) with Fe(II), the top spectrum is that obtained immediately after reaction, the bottom spectrum is after the solution had been standing for several days. It can be seen that the peak around δ 31 ppm decreases while the peak at δ 21 ppm grows in. While limited time meant that PGSE NMR studies were not carried out on this sample, these preliminary results show that perhaps a similar interconversion to that seen with the platinum(II) containing macrocycles is taking place.

5.3.5 MALDI and ES Mass Spectrometry

Mass spectrometry, both MALDI and/or ESMS, was a useful tool for characterisation of these complexes. As well as information on the molecular masses of fragments, ESMS gives information about the charges and it is possible to expand the spectra in order to see isotope patterns which can then be compared with calculated isotope patterns as another way of confirming the assignment of the fragment seen in the spectrum is correct. Figure 5.10 shows the ES mass spectrum of [Fe$_2${Pt(**1**-H)$_2$(PEt$_3$)$_2$}$_2$][PF$_6$]$_4$ in MeCN.

Peaks can be assigned to various fragments of a [2+2] macrocycle, corresponding with the information obtained from the X-ray crystal structure (see chapter 5.4.2). The most important peaks are m/z 1086.8 corresponding to [M - 2(PEt$_3$) - 2(PF$_6$-)]$^{2+}$, 755.1 [M - 3(PF$_6^-$)]$^{3+}$ and 704.9 [M - 3(Et) - 3(PF$_6^-$)]$^{3+}$.

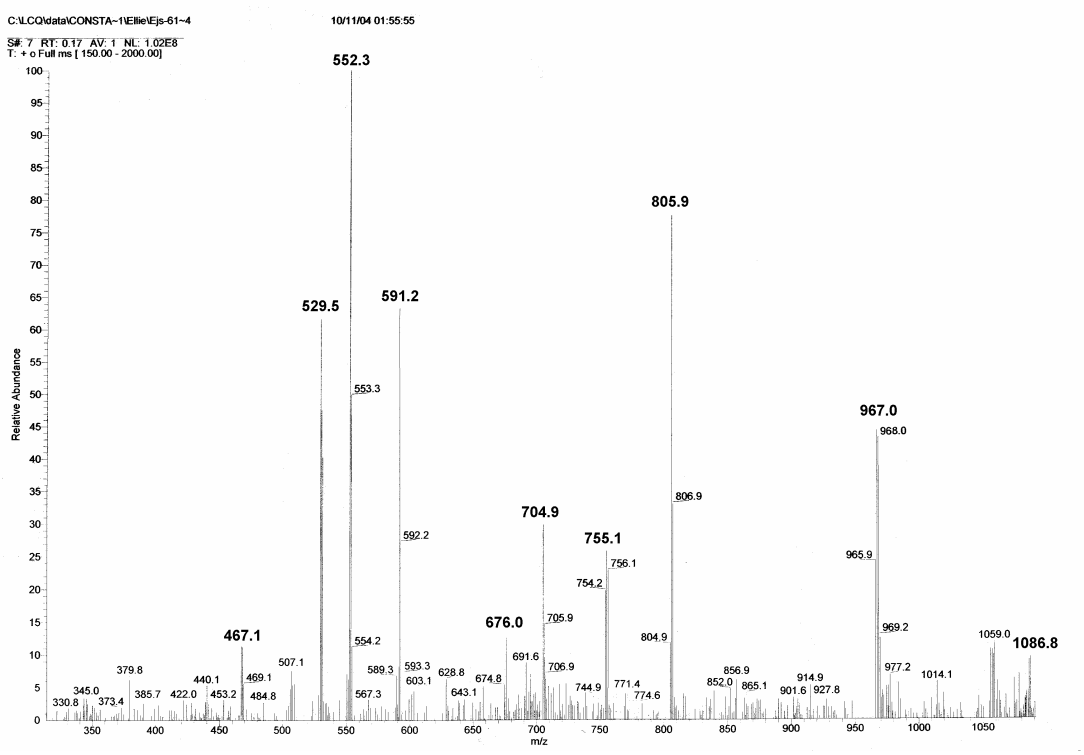

Figure 5.10: ES mass spectrum of $[Fe_2\{Pt(\mathbf{1}\text{-}H)_2(PEt_3)_2\}_2][PF_6]_4$ in MeCN.

5.3.6 UV/VIS Spectroscopy

Iron(II) complexes were characterised by UV/VIS spectroscopy in MeCN solution. The spectra were similar to those for the tpy ligands at lower wavelengths. However, the presence of an asymmetrical MLCT (metal to ligand charge transfer) band around 550 nm is further evidence for coordination of the tpy moiety.[14] This absorption is responsible for the purple colour of the iron(II) bis(tpy) complexes, since light of this wavelength is green in colour, meaning the blue and red light is reflected and the complex appears purple. The UV/VIS spectrum of $[Fe_2\{Pt(\mathbf{1}\text{-}H)_2(PEt_3)_2\}_2][PF_6]_4$ in MeCN can be seen in figure 5.11.

UV/VIS data for representative iron(II) tpy complexes synthesised in this chapter can be seen in table 5.4.

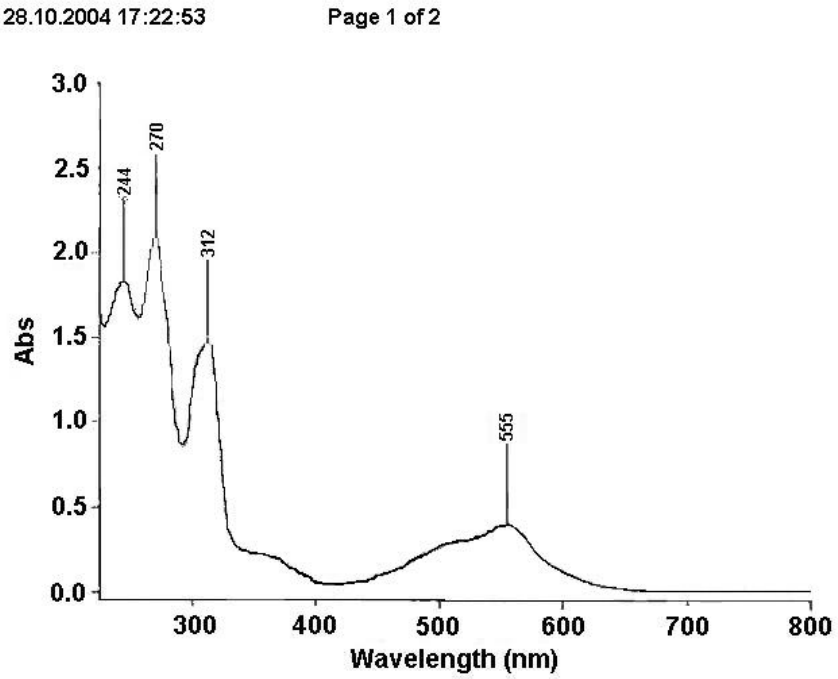

Figure 5.11: UV/VIS spectrum of $[Fe_2\{Pt(\mathbf{1}\text{-}H)_2(PEt_3)_2\}_2][PF_6]_4$ in MeCN. The MLCT band can clearly be seen at 555 nm.

	C	A (ε)	A (ε)	A (ε)	A (ε)
$[Fe_2\{Pt(\mathbf{1}\text{-}H)_2(PEt_3)_2\}_2][PF_6]_4$	$7.41x10^{-5}$	245 (99600)	272 (116400)	312 (81900)	557 (23350)
$[Fe_2\{Pt(\mathbf{1}\text{-}H)_2(P^nBu_3)_2\}_2][PF_6]_4$	$2.64x10^{-5}$	246 (67200)	271 (78500)	313 (49300)	558 (13000)
$[Fe\{Au(\mathbf{1}\text{-}H)(P^nBu_3)\}_2][PF_6]_2$	$1.75x10^{-5}$	243 (30100)	273 (29600)	315 (22600)	556 (6700)

Table 5.4: UV/VIS data for representative iron(II) bis(tpy) complexes. All spectra were recorded in MeCN. C (mol dm^{-3}), A (nm), ε ($dm^3\ mol^{-1}\ cm^{-1}$).

5.4 Crystal Structures

5.4.1 $[Fe(\mathbf{5})_2][PF_6]_2$

Crystals of $[Fe(\mathbf{5})_2][PF_6]_2$ were grown from a solution in CH_2Cl_2 layered with hexane. An ORTEP representation is shown in figure 5.12 as well as a

packing diagram in figure 5.13 and selected bond lengths and angles in table 5.5.

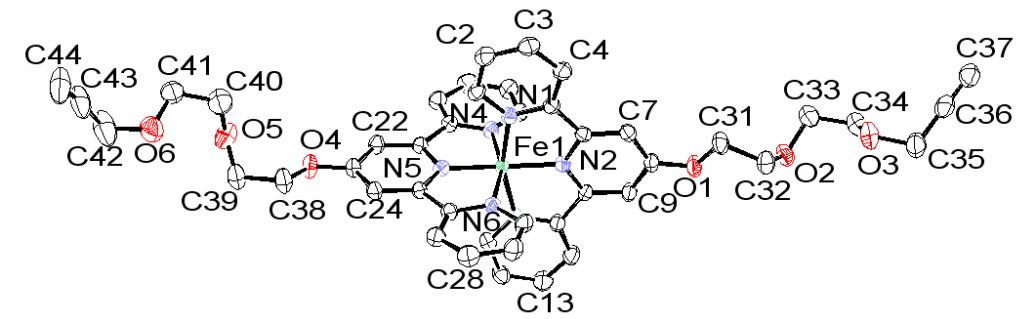

Figure 5.12: ORTEP representation of the cation in $[Fe(\mathbf{5})_2][PF_6]_2$. Crystals were grown from a solution in CH_2Cl_2 layered with hexane.

The structure of the $[Fe(\mathbf{5})_2]^{2+}$ cation in $[Fe(\mathbf{5})_2][PF_6]_2$ is not symmetrical. The conformation of each of the spacers is different, due to intermolecular hydrogen bonds between H42 and O1 as well as interactions of the chains with the PF_6^- counterions. The iron(II) is octahedrally coordinated as expected.

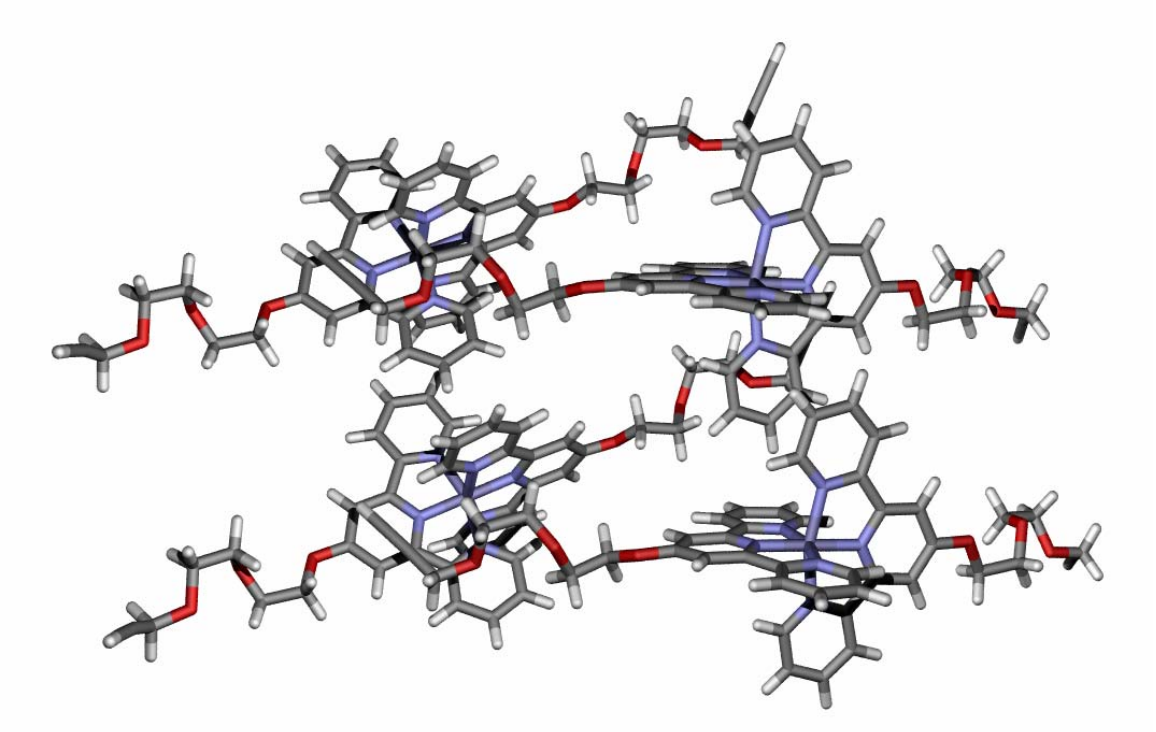

Figure 5.13: Packing diagram of $[Fe(\mathbf{5})_2][PF_6]_2$. PF_6^- ions have been removed for clarity.

Bond	Distance/Å	Bond	Distance/Å
Fe1-N1	1.982(2)	Fe1-N4	1.982(2)
Fe1-N2	1.892(2)	Fe1-N5	1.886(2)
Fe1-N3	1.983(2)	Fe1-N6	1.978(2)
C8-O1	1.334(3)	C23-O4	1.349(3)
O1-C31	1.453(3)	O4-C38	1.439(3)
C31-C32	1.504(4)	C38-C39	1.509(4)
C32-O2	1.409(4)	C39-O5	1.396(4)
O2-C33	1.424(4)	O5-C40	1.433(4)
C33-C34	1.493(5)	C40-C41	1.477(5)
C34-O3	1.416(4)	C41-O6	1.393(5)
O3-C35	1.431(4)	O6-C42	1.391(5)
C35-C36	1.449(5)	C42-C43	1.499(6)
C36-C37	1.192(5)	C43-C44	1.142(6)

Bonds	Angle/deg.	Bonds	Angle/deg.
N1-Fe1-N2	80.54(9)	C32-O2-C33	115.7(2)
N2-Fe1-N3	80.87(9)	C33-C34-O3	108.6(3)
N4-Fe1-N5	80.45(9)	C34-O3-C35	111.8(3)
N5-Fe1-N6	81.07(9)	C35-C36-C37	178.1(3)
C6-N2-C10	120.5(2)	C23-O4-C38	117.1(2)
C1-N1-C5	118.6(2)	O4-C38-C39	107.8(2)
C11-N3-C15	117.6(2)	C38-C39-O5	113.4(3)
C16-N4-C20	118.8(2)	C39-O5-C40	115.7(3)
C21-N5-C25	120.3(2)	O5-C40-C41	109.7(3)
C26-N6-C30	118.8(2)	C40-C41-O6	108.8(3)
C8-O1-C31	118.5(2)	C41-O6-C42	114.4(4)
O1-C31-C32	106.4(2)	C42-C43-C44	172.6(6)
C31-C32-O2	112.9(3)		

Table 5.5: Selected bond lengths (Å) and angles (˚) for $[Fe(\mathbf{5})_2][PF_6]_2$.

5.4.2 $[Fe_2\{Pt(\mathbf{1}\text{-}H)_2(PEt_3)_2\}_2][PF_6]_4.C_6H_5CH_3.4MeCN$

Crystals of $[Fe_2\{Pt(\mathbf{1}\text{-}H)_2(PEt_3)_2\}_2][PF_6]_4.C_6H_5CH_3.4MeCN$ were grown from a solution in MeCN layered on top of toluene. An ORTEP representation is shown in figure 5.14 and a packing diagram is shown in figure 5.15. Selected bond parameters are given in table 5.6.

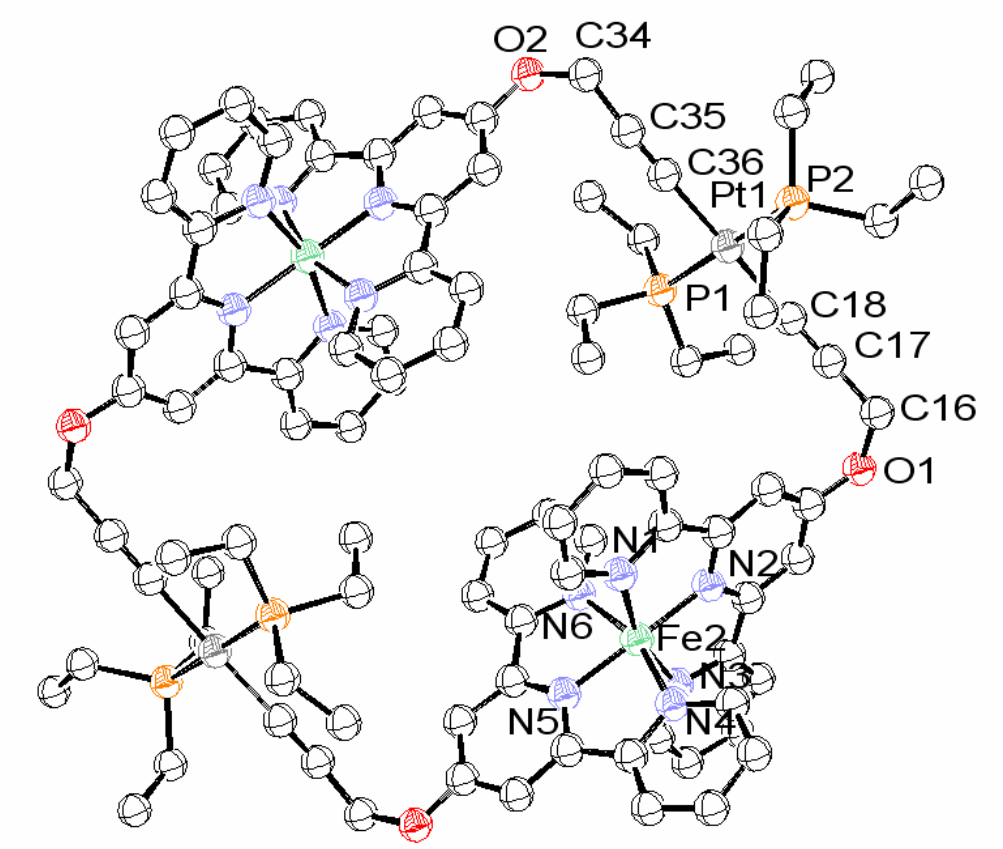

Figure 5.14: ORTEP representation of the cation in $[Fe_2\{Pt(\mathbf{1}\text{-}H)_2(PEt_3)_2\}_2][PF_6]_4$.

The [2+2] macrocycle $[Fe_2\{Pt(\mathbf{1}\text{-}H)_2(PEt_3)_2\}_2][PF_6]_4$ is symmetrical about an inversion centre at the middle of its cavity. Two phosphine groups point into the centre of the cycle and two point outside, and the corners of the rectangular structure are formed by the ether part of the spacer. The molecule measures 10.5 Å between the two iron(II) centres and 13.6 Å between the two platinum(II) centres.

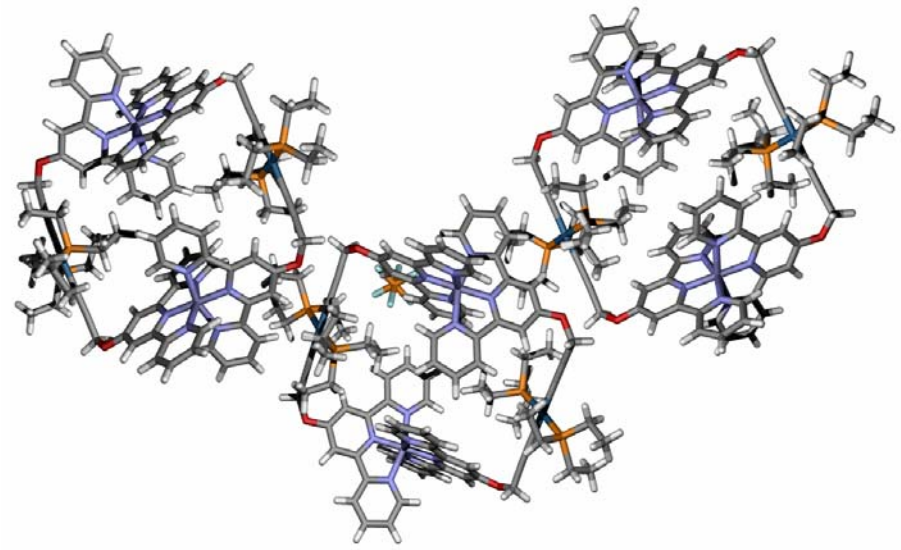

Figure 5.15: Packing diagram of $[Fe_2\{Pt(\mathbf{1}\text{-}H)_2(PEt_3)_2\}_2][PF_6]_4$.

Bond	Distance/Å	Bond	Distance/Å
Pt1-P1	2.3042(12)	C17-C16	1.465(6)
Pt1-P2	2.3068(12)	C16-O1	1.446(5)
Pt1-C36	1.992(5)	O1-C8	1.349(4)
C36-C35	1.200(6)	Fe2-N1	1.975(3)
C35-C34	1.469(7)	Fe2-N2	1.888(3)
C34-O2	1.455(6)	Fe2-N3	1.981(3)
O2-C26	1.358(4)	Fe2-N4	1.965(3)
Pt1-C18	2.003(5)	Fe2-N5	1.892(3)
C18-C17	1.204(6)	Fe2-N6	1.971(3)

Bonds	Angle/deg.	Bonds	Angle/deg.
P1-Pt1-P2	175.45(4)	C18-C17-C16	174.0(5)
C18-Pt1-C36	175.23(17)	C17-C16-O1	112.9(3)
P1-Pt1-C36	89.64(13)	C16-O1-C8	118.7(3)
P1-Pt1-C18	93.28(12)	Pt1-C36-C35	176.7(4)
P2-Pt1-C18	87.90(12)	C36-C35-C34	177.0(5)
P2-Pt1-C36	88.90(13)	C35-C34-O2	114.3(4)
Pt1-C18-C17	174.2(4)	C34-O2-C26	118.2(3)

Table 5.6: Selected bond lengths (Å) and angles (°) of $[Fe_2\{Pt(\mathbf{1}\text{-}H)_2(PEt_3)_2\}_2][PF_6]_4$.

5.5 Conclusion

Several different iron(II) bis(tpy) complexes have been synthesised. In the cases where these have been synthesised starting from a platinahomoditopic ligand, macrocyclic species of varying sizes were produced. Initial mixtures of macrocycles have been shown to interconvert to one thermodynamically stable product on standing in solution for a period of time. An example of a [2+2] macrocycle has been characterised by X-ray crystallography and this has proved that platinahomoditopic ligands are a viable precursor to the supramolecular assembly of heterometallic macrocycles.

5.6 References

[1] E. C. Constable, *Adv. Inorg. Chem. Radiochem.*, 1986 **30**, 69.

[2] P. R. Andres and U. S. Schubert, *Adv. Mater.*, 2004, **16**, 1043.

[3] B. G. Lohmeijer and U. S. Schubert, *J. Polym. Sci. Part A. Polym. Chem.*, 2003, **41**, 1413.

[4] E. C. Constable, G. Baum, E. Bill, R. Dyson, R. van Eldik, D. Fenske, S. Kaderli, D. Morris, A. Neubrand, M. Neuburger, D. R. Smith, K. Wieghardt, M. Zehnder and A. Zuberbühler, *Chem. Eur. J.*, 1999, **5**, 497.

[5] E. C. Constable, C. E. Housecroft, M. Neuburger, S. Schaffner and E. J. Shardlow, *Dalton Trans.*, 2005, 234

[6] H. Elsbernd and J. K. Beattie, *J. Inorg. Nucl. Chem.*, 1972, **34**, 771.

[7] E. C. Constable, C. E. Housecroft, M. Neuburger, S. Schaffner and E. J. Shardlow, *Inorg. Chim. Acta*, 2007, in press.

[8] A. Sebald, B. Wrackmeyer and W. Beck, *Z. Naturforsch. B*, 1983, **38**, 45.

[9] J. E. Beves, E. C. Constable, C. E. Housecroft, M. Neuburger, S. Schaffner and E. J. Shardlow, *Dalton Trans*., 2007, in press.

[10] E. Martínez-Viviente and P. S. Pregosin, *Helv. Chim. Acta*, 2003, **86**, 2364.

[11] Y. Cohen, L. Avram and L. Frish, *Angew. Chem. Int. Ed.*, 2005, **44**, 520.

[12] W. H. Otto, M. H. Keefe, K. E. Splan, J. T. Hupp and C. K. Larive, *Inorg. Chem.*, 2002, **41**, 6172.

[13] J. E. Beves, B. E. Chapman, P. W. Kuchel, L. F. Lindoy, J. McMurtrie, M. McPartlin, P. Thordarson and G. Wei, *Dalton Trans.*, 2006, 744.
[14] E. C. Constable and A. M. W. Cargill Thompson, *J. Chem. Soc. Dalton Trans.*, 1994, 1409.

Chapter 6 Experimental

6.1 2,2':6',2"-Terpyridine Ligands

6.1.1 4'-Hydroxy-2,2':6',2"-terpyridine **HO-tpy**[1]

A solution of 1,5-bis(2'-pyridyl)pentane-1,3,5-trione (1.99 g, 7.42 mmol) and ammonium acetate (4.0 g) in ethanol (50 ml) was heated to reflux for 6 hours. The dark brown solution was then concentrated to half volume. The solution was cooled in ice and a precipitate formed. This was filtered, washed with diethyl ether and recrystallised from ethanol (1.08 g, 4.33 mmol, 58 %).

^{1}H NMR ($CDCl_3$, 250 MHz): δ/ppm 12.05 (s, NH, 1H); 8.80 (dt, 2H, *J* 4.8, 1.2 Hz, 2H, A6,); 7.90 (m, 4H, A3 and A4); 7.44 (td, *J* 4.8, 1.6 Hz, 2H, A5); 7.18 (s, 2H, B3).

6.1.2 4'-(2-Propyn-1-oxy)-2,2':6',2"-terpyridine **1**[2]

A solution of **HO-tpy** (0.451 g, 1.81 mmol) in acetonitrile (60 ml) was stirred, then treated with potassium carbonate (1.50 g, 10.9 mmol) then 3-bromoprop-1-yne (80 % solution in toluene) (0.225 ml, 2.09 mmol) was added. The suspension was heated at 60 ˚C for 12 hours. The reaction mixture was then cooled to room temperature and poured into water (100 ml). The precipitate formed was collected by filtration. The product was recrystallised from a solution in CH_2Cl_2 layered with hexane. The ^{13}C NMR spectrum had not previously been assigned and was recorded (0.360 g, 1.25 mmol, 66 %).

^{1}H NMR ($CDCl_3$, 500 MHz): δ/ppm 8.69 (dq, *J* 4.8, 0.9 Hz, 2H, A6); 8.61 (dt, *J* 7.9, 1.0 Hz, 2H, A3); 8.09 (s, 2H, B3); 7.84 (td, *J* 7.9, 1.8 Hz, 2H, A4); 7.33 (ddd, *J* 7.5, 4.8, 1.2 Hz, 2H, A5); 4.93 (d, *J* 2.4 Hz, 2H, CH_2); 2.58 (t, *J* 2.4 Hz, 1H, C≡C*H*).

^{13}C NMR ($CDCl_3$, 125 MHz): δ/ppm 165.85 (B4); 157.28 (A2/B2); 155.92 (A2/B2); 149.11 (A6); 136.80 (A4); 123.91 (A5); 121.37 (A3); 107.57 (B3); 77.59 (*C*≡CH); 76.32 (C≡*C*H); 55.85 (a).

6.1.3 4'-(4-Pentyn-1-oxy)-2,2':6',2''-terpyridine **2**

HO-tpy (0.219 g, 0.879 mmol) in MeCN (30 ml) was stirred then treated with K_2CO_3 (1 g, excess) and 5-bromopent-1-yne (0.264 g, 1.80 mmol). The suspension was heated at 60°C for 12 hours. It was then poured into iced water and the precipitate was collected by filtration. The product was purified by recrystallisation from CH_2Cl_2/hexane (0.0881 g, 0.279 mmol, 29 %).

^{1}H NMR ($CDCl_3$, 400 MHz): δ/ppm 8.69 (d, *J* 4.5 Hz, 2H, A6); 8.62 (d, *J* 7.8 Hz, 2H, A3); 8.03 (s, 2H, B3); 7.83 (td, *J* 7.8, 1.5 Hz, 2H, A4); 7.33 (dd, *J* 7.3, 5.1 Hz, 2H, A5); 4.35 (t, *J* 6.1 Hz, 2H, a); 2.45 (td, *J* 6.9, 2.5 Hz, 2H, c); 2.08 (m, *J* 6.6 Hz, 2H, b); 1.98 (t, *J* 2.5 Hz, 1H, C≡C*H*).

^{13}C NMR ($CDCl_3$ 100 MHz): δ/ppm 167.6 (B4); 157.4 (A2/B2); 156.4 (A2/B2); 149.4 (A6); 137.4 (A4); 124.3 (A5); 121.8 (A3); 107.79 (B3); 83.6 (*C*≡CH); 69.5 (C≡*C*H); 66.8 (a); 28.4 (b); 15.5 (c).

MALDI: M/z 316 $[M]^+$.

IR (solid, cm^{-1}): 3296w, 3258w, 3194w, 2937w, 1599m, 1582s, 1559s, 1466s, 1443s, 1404s, 1364s, 1342s, 1252m, 1200s, 1117w, 1094m, 1040s, 991s, 960m, 903w, 885m, 860m, 795s, 743s, 696s, 658s, 621s.

UV/VIS λ_{max}/nm (2.41×10^{-5} mol dm^{-3} CH_2Cl_2) 278 (ε/dm^3 mol^{-1} cm^{-1} 12000).

Elemental analysis: Calc. C 76.17 %, H 5.43 %, N 13.32 %; Found C 75.32/75.41 %, H 5.33/5.43 %, N 13.04/13.06 %.

Melting Point: STA shows two different phase changes at 96 and 115 ˚C.

6.1.4 4'-(5-Hexyn-1-oxy)-2,2':6',2"-terpyridine **3**[3]

HO-tpy (0.520 g, 2.09 mmol), K_2CO_3 (2.2 g, excess) and 6-bromohex-1-yne (0.697 g, 4.33 mmol) in MeCN (50 ml) were stirred at 60°C for 12 hours. The reaction was poured into iced water and the precipitate collected by filtration and purified by recrystallisation from EtOH (0.384 g, 1.15 mmol, 56 %).

^{1}H NMR ($CDCl_3$, 400 MHz): δ/ppm 8.70 (ddd, *J* 4.8, 1.6, 0.8 Hz, 2H, A6); 8.63 (dt, *J* 8.0, 1.1 Hz, 2H, A3); 8.04 (s, 2H, B3); 7.88 (td, *J* 7.6, 1.6 Hz, 2H, A4); 7.35 (ddd, *J* 7.2, 4.8, 1.2 Hz, 2H, A5); 4.28 (t, *J* 6.4 Hz, 2H, a); 2.30 (td, *J* 7.2, 2.4 Hz, 2H, d); 2.00 (quintet, *J* 6.8 Hz, 2H, b); 1.99 (t, *J* 2.4 Hz, 1H, C≡C*H*); 1.77 (quintet, *J* 6.8 Hz, 2H, c).

^{13}C NMR ($CDCl_3$ 125 MHz): δ/ppm 167.4 (B4), 157.0 (A2/B2), 156.0 (A2/B2), 149.0 (A6), 136.9 (A4), 123.9 (A5), 121.4 (A3), 107.4 (B3), 84.0 (*C*≡CH), 68.8 (C≡*C*H), 67.6 (a), 28.0 (b), 24.9 (c), 18.1 (d).

MALDI: M/z 331 $[M]^+$.

IR (solid, cm^{-1}): 3202w, 2947w, 2870w, 1558s, 1466m, 1442.66s, 1404s, 1358s, 1250m, 1204s, 1157m, 1119m, 1088m, 1018s, 987s, 918s, 864s, 787s, 733s, 694s, 656s, 617s.

UV/VIS λ_{max}/nm (1.82×10^{-5} mol dm^{-3} CH_2Cl_2) 211 (ε/dm^3 mol^{-1} cm^{-1} 34500), 242 (28600).

Elemental analysis: Calc. C 76.57 %, H 5.81 %, N 12.76 %; Found C 74.97/74.90 %, H 5.70/5.80 %, N 12.37/12.53 %.

Melting Point: 97.1 - 98.9 °C (both polymorphs).

6.1.5 4'-[2-(2-Hydroxyethoxy)ethoxy]-2,2':6',2"-terpyridine **4**[4]

HO-tpy (0.509 g, 2.04 mmol), KI (0.310 g, 2.06 mmol) and K_2CO_3 (1.13 g, 8.16 mmol) in DMF (20 ml) were stirred at 70°C for 1 hour. 2-(2-Chloroethoxy)ethanol (0.23 ml, 2.18 mmol) was added and the reaction stirred at this temperature for 48 hours. The solvent was removed and the residue suspended in CH_2Cl_2. This was washed with 2M NaOH solution, saturated $NaHCO_3$ and finally water. The water phase was washed with CH_2Cl_2 and the combined CH_2Cl_2 phases dried over $MgSO_4$. The solvent was removed to leave a brown oil which later solidified. The ^{1}H NMR spectrum agreed with those values reported in the literature. The ^{13}C NMR spectrum had been reported[4] but the peaks had not been assigned (0.41 g, 1.18 mmol, 57 %).

^{1}H NMR ($CDCl_3$, 500 MHz): δ/ppm 8.66 (dq, *J* 4.8, 0.9 Hz, 2H, A6); 8.57 (dt, *J* 7.9, 0.9 Hz, 2H, A3); 8.07 (s, 2H, B3); 7.82 (td, *J* 7.9, 1.4 Hz, 2H, A4); 7.31 (ddd, *J* 7.4, 4.8, 1.1 Hz, 2H, A5); 4.41 (t, *J* 4.5 Hz, 2H, a); 3.91 (t, *J* 4.5 Hz, 2H, b); 3.76 (t, *J* 4.7 Hz, 2H, d); 3.66 (t, *J* 4.0 Hz, 2H, c).

^{13}C NMR ($CDCl_3$, 125 MHz): δ/ppm 167.0 (B4); 156.9 (A2/B2); 155.9 (A2/B2); 148.9 (A6); 136.8 (A4); 123.8 (A5); 121.3 (A3); 107.7 (B3); 72.8 (c); 69.9 (b); 67.9 (a); 61.7 (d).

6.1.6 4'-(4,7,10-Trioxa-10-dec-1-ynyl)-2,2':6',2"-terpyridine **5**[5]

Ligand **4** (0.398 g, 1.15 mmol) in MeCN with KOH (0.687 g, 12.2 mmol) were stirred for 1 hour at room temperature. Propargyl bromide (80 % in toluene) (0.14 ml, 1.26 mmol) was added and the mixture stirred at 60°C for 24 hours. The reaction mixture was poured into water and extracted with CH_2Cl_2. The CH_2Cl_2 layer was dried over $MgSO_4$ and the solvent was removed to yield a brown oil (0.23 g, 0.597 mmol, 53 %).

^{1}H NMR ($CDCl_3$, 400 MHz): δ/ppm 8.68 (d, *J* 4.5 Hz, 2H, A6); 8.59 (d, *J* 8.1 Hz, 2H, A3); 8.03 (s, 2H, B3); 7.84 (td, *J* 7.6, 1.5 Hz, 2H, A4); 7.32 (dd, *J* 7.6, 4.5 Hz, 2H, A5); 4.40 (t, *J* 4.5 Hz, 2H, a); 4.21 (d, *J* 2.0 Hz, 2H, e); 3.89 (t, *J* 4.5 Hz, 2H, b); 3.78 (m, 2H, d); 3.73 (m, 2H, c); 2.44 (t, *J* 2.0 Hz, 2H, C≡C*H*).

^{13}C NMR ($CDCl_3$ 100 MHz): δ/ppm 167.3 (B4); 157.5 (A2/B2); 156.4 (A2/B2); 149.4 (A6); 137.2 (A4); 124.22 (A5); 121.7 (A3); 107.8 (B3); 79.6 (*C*≡CH); 74.6 (C≡*C*H); 70.3 (c); 69.4 (b); 69.1 (d); 67.8 (a); 58.4 (e).

MALDI: M/z 377 $[M]^+$.

IR (solid, cm^{-1}): 3232w, 2947w, 2878w, 1983w, 1558s, 1466m, 1443m, 1404s, 1366m, 1250w, 1204s, 1119s, 1065m, 1034s, 987m, 926m, 895m, 864m, 787s, 741s, 694m, 656m, 617m.

UV/VIS λ_{max}/nm (3.18×10^{-5} mol dm^{-3} CH_2Cl_2) 242 (ε/dm^3 mol^{-1} cm^{-1} 25000), 278 (23800).

Elemental analysis: Calc. +0.5 H_2O C 68.73 %, H 5.77 %, N 10.93 %; Found C 69.19/69.49 %, H 5.79/5.65 %, N 10.80/10.83 %.

6.1.7 4'-(4-Bromophenyl)-2,2':6',2''-terpyridine **6**[6]

4-Bromobenzaldehyde (1.10 g, 5.96 mmol) and 2-acetylpyridine (1.32 g, 10.9 mmol) were ground with powdered NaOH (0.477 g, 11.9 mmol) until a yellow solid formed. The solid was washed with water and collected by filtration. This was then heated to reflux with ammonium acetate (5 g, excess) in acetic acid (25 ml). Water (50 ml) was then added and the precipitate was collected. The product was purified by recrystallisation from ethanol. The ^{1}H NMR agreed well with that published in the literature (0.692 g, 1.78 mmol, 30 %).

^{1}H NMR ($CDCl_3$, 250 MHz): δ/ppm 8.76 (d, *J* 6.4 Hz, 2H, A6); 8.74 (s, 2H, B3); 8.70 (d, *J* 8.0 Hz, 2H, A3); 7.93 (td, *J* 8.0, 1.7 Hz, 2H, A4); 7.75 (m, 4H, C2 and C3); 7.41 (ddd, *J* 7.4, 4.7, 1.3 Hz, 2H, A5).

6.1.8 4'-(4-Ethynylphenyl)-2,2':6',2"-terpyridine **7**[7]

Ligand **6** (0.307 g, 0.792 mmol), $[(Ph_3P)_2PdCl_2]$ (0.0362 g, 0.0516 mmol), PPh_3 (0.0104 g, 0.0534 mmol) and CuI (0.0218 g, 0.115 mmol) were stirred in NEt_3 (30 ml) for 1 hour, during which the reaction was heated to 73 °C and cooled back to 40 °C. Ethynyl TMS (0.055 ml, 3.96 mmol) was added and the reaction was stirred at 40 °C for 5 days. The solvent was removed and chromatographed using an alumina column with CH_2Cl_2 as the eluent. A brown solid was obtained. This solid was then stirred with K_2CO_3 (1.05 g, excess) for 1 day. Water and CH_2Cl_2 were added and the CH_2Cl_2 layer was extracted and dried with $MgSO_4$. The solvent was evaporated to give the solid product. The ^{1}H NMR spectrum agreed well with that published in the literature (0.18 g, 0.540 mmol, 79 %).

^{1}H NMR ($CDCl_3$, 250 MHz): δ/ppm 8.78 (s, 2H, B3); 8.77 (d, *J* 5.4 Hz, 2H, A6); 8.71 (d, *J* 8.0 Hz, 2H, A3); 7.94 (td, *J* 7.4, 1.7 Hz, 2H, A4); 7.80 (m, 4H, C2 and C3); 7.41 (dd, *J* 7.4, 4.7 Hz, 2H, A5); 3.22 (s, 1H, C≡C*H*).

6.1.9 4'-(3-Bromophenyl)- 2,2':6',2"-terpyridine **8**[8]

2-Acetylpyridine (4.0 ml, 35.7 mmol) was added to a solution of 3-bromobenzaldehyde (2.1 ml, 17.9 mmol) in EtOH (100 ml) and stirred. Ground KOH pellets (2.07 g, 36.9 mmol) and aqueous NH_3 (25 %) (56 ml) were added and the reaction stirred at room temperature for 4 hours. The solid that precipitated was collected by filtration and recrystallised from CH_2Cl_2/MeOH. The ^{1}H NMR spectrum agreed well with that published in the literature (4.97 g, 12.8 mmol, 71 %).

^{1}H NMR ($CDCl_3$, 500 MHz): δ/ppm 8.66 (d, *J* 5.6 Hz, 2H, A6); 8.59 (s, 2H, B3); 8.58 (dt, *J* 8.1, 1.0 Hz, 2H, A3); 8.00 (t, *J* 1.5 Hz, 1H, C2); 7.84 (td, *J* 8.1, 1.5 Hz, 2H, A4); 7.78 (ddd, *J* 7.8, 1,7, 1.0 Hz, 1H, C4/C6); 7.53 (ddd, *J* 8.0, 1.9, 1.0 Hz, 1H, C4/C6); 7.33 (m, 3H, A5 and C5).

6.1.10 4'-(3-Ethynylphenyl)-2,2':6',2"-terpyridine **9**

Ligand **8** (0.686 g, 1.77 mmol), $[(Ph_3P)_2PdCl_2]$ (0.0836 g, 0.119 mmol), PPh_3 (0.0339 g, 0.129 mmol) and CuI (0.0447 g, 0.235 mmol) in NEt_3 (50 ml) were heated to 70 °C and cooled back to 40 °C over 1 hour. Ethynyl TMS (1.22 ml, 8.81 mmol) was added and the reaction stirred for 5 days. The mixture was filtered through Celite and the solvent removed from the filtrate. The solid obtained was purified with column chromatography using 1 % acetone in CH_2Cl_2 over an alumina column. The single terpyridine fraction was identified by spotting a small amount of the eluent onto an alumina covered TLC plate which was then dipped in an aqueous solution of $FeCl_2.4H_2O$. If the spot showed up purple the fraction contained a tpy ligand. This fraction was collected and the solvent removed. K_2CO_3 (1.9 g, excess) was added as well as MeOH (15 ml) and THF (15 ml) and the reaction stirred overnight. Water (30 ml) and CH_2Cl_2 (30 ml) were added and the organic layer was extracted. It was dried over Na_2SO_4 and the solvent was removed to yield a brown solid. This was purified by column chromatography with 1 % acetone in CH_2Cl_2 over alumina. The terpyridine fraction was identified as above and collected, and the solvent removed. Due to its poor solubility it was not possible to purify this compound in order to obtain an elemental analysis (0.265 g, 0.795 mmol, 45 %).

^{1}H NMR ($(CD_3)_2SO$, 500 MHz): δ/ppm 8.77 (dq, *J* 4.7, 0.9 Hz, 2H, A6); 8.68 (s, 2H, B3); 8.66 (dt, *J* 8.0, 1.0 Hz, 2H, A3); 8.06 (t, *J* 1.8 Hz, 1H, C2); 8.04 (td, *J* 7.6, 1.8 Hz, 2H, A4); 7.93 (dq, *J* 7.8, 0.9 Hz, 1H, C6); 7.74 (dq, *J* 8.0, 0.9 Hz, 1H, C4); 7.55 (t, *J* 8.0 Hz, 1H, C5); 7.54 (td, *J* 4.7, 1.1 Hz, 2H, A5); 4.34 (s, 1H, C≡C*H*).

^{13}C NMR ($(CD_3)_2SO$, 125 MHz): δ/ppm 155.7 (A2/B2); 154.7 (A2/B2); 149.3 (A6); 148.0 (C1); 140.0 (B4); 137.5 (A5); 132.2 (C4); 131.5 (C5); 129.5 (C2); 126.1 (C6); 124.6 (A4); 122.6 (C3); 120.9 (A3); 118.1 (B3); 82.9 (*C*≡CH); 81.6 (C≡*C*H).

MALDI: M/z 395 $[M + K + Na]^+$.

IR (solid, cm^{-1}): 3153w, 3060w, 3019w, 1605w, 1583s, 1566s, 1539s, 1466s, 1440.73m, 1414m, 1381s, 1263m, 1231w, 1175w, 1124m, 1094w, 1078m, 1038s 989s, 960w, 914w, 876s, 845m, 775s.

UV/VIS λ_{max}/nm ($1.20x10^{-5}$ mol dm^{-3} CH_2Cl_2) 212 (ε/dm^3 mol^{-1} cm^{-1} 46000), 231 (38000), 315 (8000).

Melting Point: 142.0-148.3 °C.

6.1.11 4'-[1,1,1-Tris(2-propyn-1-oxymethyl)methoxy]-2,2':6',2"-terpyridine **12**

4'-[1,1,1-Tris(hydroxymethyl)methoxy]-2,2':6',2"-terpyridine[9] (0.194 g, 0.528 mmol) and ground KOH (0.299 g, 5.33 mmol) lin DMSO (3 ml) were stirred at room temperature for 30 minutes until the mixture became a white suspension. 3-Bromoprop-1-yne (80 % in toluene) (0.59 ml, 5.28 mmol) was added and the reaction stirred at room temperature for 4 days. The reaction mixture was then poured into water (100 ml) and extracted with CH_2Cl_2 (30 ml) until both layers were no longer cloudy. The solvent was removed from the organic layer. The product was purified by column chromatography on alumina using 5 % MeOH in $CHCl_3$ as the eluent. The first fraction contained the product, and was collected as a yellow oil (0.0583 g, 0.121 mmol, 23 %). The second fraction was found to be the bis-alkyne complex (0.0180 g, 0.0406 mmol, 17 %).

^{1}H NMR ($CDCl_3$, 500 MHz): δ/ppm 8.69 (dq, *J* 4.8, 0.9 Hz, 2H, A6); 8.62 (dt, *J* 7.9, 0.9 Hz, 2H, A3); 8.03 (s, 2H, B3); 7.85 (td, *J* 7.6, 1.8 Hz, 2H, A4); 7.33 (ddd, *J* 7.4, 4.8, 1.2 Hz, 2H, A5); 4.27 (s, 2H, a); 4.13 (d, *J* 2.4 Hz, 6H, c); 3.68 (s, 6H, b); 2.41 (t, *J* 2.4 Hz, 3H, C≡C*H*).

^{13}C NMR ($CDCl_3$, 125 MHz): δ/ppm 167.2 (B4); 156.7 (A2/B2); 155.9 (A2/B2); 148.9 (A6); 137.1 (A4); 123.8 (A5); 121.3 (A3); 107.6 (B3); 79.8 (*C*≡CH); 74.3 (C≡*C*H); 68.5 (b); 66.9 (a); 58.7 (c); 44.8 (*C*$(CH_2)_4$).

6.2 Platinahomoditopic Ligands

6.2.1 $Pt(\mathbf{1}\text{-}H)_2(PEt_3)_2$[10]

Ligand **1**[2] (0.108 g, 0.376 mmol) and *trans*-$PtI_2(PEt_3)_2$ (0.128 g, 0.186 mmol) and CuI (0.0050 g, 0.0263 mmol) in NEt_3 (5 ml) were stirred for 2 hours at room temperature. The white precipitate formed was collected by filtration. It was separated by column chromatography on alumina using CH_2Cl_2/acetone 4:1 as the eluent and recrystallised from hexane/CH_2Cl_2 (0.113 g, 0.113 mmol, 71 %).

^{1}H NMR ($CDCl_3$, 500 MHz): δ/ppm 8.65 (dm, *J* 4.0 Hz, 4H, A6); 8.58 (dt, *J* 8.0, 1.0 Hz, 4H, A3); 8.06 (s, 4H, B3); 7.82 (td, *J* 7.6, 1.8 Hz, 4H, A4); 7.30 (ddd, *J* 7.5, 5.2, 1.2 Hz, 4H, A5); 4.96 (s, 4H, a); 1.83 (ddq, J_{HH} 7.5, J_{PH} 4.2, $J_{P'H}$ 3.8 Hz, 12H, y); 0.88 (dt + ddt, J_{HH} 7.5, J_{PH} 15.5, J_{PtH} 120 Hz, 18H, z).

^{13}C NMR ($CDCl_3$ 125 MHz): δ/ppm 166.6 (B4); 156.6 (A2/B2); 156.2 (A2/B2); 148.8 (A6); 136.6 (A4); 123.5 (A5); 121.1 (A3); 108.1 (B3); 104.8 (t+d, J_{PC} 14.4, J_{PtC} 963 Hz, C≡*C*Pt); 101.2 (s+d, J_{PtC} 270 Hz, *C*≡CPt); 58.7 (s+d, J_{PtC} 18 Hz, a); 15.8 (t+dt, J_{PC} 17.4 Hz, J_{PtC} 35 Hz, y); 8.0 (s+d, J_{PtC} 20 Hz, z).

^{31}P NMR ($CDCl_3$ 202 MHz): δ/ppm 10.8 (s+d, *J* 2352 Hz).

^{195}Pt NMR $CDCl_3$ 107 MHz): δ/ppm -4873 (t, *J* 2353 Hz).

MALDI: M/z 1003 $[M]^+$.

IR (solid, cm^{-1}): 29620w, 2924w, 2870w, 21210m, 1736w, 1558s, 1443m, 1404m, 1335m, 1258m, 1188m, 1088w, 1011s, 972m, 864m, 787m, 733s, 617m, 563w, 525w.

UV/VIS λ_{max}/nm ($1.88x10^{-5}$ mol dm^{-3} CH_2Cl_2) 246 (ε/dm^3 mol^{-1} cm^{-1} 68900), 278 (69550).

Fluorescence (CH_2Cl_2, $1.88x10^{-5}$ mol dm^{-3}): 450 nm on excitation at 292 nm.

Elemental analysis: Calc. C 57.422 %, H 5.421 %, N 8.371 %; Calc. $+H_2O$ C 56.41 %, H 5.52 %, N 8.22 %; Found C 56.69/56.85 %, H 5.40/5.46 %, N 8.23/8.19 %.

6.2.2 Pt(**1**-H)$_2$(P^{n}Bu$_3$)$_2$[11]

Ligand **1**[2] (0.1350 g, 0.4699 mmol) and *trans*-$PtI_2(P^nBu_3)_2$ (0.2067 g, 0.2422 mmol) and CuI (cat.) in NEt_3 (5 ml) were stirred for 2 hours at room temperature. The white precipitate formed was collected by filtration. The product was purified by recrystallisation from hexane/CH_2Cl_2 (0.186 g, 0.159 mmol, 68 %).

^{1}H NMR ($CDCl_3$ 500 MHz): δ/ppm 8.65 (ddd, *J* 4.8, 1.8, 1.0 Hz, 4H, A6); 8.58 (dt, *J* 8.6, 1.0 Hz, 4H, A3); 8.05 (s, 4H, B3); 7.82 (td, *J* 7.6, 1.8 Hz, 4H, A4); 7.30 (ddd, *J* 7.6, 4.8, 1.0 Hz, 4H, A5); 4.94 (s, 4H, C*H*$_2$O); 1.85 (m, 12H, w); 1.34 (m, 12H, x); 1.24 (q, *J* 7.2 Hz, 12H, y); 0.77 (t, *J* 7.2 Hz, 18H, z).

^{13}C NMR ($CDCl_3$ 100 MHz): δ/ppm 167.1 (B4); 157.0 (A2/B2); 156.6 (A2/B2); 149.3 (A6); 137.2 (A4); 124.1 (A5); 121.7 (A3); 108.7 (B3); 104.9 (t, J_{PC} 14.3 Hz, C≡*C*Pt); 100.4 (s+d, J_{PtC} 270 Hz, *C*≡CPt); 58.7 (a); 26.5 (x/y); 24.1 (x/y); 23.4 (t, J_{PC} 17 Hz, w); 13.7 (z).

^{31}P NMR ($CDCl_3$ 162 MHz): δ/ppm -0.4 (s+d, J_{PPt} 2340 Hz).

^{195}Pt NMR ($CDCl_3$ 107 MHz) : δ/ppm -4843 (t, J_{PPt} 2329 Hz).

MALDI: M/z 1174 $[M]^+$.

IR (solid, cm^{-1}): 2947m, 2924m, 2856m, 2123m, 1582s, 1560s, 1466m, 1423m, 1404m, 1377w, 1337m, 1258w, 1184s, 1090m, 1064w, 1049w, 1009s, 989s, 970s, 903m, 866m, 791s, 746s, 746m, 733m, 692m, 660m, 609s.

UV/VIS λ_{max}/nm ($3.75x10^{-5}$ mol dm^{-3} CH_2Cl_2) 254 (ε/dm^3 mol^{-1} cm^{-1} 19100), 279 (20700).

Fluorescence (CH_2Cl_2, $3.75x10^{-5}$mol dm^{-3}): emission at 452 nm on excitation at 322 nm.

Elemental analysis: Calc. C 61.47 %, H 6.71 %, N 7.17 %; Calc. $+3H_2O$ C 58.76 %, H 6.90 %, N 6.85 %; Found C 58.89/59.22 %, H 6.30/6.36 %, N 6.66/6.78 %.

6.2.3 Pt(**1**-H)$_2$(PPh$_3$)$_2$[11]

Ligand **1**[2] (0.0789 g, 0.275 mmol), *trans*-$PtI_2(PPh_3)_2$ (0.0409 g, 0.0449 mmol) and CuI (0.0020 g, 0.0110 mmol) in CH_2Cl_2 (7 ml) and NEt_3 (7 ml) were stirred for 5 days at room temperature. The green precipitate was removed by filtration. It was chromatographed over alumina with CH_2Cl_2/acetone (99:1) as the eluent. The second fraction was isolated as a white crystalline solid (0.0283 g, 0.0219 mmol, 49 %).

^{1}H NMR (C_6D_6, 400 MHz): δ/ppm 8.74 (dt, *J* 7.9, 1.0 Hz, 4H, A3); 8.38 (ddd, *J* 4.7, 1.8, 1.0 Hz, 4H, A6); 8.33 (s, 4H, B3); 7.85 (m, 12H, Ph); 7.30 (td, *J* 7.6,

1.8 Hz, 4H, A4); 6.95 (m, 18H, Ph); 6.70 (ddd, *J* 7.6, 4.8, 1.0 Hz, 4H, A5); 4.18 (s, 4H, a).

^{13}C NMR (C_6D_6, 100 MHz): δ/ppm 167.4 (B4); 157.2 (A2/B2); 157.0 (A2/B2); 149.3 (A6); 136.3 (A4); 135.5 (t, J_{PC} 6.3 Hz, x); 131.6 (t, J_{PC} 28.8 Hz, w); 130.3 (y, z); 123.4 (A5); 121.2 (A3); 109.0 (B3); 108.2 (C^{alkyne}); 105.2 (C^{alkyne}); 58.8 (a).

^{31}P NMR (C_6D_6 162 MHz): δ/ppm 20.2 (s+d, J_{PPt} 2635 Hz).

^{195}Pt NMR (C_6D_6 107 MHz): δ/ppm -4921 (t, J_{PPt} 2625 Hz).

MALDI: M/z 1292 $[M]^+$.

IR (solid, cm^{-1}): 3047w, 2920w, 2858w, 2131m, 1580s, 1560s, 1433m, 1406m, 1329m, 1259w, 1184m, 1090m, 1014s, 989m, 972m, 883m, 862.12w, 791w, 692s.

UV/VIS λ_{max}/nm ($1.30x10^{-5}$ mol dm^{-3} $CHCl_3$) 246 (ε/dm^3 mol^{-1} cm^{-1} 70500), 278 (66700), 302 (36600).

Fluorescence ($CHCl_3$, $1.30x10^{-5}$ mol dm^{-3}): emission at 455 nm on excitation at 325 nm.

Elemental analysis: Calc. C 66.92 %, H 4.21 %, N 6.50 %; Calc. +C_6D_6 C 68.06 %, H 3.95 %, N 6.11 %; Found C 68.03/67.83 %, H 4.45/4.53 %, N 6.31/6.38 %.

6.2.4 PtI(**5**-H)$(PEt_3)_2$[5]

Ligand **5** (0.0492 g, 0.131 mmol) and CuI (0.0004 g, 0.002 mmol) were added to THF (1.5 ml). The suspension was added to a solution of $PtI_2(PEt_3)_2$ (0.0479 g, 0.0699 mmol) in DMF (1.5 ml) and NEt_3 (3 ml). The reaction was

stirred at room temperature for 4 days. Water was added to separate the product as a sticky oil. The product was purified by chromatography over alumina using CH_2Cl_2/acetone (99:1) as the eluent. The second fraction was collected and after removal of the solvent the product was isolated as a white oil (0.133 g, 0.0143 mmol, 20.5 %).

^{1}H NMR ($CDCl_3$, 500 MHz): δ/ppm 8.72 (d, *J* 4.7 Hz, 2H, A6); 8.66 (d, *J* 8.0 Hz, 2H, A3); 8.08 (s, 2H, B3); 7.89 (td, *J* 7.8, 1.8 Hz, 2H, A4); 7.37 (ddd, *J* 7.4, 4.8, 1.0 Hz, 2H, A5); 4.44 (t, *J* 4.6 Hz, 2H, a); 4.29 (t, J_{PH} 1.7 Hz, 2H, e); 3.98 (t, *J* 4.8 Hz, 2H, b); 3.77 (m, 2H, c); 3.73 (m, 2H, d); 2.18 (m, 12H, y); 1.15 (m, 18H, z).

^{13}C NMR ($CDCl_3$, 125 MHz): δ/ppm 167.0 (B4); 157.1 (A2/B2); 156.0 (A2/B2); 149.0 (A6); 136.8 (A4); 123.9 (A5); 121.4 (A3); 107.4 (B3); 94.9 (C≡*C*Pt); 71.0 (c); 69.4 (b); 68.3 (d); 67.9 (a); 61.2 (e); 16.5 (y); 8.3 (z).

^{31}P NMR ($CDCl_3$ 202 MHz): δ/ppm 8.8 (s+d, *J* 2323 Hz).

^{195}Pt NMR ($CDCl_3$ 107 MHz): δ/ppm -4936 (t, J_{PPt} 2354 Hz).

MALDI: M/z 957 $[M + Na]^+$, $[M – I]^+$.

IR (solid, cm^{-1}): 3055w, 2924m, 2878m, 2129w, 1728w, 1566s, 1450s, 1412s, 1350m, 1258m, 1204m, 1126m, 1095s, 1034s, 995w, 872w, 795w, 632w, 540s.

UV/VIS λ_{max}/nm (4.80×10^{-5} mol dm^{-3} CH_2Cl_2) 239 (ε/dm^3 mol^{-1} cm^{-1} 48000), 276 (40400).

6.2.5 Pt(**5**-H)$_2$(PEt$_3$)$_2$[5]

Ligand **5**[5] (0.139 g, 0.396 mmol), $PtI_2(PEt_3)_2$ (0.0454 g, 0.0663 mmol) and CuI (0.0028 g, 0.0147 mmol) in CH_2Cl_2 (20 ml) and NEt_3 (20 ml) were

stirred for 5 days at room temperature. The precipitate was removed by filtration. The solvent was removed from the filtrate and the resulting solid separated by column chromatography over alumina using CH_2Cl_2:acetone 99:1 as the eluent. The second fraction was collected as a white oil (0.0281 g, 0.0248 mmol, 36 %).

^{1}H NMR ($CDCl_3$, 500 MHz): δ/ppm 8.67 (dm, *J* 5.0 Hz, 4H, A6); 8.52 (dm, *J* 8.0 Hz, 4H, A3); 8.03 (s, 4H, B3); 7.84 (td, *J* 4.9, 1.8 Hz, 4H, A4); 7.33 (ddd, *J* 3.5, 6.0, 1.2 Hz, 4H, A5); 4.39 (t, *J* 4.6 Hz, 4H, a); 4.26 (t, *J* 1.4 Hz, 4H, e); 3.93 (dd, *J* 3.8, 4.8 Hz, 4H, b); 3.74 (m, 8H, c and d); 2.03 (m, 12H, y); 1.10 (m, 18H, z).

^{13}C NMR ($CDCl_3$ 125 MHz): δ/ppm 167.0 (B4); 157.1 (A2/B2); 156.1 (A2/B2); 149.0 (A6); 136.8 (A4); 123.8 (A5); 121.3 (A3); 107.4 (B3); 103.2 (*C*≡CPt); 101.4 (t, J_{PC} 14.5 Hz, C≡*C*Pt); 71.0 (c); 69.4 (b); 67.9 (d); 67.8 (a); 60.9 (e); 16.1 (t, J_{PC} 17.5 Hz, y); 8.2 (z).

^{31}P NMR ($CDCl_3$ 202 MHz): δ/ppm 7.9 (s+d, *J* 2379 Hz).

^{195}Pt NMR ($CDCl_3$ 107 MHz): δ/ppm -4875 (t, *J* 2366 Hz).

MALDI: M/z 1181 $[M]^+$, 945 $[M\text{-}2(PEt_3)]^+$.

IR (solid, cm^{-1}): 2959m, 2920m, 2874m, 2853m, 2114m, 1727w, 1676s, 1582s, 1562s, 1468m, 1441m, 1406s, 1379w, 1346m, 1278w, 1252w, 1204m, 1134m, 1090s, 1057m, 1036s, 991m, 968m, 870m,795s, 758m, 735s, 698w, 660m, 635m, 621m.

UV/VIS λ_{max}/nm ($3.89x10^{-5}$ mol dm^{-3} CH_2Cl_2) 242 (ε/dm^3 mol^{-1} cm^{-1} 27450), 277 (27200), 308 (10300).

Fluorescence ($CHCl_3$, $3.89x10^{-5}$ mol dm^{-3}): emission at 440 nm on excitation at 300 nm.

6.2.6 $Pt(\mathbf{7}\text{-}H)_2(PEt_3)_2$

Ligand **7**[7] (0.103 g, 0.310 mmol) and CuI (0.0013 g, 0.0068 mmol) in THF (15 ml) and a solution of $PtI_2(PEt_3)_2$ (0.0220 g, 0.0321 mmol) in DMF (3 ml) and NEt_3 (3 ml) were sonicated for 1 hour then stirred at room temperature for 4 days. The orange solution was poured into water (50 ml) and the precipitate formed was collected by filtration. The precipitate was washed with CH_2Cl_2 to give a yellow solution and a small amount of insoluble orange solid. The yellow solution was dried over Na_2SO_4 and the solvent was removed to yield an off-white solid. This was then separated using column chromatography over alumina, with CH_2Cl_2 as the eluent. Tpy fractions were identified by spotting a small amount of eluent on an alumina covered TLC plate then dipping this in an aqueous solution of $FeCl_2.4H_2O$. Fractions showing up purple after this test contained tpy. The second tpy-containing fraction was collected. The solvent was removed to give a yellow solid. Due to the low solubility as well as decomposition of the complex it was not possible to obtain a ^{13}C NMR spectrum well enough resolved to assign the signals (0.0279 g, 0.025 mmol, 79 %).

^1H NMR ($CDCl_3$, 500 MHz): δ/ppm 8.73 (m, 8H, A6 and B3); 8.67 (dt, *J* 7.9, 1.0 Hz, 4H, A3); 7.88 (td, *J* 5.9, 1.7 Hz, 4H, A5); 7.81 (d, *J* 8.5 Hz, 4H, C2/C3); 7.41 (d, *J* 4.7 Hz, 4H, C2/C3); 7.38 (ddd, *J* 3.6, 8.1, 1.1 Hz, 4H, A4); 2.23 (m, 12H, y); 1.28 (m, 18H, z).

^{13}C NMR ($CDCl_3$, 125 MHz): δ/ppm 156.3, 155.8, 150.1, 149.2, 149.1, 136.9, 134.7, 131.4, 126.9, 123.8, 121.4, 118.5, 110.7, 109.6, 16.4 (s+d, *J* 0.04 Hz), 8.4.

^{31}P NMR ($CDCl_3$, 202 MHz): δ/ppm 11.6 (s+d, *J* 2357 Hz).

^{195}Pt NMR ($CDCl_3$, 107 MHz): δ/ppm -4839 (t, *J* 4.7 Hz).

MALDI: M/z 450 $[M\text{-}2(tpy\text{-}ph)]^+$.

IR (solid, cm^{-1}): 2098m, 1582m, 1504m, 1458m, 1381m, 1242w, 1211w, 1180w, 1034m, 895m, 833s, 795s, 733s, 617m, 579w.

UV/VIS λ_{max}/nm ($9.12x10^{-5}$ mol dm^{-3} CH_2Cl_2) 291 (ε/dm^3 mol^{-1} cm^{-1} 16700).

Fluorescence (CH_2Cl_2, $9.12x10^{-6}$ mol dm^{-3}): 396 nm on excitation at 300 nm.

6.2.7 Pt(**7**-H)$_2$(P^nBu_3)$_2$

Ligand **7**[7] (0.0826 g, 0.284 mmol), $PtI_2(P^nBu_3)_2$ (0.121 g, 0.141 mmol) and CuI (0.0054 g, 0.0282 mmol) in NEt_3 (5 ml) were stirred at room temperature for 1 hour. The precipitate was removed by filtration and the solvent was removed from the filtrate. Purification by both chromatography and recrystallisation was unsuccessful and resulted in the decomposition so the product was characterised as crude (0.0899 g, 0.0711 mmol, 50 %). Due to the poor solubility of the product it was not possible to obtain a well resolved ^{13}C NMR spectrum.

^1H NMR (C_6D_6, 400 MHz): δ/ppm 9.18 (s, 4H, B3); 8.78 (d, *J* 7.9, 4H, A3); 8.61 (d, *J* 3.9 Hz, 4H, A6); 7.65 (d, *J* 8.3 Hz, 4H, C2/C3); 7.57 (d, *J* 8.3 Hz, 4H, C2/C3); 7.36 (td, *J* 7.6, 1.7 Hz, 4H, A4); 6.69 (ddd, *J* 7.4, 4.8, 1.0 Hz, 4H, A5); 2.19 (m, 12H, w); 1.73 (m, 12H, x); 1.48 (septuplet, *J* 7.4 Hz, 12H, y); 0.96 (t, *J* 7.4 Hz, 18H, z).

^{31}P NMR (C_6D_6, 162 MHz): δ/ppm 0.9 (s+d, *J* 2365 Hz).

MALDI: M/z 1266 $[M]^+$.

IR (solid, cm^{-1}): 2947m, 2924m, 2862m, 2098s, 1975w, 1898w, 1697w, 1581s, 1504s, 1466s, 1381s, 1265w, 1211w, 1180w, 1072m, 1034m, 964w, 895m, 833s.

UV/VIS λ_{max}/nm ($1.11x10^{-5}$ mol dm^{-3} CH_2Cl_2) 233 (ε/dm^3 mol^{-1} cm^{-1} 73250), 285 (67900), 348 (61500).

Fluorescence (CH_2Cl_2, $1.11x10^{-5}$ mol dm^{-3}): 416 nm on excitation at 348 nm.

6.3 Gold(I) Complexes

6.3.1 Au(**1**-H)(P^nBu_3)

Ligand **1**[2] (0.219 g, 0.763 mmol) and AuCl(P^nBu_3)[12] (0.330 g, 0.750 mmol) and CuI (0.0147 g, 0.0772 mmol) in NEt_3 (10 ml) were stirred for 4 hours at room temperature. The solvent was removed from the reaction mixture and the product was separated by column chromatography on alumina using CH_2Cl_2/acetone 99:1 as the eluent. The only fraction was collected and the solvent was removed (0.233 g, 0.340 mmol, 45 %).

^{1}H NMR ($CDCl_3$, 400 MHz): δ/ppm 8.65 (ddd, *J* 4.7, 1.8, 0.8 Hz, 2H, A6); 8.54 (dt, *J* 7.9, 0.9 Hz, 2H, A3); 8.04 (s, 2H, B3); 7.79 (td, *J* 7.6, 2.0 Hz, 2H, A4); 7.26 (ddd, *J* 5.1, 7.6, 1.0 Hz, 2H, A5); 5.01 (s, 2H, a); 1.67 (m, 6H, w); 1.48 (m, 6H, x); 1.38 (septuplet, *J* 7.6 Hz, 6H, y); 0.87 (t, *J* 7.6 Hz, 9H, z).

^{13}C NMR ($CDCl_3$ 100 MHz): δ/ppm 166.9 (B4); 157.4 (A2/B2); 156.7 (A2/B2); 149.4 (A6); 137.0 (A4); 124.0 (A5); 121.7 (A3); 108.20 (B3); 108.0 (C≡*C*Au); 97.2 (*C*≡CAu); 57.7 (a); 27.6 (y); 25.9 (d, J_{PC} 32.2 Hz, w); 24.6 (d, J_{PC} 14.6 Hz, x); 14.0 (z).

^{31}P NMR ($CDCl_3$ 162 MHz): δ/ppm 25.7 (s).

MALDI: M/z 686 $[M]^+$.

IR (cm^{-1}, solid): 2955w, 2924w, 2862w, 2361w, 2130w, 1376w, 1558m, 1450m, 1404m, 1335m, 1188m, 1088m, 1018s, 879w, 795m, 741m, 6178w, 563w, 525w.

UV/VIS λ_{max}/nm (CH_2Cl_2) 247, 277.

Fluorescence: no fluorescence observed.

6.3.2 (Au(**1**-H))$_2$(dppe)

$(AuCl)_2(dppe)$[13] (0.405 g, 0.447 mmol), ligand **1**[2] (0.270 g, 0.934 mmol) and CuI (0.0094 g, 0.0494 mmol) in NEt_3 (12 ml) and CH_2Cl_2 (12 ml) were stirred at room temperature for 4 days. The precipitate formed was collected by filtration and purified by column chromatography over alumina, using CH_2Cl_2/acetone 90:10 as the eluent. The single tpy fraction (no other fractions were present) was identified by spotting a small amount of the eluent onto an alumina covered TLC plate which was then dipped in aqueous $FeCl_2.4H_2O$ solution, the resulting purple colour confirming the presence of a tpy moiety. The solvent was removed (0.253 g, 0.185 mmol, 40 %).

^{1}H NMR ($CDCl_3$, 400 MHz): δ/ppm 8.63 (ddd, *J* 4.8, 1.8, 0.8 Hz, 4H, A6); 8.55 (dt, *J* 8.1, 1.0 Hz, 4H, A3); 8.06 (s, 4H, B3); 7.78 (td, *J* 7.6, 1.8 Hz, 4H, A4); 7.56 (q, *J* 6.6 Hz, 8H, PPh_2); 7.34 (m, 12H, PPh_2); 7.25 (ddd, *J* 7.6, 4.8, 1.0 Hz, 4H, A5); 5.00 (s, 4H, a); 1.94 (s, 4H, b).

^{13}C NMR ($CDCl_3$ 100 MHz): δ/ppm 166.4 (B4); 157.0 (A2/B2); 156.2 (A2/B2); 149.0 (A6); 136.7 (A4); 133.3 (x/y/z); 132.2 (x/y/z); 129.5 (x/y/z); 128.5 (w); 123.9 (A5); 121.3 (A3); 107.8 (B3); 107.5 (Au-*C*≡C); 97.0 (Au-C≡*C*); 57.1 (a); 23.7 (b).

^{31}P NMR ($CDCl_3$ 162 MHz): δ/ppm 36.5 (s).

MALDI: M/z 1388.38 $[M + Na]^+$, 1406 $[M + K]^+$.

IR (solid, cm^{-1}): 3055w, 2924m, 285m, 1697w, 1558s, 1435s, 1404s, 1335s, 1258m, 1188s, 1103m, 1018s, 879s, 795m, 725s, 687s.

UV/VIS λ_{max}/nm (4.62×10^{-5} mol dm^{-3} CH_2Cl_2) 233 (ε/dm^3 mol^{-1} cm^{-1} 55500), 253 (sh) (37900), 277 (30400).

Fluorescence: no fluorescence observed.

6.3.3 (AuP^{n}Bu$_3$)$_3$(**12**-3H)

Ligand **12** (0.161 g, 0.335 mmol), CuI (0.0094 g, 0.0494 mmol) and ClAu(P^{n}Bu$_3$) (0.462 g, 0.0133 mmol) were stirred in NEt_3 (5 ml) and CH_2Cl_2 (5 ml) for 2 days. The precipitate which formed was collected by filtration. It was purified by column chromatography on alumina using 1 % acetone in CH_2Cl_2 as the eluent. The single tpy fraction was eluted first and was identified by spotting a small amount of the eluent onto an alumina covered TLC plate and then dipping this in an aqueous solution of $FeCl_2.4H_2O$, the tpy fraction giving a purple colour and non-tpy fractions staying colourless. The solvent was removed from the tpy fraction to yield a white oil (0.0453 g, 0.0270 mmol, 8 %). NMR chemical shifts were assigned based on comparison with ligand **12**.

^{1}H NMR ($CDCl_3$, 400 MHz): δ/ppm 8.66 (dq, *J* 4.8, 0.9 Hz, 2H, A6); 8.56 (dt, *J* 7.9, 1.0 Hz, 2H, A3); 7.98 (s, 2H, B3); 7.79 (d, *J* 7.5, 1.8 Hz, 2H, A4); 7.26 (ddd, *J* 7.5, 4.8, 1.2 Hz, 2H, A5); 4.30 (s, 2H, a); 4.23 (s, 6H, c); 3.71 (s, 6H, b); 1.67 (m, 18H, w); 1.51 (m, 18H, x); 1.47 (septuplet, *J* 7.3 Hz, 18H, y); 0.88 (t, *J* 7.3 Hz, 27H, z).

^{13}C NMR ($CDCl_3$ 100 MHz): δ/ppm 167.4 (B4); 156.6 (A2/B2); 156.4 (A2/B2); 148.9 (A6); 136.5 (A4); 123.3 (A5); 121.1 (A3); 107.8 (B3); 100.1 (d, J_{PC} 25.9 Hz, *C*≡*C*Au); 69.3 (b); 68.0 (a); 60.0 (c); 44.9 (*C*$(CH_2)_4$); 27.1 (y); 25.4 (d, J_{PC} 32.3 Hz, w); 24.2 (d, J_{PC} 14.4 Hz, x); 13.6 (z).

^{31}P NMR ($CDCl_3$ 162 MHz): δ/ppm 25.8 (s).

MALDI: M/z 1678 $[M]^+$.

IR (solid, cm^{-1}): 2955m, 2924m, 2862m, 2361w, 2129w, 1713m, 1566m, 1443m, 1404m, 1350m, 1204m, 1088s, 1026m, 988w, 910w, 795m, 733w, 640s, 617s, 517m, 463m.

UV/VIS λ_{max}/nm ($2.39x10^{-5}$ mol dm^{-3} CH_2Cl_2) 249 (ε/dm^3 mol^{-1} cm^{-1} 106200), 278 (72700).

Fluorescence: no fluorescence observed.

6.4 Iron 2,2':6',2"-Terpyridine Complexes and Macrocycles

6.4.1 $[Fe(\mathbf{4})_2][PF_6]_2$

Ligand **4** (0.0299 g, 0.0887 mmol) and $FeCl_2.4H_2O$ (0.0095 g, 0.0477 mmol) were added to MeOH (5 ml) and stirred for 30 minutes at room temperature. Aqueous NH_4PF_6 was added and the precipitated product was collected by filtration. No purification was necessary (0.0431 g, 0.0422 mmol, 95 %).

^1H NMR (CD_3CN 400 MHz): δ/ppm 8.49 (s, 4H, B3); 8.44 (d, *J* 8.0 Hz, 4H, A3); 7.86 (t, *J* 7.6 Hz, 4H, A4); 7.16 (d, *J* 5.2 Hz, 4H, A6); 7.07 (t, *J* 6.8 Hz, 4H, A5); 4.76 (m, 4H, a); 4.10 (m, 4H, b); 3.73 (s, 8H, c and d); 2.84 (br, OH).

^{13}C NMR (CD_3CN 100 MHz): δ/ppm 168.8 (B4); 161.7 (A2/B2); 158.9 (A2/B2), 154.3 (A6); 139.3 (A4); 128.1 (A5); 124.5 (A3); 112.3 (B3); 73.7 (c/d); 71.0 (a); 69.8 (b); 62.0 (c/d).

MALDI: M/z 979 $[M - 2PF_6 + matrix + Na]^+$, 617 $[M - 2PF_6 - \mathbf{4} + matrix]^+$, 338 $[\mathbf{4} + H]^+$.

IR (solid, cm^{-1}): 2924w, 2878w, 1668w, 1614m, 1551w, 1495w, 1474m, 1441m, 1424m, 1354m, 1300w, 1252w, 1216m, 1161w, 1128m, 1117m,

1059m, 1045m, 966w, 924w, 825s, 787s, 754s, 739s, 727m, 698m, 663m, 652m, 639w, 615w, 590m, 554m.
UV/VIS λ_{max}/nm (2.06×10^{-5} mol dm^{-3} CH_3CN) 207 (ε/dm^3 mol^{-1} cm^{-1} 57800), 244 (52500), 272 (53500), 315 (40350), 555 (10700).

6.4.2 [Fe(**5**)$_2$][PF_6]$_2$

Ligand **5** (0.0198 g, 0.0563 mmol) and $FeCl_2.4H_2O$ (0.0056 g, 0.0282 mmol) in MeOH (10 ml) were stirred for 1 hour at room temperature. Aqueous NH_4PF_6 was added and the precipitate collected by filtration. The product was recrystallised from various solvent combinations (Et_2O/CH_3CN, CH_3CN/toluene and CH_2Cl_2/hexane) (0.0275 g, 0.0251 mmol, 89 %) (total from all recrystallisations).

^{1}H NMR (CD_3CN, 500 MHz): δ/ppm 8.48 (s, 4H, B3); 8.43 (d, *J* 8.0 Hz, 4H, A3); 7.86 (td, *J* 8.0, 1.5 Hz, 4H, A4); 7.16 (ddd, *J* 5.5, 1.5, 0.9 Hz, 4H, A6); 7.06 (ddd, *J* 7.0, 5.5, 1.3 Hz, 4H, A5); 4.74 (m, 4H, a); 4.21 (d, *J* 2.0 Hz, 4H, e); 4.09 (m, 4H, b); 3.82 (m, 4H, d); 3.73 (m, 4H, c); 2.71 (t, *J* 2.5 Hz, C≡C*H*).

^{13}C NMR ($CDCl_3$ 125 MHz): δ/ppm 169.7 (B4); 161.7 (A2/B2); 158.9 (A2/B2); 154.3 (A6); 139.3 (A4); 128.0 (A5); 124.4 (A3); 112.4 (B3); 80.8 (*C*≡CH); 75.7 (C≡*C*H); 71.3 (d); 70.9 (a); 69.9 (c); 69.8 (b); 58.7 (e).

ESMS: M/z 951 $[M - PF_6]^+$, 403 $[M - 2PF_6]^{2+}$.

IR (cm^{-1}, solid): 2930w, 2876w, 1714.60w, 1614m, 1562w, 1551w, 1474m, 1441m, 1423m, 1352m, 1288w, 1250w, 1215m, 1161w, 1130w, 1115w, 1092w, 1059m, 1043m, 966 w, 825s, 789s, 754s, 729s, 698m, 663m, 652m.

UV/VIS λ_{max}/nm (5.72×10^{-5} mol dm^{-3} CH_3CN) 281 (ε/dm^3 mol^{-1} cm^{-1} 7600), 313 (14000), 354(sh) (2000), 552 (4050).

6.4.3 $[Fe_2\{Pt(\mathbf{1}\text{-}H)_2(PEt_3)_2\}_2][PF_6]_4$[10,11]

$Pt(\mathbf{1}\text{-}H)_2(PEt_3)_2$ (0.0129 g, 0.0128 mmol) and $FeCl_2.4H_2O$ (0.0025 g, 0.0128 mmol) in MeOH (3 ml) were stirred for half an hour at room temperature. Aqueous NH_4PF_6 was added and the precipitate formed was collected by filtration. The purple solid was recrystallised from CH_2Cl_2/hexane (0.0124 g, 0.00459 mmol, 72 %).

^{1}H NMR (CD_3CN, 400 MHz): δ/ppm 8.56 (s, 8H, B3); 8.27 (d, *J* 7.6 Hz, 8H, A3); 7.79 (td, *J* 7.2, 1.9 Hz, 8H, A4); 6.93-6.96 (m, 16H, A5 and A6); 5.35 (s, 8H, a); 2.03 (m, 24H, y); 0.96 (m, $J_{P\text{-}H}$ 8, $J_{P'\text{-}H}$ 8, $J_{H\text{-}H}$ 8 Hz, 36H, z).

^{13}C NMR ($CDCl_3$ 125 MHz): δ/ppm 163.1; 161.1; 159.0; 153.9; 139.4; 127.9; 124.3; 118.3; 113.2; 61.7; 17.1 (t, *J* 17.6 Hz, 12C,); 8.8.

^{31}P NMR (CD_3CN 162 MHz): δ/ppm 12.0 (s+d, J_{PPt} 2334 Hz); -144.6 (septet, J_{PF} 707 Hz).

^{195}Pt NMR (CD_3CN 107 MHz): δ/ppm -4875 (t, *J* 2332 Hz).

ESMS: M/z 1086 $[M\text{-}2PF_6\text{-}2PEt_3]^{2+}$, 755 $[M\text{-}3PF_6]^{3+}$.

IR (solid, cm^{-1}): 3661w, 3119w, 3043w, 2961w, 2120w, 1610m, 1549w, 1474m, 1441m, 1421m, 1377m, 1340m, 1298w, 1256w, 1200s, 1159w, 1117w, 1040m, 1007m, 970m, 878m, 829s, 787s, 752s, 729s, 673s, 650s, 586s, 555s.

UV/VIS λ_{max}/nm ($7.41x10^{-5}$ mol dm^{-3} CH_3CN) 245 (ε/dm^3 mol^{-1} cm^{-1} 99600), 272 (116400), 312 (81900), 557 (23350).

Fluorescence: no observed fluorescence.

Elemental analysis: Calc. C 44.03 %, H 4.23 %, N 5.98 %; Found C 43.01 %, H 4.68 %, N 5.58 %.

6.4.4 $[Fe_2\{Pt(\mathbf{1}\text{-}H)_2(P^nBu_3)_2\}_2][PF_6]_4$[11]

$Pt(\mathbf{1}\text{-}H)_2(P^nBu_3)_2$ (0.1055 g, 0.0900 mmol) and $FeCl_2.4H_2O$ (0.0180 g, 0.0905 mmol) in MeOH (20 ml) were stirred for half an hour at room temperature. Aqueous NH_4PF_6 was added and the precipitate formed was collected by filtration (0.105 g, 0.0346 mmol, 95 %).

^1H NMR (CD_3CN, 500 MHz): δ/ppm 8.49 (s, 8H, B3); 8.27 (d, *J* 7.5 Hz, 8H, A6); 7.86 (t, *J* 7.5 Hz, 8H, A3); 6.99 (m, 8H, A5); 6.93 (m, 8H, a6); 5.32 (s, 8H, a); 1.94 (overlaps with solvent, w); 1.47 (m, 24H, x); 1.25 (septet, *J* 7.5 Hz, 24H, y); 0.60 (t, *J* 7.5 Hz, 36H, z).

^{31}P NMR ($CDCl_3$ 162 MHz): δ/ppm 3.0 (s+d, J_{PPt} 2315 Hz); -144.6 (septet, *J* 707 Hz).

ESMS: M/z 1373 $[M - 2PF_6]^{2+}$.

IR (solid, cm^{-1}): 2953w, 2926w, 2868w, 2116w, 1609m, 1472m, 1421m, 1377w, 1339m, 1298w, 1256w, 1196m, 1163w, 1092w, 1040w, 1003w, 966m, 875.62w, 829s, 787s, 752m, 727w.

UV/VIS λ_{max}/nm (2.64^{-5} mol dm^{-3} CH_3CN) 246 (ε/dm^3 mol^{-1} cm^{-1} 67200), 271 (78500), 313 (49300), 558 (13000).

Fluorescence: no observed fluorescence.

6.4.5 $[Fe_n\{Pt(\mathbf{1}\text{-}H)_2(PPh_3)_2\}_n][PF_6]_{2n}$[11]

$Pt(\mathbf{1}\text{-}H)_2(PPh_3)_2$ (0.0307 g, 0.0238 mmol) and $FeCl_2.4H_2O$ (0.0048 g, 0.0241 mmol) in MeOH (5 ml) were stirred for half an hour at room

temperature. Aqueous NH_4PF_6 was added and the precipitate formed was collected by filtration (0.0346 g). Since the product was an inseparable mixture it was not possible to characterise it fully.

^{31}P NMR ($CDCl_3$ 162 MHz): δ/ppm 18.5 (s+d, *J* 2611 Hz), 18.0 (s+d, *J* 2605 Hz), -144.6 (septet, *J* 706 Hz).

ESMS: M/z 793 $[M - 3PF_6 - 6Ph]^{3+}$.

IR (solid, cm^{-1}): 3047w, 2908w, 2851w, 2122w, 1609m, 1549w, 1472m, 1435m, 1421m, 1377w, 1337m, 1298w, 1248w, 1196m, 1161m, 1095m, 1007m, 876w, 829s, 787s, 743s, 690s, 617s.

Fluorescence: no fluorescence observed.

6.4.6 $[Fe\{Pt(\mathbf{5}\text{-}H)_2(PEt_3)_2\}][PF_6]_2$[5]

$Pt(\mathbf{5}\text{-}H)_2(PEt_3)_2$ (0.0182 g, 0.0154 mmol) and $FeCl_2.4H_2O$ (0.0039 g, 0.0196 mmol) were added to MeOH (2 ml) and stirred at room temperature for 30 minutes. Aqueous NH_4PF_6 was added and the precipitate was collected by filtration. Thin layer chromatography showed that there were two purple fractions as well as some purple material remaining on the baseline. Attempts to separate the products were however unsuccessful and the product was partly characterised as a component of a mixture.

^1H NMR (CD_3CN, 500 MHz): δ/ppm 8.63 (s, 4H, B3); 8.39 (d, *J* 8.0 Hz, 4H, A3); 8.01 (t, *J* 7.2 Hz, 4H, A4); 7.15 (m, 4H, A5); 7.07 (m, 4H, A6); 4.92 (m, 4H, a); 4.12 (m, 4H, e); 4.04 (m, 4H, b); 3.65 (t, *J* 6.2 Hz, 4H, d); 1.66 (m, 12H, y); 0.72 (m, 18H, z).

^{31}P NMR ($CDCl_3$ 162 MHz): δ/ppm 8.8 (s+d, J_{PPt} 2313 Hz), -144.6 (septet, J_{PF} 707 Hz).

ESMS: M/z 617 $[M - 2PF_6]^{2+}$.

MALDI: M/z 1457 $[M - 2PF_6 + matrix]^+$.

6.4.7 [Fe{Au(**1**-H)(P^{n}Bu$_3$)}$_2$][PF$_6$]$_2$

Au(**1**-H)(P^{n}Bu$_3$) (0.132 g, 0.192 mmol) and $FeCl_2.4H_2O$ (0.0191 g, 0.0961 mmol) in MeOH (20 ml) and CH_2Cl_2 (10 ml) were stirred for 30 minutes at room temperature. Some of the solvent was removed and aqueous NH_4PF_6 was added. The precipitate was collected by filtration. Purification was attempted by chromatography on alumina using a mixture of CH_3CN, saturated aqueous KNO_3 and water in a 7:1:0.5 ratio as the eluent. The first band was collected (0.0952 g, 0.0554 mmol, 70 %). The product was still a mixture however, and a brown decomposition product was observed after a short time in solution, therefore it was not possible to obtain well resolved ^{1}H and ^{13}C NMR spectra.

^{31}P NMR (CD_3CN 162 MHz): δ/ppm 36.3 (s); 25.2(br); -144.6 (septet, *J* 706 Hz)

ESMS: M/z 1442 $[M – P^nBu_3 - PF_6]^+$; 913 $[Fe(\mathbf{1})_2 - PF_6]^+$.

IR (solid, cm^{-1}): 3279w, 3086w, 2924m, 2862m, 2129w, 1278w, 1612m, 1558w, 1469m, 1420m, 1381w, 1350m, 1296w, 1250w, 1204m, 1165w, 1095w, 1041w, 1011w, 980w, 825s, 787s, 748m, 717m, 663m, 617w, 555s.

UV/VIS λ_{max}/nm (1.75x10^{-5} mol dm^{-3} CH_3CN) 243 (ε/dm^3 mol^{-1} cm^{-1} 30100), 273 (29600), 283(sh), 315 (22600), 556 (6700).

Fluorescence: no fluorescence observed.

6.4.8 $[Fe_n\{(Au(\mathbf{1}\text{-}H))_2(dppe)\}_n][PF_6]_{2n}$

$(Au(\mathbf{1}\text{-}H))_2(dppe)$ (0.1141 g, 0.0836 mmol) and $FeCl_2.4H_2O$ (0.0165 g, 0.0830 mmol) in MeOH (15 ml) were stirred at room temperature for 30 minutes. Aqueous NH_4PF_6 was added and the precipitate was collected by filtration. Attempts to separate the three products were unsuccessful and attempts to grow crystals of the product resulted in a change in the ^{31}P NMR chemical shifts.

6.5 References

[1] E. C. Constable and M. D. Ward, *J. Chem. Soc. Dalton Trans.*, 1990, 1405.

[2] D. Armspach, E. C. Constable, C. E. Housecroft, M. Neuburger and M. Zehnder, *J. Organomet. Chem.*, 1997, **550**, 193.

[3] E. C. Constable, C. E. Housecroft, M. Neuburger, S. Schaffner and E. J. Shardlow, *CrystEngComm*, 2005, **7**, 599.

[4] D. Armspach, E. C. Constable, F. Diederich, C. E. Housecroft and J.-F. Nierengarten, *Chem. Eur. J.*, 1998, **4**, 723.

[5] E. C. Constable, C. E. Housecroft, M. Neuburger, S. Schaffner and E. J. Shardlow, *Inorg. Chim. Acta*, 2007, in press.

[6] G. W. Cave and C. L. Raston, *J. Chem. Soc. Perkin Trans.*, 2001, 3258.

[7] E. C. Constable, C. E. Housecroft, L. A. Johnston, D. Armspach, M. Neuburger and M. Zehnder, *Polyhedron*, 2001, **20**, 483.

[8] S. Bonnet, J.-P. Collin and J.-P. Sauvage, *Chem. Commun.*, 2005, 3195.

[9] E. C. Constable, C. E. Housecroft, M. Cattalini and D. Phillips, *New J. Chem.*, 1998, 193.

[10] E. C. Constable, C. E. Housecroft, M. Neuburger, S. Schaffner and E. J. Shardlow, *Dalton Trans.*, 2005, 234.

[11] J. E. Beves, E. C. Constable, C. E. Housecroft, M. Neuburger, S. Schaffner and E. J. Shardlow, *Dalton Trans.*, 2007, in press.

[12] M. I. Bruce, E. Horn, J. G. Matisons and M. R. Snow, *Aust. J. Chem.*, 1984, 1163.

[13] S. J. Berners-Price, M. A. Mazid and P. J. Sadler, *J. Chem. Soc. Dalton Trans.*, 1984, 969.

Crystal Data for Ligand **1**	
Formula	$C_{18}H_{13}N_3O_1$
Formula weight	287.32
Crystal system	Triclinic
Space group	P -1
a, b, c, [Å]	3.95720(10), 12.1228(4), 14.6442(4)
α, β, γ [◦]	87.7010(19), 83.9528(19), 82.9919(17)
V [$Å^3$]	693.12(3)
Z	2
D (calc) [gcm^{-3}]	1.377
μ (MoK_α) [mm^{-1}]	0.088
F(000)	300
Crystal size [mm]	0.14 x 0.14 x 0.16
Data Collection	
Temperature [K]	173
Radiation [Å]	MoK_α, 0.71073
θ Min (Max) [◦]	3 (30)
Total number of reflections	8003
Number of unique reflections	4065
Observed data [I>3.0 σ(I)]	2496
Refinement	
Number of reflections	2496
Number of parameters	200
R1	0.0376
R1 (all data)	0.0630
wR2	0.0437
wR2 (all data)	0.0780
Goodness of fit (GOF)	1.1079
Min. and Max. residual electron density [e $Å^{-3}$]	-0.18, 0.28

Crystal Data for Ligand **2**	
Formula	$C_{20}H_{17}N_3O_1$
Formula weight	315.37
Crystal system	Orthorhombic
Space group	P n a 2_1
a, b, c, [Å]	21.6358(4), 5.84320(10), 12.7032(2)
V [$Å^3$]	1605.97(5)
Z	4
D (calc) [gcm^{-3}]	1.304
μ (MoK_α) [mm^{-1}]	0.083
F(000)	664
Crystal size [mm]	0.12 x 0.18 x 0.38
Data Collection	
Temperature [K]	173
Radiation [Å]	MoK_α, 0.71073
θ Min (Max) [◦]	1 (28)
Total number of reflections	12986
Number of unique reflections	2011
Observed data [I>0.5 σ(I)]	1748
Refinement	
Number of reflections	1748
Number of parameters	217
R1	0.0351
R1 (all data)	0.0416
wR2	0.0328
wR2 (all data)	0.0342
Goodness of fit (GOF)	1.0949
Min. and Max. residual electron density [e $Å^{-3}$]	-0.12, 0.20

Crystal Data for Ligand **3a**	
Formula	$C_{21}H_{19}N_3O_1$
Formula weight	329.40
Crystal system	Monoclinic
Space group	P 2_1/n
a, b, c, [Å]	5.6534(2), 25.5246(9), 12.1459(3)
β [◦]	94.310(2)
V [$Å^3$]	1747.71(10)
Z	4
D (calc) [gcm^{-3}]	1.252
μ (MoK_α) [mm^{-1}]	0.079
F(000)	696
Crystal size [mm]	0.07 x 0.12 x 0.34
Data Collection	
Temperature [K]	173
Radiation [Å]	MoK_α, 0.71073
θ Min (Max) [◦]	1 (27)
Total number of reflections	12169
Number of unique reflections	3981
Observed data [I>1.0 σ(I)]	2472
Refinement	
Number of reflections	2472
Number of parameters	226
R1	0.0595
R1 (all data)	0.0974
wR2	0.0698
wR2 (all data)	0.2981
Goodness of fit (GOF)	0.9646
Min. and Max. residual electron density [e $Å^{-3}$]	-0.17, 0.82

Crystal Data for Ligand **3b**	
Formula	$C_{21}H_{19}N_3O_1$
Formula weight	329.40
Crystal system	Monoclinic
Space group	C2/c
a, b, c, [Å]	35.6129(12), 5.4646(2), 20.5952(7)
β [◦]	120.439(2)
V [$Å^3$]	3455.6(2)
Z	8
D (calc) [gcm^{-3}]	1.266
μ (MoK_α) [mm^{-1}]	0.080
F(000)	1392
Crystal size [mm]	0.04 x 0.16 x 0.54
Data Collection	
Temperature [K]	173
Radiation [Å]	MoK_α, 0.71073
θ Min (Max) [◦]	1 (30)
Total number of reflections	48465
Number of unique reflections	5038
Observed data [I>3.0 σ(I)]	2605
Refinement	
Number of reflections	2605
Number of parameters	226
R1	0.0504
R1 (all data)	0.1034
wR2	0.0326
wR2 (all data)	0.0443
Goodness of fit (GOF)	1.2421
Min. and Max. residual electron density [e $Å^{-3}$]	-0.22, 1.02

Crystal Data for Ligand **5**	
Formula	$C_{22}H_{21}N_3O_3$
Formula weight	375.43
Crystal system	Monoclinic
Space group	C 2/c
a, b, c, [Å]	36.842(36), 5.040(4), 20.626(16)
β [◦]	101.23(10)
V [$Å^3$]	3756.2(57)
Z	8
D (calc) [gcm^{-3}]	1.328
μ (MoK_α) [mm^{-1}]	0.090
F(000)	1584
Crystal size [mm]	0.06 x 0.31 x 0.35
Data Collection	
Temperature [K]	173
Radiation [Å]	MoK_α, 0.71073
θ Min (Max) [◦]	1 (27)
Total number of reflections	30509
Number of unique reflections	4317
Observed data [I>2.0 σ(I)]	2565
Refinement	
Number of reflections	2565
Number of parameters	254
R1	0.0565
R1 (all data)	0.0576
wR2	0.0497
wR2 (all data)	0.0503
Goodness of fit (GOF)	1.0740
Min. and Max. residual electron density [e $Å^{-3}$]	-0.24, 0.22

Crystal Data for Pt(**1**-H)$_2$(P^nBu_3)$_2$	
Formula	$C_{60}H_{78}N_6O_2P_2Pt_1$
Formula weight	1172.36
Crystal system	Triclinic
Space group	P -1
a, b, c, [Å]	9.39830(10), 10.99710(10), 13.79160(10)
α, β, γ [◦]	100.6520(6), 99.7287(6), 91.2631(6)
V [$Å^3$]	1378.62(2)
Z	1
D (calc) [gcm^{-3}]	1.412
μ (MoK_α) [mm^{-1}]	2.651
F(000)	604
Crystal size [mm]	0.04 x 0.16 x 0.28
Data Collection	
Temperature [K]	123
Radiation [Å]	MoK_α, 0.71073
θ Min (Max) [◦]	3 (28)
Total number of reflections	13016
Number of unique reflections	6560
Observed data [I>3.0 σ(I)]	6490
Refinement	
Number of reflections	6490
Number of parameters	322
R1	0.0203
R1 (all data)	0.0206
wR2	0.0228
wR2 (all data)	0.0229
Goodness of fit (GOF)	1.0943
Min. and Max. residual electron density [e $Å^{-3}$]	-1.20, 1.11

Crystal Data for Pt(**1**-H)$_2$(PPh$_3$)$_2$.2C$_6$H$_6$	
Formula	$C_{84}H_{66}N_6O_2P_2Pt_1$
Formula weight	1448.52
Crystal system	Triclinic
Space group	P -1
a, b, c, [Å]	9.3237(5), 13.3692(7), 15.5613(7)
α, β, γ [◦]	104.458(3), 104.998(3), 107.061(2)
V [Å^3]	1676.16(16)
Z	1
D (calc) [gcm^{-3}]	1.435
μ (MoK$_\alpha$) [mm^{-1}]	2.196
F(000)	736
Crystal size [mm]	0.25 x 0.27 x 0.48
Data Collection	
Temperature [K]	173
Radiation [Å]	MoK$_\alpha$, 0.71073
θ Min (Max) [◦]	2.933 (27.456)
Total number of reflections	12703
Number of unique reflections	7414
R (int)	0.042
Observed data [I>3.0 σ(I)]	6362
Refinement	
Number of reflections	6362
Number of parameters	430
R1	0.0431
R1 (all data)	0.0511
wR2	0.0475
wR2 (all data)	0.0520
Goodness of fit (GOF)	1.1209
Min. and Max. residual electron density [e Å^{-3}]	-1.48, 2.02

Crystal Data for $[Cu_2(PPh_3)_2(\mu\text{-}I)(\mu\text{-}\mathbf{7})]I$	
Formula	$C_{59}H_{45}Cu_2I_2N_3P_2$
Formula weight	1238.87
Crystal system	Orthorhombic
Space group	C 2 2 2_1
a, b, c, [Å]	18.4993(2), 26.7904(4), 10.46600(10)
V [$Å^3$]	5186.99(11)
Z	4
D (calc) [gcm^{-3}]	1.586
μ (MoK_α) [mm^{-1}]	2.113
F(000)	2456
Crystal size [mm]	0.02 x 0.16 x 0.33
Data Collection	
Temperature [K]	173
Radiation [Å]	MoK_α, 0.71073
θ Min (Max) [◦]	1 (27)
Total number of reflections	39838
Number of unique reflections	5950
Observed data [I>3.0 σ(I)]	5133
Refinement	
Number of reflections	5133
Number of parameters	314
R1	0.0330
R1 (all data)	0.0384
wR2	0.0397
wR2 (all data)	0.0422
Goodness of fit (GOF)	1.0751
Min. and Max. residual electron density [e $Å^{-3}$]	-2.63, 2.64

Crystal Data for Au(**1**-H)(P^nBu_3)	
Formula	$C_{30}H_{39}Au_1N_3O_1P_1$
Formula weight	685.60
Crystal system	Triclinic
Space group	P -1
a, b, c, [Å]	11.1882(2), 11.3401(2), 14.3037(2)
α, β, γ [◦]	92.6970(9), 110.5440(7), 116.1495(8)
V [$Å^3$]	1480.86(5)
Z	2
D (calc) [gcm^{-3}]	1.537
μ (MoK_α) [mm^{-1}]	5.047
F(000)	684
Crystal size [mm]	0.12 x 0.22 x 0.23
Data Collection	
Temperature [K]	173
Radiation [Å]	MoK_α, 0.71073
θ Min (Max) [◦]	1.566 (29.988)
Total number of reflections	17126
Number of unique reflections	8610
Observed data [I>2.0 σ(I)]	6366
Refinement	
Number of reflections	6366
Number of parameters	325
R1	0.0315
R1 (all data)	0.0498
wR2	0.0491
wR2 (all data)	0.0592
Goodness of fit (GOF)	0.9678
Min. and Max. residual electron density [e $Å^{-3}$]	-2.19, 1.67

Crystal Data for $(AuP^nBu_3)_3$(**12** – 3H)	
Formula	$C_{65}H_{105}Au_3N_3O_4P_3$
Formula weight	1676.39
Crystal system	Monoclinic
Space group	P 2_1/c
a, b, c, [Å]	14.5969(4), 17.5045(3), 27.8698(6)
β [◦]	98.7409(9)
V [$Å^3$]	7038.3(3)
Z	4
D (calc) [gcm^{-3}]	1.582
μ (MoK_α) [mm^{-1}]	6.350
F(000)	3320
Crystal size [mm]	0.04 x 0.07 x 0.21
Data Collection	
Temperature [K]	173
Radiation [Å]	MoK_α, 0.71073
θ Min (Max) [◦]	2.958 (26.002)
Total number of reflections	27178
Number of unique reflections	13775
Observed data [I>2.0 σ(I)]	7109
Refinement	
Number of reflections	7109
Number of parameters	703
R1	0.0866
R1 (all data)	0.1538
wR2	0.0830
wR2 (all data)	0.1152
Goodness of fit (GOF)	1.0481
Min. and Max. residual electron density [e $Å^{-3}$]	-2.08, 5.25

Crystal Data for $[Au_3Cl_2(dppm)_2][PF_6]$	
Formula	$C_{50}H_{44}Au_3Cl_2F_6P_5$
Formula weight	1575.56
Crystal system	Triclinic
Space group	P -1
a, b, c, [Å]	9.67400(10), 15.4549(2), 18.9003(3)
α, β, γ [◦]	105.9872(8), 101.5928(7), 101.6696(8)
V [$Å^3$]	2559.58(6)
Z	2
D (calc) [gcm^{-3}]	2.044
μ (MoK_α) [mm^{-1}]	8.893
F(000)	1488
Crystal size [mm]	0.09 x 0.09 x 0.11
Data Collection	
Temperature [K]	173
Radiation [Å]	MoK_α, 0.71073
θ Min (Max) [◦]	1.165 (27.865)
Total number of reflections	23737
Number of unique reflections	12197
Observed data [I>3.0 σ(I)]	8452
Refinement	
Number of reflections	8452
Number of parameters	650
R1	0.0361
R1 (all data)	0.0548
wR2	0.0408
wR2 (all data)	0.0578
Goodness of fit (GOF)	1.1149
Min. and Max. residual electron density [e $Å^{-3}$]	-4.00, 2.84

Crystal Data for $(Au(\mathbf{1}\text{-}H))_2(dppe).4CHCl_3$	
Formula	$C_{66}H_{52}Au_2Cl_{12}N_6O_2P_2$
Formula weight	1842.49
Crystal system	Triclinic
Space group	P -1
a, b, c, [Å]	8.7136(3), 13.3106(4), 15.9758(4)
α, β, γ [◦]	110.0374(18), 91.133(2), 95.8007(16)
V [$Å^3$]	1728.92(9)
Z	1
D (calc) [gcm^{-3}]	1.770
μ (MoK_α) [mm^{-1}]	4.797
F(000)	898
Crystal size [mm]	0.02 x 0.05 x 0.37
Data Collection	
Temperature [K]	173
Radiation [Å]	MoK_α, 0.71073
θ Min (Max) [◦]	1.359 (27.491)
Total number of reflections	14873
Number of unique reflections	7916
Observed data [I>3.0 σ(I)]	5094
Refinement	
Number of reflections	5094
Number of parameters	442
R1	0.0325
R1 (all data)	0.0626
wR2	0.0359
wR2 (all data)	0.0574
Goodness of fit (GOF)	1.1116
Min. and Max. residual electron density [e $Å^{-3}$]	-0.72, 0.79

Crystal Data for $(AuCl)_2(dppf)$	
Formula	$C_{34}H_{28}Au_2Cl_2Fe_1P_2$
Formula weight	1019.23
Crystal system	Triclinic
Space group	P -1
a, b, c, [Å]	8.62730(10), 9.04010(10), 10.37150(10)
α, β, γ [◦]	80.9701(7), 86.0279(7), 81.6056(7)
V [$Å^3$]	789.417(14)
Z	1
D (calc) [gcm^{-3}]	2.144
μ (MoK_α) [mm^{-1}]	10.017
F(000)	480
Crystal size [mm]	0.03 x 0.08 x 0.15
Data Collection	
Temperature [K]	173
Radiation [Å]	MoK_α, 0.71073
θ Min (Max) [◦]	1.990 (30.004)
Total number of reflections	9181
Number of unique reflections	4616
Observed data [I>2.0 σ(I)]	4217
Refinement	
Number of reflections	4592
Number of parameters	188
R1	0.0233
R1 (all data)	0.0258
wR2	0.0595
wR2 (all data)	0.0604
Goodness of fit (GOF)	0.9738
Min. and Max. residual electron density [e $Å^{-3}$]	-1.28, 1.50

Crystal Data for $[Fe(\mathbf{5})_2][PF_6]_2$	
Formula	$C_{44}H_{42}F_{12}Fe_1N_6O_6P_2$
Formula weight	1096.62
Crystal system	Orthorhombic
Space group	P 2_1 2_1 2_1
a, b, c, [Å]	8.691(2), 38.232(5), 13.7060(15)
V [Å3]	4554.3(13)
Z	4
D (calc) [gcm-3]	1.599
μ (MoKα) [mm-1]	0.507
F(000)	2240
Crystal size [mm]	0.05 x 0.12 x 0.34
Data Collection	
Temperature [K]	173
Radiation [Å]	MoK_α, 0.71073
θ Min (Max) [◦]	1.578 (26.836)
Total number of reflections	45472
Number of unique reflections	9428
Observed data [I>3.0 σ(I)]	8139
Refinement	
Number of reflections	8139
Number of parameters	641
R1	0.0399
R1 (all data)	0.0460
wR2	0.0432
wR2 (all data)	0.0441
Goodness of fit (GOF)	1.0536
Min. and Max. residual electron density [e Å-3]	-0.40, 0.41

Crystal Data for $[Fe_2\{Pt(\mathbf{1}\text{-}H)_2(PEt_3)_2\}_2][PF_6]_4.C_6H_5CH_3.4MeCN$	
Formula	$C_{55.5}H_{64}F_{12}Fe_1N_8O_2P_4Pt_1$
Formula weight	1477.98
Crystal system	Monoclinic
Space group	P 2_1/n
a, b, c, [Å]	13.8860(2), 18.4187(2), 24.1365(3)
α, β, γ [◦]	90, 94.6196(7), 90
V [$Å^3$]	6153.15(13)
Z	4
D (calc) [gcm^{-3}]	1.595
μ (MoK_α) [mm^{-1}]	2.694
F(000)	2964
Crystal size [mm]	0.10 x 0.13 x 0.20
Data Collection	
Temperature [K]	123
Radiation [Å]	MoK_α, 0.71073
θ Min (Max) [◦]	2.943 (27.875)
Total number of reflections	55770
Number of unique reflections	14640
Observed data [I>2.0 σ(I)]	9363
Refinement	
Number of reflections	9363
Number of parameters	901
R1	0.0318
R1 (all data)	0.0582
wR2	0.0346
wR2 (all data)	0.0391
Goodness of fit (GOF)	1.0070
Min. and Max. residual electron density [e $Å^{-3}$]	-0.66, 0.98

Ellen Jane Shardlow MChem PhD MRSC

PERSONAL INFORMATION

Address:	Schützengraben 16 CH-4051 Basel Switzerland	Date of Birth: Nationality: Marital status:	25th September 1980 British Single

Home: +41 61 2616368
Work: +41 61 2671034
Mobile: +41 78 6625502
Email: Ellie.Shardlow@unibas.ch

EDUCATION

2003-2007 PhD, Universität Basel, Switzerland
"Metal Complexes of Alkyne-Functionalised 2,2':6',2"-Terpyridine Ligands" under the supervision of Prof. Edwin Constable and Prof. Catherine Housecroft.

1999-2003 MChem (2.1 with Honours) Chemistry with a European Language (French), Heriot-Watt University, Edinburgh, UK.
Masters project under the supervision of Prof. Alan Welch "Supraicosahedral Carboranes".

2000-2001 ERASMUS placement
One year spent studying at the École Supérieure Chimie Physique Électronique de Lyon, France.

1996-1999 A levels, South Craven School, Crosshills, UK.
Grade A in Biology, Chemistry, French and General Studies.

1992-1996 GCSEs, South Craven School, Crosshills, UK.
Grade A* in Science (dual award), Music and French.
Grade A in Mathematics, English language, English Literature and Humanities.
Grade B in History and Technology.

PRIZES

2003 Sandilands Prize for Inorganic Research awarded for masters project.

EMPLOYMENT

2003-1999 Various Sales Assistant positions, Harvey Nichols and House of Fraser, Edinburgh and Skipton, UK.

RESEARCH EXPERIENCE

I have experience in the synthesis of organic ligands and transition metal complexes including Schlenk line skills. I am group user for ESI mass spectrometry and I also have experience in fluorescence, IR, UV/VIS and NMR spectroscopies.

KEY SKILLS

As the president of the Swiss Young Chemists Association, I have good communication and teamwork skills and experience of chairing meetings, organising events, producing publicity for the association as well as taking part in meetings as a delegate to the Swiss Chemical Society Chemical Research Division.

POSITIONS OF RESPONSIBILITY

I have experience of working as a Laboratory Teaching Assistant in the Advanced Inorganic Chemistry lab course for second year students, including teaching Schlenk line techniques, correcting reports and having responsibility for the safety of the students.

LANGUAGES

English (fluent), French (fluent), German (intermediate).

HOBBIES AND INTERESTS

I have played the oboe since the age of eight and have a distinction at grade eight. I have been a member of several orchestras as well as performing solos and playing in small groups. I also enjoy Scottish dancing and swimming.

REFERENCES

Prof. Catherine Housecroft
University Of Basel
Spitalstrasse 51
CH-4056
Basel
Switzerland
Catherine.Housecroft@unibas.ch

Prof. Edwin Constable
University of Basel
Spitalstrasse 51
CH-4056
Basel
Switzerland
Edwin.Constable@unibas.ch

Prof. Alan Welch
Department of Chemistry
Heriot-Watt University
Edinburgh
EH14 4AS
UK
A.J.Welch@hw.ac.uk

PUBLICATIONS

1. E. C. Constable, C. E. Housecroft, M. Neuburger, S. Schaffner, E. J. Shardlow, *Dalton Trans.,* 234-235, (2005).

2. E. C. Constable, C. E. Housecroft, M. Neuburger, S. Schaffner, E. J. Shardlow, *Inorg. Chem. Comm.,* **8**, 743-745, (2005).

3. E. C. Constable, C. E. Housecroft, M. Neuburger, S. Schaffner, E. J. Shardlow, *Cryst. Eng. Comm.,* **7**, 599-602, (2005).

4. E. C. Constable, C. E. Housecroft, M. Neuburger, S. Schaffner, E. J. Shardlow, *Acta Cryst.*, **E62**, m2210-2212, (2006).

5. E. C. Constable, C. E. Housecroft, M. Neuburger, S. Schaffner, E. J. Shardlow, *Inorg. Chim. Acta*, in press, (2007).

6. J. E. Beves, E. C. Constable, C. E. Housecroft, M. Neuburger, S. Schaffner, E. J. Shardlow, *Dalton Trans*., in press, (2007).

PRESENTATIONS

February 2005 Oral Presentation- Swiss Young Chemists' Association Snow Symposium.

June 2005 Poster Presentation- Royal Society of Chemistry European Industry Tour.

October 2005 Poster Presentation- Swiss Chemical Society Fall Meeting.

August 2006 Oral Presentation- 37th ICCC, Cape Town, South Africa.